Measuring and modelling of volcanic pollutants from White Island and Ruapehu volcanoes: assessment of related hazard in the North Island

A thesis

submitted in fulfilment

of the requirements for the Degree

of

Doctor of Philosophy

at the

University of Canterbury

by

Uwe Grunewald

University of Canterbury

May 2007

Acknowledgements

This thesis would not have been possible without the support of many, which is greatly appreciated. First of all, I would like to express my sincere thanks to Cindy Werner, who supervised my work in its initial stages regarding DOAS and aerosol sampling. I would also like to take the opportunity to express my utmost thanks to Peyman Zawar-Reza, who advised my work with TAPM and tolerated my numerous questions concerning modelling. Many thanks to Jim Cole my principle supervisor, who supervised the complete thesis and who endured the proof reading and editing of my German-English.

Karen Britten and Jeremy Cole-Baker (Geological & Nuclear Sciences) are thanked very much for their help and for providing monitoring data from White Island volcano. I am also thankful to Brad Scott, Dave Keen and Fred Langford (GNS) for their work on the weather station on White Island. Thanks to Justin Harrison (Geography Department) for the MiniVol instruments and filters. More filters were supplied from Catherine Chagué-Goff (NIWA Christchurch). Thanks also to Brian Daly, Linda Hill and Gareth Salt (Landcare Palmerston North) for the filter analyses. I am very grateful to Tamsin Mather who gave me much advise before and after aerosol sampling on White Island and read through the results. Many thanks to Ross Marsden (MetService New Zealand) for providing me the weather data from Whakatane, Auckland, Wellington and Rotorua, as well as Elaine Fouhy (NIWA Wellington) for weather data from Ruapehu. The emails of Peter Hurley (CSIRO), containing valuable information regarding TAPM, are very much appreciated. Thanks to Neil Andrews (Biology Department) for his help on SEM.

Other people who answered my questions: Thanks to Nicole Bobrowski, Marie Edmonds, Richard Herd, Andrew McGonigle, Ashok Luhar, John Thyne, Vicky Hards and Katrin Tschirpke. Special thanks to Naomi Matthew, Kate Bodger, Heather Taylor, Rose Turnbull and Clinton Rissmann who read through individual chapters of the thesis and corrected my German-English before printing. I also received great support from the University of Canterbury, which provided me with 3-years funding. Thanks to the people in my department, especially John Southward and Pat Roberts for their help. Thanks also to all the friendly people in New Zealand who crossed my way in these three years. Many thanks also to my friends in Germany, Europe and the rest of the world who supported me from afar and even more thanks to all of you who visited me!!! Last but not least, greatest thanks to my parents for their unconditional support over ALL the years!!!

CONTENTS

CHAPTER 5: The Air Pollution Model (TAPM)

CHAPTER 6: Evaluation of meteorological data from annual modelling

CHAPTER 7: Results of annual SO_2 and PM_{10} dispersion modelling

CHAPTER 8: Hazard assessment to population

CHAPTER 9: Verification of meteorology and SO_2 dispersion modelling from WIV

CHAPTER 10: Dimension of the non-eruptive plumes from White Island volcano

CHAPTER 11: Summary and conclusions

List of Figures

List of Tables

Abstract

White Island and Ruapehu are currently the most active volcanoes in New Zealand. During non-eruptive periods, intense quiescent degassing through fumaroles can occur. The current project studies the quiescent degassing plumes, including aerosol sampling on White Island and dispersion modelling of SO_2 and PM_{10} from White Island and Ruapehu volcanoes.

Aerosol sampling from fumaroles at the crater floor on White Island volcano was carried out on 9 February and 6 April 2005. The exposed filters were analysed for various anions and cations and the particle mass concentration and molar concentration determined. Major elemental constituents were sodium and chlorine (Na^+: 413 µg m^{-3}, Cl^-: 1520 µg m^{-3}), which show best correlation at both sampling sessions. Other ions detected, with little correlation, are Ca^{2+}, PO_4^{3-} and to a certain extent Mg^{2+}. Other constituents found, which cannot correlate explicitly to other ions, are K^+, NH_4^+, NO_3^-, and SO_4^{2-}. SEM study of one exposed filter was performed and mainly NaCl particles could be distinguished due to their well-defined cubic shape.

The Air Pollution Model (TAPM) was used for dispersion modelling of SO_2 (models 1-4) and PM_{10} (models 5 and 6) from White Island and Ruapehu volcanoes. Annual modelling was performed using different parameters of emission rate, exit temperature and exit velocity. The resulting plume dispersions show relatively low concentrations at ground level (≤10 m), particularly for the models of PM_{10} dispersion. TAPM calculated the highest SO_2 ground level concentrations with model 4, where the NES values of 350 and 570 µg m^{-3} were exceeded several times. The data was then used for detailed hazard assessment of urban population in the North Island. The meteorological data from annual modelling was used for model evaluation and compared with observation data from different weather stations by statistical calculations. Overall, TAPM performed well with most good and very good results.

To evaluate SO_2 dispersion modelling, airborne plume measurements were carried out on 22 November 2006 by plume traverses at 3, 10 and 20 km. Although there is some variation, the calculated correlation coefficients indicate good model results for two plume traverses at 3 and 20 km and one plume traverse at 10 km. The meteorological data was also used for model evaluation, and the results indicate good model performance. TAPM is therefore suggested for future studies when more observation data are available to verify the calculated model data.

CHAPTER 1: Introduction

The North Island of New Zealand is an area with several active volcanoes that are mainly located in the Taupo Volcanic Zone. The two most active volcanoes, White Island and Ruapehu, are associated with numerous active events in historical time and are characterised by continuous, quiescent degassing.

Volcanoes represent a major source for emission of pollutants into the atmosphere. Emitted pollutants can be divided into gases and suspended particulate matter. Depending on the alert level of the volcano, several hundred or thousand tonnes of gas per day can be discharged daily out of the vent and into the atmosphere. During quiescent degassing the released gases and aerosols are emitted into the troposphere, whereas highly explosive events cause the emission of volcanic pollutants into the stratosphere, although substantial quantity of gases and aerosols are also emitted into the troposphere. The amount of individual pollutants and the height of the plume column determine the elevation at which the elevation the gases and aerosols are emitted into the atmosphere as well as how long and how far the volcanic plume is transported and dispersed in the atmosphere.

Monitoring of volcanoes is essential for predicting volcanic activity and to protect the population living in volcanic areas or close to volcanic vents, respectively. Volcano surveillance includes mainly geophysical and geochemical investigations providing indications about signs of unrest and alert level of the individual volcano studied. One of the major gas species emitted from volcanoes is sulphur dioxide (SO_2), whose monitoring is a standard procedure of volcano surveillance in all regions with active volcanism. Although the emission of volcanic gases and aerosols is not the highest risk for people living near volcanoes, this type of hazard is often underestimated since their health effects, causing various chronic illnesses, are typically delayed. In comparison to other volcanic hazards, the number of deaths due to volcanic gases is quite low. Monitoring and mitigation of volcanic hazards do not simply imply the prediction of volcano alert levels but also involve the assessment of volcanic hazards and the prevention of victims and accidents relating to volcanic activity.

Study of volcanic gas composition and gas emission rates is undertaken regularly at many volcanoes worldwide, including White Island and Ruapehu. In New Zealand this is carried out by scientists of the Institute of Geological & Nuclear Sciences (GNS). A standard instrument for plume measurements to determine the emission rate of sulphur dioxide (SO_2) is the correlation spectrometer (COSPEC). Such monitoring is carried out regularly in New Zealand but only at intervals of several weeks due to the high costs involved. Since this is somewhat inadequate for volcano surveillance, GNS have purchased two Differential Optical Absorption Spectrometers (DOAS), which were installed on White Island in 2006 and which should measure the SO_2 emission rate continuously from sunrise to sunset. Sampling of volcanic aerosols in New Zealand was only performed once before in 1983.

The original subject of the present research project was to carry out permanent SO_2 measurements using DOAS, which had improved the surveillance of the alert level of the White Island volcano and the results had been used for hazard assessment and risk mitigation. Unfortunately, there appeared much delay in the process of purchasing these spectrometers. Therefore, the research topic had to be changed after more than one year and modelling became the main subject of the present study.

The application of numerical models has become an important tool for volcano monitoring. There are several computer programs available to perform modelling of the different types of volcanic hazard. In order to model the dispersion of pollutants in the troposphere, atmospheric scientists of the Commonwealth Scientific and Industrial Research Organisation (CSIRO) in Australia have developed the program *The Air Pollution Model (TAPM)*, which is mainly used for dispersion modelling of pollutants from anthropogenic sources, such as industrial chimneys.

Modelling the dispersion of pollutants in the atmosphere assists in the prediction of air pollution and the exposure of human and environment to pollutants under defined and varying meteorological conditions. Due to the effects of air pollution on the natural environment and human activities, organisations and governments in many countries have developed national protocols with guidelines for many pollutant compounds to protect environment and population. There are several National Environmental Standards (NES) that have been developed for New Zealand to regulate the cleanness of land, water and air. These are issued by the Ministry for the Environment to ameliorate adverse effects on people and environment. NES include 14 standards to prevent toxic emissions of gases and aerosols, including sulphur dioxide (SO_2) and particulate matter with aerodynamic diameter of 10 μm (PM_{10}), and to protect air quality.

Research objectives

The present study is divided into two parts: first the sampling of particulate matter (PM_{10}) on White Island volcano and second the modelling of SO_2 and PM_{10} dispersion in the troposphere from White Island and Ruapehu volcanoes. Two sampling sessions were undertaken to address the first part of this study. The analyses include the determination of the chemical composition of soluble ions as well as the morphology and elemental composition of solid particles that are deposited onto the exposed filters. In order to address the second part of this project, TAPM is applied to model different scenarios of plume dispersions from White Island and Ruapehu volcanoes, containing either SO_2 or PM_{10}.

The goals of this study are:

(1) to determine the chemistry and concentration of emitted particulate matter (PM_{10}) from quiescent degassing fumaroles of White Island volcano and to compare the present results with data from previous studies as well as other volcanoes

(2) to model different scenarios of SO_2 and PM_{10} dispersion from White Island and Ruapehu volcanoes and to evaluate the model using statistical measures

(3) to provide images of modelled plume dispersion for hazard assessment in the North Island using the results of modelled SO_2 and PM_{10} dispersion scenarios

(4) to perform detailed hazard assessment of modelled SO_2 dispersion from scenario with the highest ground level concentration (from each source) for various locations in the North Island by comparing the modelled SO_2 dispersion data with issued concentration values of the National Environmental Standard (NES) of New Zealand
(5) to verify the accuracy of SO_2 dispersion modelling using data from airborne plume measurements and to evaluate the accuracy of annual modelling by comparing the results of observed and predicted meteorological and pollution data using statistical measures
(6) to appraise the model program 'TAPM' about the possibility for future application of hazard assessment of volcanic degassing

The results will show if quiescent volcanic degassing poses any hazards to New Zealand's population. The results of aerosol sampling should also indicate which aerosol species exist in the atmosphere at White Island and the concentration people are exposed to when visiting the volcano. While this part is a proximal hazard assessment, the modelling of plume dispersion is thought to represent distal hazard assessment. Depending on the accuracy of the models, their results can be used to evaluate the pollution concentration in affected areas due to volcanic degassing.

Resultant data will also contribute to NES of issued SO_2 and PM_{10} concentrations ultimately providing information concerning the compliance with threshold values of NES.

Structure of the thesis

This thesis is organised into 11 chapters as follows:

Chapter 1: Introduces the issue addressed by this project, outlines the study objectives and provides the thesis structure.

Chapter 2: Contains general background of all aspects related to the present study. In particular, it gives information about meteorology, troposphere, plume dispersion in the troposphere, impacts of SO_2 and aerosols on human health and environment, existing National Environmental Standards in New Zealand and modelling of air pollution.

Chapter 3: Describes monitoring methods that are applied at White Island and Ruapehu volcanoes, which represent the prime objectives of this study.

Chapter 4: Deals with the fieldwork on White Island, where two aerosol-sampling sessions were carried out. It describes the sampling method and it discusses the results of the different analyses of the present study This chapter also provides a comparison of the present results with those of previous studies on White Island and other volcanoes.

Chapter 5: Describes the software 'The Air Pollution Model' (TAPM), which is used for dispersion modelling of sulphur dioxide (SO_2) and particulate matter (PM_{10}) from White Island and Ruapehu volcanoes. It explains the meteorology and the pollution module of the model program as well as it gives a short summary about modelled scenarios.

Chapter 6: Analyses the results of the meteorological part of the present modelling studies. It evaluates the accuracy of the present modelling using a set of statistical measures that enable comparison between recorded observation data from different weather stations in the North Island and modelled prediction data from TAPM. There is also presented a comparison with other previous published model analyses.

Chapter 7: Provides the results of the dispersion modelling of SO_2 and PM_{10}. First there are explained the reasoning behind the choices of certain input parameters to model the different scenarios. The output data consists of gridded summary statistics of the whole modelled area and time series data of individual location in the North Island. The results of the gridded summary statistic files are projected onto digital elevation images of the North Island. This chapter also discusses modelled ground level concentration of SO_2 and PM_{10} in the North Island in relation to the threshold values of the National Environmental Standards (NES) of New Zealand. Where useful, the output data of the time series are used for detailed pollution concentration at individual locations.

Chapter 8: Presents a detailed analysis of SO_2 dispersion based on the results of modelling with the highest ground level concentrations. Different locations, including all main urban areas, in the North Island were chosen to perform this analysis of hazard assessment to population.

Chapter 9: Analyses the results of the pollution part of the present modelling studies. It verifies the accuracy of modelled SO_2 dispersion data with airborne plume measurements, which were carried out on 22 November 2006 at different distances from the volcanic vent. The evaluation is performed using statistical calculations.

Chapter 10: Gives a short summary about the dimension of the quiescent degassing plumes from White Island volcano. This chapter is based on a previous study of the non-eruptive plume from Mount St. Helens. The results of the present study compares are compared with known data from other volcanoes.

Chapter 11: Provides a summary of the present study findings and conclusions and gives an outlook for possible future work.

Chapter 2: General background

2. 1. Introduction

This chapter will cover the general background to this study. It includes information about meteorology, plume dispersion, impacts of SO_2 and aerosols on the environment and air pollution modelling.

2. 2. Atmosphere and meteorology

2. 2. 1. Gases and aerosols in the atmosphere

The Earth's atmosphere is a mixture of gas that consists of the major gas species nitrogen (N_2) and oxygen (O_2) as well as many trace gas and aerosol species. Atmospheric aerosols are in air suspending liquid droplets and/or solid particles, whose concentration is decreasing with increasing elevation in the atmosphere [e.g. Roedel 2000]. Aerosol particles are also referred to as particulate matter (PM). They may vary in shape and their size ranges from a few tens of angstroms (Å) to several hundred micrometers. Particulate matter is mainly divided into coarse particles (>2.5 μm) and fine particles ≤2.5 μm [e.g. Seinfeld & Pandis 1998, Mather et al. 2003b], which differ widely. For example, they have different chemical compositions, have different optical properties, are removed from the atmosphere by different mechanisms and differ in their deposition patterns in the respiratory tract. Thus the differentiation of fine and coarse particles is fundamental in all discussions regarding physics, chemistry, measurement and/or health effects of aerosols [Seinfeld & Pandis 1998].

There are numerous sources of atmospheric particulate matter, such as sea salt spray, combustion of materials, erosion of rocks, dispersion of biological substances and gaseous emissions. The latter source includes the discharge of gas and aerosol species from degassing volcanoes.

Many gas and aerosol species are removed from the atmosphere by dry and wet depositional processes [e.g. Arya 1999, Warneck 2000, Horrocks et al. 2003]. Dry deposition includes the irreversible absorption of individual compounds on soil, water or vegetation surfaces [Arya 1999]. Experimental studies by Seinfeld [1986] showed that the velocity of dry deposition depends on surface roughness and wind

speed. The rate of acid deposition increases when leaf surfaces are wet [Horrocks et al. 2003]. Dry deposition velocities of SO_2 were experimentally determined with 0.1-2 cm s^{-1} [Seinfeld 1986] and field studies of Delmelle et al. [2001] at Masaya volcano, Nicaragua, result in SO_2 and HCl deposition rates of 1.6 cm s^{-1} [Delmelle et al. 2001]. During wet deposition, the gas and aerosol species are incorporated into precipitation elements, such as clouds, rain droplets and ice particles [Arya 1999]. Particulate matter act as condensation nuclei and fall out with water droplets, whereas gases are easily dissolved in water droplets and are removed by fallout from the atmosphere [Horrocks et al. 2003].

2. 2. 2. Troposphere

The troposphere is the lowest layer of the Earth's atmosphere and hence, most relevant to atmospheric pollutants. Stull [1989] reported that the troposphere consists of a planetary boundary layer (PBL) near the Earth's surface and a free atmosphere above it (Figure 2. 1). The boundary layer is defined as the lowest part of the troposphere, which is directly influenced by the presence of the earth's surface responding to surface forces and processes within a time period of approximately one day [Oke 1987] to one hour or less [Stull 1989]. Generally, the depth of the boundary layer is less in high-pressure than in low-pressure regions. In regions of low pressure, the air of the boundary layer moves upward away from the ground to large altitudes throughout the troposphere [Stull 1989].

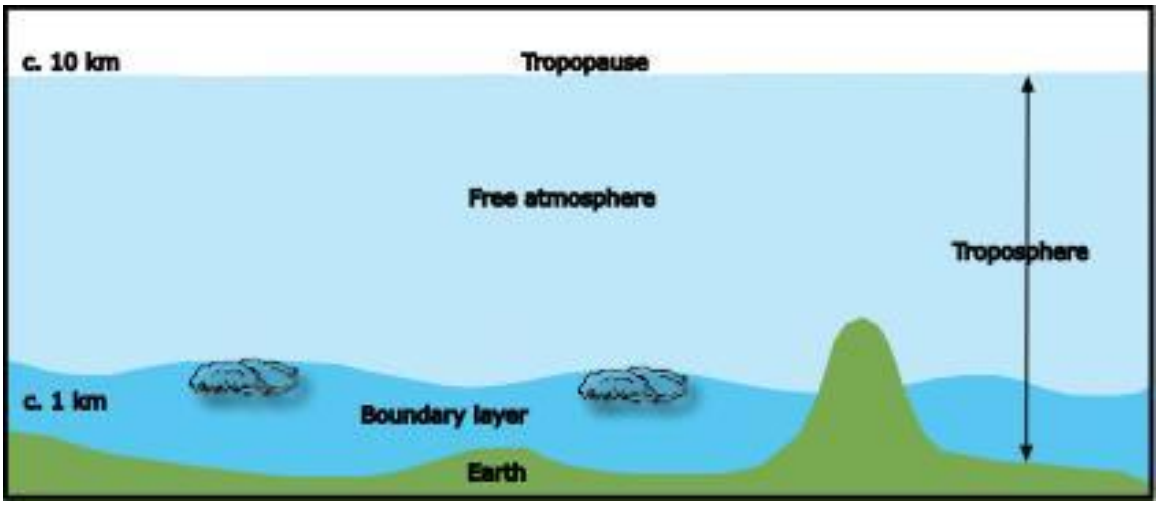

Figure 2. 1 Location of the boundary layer (adopted from Stull 1989).

According to Stull [1989], PBL forms a well-defined structure with diurnal cycle over land surfaces in high-pressure regions (Figure 2. 2). The three major parts are the *mixed layer*, the *stable boundary layer* and the *residual layer*. The presence of clouds results in generation of a *cloud layer* at the top of the mixed layer. At the bottom of the boundary layer is the *surface layer* where the magnitude of turbulence and stress vary by less than 10 %. The surface layer is always present and is either part of the mixed layer or the stable boundary layer [Stull 1989]. The surface layer often undergoes strong wind shear caused by friction [Piironen 1994].

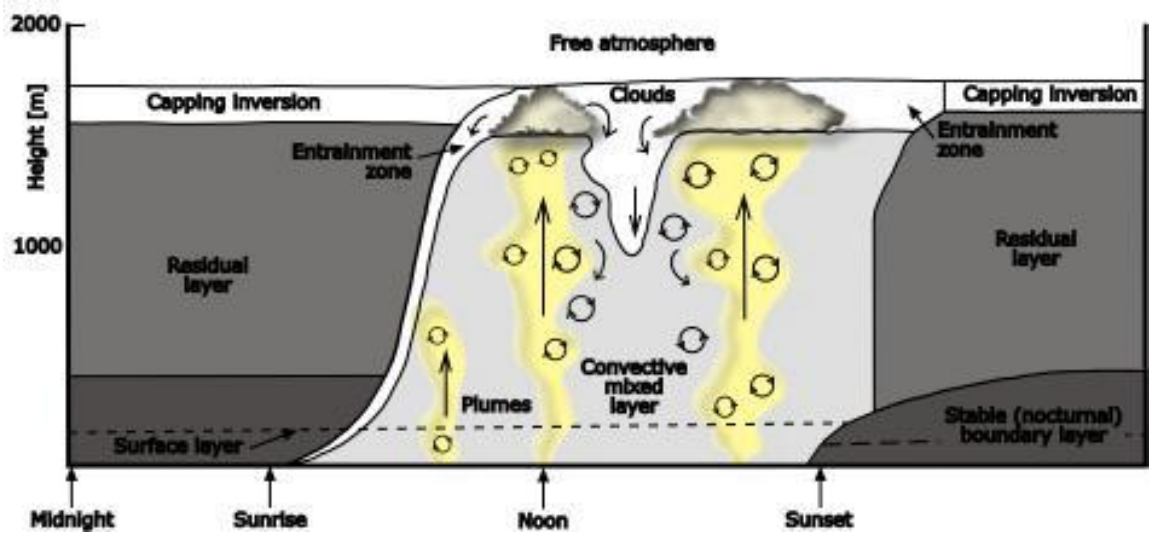

Figure 2. 2 Structure of the boundary layer in fair weather (adapted from Stull, 1989, 1995 and Piironen 1994).

The mixed layer is characterised by turbulence caused by heat transfer from a warm ground surface and radiative cooling from the top of the cloud layer. When buoyant turbulence takes over the mixed layer, it is also called the *convective boundary layer* [Stull 1989, Piironen 1994]. The generation of the mixed layer usually starts about half an hour after sunrise. It grows by entraining and mixing less turbulent air from above into it and reaches its maximum depth in the late afternoon [Stull 1989]. An *entrainment zone* occurs between the sinking dry air parcels from the free atmosphere and rising thermals from the mixed layer [Stull 1989, Piironen 1994]. At night, the entrainment zone becomes a non-turbulent capping inversion [Stull 1989, 1995].

The intensity of the thermals in the mixed layer weakens and ceases before sunset, generating the so-called *residual layer*. From sunset to sunrise, the lowest part of the residual layer transforms by its contact with the ground into the stable (nocturnal) boundary layer [Stull 1989]. Due to the end of solar heating, radiative cooling and surface friction stabilise this part of the planetary boundary layer. However, during periods of cold air advection over warm surfaces the nocturnal boundary layer may also be convective [Piironen 1994].

The atmospheric boundary layer over oceans is called the *marine boundary layer*. There is little variation of the sea surface temperature during the day due to vigorous mixing within the top of the ocean. Additionally, due to the large heat capacity, water can absorb large amounts of heat from the sun with relatively little temperature change. As a consequence, the depth of the marine boundary layer only shows little variation in time and space [Stull 1989, Arya 1999].

Above the planetary boundary layer (PBL) is the free atmosphere. While the wind in the PBL is characterised by turbulences and vertical mixing, the wind in the free atmosphere behaves approximately geostrophic (parallel to the isobars), as this layer is usually non-turbulent or only intermittently turbulent [Stull 1989].

2. 2. 3. The general circulation of the atmosphere

In the troposphere, the amount of energy from the sun at tropical (0-30°) and subtropical (30-40°) latitudes is greater than that given off by outgoing terrestrial radiation, for both land areas and oceans. As a result, there is a year-round energy transfer from low to high latitudes, driving the general circulation of the atmosphere [Graedel & Crutzen 1993].

The rotation of the Earth also results in the generation of a complex atmospheric circulation pattern [e.g. Lutgens & Tarbuck 1979, Miller & Anthes 1980, Graedel & Crutzen 1993, Sturman & Tapper 1996]. As these authors reported, the transport of air between equator and pole areas is driven by the energy received from the sun and occur in three large convection cells (Figure 2. 3). A description of the general circulation of the Earth's atmosphere is summarised in the following paragraph using the publications of the authors mentioned above.

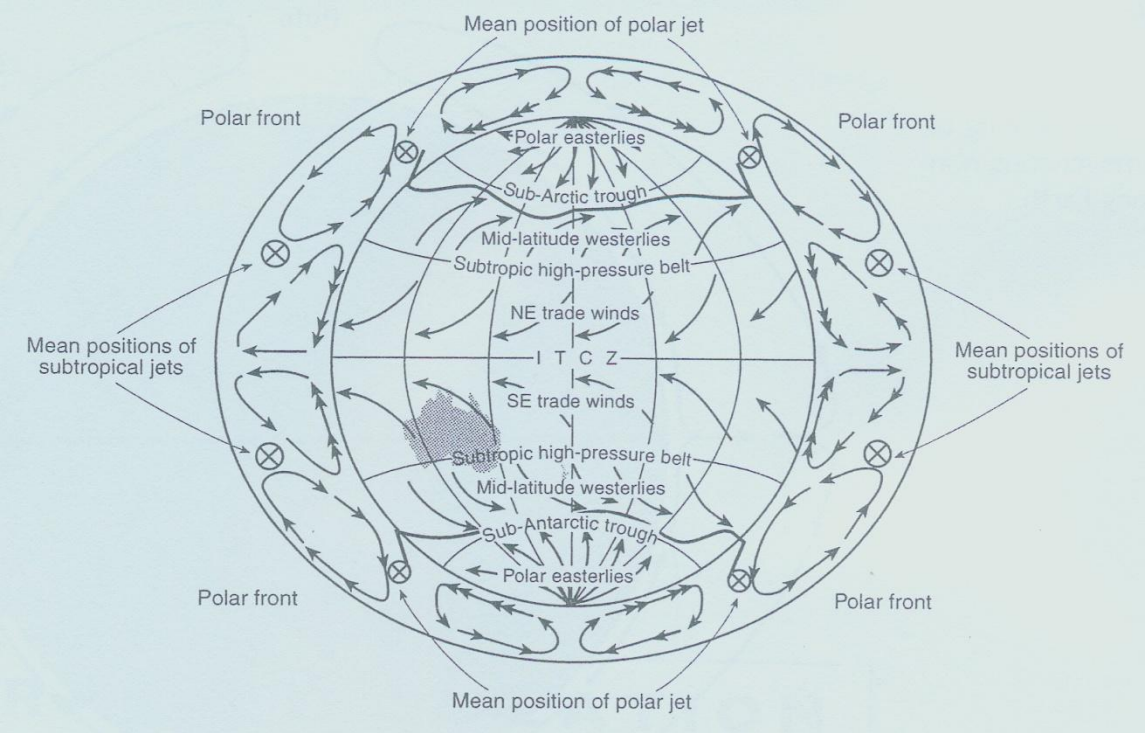

Figure 2. 3 General circulation of the global atmosphere. Single- and double-headed arrows in the cross sections indicate wind components from the west and east, respectively [from Sturman & Tapper 1996].

The zone of circulation between the equator and about 30 degrees latitudes is called the *Hadley cell*. Within the equatorial region is the *intertropical convergence zone* (ITCZ). This is the zone of maximum solar heating, in which warm air rises to high altitudes. Due to the Coriolis force, the poleward flowing air in the two hemispheres becomes west winds, reaching more than 40 m/s at an average latitude of 30 degree. These are the *subtropical jet streams*. Cooling causes some of the air to descend again towards the Earth's surface at c. 30 degrees north and south latitudes. These zones are called the *horse latitudes* and are characterised by cloudiness and precipitation. Near the surface, some air returns back to the tropics. The Coriolis force causes a deflection of the wind again, which results in generation of NE-winds in the Northern Hemisphere and SE-winds in the Southern Hemisphere. These are called 'trade winds'.

The Coriolis force also deflects the air that moves from the horse latitudes poleward. These are named the *prevailing westerlies* and occur in both hemispheres. Cold Arctic and Antarctic air moves from the pole areas to lower latitudes. The Coriolis force is again responsible for deflection of the winds, which are called the *polar easterlies*. The warm westerlies encounter the polar easterlies at latitudes between 40 to 60 degrees, forming a boundary that is known as the *polar front*. Warm air from the horse latitudes rises over the cold dense air from the poles. Some of the warm air returns at high altitudes back toward the equator, whereas the other portion of air moves toward the poles.

The planetary circulation is accompanied by a compatible distribution of surface pressure [e.g. Lutgens & Tarbuck 1979]. The large-scale global pressure and current systems between the Northern and Southern Hemisphere have the same main features (Figure 2. 3). However, the weather and atmospheric circulation in the Northern Hemisphere is significantly modified by the larger landmasses that cause semi-permanent pressure systems between the summer and winter seasons and the formation of monsoonal circulations. The weather systems in the Southern Hemisphere are more influenced by the oceans. Monsoonal circulations are less important but eastward-migrating high- and low-pressure systems are the dominant feature [e.g. Steiner 1980].

2. 2. 4. Meteorology of New Zealand

As described by Linacre & Geerts [1997], the weather, and consequently the climate, depend on three factors:

(1) atmospheric processes (e.g. wind, radiation, instability and turbulence)

(2) surface characteristics (e.g. albedo, roughness, ocean currents)

(3) features of geography (e.g. latitude, altitude, proximity to the sea)

The general circulation represents a global-scale wind system, which determines the broad patterns of the Earth's climate. Parts of the planetary circulation also influence the Australasian region [Sturman & Tapper 1996], which includes New Zealand. From a meteorological point of view, New Zealand is situated in a zone between the high-pressure belt in the sub-tropics and the low-pressure trough in the Southern Ocean [De Lisle & Kerr 1963].

Throughout the year, the Southern Hemisphere surface pressure field is characterised by large, semi-permanent high-pressure cells over the subtropical oceans, namely the eastern South Pacific High, the South Atlantic High and the South Indian Ocean High [Sturman & Tapper 1996]. While they all undergo a northward shift of 5 to 10° during the winter months, the South Indian Ocean High shifts up to 30° to the north, lying closer to the Australian continent in summer. With the exception of Antarctica, surface heating results in lower air pressures over the landmasses in summer than over the surrounding oceans. Conversely, there is a cell of high pressure over the Australian continent during the winter season [Sturman & Tapper 1996]. As these authors reported, patterns of 'anticyclonicity' and 'cyclonicity' occur in the Southern Hemisphere, which are partly caused by features mentioned above. In January, high-pressure cells of anticyclones are preferentially located in the eastern ocean sectors between 30 and 40° latitude as well as in the Great Australian Bight, just west of the North Island of New Zealand [Sturman & Tapper 1996].

A weather pattern, which affects the climate of large parts of the world every few years, is known as El Niño-Southern Oscillation (ENSO) and is centred in the ocean and atmosphere of the tropical Pacific [e.g. Walker 1924, Gordon 1986, Brenstrum 1998]. ENSO has caused droughts in New Zealand particularly in 1982-83 and 1997-98 and the Auckland water crisis in 1994. The factors that influence the generation of the Southern Oscillation (air pressure and sea surface temperature) are known and help to forecast much of the weather in the Pacific region (e.g. New Zealand), it is not particularly predictable. While, for example, the El Niño in 1982-83 caused a severe drought in Gisborne and Hawkes Bay, the El Niño in 1987-88 did not [Brenstrum 1998].

Any climate depends on local factors, such as radiation, rainfall and evaporation as well as advection that includes heat and moisture brought by oceans and winds [Linacre & Geerts 1997]. Winds are distinguished on their scale. The global wind circulation is the sum of the synoptic-scale winds that are averaged over space and time. The term synoptic means 'seen together' and refers to the observation of measurements from a wide area, such as Australia or New Zealand [Linacre & Geerts 1997]. To the group of synoptic-scale winds belong air masses. They represent bodies of streaming air with more or less uniform characteristics with regard to temperature, humidity, stability, wind speed and direction [Sturman & Tapper 1996, Linacre & Geerts 1997]. According to Sturman & Tapper [1996], the largest air masses source areas in the Southern Hemisphere are over the oceans, in which there are four major air mass types affecting New Zealand (Figure 2. 4):

(1) The modified polar maritime (Npm) has its origin in the Southern Ocean (55-68°S) and brings a cold, moist and unstable air mass to the southern parts of Australia and New Zealand.

(2) The air mass of the southern maritime (Sm) is characterised by cool, moist air, in which the source is the lower latitudes in the Southern Ocean (35-55°S). New Zealand is often affected by large quantities of rain.

(3) The tropical maritime Tasman (tTm) comes from the north Tasman Sea, in which the air mass is warm, unstable and moist to high levels. The north-western parts of New Zealand get cloudy and drizzly weather, whereas heavier rainfall occurs where there is orographic lifting.

(4) The air mass of the tropical maritime Pacific (pTm) is warmer than tTm and has its origin further north over the tropical western Pacific. Heavy rainfalls affect the northern parts of New Zealand when the air mass is associated with tropical cyclones [Sturman & Tapper 1996].

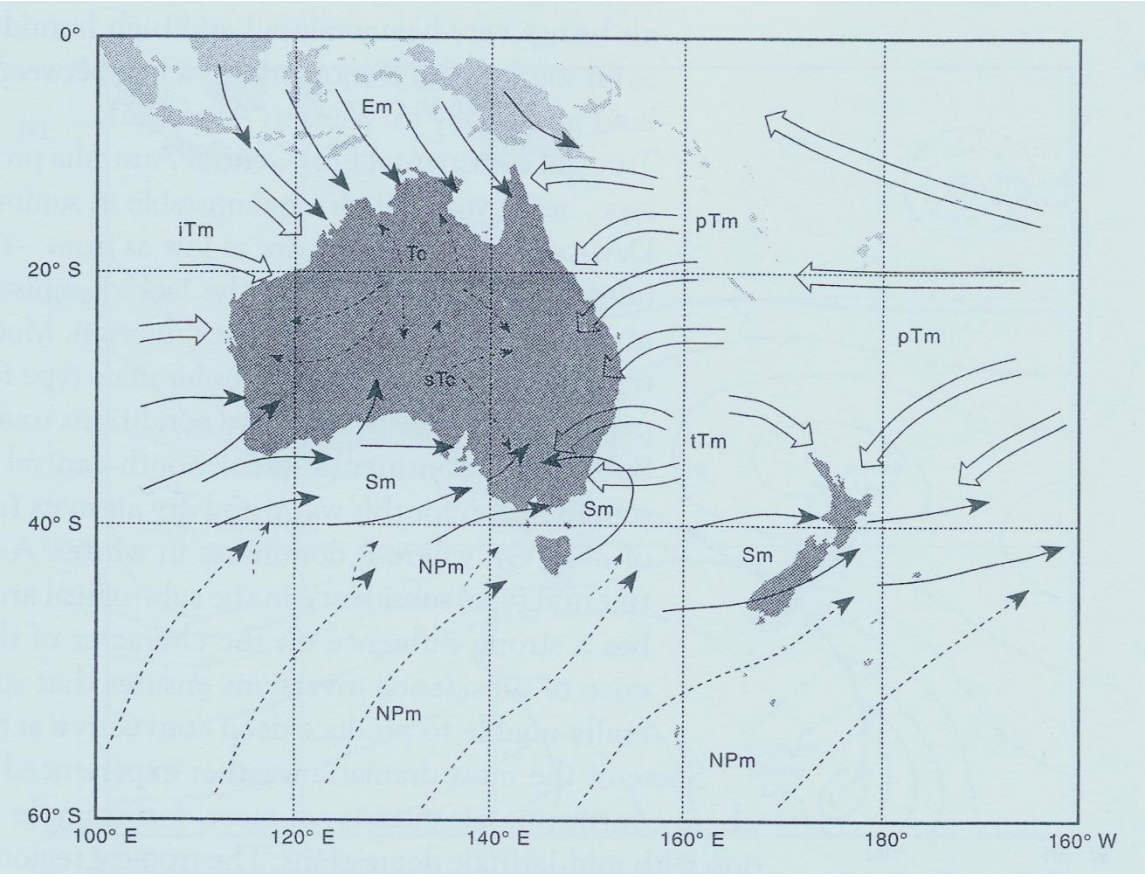

Figure 2. 4 Distribution of important air masses of the Australia and New Zealand region [from Sturman & Tapper 1996].

The synoptic-scale winds contain local surface winds. Linacre & Geerts [1997] mentioned four ways how a surface wind can be created:

(1) they are the synoptic-scale wind

(2) a horizontal difference of temperature in the planetary boundary layer

(3) the topography, causing cold air flow downhill and warm air upwards

(4) storms, especially thunderstorms.

If none of these occur, then the air is 'calm' meaning wind speeds of less than 1.5 m s^{-1} [Linacre & Geerts 1997]. Local surface winds include sea and land breezes, which are common features of the coastal regions of New Zealand. One example is in the Auckland area where the sea breezes have their origin on both sides of the Northlands peninsula [Sturman & Tapper 1996].

Generally, the climate of New Zealand is complex and shows much variation. As mentioned by Drost et al. [2007], the ocean influences the main climate, whereas regional differences are induced by topography. Whilst there is a warm subtropical climate in the far north, the south of New Zealand undergoes cool temperature climates. Located between the subtropical ridge and sub-Antarctic trough is the zone of the mid-latitude westerlies, which affect New Zealand throughout the year [Sturman & Tapper 1996]. Besides the alpine chain in the South Island, the Tongariro Volcanic Massif and Taranaki in the North Island is the only other mountainous area that experiences alpine weather conditions. The edifice of Mt. Ruapehu (2797 m a.s.l.) is part of this volcanic massif and represents the highest peak in the North Island.

The dominant westerly winds increase rainfall activity in spring time along the west coast but decrease precipitation on the east side. Convection and convergence of sea breezes result in more inland showers during summer, especially on the North Island [Linacre & Geerts 1997]. As these authors reported, there are at least 150 days of rain each year over the North Island. Salinger [1979] classified 10 rainfall regions over the North Island (Figure 2. 5).

The volcanic centre of White Island is located approximately 50 km offshore from the coast of Bay of Plenty, where Quayle [1984] noted high rainfall variability within the Bay of Plenty region. Although there is no difference between the large weather systems at White Island and the rest of the Bay of Plenty, White Island is probably more influenced by the surrounding sea [Quayle 1984].

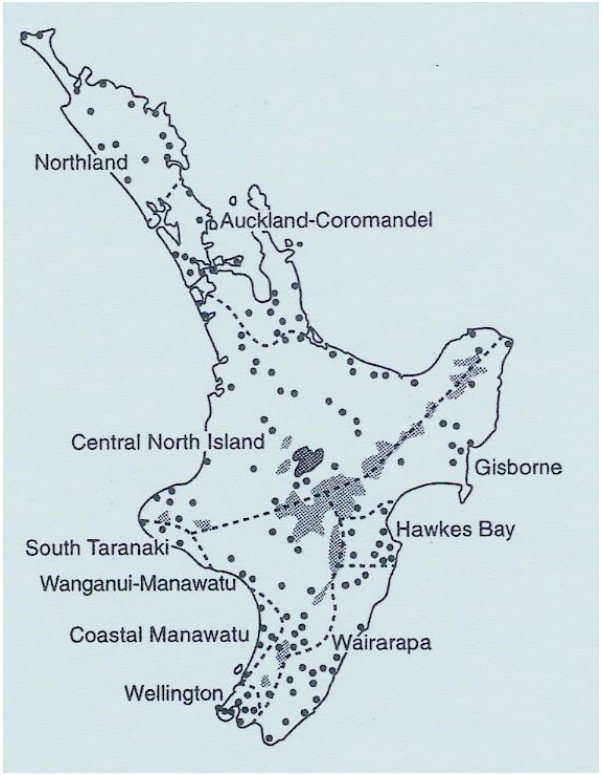

Figure 2. 5
Climate subdivision of the North Island of New Zealand based on a cluster technique applied to rainfall activity [from Sturman & Tapper 1996].

2. 3. Dispersion of plumes in the troposphere

2. 3. 1. Gases and aerosols in volcanic plumes

The most common discharged gas species from volcanoes are water vapour (H_2O), carbon dioxide (CO_2) and sulphur dioxide (SO_2). Additionally, there are compounds with lower concentrations, such as hydrogen chloride (HCl), hydrogen sulphide (H_2S) and hydrogen fluoride (HF). Although the relative concentrations of S_t ($S_t = SO_2 + H_2S$) and HCl can vary considerably, the amount of total sulphur is lower than that of CO_2 but normally higher than HCl [Symonds et al. 1994, Delmelle & Stix 2000, Delmelle 2003].

The chemical composition of volcanic gases is usually measured near the vent. Ingestion of large amounts of air after a few seconds or minutes of transport can result in dilution of tropospheric volcanic plumes by factors of c. 10^2 to 10^5 [Casadevall et al. 1984, McGee 1992, Delmelle 2003]. Delmelle [2003] concluded that only volcanic gas species of SO_2, H_2S, HCl and HF might be detected downwind from the source due to their very low background concentration in an unpolluted

atmosphere. Although there are good indications and general trends that show relationships between the magmatic volatile content and tectonic setting of a volcano, various processes (e.g. magmatic differentiation, concentration of incompatible elements in the melt and crustal assimilation) make it difficult for conclusions about the relative contribution of the individual volatile species from these sources to an individual volcano [Oppenheimer 2003].

As previously mentioned, SO_2 represents a major gas component in erupting and non-erupting volcanic plumes. Several publications point out the significance of SO_2 emission from quiescent degassing volcanoes to the (tropospheric) global sulphur cycle [e.g. Graf et al. 1997, Andres & Kasgnoc 1998, Halmer et al. 2002]. Andres & Kasgnoc [1998] published two lists of 49 continuously degassing and 25 sporadically degassing volcanoes and their individual SO_2 fluxes over the last 25 years. They calculated an estimated sum of 26,200 Mg d^{-1} and 278,000 Mg d^{-1}, respectively. The list of the 49 continuously or semi-continuously degassing volcanoes shows a SO_2 flux between <0.1 and 50 kg s^{-1} over the period of 1972-1997. This represents a total SO_2 emission rate of c. 9.66 Tg a^{-1} and is equivalent to approximately 6% of the global anthropogenic sulphur discharge [Delmelle 2003].

Several other important volatile substances, such as HNO_3 [Mather et al. 2004a] and BrO [Bobrowski et al. 2003] as well as numerous particles of aerosols and trace metals such as Cr, Cu, Zn, As, Se, Cd, Sn, Hg and Bi were detected in volcanic plumes [e.g. Phelan et al. 1982, Vié Le Sage 1983, Gauthier & Le Cloarec 1998, Obenholzner et al. 2003, Mather & Pyle 2004]. Particulate sulphur in volcanic plumes occurs as sulphuric acid (H_2SO_4) and native sulphur. Other particulate matters that were detected are chlorine and fluorine in form of acids and salts. Trace metals are emitted as compounds of halide, sulphide and sulphate into the atmosphere [Delmelle 2003]. Several publications [e.g. Vié Le Sage 1983, Casadevall et al. 1984, Rose et al. 1986, Zreda-Gostynska et al. 1997, Allen et al. 2000] report the total concentration of particulate matter from non-eruptive plumes (from above the vent to 5-6 km distance), with their results showing a range from <20 to several thousand µm m^{-3} [Delmelle 2003].

2. 3. 2. Air mixing and atmospheric stability

Vertical mixing of air is mainly determined by the vertical temperature gradient in the atmosphere. Depending on the temperature of the air that surrounds an upward moving air parcel, the atmosphere consists of combinations of stable and unstable regimes [Graedel & Crutzen 1993].

As described by Sturman & Tapper [1996], because of pressure decrease with altitude, the upward moving air parcel will expand. This expansion is associated with molecular motion with the air parcel (i.e. reduction of molecular kinetic energy). A downward moving air parcel results in an increase of its temperature as a consequence of compression. The change of temperature, caused by change of pressure, is called *adiabatic* [Sturman & Tapper 1996].

The ideal process is a decrease of temperature with altitude with no heat exchange between a dry (unsaturated) air parcel and ambient air during vertical movements. This is called *dry adiabatic lapse rate* Γ [Graedel & Crutzen 1993, Sturman & Tapper 1996]. The concepts of lapse rates are important as they influence the vertical motion and the atmospheric stability. The atmosphere is called stable when the vertical moving of air is limited, and unstable when it is enhanced [Sturman & Tapper 1996]. How far an air parcel will move upward and/or downward depends on changes in its temperature relative to that of the during vertical motion, which is a function of both the adiabatic lapse rate and the actual temperature distribution through the atmosphere (the environmental temperature profile or lapse rate).

Figure 2. 6 shows two diagrams where stable and unstable atmospheric situations are explained, and two significant different environmental temperature profiles (Γ_E) are compared with the dry adiabatic lapse rate (Γ). In each of the diagrams shown, the effect of vertical forcing on an air parcel is assessed at the middle level (O), although it can be examined at any other level [Sturman & Tapper 1996]. During stable atmospheric conditions, the observed decrease in temperature through the environmental temperature profile is small relative to the change of temperature that the vertical moving air parcel undergoes (shown by the dry adiabatic lapse rate). In this situation, the temperature difference between air parcel and the surrounding air provides buoyancy (A is less than B and C is less than D), which will act to try and return the air to its original location while the air parcel is moving up or down [Sturman & Tapper 1996].

The environmental lapse rate shows a strong temperature decrease with altitude during unstable atmospheric conditions. In this situation, a fast upward (or downward) moving air parcel, away from the middle point (O), is the consequence of its temperature increase (or decrease) with respect to the surrounding air (i.e. A greater than B or C greater than D). It is emphasised that the profile of Γ_E, not Γ, is changing between the two diagrams in Figure 2. 6 [Sturman & Tapper 1996].

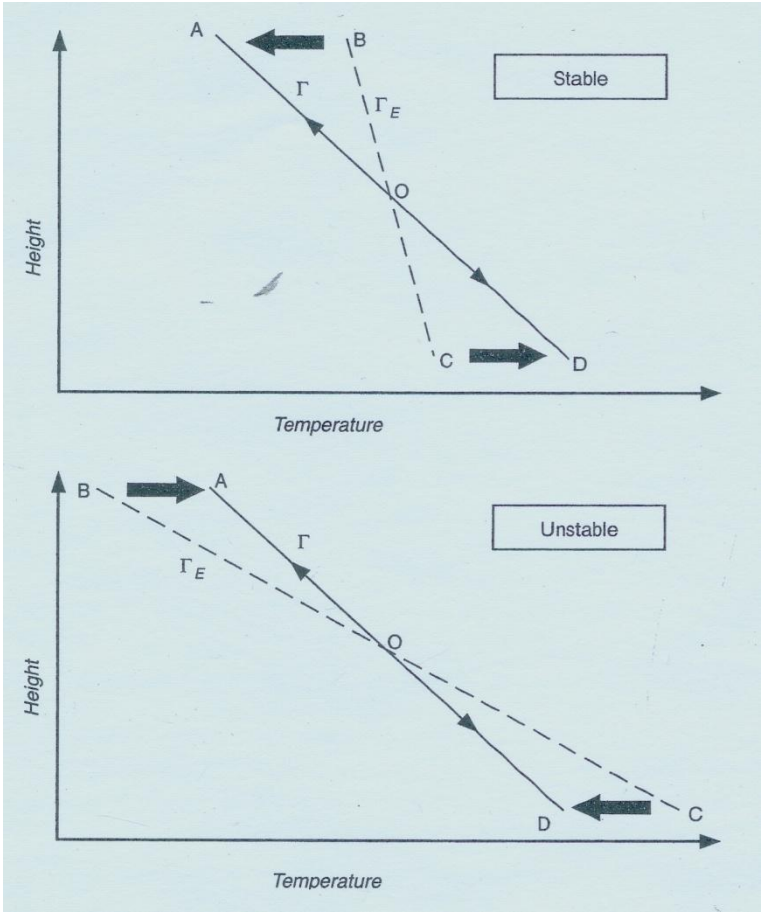

Figure 2. 6
Simplified examples of stable and unstable atmospheric situations. The dry adiabatic lapse rate and the environmental lapse rate are labelled with Γ_E and Γ, respectively. The graphs are adopted from Sturman & Tapper [1996].

2. 3. 3. Plumes of pollution

Wherever pollutants are emitted from a source into the atmosphere, either continuously or over a period of time, a plume is formed. There are various possibilities of stability conditions in the atmosphere and each of which affects mixing of pollutants in the lower atmosphere [Neiburger et al. 1973, Graedel & Crutzen 1993, Turco 2005]. Neiburger et al. [1973] reported that the level of air pollution is controlled by three factors:

(1) total amount of emitted pollutants

(2) configuration of the sources

(3) meteorological conditions

Factor (1) is very evident as the more pollutants are emitted into the atmosphere the higher is the air pollution. Factor (2) can be divided into three source types: point sources, line sources and area sources. Individual house chimneys, industrial stacks and most active volcanoes can be considered as point sources. Exhausting pipes of numerous motor vehicles, streets and highways represent line sources. Large amounts of house chimneys and industrial stacks (e.g. in cities) are regarded as area sources [Neiburger et al. 1973].

As reported by e.g. Arya [1999], transport and diffusion of any substances that are discharged into the planetary boundary layer depend on (Factor 3):

(1) wind direction
(2) vertical distribution of mean wind speed and
(3) turbulences in the planetary boundary layer.

These factors depend strongly on the stability conditions in the atmosphere, which also affects the rise of buoyant plumes and puffs [Arya 1999, Turco 2005]. The vertical mixing of pollutants with ambient air from line and area sources is similar to that of point sources, however their increased horizontal dimension reduces horizontal mixing. Particularly over area sources, pollutants of one part of the source mix with pollutants of another part of the source, rather than with clean and unpolluted air [Neiburger et al. 1973].

Neiburger et al. [1973] outline the effect of turbulent mixing by wind. Turbulence is the consequence of variations in wind direction and speed. The occurrence of more turbulence at high wind speeds results in faster mixing processes and more dilution between pollutants and clean ambient air. Conversely, low wind speeds produce less turbulence and high pollution concentrations remain [Neiburger et al. 1973].

The vertical temperature gradient, and consequently the stability of the air, controls the rate of up- and downward movement, as well as mixing of pollutants with the surrounding air. Wind direction and strength determine how much air the pollutants are initially mixed with and govern the rate of horizontal and downwind dispersion [Neiburger et al. 1973, Boubel et al. 1994, Brimblecombe 1996, Turco 2005].

As shown in Figures 2. 7 a-e, the different atmospheric stability conditions have effects on mixing of pollutants in the troposphere, producing five different shapes and patterns of plumes, which include fanning, fumigation, looping, coning and lofting [e.g. Neiburger et al. 1973, Boubel et al. 1994, Brimblecombe 1996, Turco 2005].

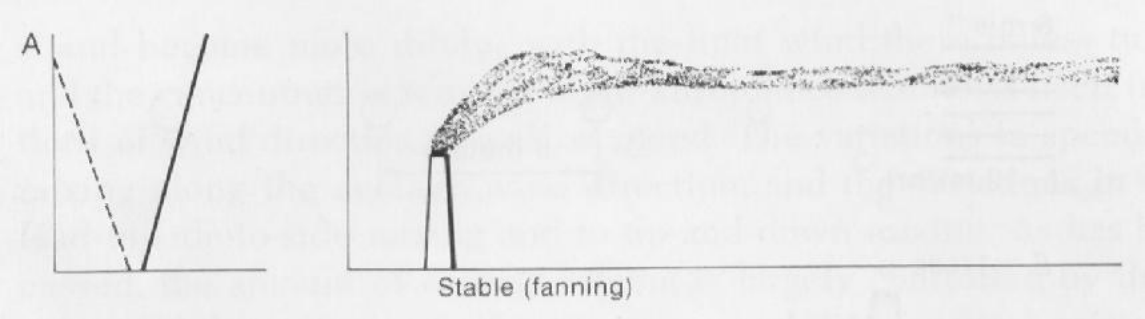

Figure 2. 7a The smoke is emitted into an inversion layer. The stable conditions prevent the diffusion of the pollutants to higher and lower altitudes, causing a vertical thin but horizontal wide spreading (V-shaped) plume. The formation of this plume pattern is called "fanning". Figure adopted from Neiburger et al. [1973].

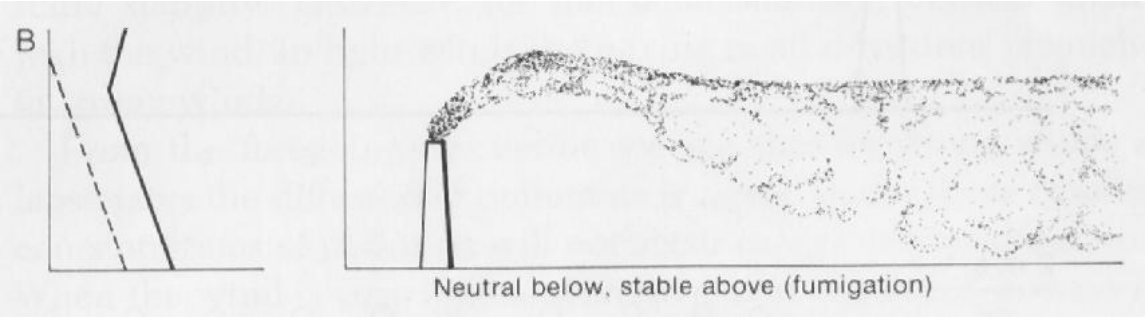

Figure 2. 7b The pollutants are emitted into the atmosphere with an adiabatic lapse rate that is topped by an inversion. The adiabatic lapse rate results in a readily mixing in the lower part of the atmosphere. Upward mixing is limited. This situation is developed during warming-up of the Earth's surface after sunrise, which pushes the inversion at the ground upward and produces a progressively thicker layer with an adiabatic lapse rate. After the level of plume emission is reached, it follows a rapid downward mixing of the pollutants with the ambient air, "fumigating" the ground. Until this moment the ground was protected from pollution by the inversion and the formation of the fumigating plume causes an abrupt increase of pollution concentration at the Earth's surface to a high value. Figure adopted from Neiburger et al. [1973].

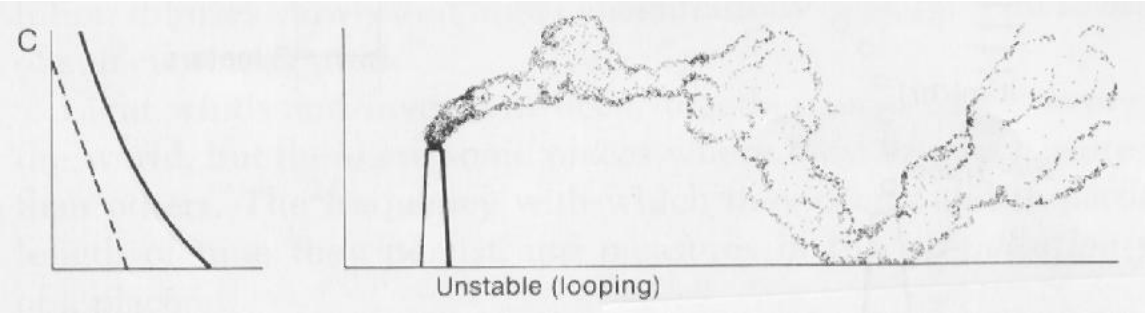

Figure 2. 7c The plume shows a "looping" pattern. At a superadiabatic lapse rate through a deep layer, convective currents carry the plume up and down. Intense vertical mixing causes a rapid dilution of the plume. Figure adopted from Neiburger et al. [1973].

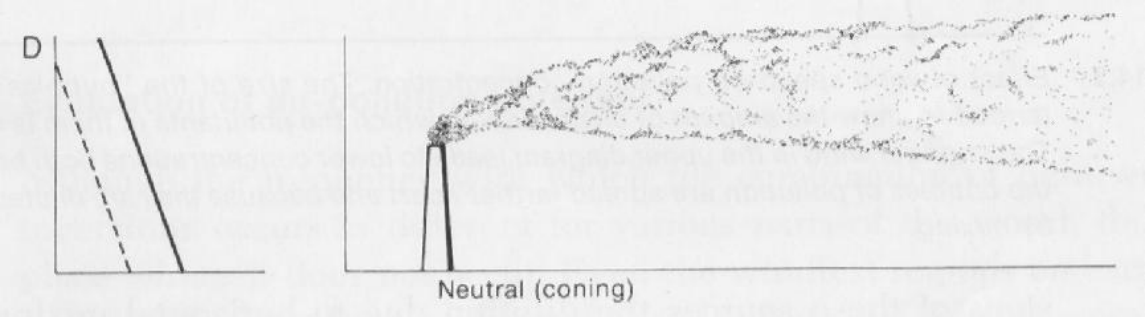

Figure 2. 7d In this case the atmosphere has a deep adiabatic lapse rate. Neutral conditions result in free vertical mixing and turbulences due to irregularities of the ground and shearing of the wind are not amplified by instability. Vertical mixing and horizontal dispersion are about equal and the plume resembles a cone. Hence the formation of this plume shape is named "coning". Figure adopted from Neiburger et al. [1973].

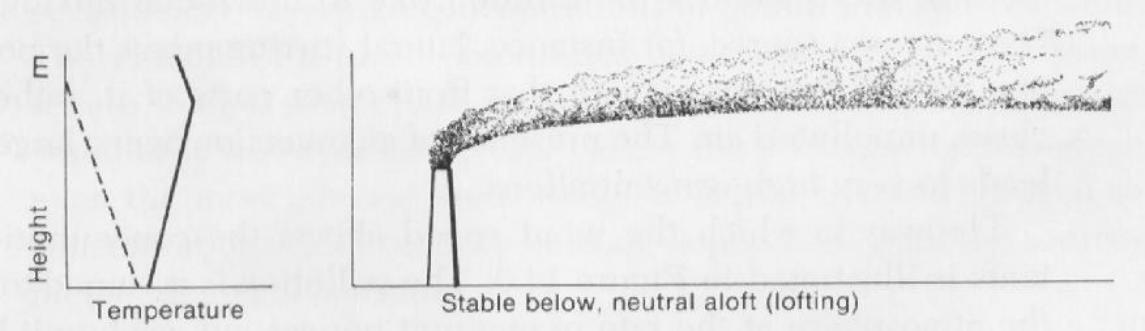

Figure 2. 7e The plume is emitted at the top of an inversion layer. As a consequence, downward mixing is prevented but upward motion goes freely. This process of plume shape formation is called "lofting". Figure adopted from Neiburger et al. [1973].

Turco [2005] reported that the plume patterns of Figures 2. 7a and e are held aloft for a long time and thus can be transported over long distances while they are being diluted. On the contrary is the behaviour of the plume configurations in Figures 2. 7b and c. In Figure 2. 7b the (fumigating) plume is trapped under an inversion (stable conditions). The (looping) plume pattern of Figure 2. 7c is the most serious with respect to surface air pollution, since there occurs very fast transport in eddies and the plume can reach the ground with high concentrations before being diluted. During neutrally stable conditions in the atmosphere (Figure 2. 7d), the plume spreads out in all directions as it travels away from the stack, forming a cone [Turco 2005].

Besides of atmospheric stability and wind conditions, there are other factors that influence the rate of dispersion of pollutants, such us the height of the smokestack, the exit velocity of the plume and the temperature of the effluent [Turco 2005]. Generally, the emitted pollutants from high smokestacks need longer to reach the ground from greater heights and produce less local pollution. Higher emission temperatures also cause long transport times of the plumes, since the heat results in upward moving of the individual air parcel into higher altitudes of the atmosphere. Great exit velocities of the plume from the source have a similar, but smaller effect [Turco 2005]. As the author also reported, the dispersion of plumes from chimneys is also affected by topography, such as mountains, hills and valleys, where the large-scale flows of air can be deflected and create wind channels, turbulences and inversions. New Zealand is characterised by extensive areas of agriculture and rural land with little drop in wind speed by surface friction as well. In other parts of the country, the wind is funnelled through gaps in the mountain ranges [Reid 1981]. Even the buildings around settlements can cause air circulation and affect the initial dispersion of plumes from smokestacks [Turco 2005].

A special case of a pollution plume is its emission from ground level sources, such as automobiles, garbage dumps and industrial holding ponds [Turco 2005]. Under normal atmospheric conditions, the highest concentration of the pollutants is found at the surface and remain high even if the plume is transported over a long distance (Figure 2. 8). Consequently, ground level plumes involving toxic substances represent a serious hazard over a large area [Turco 2005].

During an unstable atmospheric situation, vertical motions mix the emitted pollutants rapidly and the surface concentrations are diluted. Convection causes a fast upward moving of the pollutants to higher altitudes. The most hazardous situation develops during a strong, low-altitude temperature inversion, where the pollutants are trapped beneath the inversion and the pollutant concentrations remain high over a large surface area [Turco 2005].

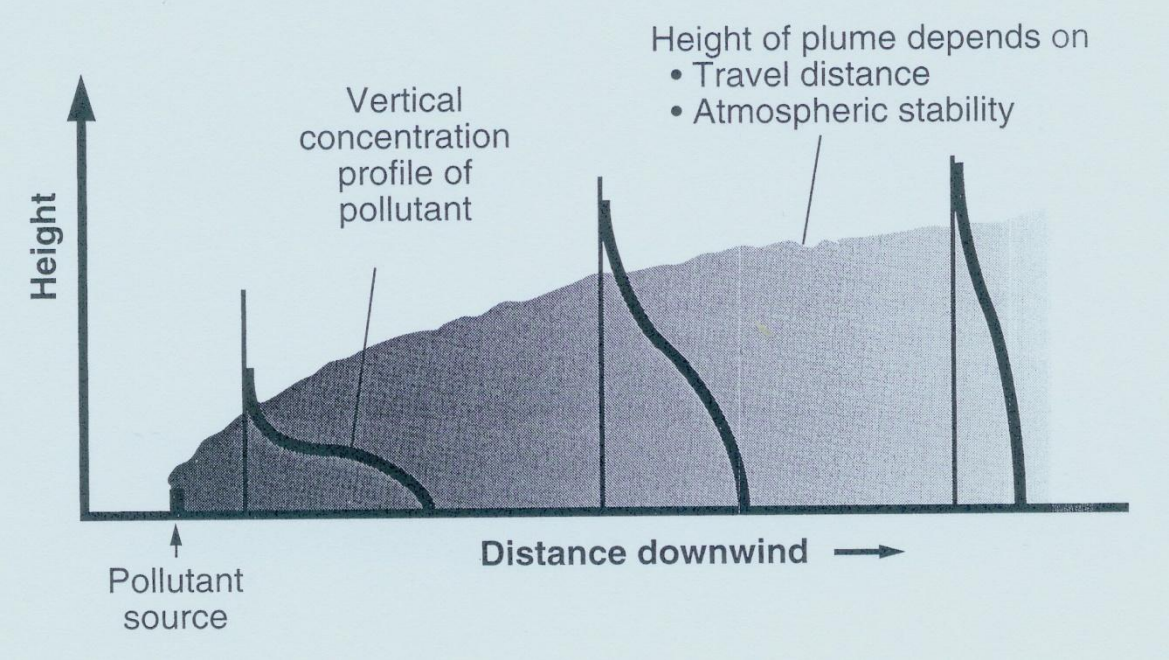

Figure 2. 8 The dispersion behaviour of a ground plume is most significantly influenced by the stability of the air near the surface. The plume is moving in horizontal and vertical direction with increasing distance from the vent. The plume expands faster during unstable and turbulent atmospheric conditions. Figure adopted from Neiburger et al. [1973].

Large-scale eddies are formed by thermal turbulences that are created above hot sources (e.g. volcanic craters) and the simultaneous descent of the surrounding cooler air [McGee 1992, Stern et al. 1984]. Diffusion of eddies results in mixing of the plume with the ambient air and lateral spreading of the plume.

2. 4. Impacts of SO_2 and aerosol particles on the environment

Sulphur dioxide (SO_2) is a colourless gas with a pungent odour. There are natural (e.g. volcanoes) and anthropogenic emissions of SO_2 into the atmosphere. Besides direct emission, SO_2 may be formed by oxidation from reduced sulphur compounds, such as hydrogen sulphide (H_2S) and dimethyl sulphide (DMS) [Warneck 2000]. The distribution of SO_2 can cause health problems to humans and animals, and it has damaging effects on the environment at certain concentrations.

Under normal conditions, the life cycle of an air pollutant involves the processes of emission, dispersion and transport, chemical transformation and deposition to the ground [Clarke 1992]. Sulphur dioxide is removed from the atmosphere by dry and wet deposition [e.g. Arya 1999]. The former term is used for

the settling of any pollutant (e.g. SO_2) to the ground, even if the removal is to a wet surface. The term 'wet deposition' can be subdivided into the processes 'rainout' and 'washout' and describes the settling of the pollutant to the ground by rainfall or by snow. 'Washout' represents the absorption of pollutants within the cloud followed by precipitation. The term 'rainout' is used if the pollutants are absorbed below the clouds (i.e. while the raindrops fall to the ground) [Arya 1999]. Sulphur dioxide represents the source of acid rain that can cause damage to the environment. In order to protect human population and the environment health protection standards were introduced in several countries in regards to the anthropogenic emission of sulphur dioxide and other pollutants into the atmosphere. In New Zealand, the Ministry for the Environment [2005] published the latest national environmental standards (NES) with represent mandatory technical environmental regulations.

2. 4. 1. Impacts of SO_2 on health

People who are exposed to SO_2 absorb the gas by breathing air into the body through the nose, with the gas entering the bloodstream through the lungs. Sulphur dioxide breaks down to sulphate within the body and leaves it through the passing of urine [e.g. US Department of Health and Human Services 1998].

Folinsbee [1993] reported that one of the first controlled experiments of SO_2 exposure to humans was carried out by Amdur et al. [1953]. They studied the effects of human breathing in up to 8 ppm SO_2 and showed that changes in respiratory pattern were the results of changing concentration, in which people react differently. While some people became tolerant even at the highest concentrations, others reacted very sensitive at very low concentrations of 1-2 ppm [Amdur et al. 1953]. Other studies followed e.g. by Frank et al. [1962] who found that SO_2 causes increased airway resistance, which Nadel et al. [1965] considered to be due to reflex bronchoconstriction. Frank et al. [1962] found out that humans react to inhalation of SO_2 fast, depending on the dose, reaching a peak after c. 10 minutes. They also mentioned possible differences between oral and nasal breathing and that the mode of breathing might alter responses. Speizer & Frank [1966] confirmed later that mouth breathing of SO_2 causes greater changes in pulmonary resistance than the same concentration inhaled through the nose. Due to the nasal mucosa, even relatively high concentrations of SO_2 can be removed nearly completely during resting breathing [Speizer & Frank 1966].

In order to assess the hazard of SO_2 exposure to human, experiments were necessary to examine responses in an active phase. Since humans typically breathe through the nose during heavier exercises, transitions are found between breathing through nose and/or mouth within and among individuals [Folinsbee 1993]. Niinimaa et al. [1980] found that most healthy people shifted from nasal to oronasal breathing at a ventilation of 35 L min^{-1}, which consequently increased the relative amount of air breathed through the mouth. The nasal resistance for SO_2 found in healthy humans does not appear in asthmatics or people suffering allergic rhinitis. Hence, they react more sensitive to SO_2 exposure [Kreisman et al. 1976, Tam et al. 1988, Folinsbee 1993]. Later experiments found out that inhalation of SO_2 in air with a low water vapour content (either cold or dry) also cause an increased responsiveness in asthmatics [Sheppard et al. 1984, Bethel et al. 1984]. Folinsbee [1993] assumed that the drying of the upper airway mucosa results in decreased scrubbing of SO_2 by the mucosa.

Roger et al. [1985] and Bethel et al. [1983] reported that asthmatics suffer from bronchoconstriction at SO_2 exposures exceeding 0.5 ppm (parts per million). Typical outdoor concentrations of SO_2 range between 0-1 ppm. People with asthmatic problems are sensitive to the respiratory effects of SO_2 at concentrations of 0.25 ppm. Exposure of up to 100 ppm is regarded as immediately dangerous to health and life. Continuous long-term exposure of low levels of SO_2 can also affect the health of the population, and short-term exposure of high levels of SO_2 can be life-threatening [US Department of Health and Human Services 1998]. Inhalation of SO_2 may result in different symptoms, such as wheezing, a tight chest and shortness of breath or coughing [Ministry for the Environment, New Zealand 2002]. Physical exercises enhance these effects, as they increase the volume of air inhalation, causing the further penetration of SO_2 into the respiratory tract [Brasseur et al. 2003].

There are few reports that describe the effects of air pollution on the health of an exposed population. For instance, the Ministry of Health in the United Kingdom reported in 1954 the recorded death of 3500-4000 people above the norm in London in December 1952, during an exceptionally high smog episode of five days [Smith 1992]. The pollution in that time was caused largely by coal combustion, resulting in numerous near-ground emissions of SO_2 and smoke. Additionally, the weather conditions in December 1952 formed a very stable high-pressure zone and an inversion layer over London, preventing the dispersion of the pollutants and their concentrations to very high levels. According to estimates, the SO_2 and smoke concentrations (48 h mean) during the London episode reached values of 1.3 ppm and 4.5 ppm, respectively [Smith 1992, from Ministry of Health, UK 1954].

No reports are found about hazard of SO_2 exposure to population in New Zealand. The most important source of SO_2 emission in New Zealand is probably active volcanism, which presently occurs in the North Island. Sulphur dioxide is a common gas species in volcanic plumes and is less quickly removed than other acidic gases such as HCl and HF [Hansell & Oppenheimer 2004].

Some studies relating to SO_2 exposures were carried out at Mt. Sakurajima in Japan. During those studies the annual SO_2 concentrations were determined in Sakurajima town between 44 and 158 ppb (μg m^{-3}) in 1979-85 [Wakisaka et al. 1988], 209 ppb (μg m^{-3}) in 1988 [Tomari et al. 1990] and 31 ppb (μg m^{-3}) in 1992 [Uda et al. 1999]. The latter two publications report that they did not find any effects on the prevalence of respiratory disease and respiratory symptoms of school children living in Sakurajima town in comparison to those schools in control areas. Tomari et al. [1990] found the same result for lung function in school children. Wakisaka et al. [1988] reported higher standardised mortality ratios for bronchitis and pneumonia for people living near the volcanic centre, but the relationship was not conclusive for asthma and emphysema [Hansell & Oppenheimer 2004]. While positive correlations were found between the annual mean SO_2 and total suspended particles and bronchitis deaths, there were inverse correlations with pneumonia deaths [Wakisaka et al. 1988, from Hansell & Oppenheimer 2004].

2. 4. 2. Impacts of SO_2 on ecosystems

2. 4. 2. 1. Impacts on terrestrial ecosystems

Vegetation is considered to be an important sink of sulphur dioxide and other air pollutants [Hill 1971, Garland et al. 1973]. Direct damage to vegetation occurs by the absorption of SO_2 at phytotoxic concentrations through stomatal pores of leaves and the subsequent dissolution of free space moisture in leaf interiors [Delmelle 2003, from Smith 1990]. The dissolved sulphur causes biochemical interferences at the physiological level and lead to leaf injury or plant death [Smith 1990 and references therein]. Siebke et al. [1990] developed a model to simulate the uptake and metabolism of SO_2 by various leaf cell compartments. Various plants showed poor growth, diminished or disappeared completely from urban areas a few decades after the industrial revolution in Europe and America. Lichens and some conifer species were particularly sensitive to sulphur dioxide and other pollutants [Smith 1992].

The concentration of volcanic SO_2 is often at the level that can cause damage to terrestrial ecosystems at phytotoxic concentration. For instance, crops and trees were damaged or devastated in many parts of Europe during the summer of 1783 as a consequence of the volcanic plume generated from the Laki fissure eruption in Iceland and the generated volcanic plume [Grattan & Pyatt 1994]. Another example is the continuous vegetative deterioration at Masaya volcano, Nicaragua, where a strong perturbation of the ecosystem has occurred for more than 140 years. Since 1852, at least five gas crises have occurred due to increased volcanic activity and associated gas emission, causing hazards to vegetation and public health [Baxter et al. 1982, Johnson & Parnell 1986, Delmelle et al. 2002]. The forest in an enclave of c. 22 km^2 within 15 km distance downwind from the vent is subject to regular acidic wet deposition, originating from the continuously degassing, low-altitude volcano [Delmelle et al. 2002, Delmelle 2003]. Similar effects were observed and reported from other volcanic areas, such as the Ka'u desert on Big Island, Hawaii [Harding & Miller 1982, Sutton & Elias 1993] or from volcanoes in Italy [Camuffo & Enzi 1995].

Sulphur dioxide from the atmosphere can be removed by diffusion to the soil [Kellogg et al. 1972]. According to these authors, the uptake of sulphur depends on the soil pH and moisture content. They also estimated that the uptake of SO_2 by soil and vegetation is 52 x 10^6 tons per year.

Continuous uptake of SO_2 and other acidic pollutants by the soil can result in soil acidification. This process is characterised by the loss of exchangeable basic cations (Mg^{2+}, Ca^{2+}, Na^+ and K^+) from the soil, the decrease of soil fertility and/or the consumption of the soil acid-neutralising capacity. This may result in a decline in pH and a rise in concentration of inorganic Al in drainage waters, which can reach ecologically significant quantities [van Breemen et al. 1984].

If atmospheric SO_2 and other chemical compounds enter the hydrological cycle, it results in groundwater contamination [Delmelle 2003]. For example, the ratio of chloride to total dissolved solids content (TDS) was constantly low during the inter-eruptive period of Mount Etna (Italy) in 1993-1995 and rose during the strombolian activity in 1996-1998 [Aiuppa et al. 2001]. These authors attributed the changes in chemistry to the fact that the groundwater around Mount Etna is derived mainly from meteoric water and the chemistry of the rainwater changed due to the degassing volcanic plume.

2. 4. 2. 2. Impact on aquatic ecosystems

Impacts due to acidification of aquatic ecosystems (lakes, streams and rivers) have been reported from several countries, such as Sweden, Norway and Canada [Hutchinson & Havas 1994]. At the beginning, acidification is noticed by changes in species composition and lower species diversity. Lower biomass is a distinctive feature of higher acidification levels [Hutchinson & Havas 1994]. Species of fish, zooplankton, insect larvae, molluscs, crustaceans and phytoplankton that are sensitive to acidification are displaced or replaced by acid-tolerant species [Havas 1986].

Fisheries biologists noticed the first evidences of impacts on aquatic ecosystems. They reported a rapid decline of some fish populations (especially brown trout and Atlantic salmon) in southern Norwegian rivers at the turn of the last century. Rivers in northern Norway that were fished did not show significant changes in fish population, which meant that overfishing was not the reason for these changes [Hutchinson & Havas 1994].

According to Hutchinson & Havas [1994], Oden [1967] reported first about the relationship between lake-water acidification and acid rain in Norway. Since that discovery, thousands of lakes with acidification have been recognised. The most acidic lakes were located at the southern tip of Norway, which showed the greatest declines to fish populations. The surface waters reached pH values of below 5.0 [Hutchinson & Havas 1994].

2. 4. 3. The situation in New Zealand and government control of SO_2

The Ministry for the Environment of New Zealand [1998] published a report about the effects of air pollution on ecosystems in New Zealand. Similar to the situation overseas, air pollutants such as SO_2, NO_X, O_3, fluoride and particulate matter have the greatest impacts on ecosystems in New Zealand. However, the effects are mainly local since the emission of SO_2, NO_X, fluoride and heavy metals are substantially lower in comparison to other parts of the world [Ministry for the Environment, New Zealand 1998]. Additionally, the oxidation rates of SO_2 and NO_X to their specific acids are approximately 1% per hour. Due to the size and extension of the country, a typical wind speed of about 5 m s^{-1} and the prevailing wind direction usually only c. 10% of emitted SO_2 and NO_X is oxidised before they are blown offshore [Ministry for the Environment, New Zealand 1998].

Forest decline is well known in New Zealand and has been reported, for instance, from the high altitude forests of the Kaimai Ranges, North Island [Jane & Green 1983]. The decline of *Nothofagus* in New Zealand's forests is usually explained by natural causes, such as fires, catastrophic winds and landslides [Wardle & Allen 1983, Ogden et al. 1993, Hosking 1993]. The decline of cabbage trees in New Zealand is due to the disappearance of wetlands through land development, as well as the grazing of farmland and stock damage that prevents regeneration of cabbage trees [Simpson 1993]. Clarkson [1990] studied the effects of historic and recent volcanic activity on New Zealand's flora. The author reported that volcanic activity has damaged or destroyed at least 20,000 ha of native vegetation in the previous 450 years, mainly by pyroclastic flows, debris flows and ash falls. Damage also occurred to the *Metrosideros* trees on White Island (Figure 2. 9), particularly after the eruptive episode of 1976-81. Although most of the damage is caused by ash fall during phases of volcanic activity, the most likely causes of pre- and post-volcanic damages are toxic fumes and acid rain [Oliver 1915, Clarkson 1990, Clarkson & Clarkson 1994].

Figure 2. 9 Little forest of *Metrosideros* trees on White Island.

Some organisations, such as the US Environmental Protection Agency (USEPA) and the World Health Organisation (WHO), introduced air quality guidelines for certain regions and defined acceptable levels for individual gas species. The Ministry for the Environment of New Zealand [2005] determined and published the latest ambient air guidelines for pollutant concentrations, including SO_2. According to this report, the standard values for SO_2 are 350 and 570 µg m^{-3} (equivalent to c. 130 and 220 ppb) for 1-hour-average. While the concentration of 350 µg m^{-3} is allowed to be exceeded up to nine hours per year, the value of 570 µg m^{-3} is not to be exceeded at any time. These values were set not only for people with health problems, such as asthmatics and those with chronic obstructive lung disease, but also to provide the population protection of lung function and prevent other respiratory symptoms.

Additionally, there are annual guideline values for various airborne pollutants (e.g. SO_2) to protect ecosystems. These values are based on guideline values of the United Nations Economic Commission for Europe/World Health Organisation (UNECE/WHO) of 1996 and the Australian and New Zealand Environment and Conservation Council (ANZECC) [Ministry for the Environment, New Zealand 2002]. According to this report, the critical levels are 30 µg m^{-3} (c. 12 ppb) for agriculture crops, 20 µg m^{-3} (c. 8 ppb) for forest and natural vegetation and 10 µg m^{-3} (4 ppb) for lichens.

In order to monitor air pollution the Ministry for the Environment [1995] published a study concerning the design and implementation of a national network that is suited for New Zealand conditions. This study used several important factors and internationally accepted criteria that determine the construction of the network, such as geography, meteorology, emission, legislation and environmental management structure. The major aim was to provide a network that quantifies the air quality of New Zealand in space and time. The results can be used by all national governments, organisation, companies and the public [Ministry for the Environment, New Zealand 1995].

SO_2 pollution is measured in New Zealand mainly by fluorescence monitoring method, in which the detection limit of this continuously measuring equipment is less than 1 ppb. Additionally, there are passive samplers in some regions for general survey [Ministry for the Environment, New Zealand 2000a]. SO_2 monitoring in New Zealand is carried out at several sites, though these are mainly limited to the Canterbury region, the Auckland region and around some industrial sources [Ministry for the Environment, New Zealand 2003a]. The results show that the SO_2 concentrations lie well within the ambient air guideline values and suggest that

major health impacts due to SO_2 exposure in New Zealand are unlikely [Ministry for the Environment, New Zealand 2003b]. Exceptions are sites in Christchurch, Auckland and some industrial areas where SO_2 concentrations reached the 'acceptable' or 'alert' categories [Ministry for the Environment, New Zealand 2003a].

Many regions in New Zealand experience weather situations in winter that are characterised by nocturnal inversion and foggy conditions by day. Such meteorological circumstances cause poorly ventilated street canyons during high volume traffic hours and inhibit the dispersion of pollutants. Additionally, the cool winter climate reflects the relatively high domestic heating requirements [Ministry for the Environment, New Zealand 1995, Aberkane et al. 2005].

According to a report from the Ministry for the Environment [2003c], major sources of SO_2 emission in New Zealand are Northland region, Christchurch, Wellington, Auckland, Dunedin, the Bay of Plenty region and Taupo. Excluding the values in the Bay of Plenty region, these values represent average wintertime emissions. Further, in most cities the emission of SO_2 is predominantly caused by industrial and vehicle emissions, whereas the major source of SO_2 in Wellington is due to shipping [Ministry for the Environment, New Zealand 2003c].

2. 4. 4. Health hazards of aerosol particles

An important aerosol from volcanic emissions is sulphuric acid (H_2SO_4), which is formed by oxidation in the atmosphere from gaseous SO_2 into (secondary) particles [e.g. Warneck 2000]. Sulphur dioxide has a lifetime in the atmosphere of 1-4 days. Approximately half of the SO_2 in the atmosphere is oxidised to sulphuric acid (H_2SO_4) or sulphate (SO_4^{2-}). According to Roedel [2000] this is caused by the extremely low vapour pressure of sulphuric acid, particularly in the presence of water vapour and, if present, ammonia (NH_3).

Similarly, the oxidation of SO_2 to sulphuric acid (H_2SO_4) is caused by the occurrence of OH-radicals. As described in several publications [e.g. Warneck 2000, Sparks et al. 1997], it includes a series of oxidation reactions:

$$SO_2\ (g) + OH \Rightarrow HOSO_2 \qquad (2.\ 1)$$

$$HOSO_2 + O_2 \Rightarrow SO_3 + HO_2 \qquad (2.\ 2)$$

$$SO_3 + H_2O \Rightarrow H_2SO_4 \qquad (2.\ 3)$$

The hygroscopic property of H_2SO_4 results from its rapid condensation, either forming new aerosols or adding to existing ones. Another way is by the partition of gaseous SO_2 into cloud droplets or pre-existing aerosols, reacting with dissolved hydrogen peroxide (H_2O_2) or ozone (O_3) to form sulphate (SO_4^{2-}). In fact, most of the sulphur is emitted as gaseous SO_2 into the atmosphere, where it represents a dangerous pollutant. The precipitation of high levels of sulphate is called 'acid rain' and is devastating on sensitive ecosystems. Sulphate aerosols have a lifetime of c. 5 days in the atmosphere before it is wet deposited to the surface. [Stevenson et al. 2003].

Aerosols of natural or anthropogenic origin represent common pollutants in the troposphere that vary in size and chemical composition. Their emission into the troposphere can cause considerable impacts on terrestrial ecosystems and human health, at both local and regional scales [e.g. Mather et al. 2003b]. There is no doubt that excessive concentration of particulate matter in the air, such as quartz dust and metal dust, lead to health damages (e.g. silicosis). For health hazard assessments due to the exposure to aerosols, it is important to consider dosage and particle size, as well as the chemical composition of the particles [Neubert 2001]. Coarse particles (2.5-10 µm) can affect human health by aggravation of respiratory conditions, such as asthma. Fine particles (<2.5 µm) can penetrate deep into the lungs and can increase heart, lung and respiratory disease, and can cause such symptoms as decreased lung function, alteration of lung tissue and premature death. In particular children, elderly people, people with chronic lung disease and asthmatics who are exposed to air pollution are most at risk and affected [e.g. Scott 2005].

However, from a medical-toxicological point of view, a single characterisation of particle sizes (e.g. $PM_{2.5}$ or PM_{10}) is unsatisfactory and a medical-toxicological judgement is not possible [Neubert 2001]. This author noted five factors that must be considered for health hazard assessment:

(1) chemical composition of the particles,
(2) residence time within the respiratory tract,
(3) potential of damages with respect to specific parts of the respiratory tract,
(4) the kind of toxic potential (e.g. irritation, acute/chronological damage) and
(5) dosage or concentration of exposed particle.

Neubert [2001] also noted that health hazards as a result of pollutant exposure become difficult to assess, since spatial and temporal concentration variations make it impossible to identify exactly which component is responsible for which biological effects. The individual situation becomes even more complicated, as most pollutant components do not affect the human body alone. Therefore, Neubert [2001] expects combined effects of several aerosol compounds on human bodies.

Neubert [2001] reviewed numerous reports of research groups, which performed experiments on men and animals and studied the effects of different pure single sulphate aerosols (e.g. H_2SO_4), as well as the combination of different aerosol species. According to his report, it seems that the effects of sulphate aerosol particles on the respiratory tract depend on H^+ concentration, and thus on the acidity of the particles. The exposure of humans to sulphuric acid relates to acute effects between dosage and effects: concentrations up to 100 µg m^{-3} seem to have no effects in healthy people, whereas it can cause minor effects in asthmatics. A concentration of 450 µg m^{-3} of H_2SO_4 aerosols seems to be a critical value for some healthy people, where the first acute damaging effects can emerge. In consideration of the experimental conditions, Neubert [2001] concluded that a concentration of 1000 µg m^{-3} of pure H_2SO_4 aerosols is regarded as a value where damaging effects appear, even to healthy people. It is emphasised that these concentration limits are only valid to the exposure to pure sulphuric acid and not for particles connected with soot or metal oxides. Generally, the formation and effectiveness of acid aerosols can be amplified due to the presence of heavy metals [Neubert 2001].

Particulate matter also affects the environment. Fine particles represent the major reason for reduced visibility in areas with air pollution and they can deposit onto soils, plants, water and/or material [Gallaher & Depro 2005]. As the authors further reported, particularly compounds of nitrogen and sulphur that deposit onto land or water bodies may affect the nutrient balance and acidity of the affected environment. Depending on the chemical composition of particles that are deposited directly onto plants, they can cause corrosion of leaf surfaces or interfere with plant metabolism [Gallaher & Depro 2005].

During explosive volcanism, a large amount of sulphate can penetrate the tropopause and can be dispersed widely in the stratosphere, having effects on global radiation budget and climate change [e.g. Rampino & Self 1982, Ackerman & Strabala 1994, Fiacco et al. 1994, Zielinski et al. 1996, Mills 2000].

2. 4. 5. The situation in New Zealand and government control of PM_{10}

Particulate matter (PM_{10} and $PM_{2.5}$) is likely to represent the most important air contaminant in New Zealand [Ministry for the Environment 2000b]. According to a report in 1998 by the Ministry for the Environment of New Zealand, the cities of Auckland and Christchurch represent the largest areas in New Zealand that are affected by air pollution, as they have the highest emission of pollutants. Additionally, there are several other smaller and less polluted cities with more localised pollution. Pollution of particulate matter originates from single point sources, such as fertiliser works, open mines, power stations and dairy factories, where particulate matter is released into the troposphere. The major cities also have heavy traffic, in which State Highway One between Auckland and Hamilton is the busiest section of highway on the country. Although there is a lack of information available, the effects of particulate matter on New Zealand's environment is probably low. The deposition of particulate matter and its concentration through food chains may be possible in isolated cases [Ministry for the Environment, New Zealand 1998].

As mentioned earlier, volcanoes represent an important source of aerosol particles and New Zealand has a high incidence of volcanic activity. Although no negative effects of aerosols on ecology as a result of volcanic activity have been reported, future events by large eruptions cannot be excluded.

The Ministry for the Environment in New Zealand [2005] published, among others, the National Environmental Standards for PM_{10}. According to this report, the threshold value for PM_{10} is 50 µg m^{-3} as a 24-hour mean and with a permissible excess of one 24-hour period per year. Additionally, there was introduced a critical level for sulphate particle concentrations in forests, where ground-level cloud is present >10% of time [Ministry for the Environment, New Zealand 2002].

2. 5. Air pollution modelling

Modelling of air pollution describes the dispersion of pollutants in the atmosphere, in which some aspects of an environmental system are reproduced with reasonable accuracy [Barrett 2001]. Depending on their complexity, dispersion models take into account many physico-chemical processes that occur in the atmosphere, such as type and scale of emissions, plume rise, plume transport, diffusion by turbulence, dry and wet deposition and topographical effects. These atmospheric processes are included within the models using mathematical equations, although not all of them may be well known [Barrett 2001]. Due to the lack of quantitative data for writing dispersion models, several assumptions have to be made to determine variations of certain parameters and appropriate boundary conditions. Consequently, there are diverse atmospheric dispersion models that predict the concentration of individual compounds in the atmosphere. Each model makes different assumptions to evaluate the impact of a specific source that include several factors, such as type of pollutants, spatial scale or size of the area as well as the meteorological and topographical complexities of the area [Barrett 2001].

From the meteorological point of view, there are three groups of dispersion models to predict the concentration of pollutants for environmental impact assessment:

(1) models using observed meteorological data,

(2) models using diagnostic meteorology and

(3) models using prognostic meteorology [Luhar et al. 2004].

The use of data from meteorological observations is needed in simple Gaussian plume or puff models and some non-Gaussian analytical models. The typical meteorological data used in these models are the near-surface (<10 m a.g.l.) observations of wind speed, wind direction and ambient temperature, as well as estimates of mixing heights and atmospheric stability. These models can be used to predict air pollution dispersion from distinct sources (point, line or area source) at high spatial resolution (e.g. 100 m spaced pollutant grids), although chemical reactions are either ignored or treated as very simple [Luhar et al. 2004]. These types of models are either not applicable or the models show inappropriate results in areas with high complex airflow and diffusion conditions, such as coastal areas and/or complex terrains. Examples of such models are AUSPLUME and CALPUFF [Luhar et al. 2004].

Models using diagnostic meteorology are used for predicting air pollution in complex terrains where insufficient near-surface weather data are available to simulate accurately the complex meteorological field [Luhar et al. 2004]. Instead, diagnostic models perform an objective analysis by extrapolating and interpolating available meteorological observation data, which results in a three-dimensional model of meteorological parameters [Goodin et al. 1980]. Diagnostic models are not able to forecast the meteorology, but provide the best estimation of steady-state (or quasi steady-state) conditions [Luhar et al. 2004]. In simple diagnostic models the influence of observations on the calculated meteorology decreases steeply with increasing distance from the location of the monitoring site [Luhar & Rao 1994, Luhar et al. 2004]. However, typical diagnostic models perform various calculations that result in mass-derived flow fields, in which the conservation of mass equation, as well as differences between the observations and the modelled predictions, are considered at the same time [Ratto et al. 1994, Luhar et al. 2004]. Such diagnostic models require the near-surface meteorological data from a dense network of monitoring sites. Examples of diagnostic meteorological models are NUATMOS and the CALMET processor of the CALPUFF model [Luhar et al. 2004].

Prognostic models are the most complex of air pollution models. They can be used to forecast the meteorology through the space-time integration of fundamental equations, such as conservation of mass, heat, motion and water [Luhar et al. 2004]. Prognostic air pollution modelling is mostly used in a mesoscale range (between a few to several hundred kilometres) and is applicable in territories with difficult horizontal and vertical airflow structure, such as coastal areas and complex terrains. A very characteristic feature of prognostic models is that they do not need site-specific observation data, but can assimilate recorded meteorological data if they are available [Luhar et al. 2004].

Prognostic air pollution models can perform complex coupled chemical reactions, in which they are able to handle urban sources on a gridded emission inventory (e.g. vehicle, domestic, industrial and biogenic emissions). Additionally, prognostic models can calculate accurately the near-source diffusion of point source plumes [Luhar et al. 2004]. Examples of prognostic models are the Mesoscale Model 5 (MM5) and The Air Pollution Model (TAPM). The latter is used for dispersion modelling during the present study. A description about TAPM and its application follows in chapter 5.

The air pollution models of AUSPLUME, CALPUFF and TAPM are commonly used in Australia and New Zealand. For example Hurley & Luhar [2005] and Hurley et al. [2005] used these programs for air pollution modelling at several locations in Australia, in which the results were evaluated and inter-compared. Although the statistics showed often acceptable or good results for various locations, the authors could also show that the results from TAPM proved to be better. There are numerous other publications in which CSIRO scientists used TAPM and other computer programs to model the dispersion of different atmospheric pollutants at numerous locations in Australia, such as Physick et al. [2002], Hurley et al. [2002], Luhar & Hurley [2003], Hill & Hurley [2005], Physick & Edwards [2005a, b] and Hurley [2006].

TAPM was also applied for pollution modelling in New Zealand. Zawar-Reza et al. [2005] modelled the meteorology and dispersion of PM_{10} for 1999 over the coastal city of Christchurch. Due to formation of nocturnal inversion layers and the emission of particulate matter from solid fuel home heating, this city frequently experiences severe degradation of air quality during winter. The resulting statistical measures are in good agreement with observation data from the monitoring sites [Zawar-Reza et al. 2005]. Other work was carried out by Gimson [2005] who modelled the air quality in the Auckland region using two different programs, CALGRID and TAPM.

Chapter 3: Monitoring of White Island and Ruapehu volcanoes

3. 1. Introduction

The two study areas of the present project are White Island and Ruapehu volcanoes. They represent the two most active volcanoes in New Zealand and are located at the northern and southern end of the Taupo Volcanic Zone (TVZ). TVZ is situated in the central North Island and is the result of westward subduction of the oceanic Pacific plate underneath the continental Australian (Indian) plate. It represents the main site of ongoing volcanism in New Zealand that strikes over nearly 300 km (c. 200 km on land) in NE-SW direction and has a width of approximately 60 km [Wilson et al. 1995]. Volcanism in TVZ began about 2 Ma ago with present zone volcanism in a NNE-SSW-trending zone, which strikes over c. 250 km from Ruapehu to White Island [Houghton et al. 1995, Wilson et al. 1995, Spinks et al. 2005]. The Taupo Volcanic Zone extends offshore as a graben structure of c. 45 km width in north-eastern direction into the Bay of Plenty forming two fault zones, the western Tauranga Fault Zone and the eastern White Island Fault Zone. The latter one represents the current active volcanic front [Gamble et al. 1993, Cole et al. 2000]. While the central part of TVZ includes several calderas with large volumes of rhyolitic deposits, the lateral parts (Ruapehu to the SW and Whakatane and White Island to the NE) are characterised by andesitic stratovolcanoes [e.g. Houghton et al. 1995, Wilson et al. 1995, Spinks et al. 2005]. An image of TVZ is shown in Figure 3. 1.

Scientists from the Institute of Geological & Nuclear Sciences (GNS) employ various monitoring methods at New Zealand's volcanoes, which include several geophysical and gas monitoring techniques. This chapter gives a geoscientific overview of the monitoring program that is applied at these two volcanoes. Although aerosol-sampling campaigns were only carried out on White Island, both volcanic centres, White Island and Ruapehu, are used as point sources for gas and aerosol dispersion modelling during this project.

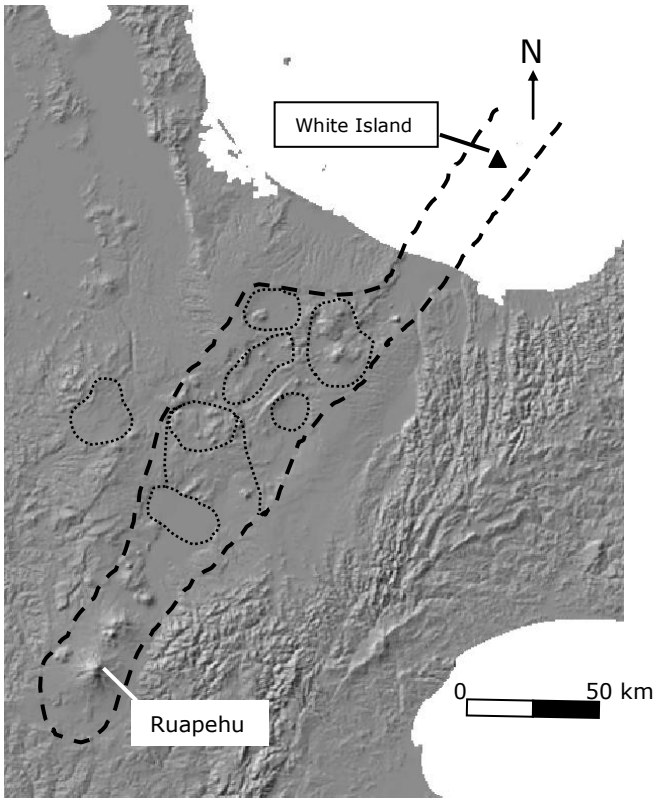

Figure 3. 1
Taupo Volcanic Zone and the locations of White Island and Ruapehu volcanoes.

3. 2. White Island volcano

White Island volcano (WIV) is located about 50 km offshore in the Bay of Plenty at the north-eastern edge of the continental shelf of New Zealand. It has been built up over the past 150,000 years. Its submarine base is at nearly 3000 m depth and covers an area of 16 km x 18 km [Duncan 1970, Cole et al. 2000], whereas Mt. Gisborne (320 m a.s.l.) represents the summit of White Island volcano. The stratigraphy shows alternating sequences of lava flows as well as pyroclastic and epiclastic deposits with a total of 22 eruption units [Cole et al. 2000].

Its present activity is centered inside a horseshoe-shaped crater breached to the southeast, which includes three coalescing subcraters. Numerous fumaroles and hot springs are distributed over the floor of the main crater area, representing surface expressions of White Island's geothermal system [Giggenbach & Sheppard 1989]. They emit gases at rates of several hundred to several thousand tons per day. The gases are mostly steam, carbon dioxide and sulphur dioxide, with small quantities of chlorine and fluorine [Giggenbach & Sheppard 1989]. Fumaroles and hot springs are also observed offshore along the coastline of White Island.

Presently, White Island is New Zealand's most active volcano and is in a state of continuous sulfataric and fumarolic activity, with sporadic episodes of phreatic, phreatomagmatic and strombolian eruptions [e.g. Houghton & Nairn 1989, Cole et al. 2000]. One of the largest major eruptive phases occurred in 1976. The latest phase of activity occurred from March 1998 to early 2000 with several explosive events. This phase of activity was accompanied by a fourfold increase in SO_2 emission rates (Cindy Werner 2004, *pers. comm.*). This observation confirms the present knowledge that volcanic gas surveillance represents an important part of forecasting volcanic events.

3. 2. 1. Geophysical monitoring

The seismicity of White Island volcano has been continuously recorded since December 1976 [e.g. Cole 1986]. In 1992, scientists from Japan and New Zealand carried out a detailed temporary seismic survey, whose results were published by Nishi et al. [1996]. During this study, two types of high-frequency seismic signals, volcano-tectonic earthquakes and spasmodic bursts with individual characteristic features were recorded. Nishi et al. [1996] reported that most volcano-tectonic earthquakes and few spasmodic bursts occurred at a depth of <1 km, in a single seismically active zone beneath the central and eastern subcraters of the main crater area. Very few events were located near the western subcrater at about 3 km depth, but no earthquakes were recorded west of Mt. Gisborne. The magnitudes of located earthquakes varied between 0.7 and 2.7. The small-magnitude events occurred mainly beneath the main crater area, whereas the large-magnitude events were limited to the active vents, an area including parts of the western and central subcraters [Nishi et al. 1996].

Level surveys began at White Island volcano on 12 July 1967. Nine survey stations were installed on the Main crater area to form a closed loop of approximately 2 km in circumference. This level net was extended to 32 stations in 1969 and 1971. Due to volcanic activity some sites of the net were destroyed (e.g. 1976-77) but later (e.g. 1978) replaced by new stations [Clark & Cole 1989].

Deformation survey at White Island is carried out about three times per year during quiet periods and more frequently during phases of eruptive activity [Clark & Otway 1989]. The periodic survey of the main crater floor shows episodes of inflation and deflation at well-defined areas. Volcanic eruptions of different styles and at different locations have shown that a correlation between volcanic deformation and the onset of eruptive activity exists [e.g. Clark 1970, 1973].

A survey of the total magnetic field of White Island began in April 1968 and it has proven to be a useful tool for magnetic monitoring for two reasons. Firstly, the easy access to the more or less flat crater floor and secondly, there were measured large magnetic changes with time due to varying degrees of thermal demagnetisation of the crater material [Hurst et al. 2004]. Hurst & Christoffel [1973] and Christoffel [1989] reported changes of some hundreds nanoTesla (nT) during periods of months or years at various points measured along the crater floor. In Figure 3. 2 are shown two graphs, where the total magnetic field is compared with the maximum fumarole temperature of one measuring point in Donald Mound area. In the last few years, however, little relationship has been recognised between magnetic data and volcanic activity [Hurst et al. 2004]. The topography of the main crater area changed during volcanic activity on White Island. Some pegs and markers of the network were destroyed causing the disruption of the continuity of magnetic field measurements at these sites. Up to the present time the topography of the main crater area and the magnetic survey network are considered to have had four distinctive stages [Hurst et al. 2004].

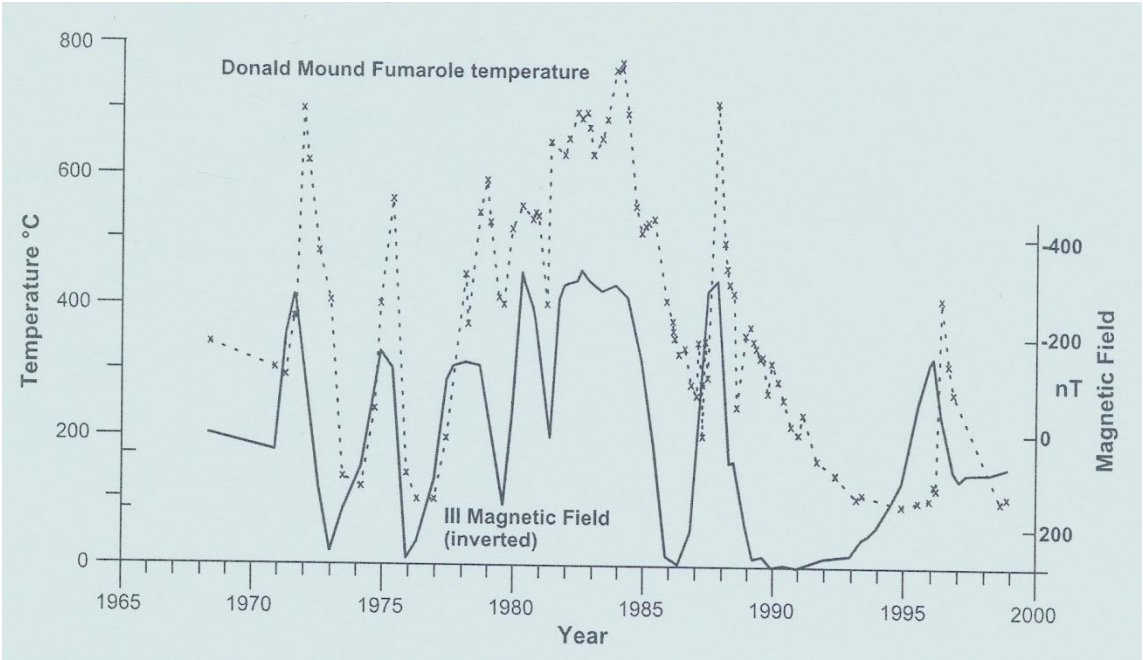

Figure 3. 2 Comparison of total magnetic field with maximum fumarole temperature at site III in Donald Mound area. Figure from Hurst et al. [2004].

3. 2. 2. Gas monitoring

White Island volcano (WIV) is characterised by uninterrupted sulfataric and fumarolic gas emissions that are governed by a shallow magma body and its associated hydrothermal system [e.g. Giggenbach 1987]. White Island is a volcano where the crater area is easily accessible and high temperature volcanic gases can be sampled and examined between eruptive phases [Marty & Giggenbach 1990]. The emission of volcanic gases on White Island volcano has been monitored for many years by ground-based as well as airborne measurements and their several analyses and results have been published [e.g. Torgersen et al. 1982, Rose et al. 1986, Giggenbach 1987, Giggenbach & Sheppard 1989, Marty & Giggenbach 1990, Tedesco & Toutain 1991, Wardell et al. 2001].

Regular ground-based direct sampling of volcanic gases on White Island has been carried out since about 1970. Giggenbach [1982] reported a cyclic behaviour of the gas emission between 1970 and 1979, which was characterised by variations in emission temperatures between 100 and about 600 °C associated with immense changes in the fumarole chemistry. Based on a systematic thermodynamic evaluation, Giggenbach [1987] published the results of more than 250 gas analyses from fumaroles on White Island with temperatures between 100-800°C. The author discovered that the emitted gases consist of two source components:

(1) a primary "magmatic" component with high SO_2 content that rises rapidly and directly from the underlying magma reservoir and
(2) a secondary "hydrothermal" component that rises slowly from a two phases (saline brine – vapour) envelope surrounding the magmatic system.

The results of two sets of gas samplings, taken from Giggenbach [1987], are listed in Table 3. 1.

A correlation spectrometer (COSPEC) is commonly used for airborne measurements of SO_2 emission. The COSPEC instrument detects the slant or vertical SO_2 column mass in the atmosphere by differential measurements, traversing beneath a volcanic plume and recording the absorption of diffuse ultraviolet (UV) sunlight. The emission rate can subsequently be calculated by multiplying the integrated SO_2 cross-section (COSPEC output) by the plume width and the estimated plume transport. The latter is usually assumed to be equivalent to the wind speed [Edmonds et al. 2001, McGonigle et al. 2002]. The geographic position during the time of airborne measurements is also recorded every second by the GPS system of the aircraft.

Table 3. 1 A selected set of samples showing the temporal changes of chemical composition of few gas species from White Island (in µmol/mol). Data are taken from Giggenbach [1987]. (S_t = total sulphur; - = not determined)

No.	Date	°C	H_2O	CO_2	CH_4	S_t	HCl	NH_3
Donald Mound								
W1	8/74	122	632,000	323,000	8.4	42,500	44	-
W2	11/74	400	898,000	61,200	1.8	27,900	12,040	1.6
W3	5/75	560	949,000	37,000	7.9	8000	4590	20.3
W4	11/75	105	961,000	35,800	12.2	2800	102	4.0
W5	4/76	100	900,000	96,700	10.1	3400	152	0.9
W6	12/76	100	836,000	146,300	1.0	14,400	2460	10.4
W7	5/77	195	932,000	48,100	0.7	15,300	2880	270.0
W8	2/78	445	876,000	83,500	3.5	31,700	4960	42.0
W9	8/78	540	881,000	98,100	3.3	15,600	2260	6.0
W10	11/79	512	575,000	367,200	2.6	52,400	2940	5.1

Several airborne plume measurements have been carried out at White Island. Wardell et al. [2001] listed the results of 20 measurements that were carried out using a correlation spectrometer (COSPEC) between 1983 and 1999, which ranging between 171 and 1230 Mg d^{-1}. The overall mean emission rate of SO_2 from White Island volcano during the same period is 430±70 Mg d^{-1} [Wardell et al. 2001].

Due to dependence of weather conditions as well as high costs by aircraft use, airborne measurements are applied at White Island volcano regularly but in long-term intervals between 6 to 12 weeks (Cindy Werner, *pers. comm.*). Future monitoring of SO_2 emission will be carried out daily from sunrise to sunset using two Differential Optical Absorption Spectrometer (DOAS). The installation of the two spectrometers was in process during this study.

3. 2. 3. Aerosol sampling

Rose et al. [1986] published the results of the first aerosol-sampling campaigns on White Island volcano. They used a 10-stage cascade impactor with quartz crystal microbalance (QMC) impactor plates for the particle measurement. This device separated the collected airborne particles into ten aerodynamic size groups and electronically measured the mass of particles on each stage. With this instrument, [Rose et al. 1986] were able to examine the small grain size fraction of the collected particles before modification by chemical processes in the atmosphere or weathering on the ground occurred. All other collected particles were analysed in the laboratory by scanning electron microscopy (SEM) and energy dispersive spectroscopy (EDS).

Ground-based sampling was carried out on 23 November 1983 by inserting a titanium sampling tube into the exit of the fumarole. The results show bimodal particle size distribution, in which 70% of the total mass represents particles larger than 10 µm (Figure 3. 3). The large particles were specified as water droplets, native sulphur crystals and probably non-volcanic, spherical-shaped Ti-rich particles. The smaller particles (<1 µm) were ascertained to be mixtures of sulphuric acid droplets and sublimates [Rose et al. 1986].

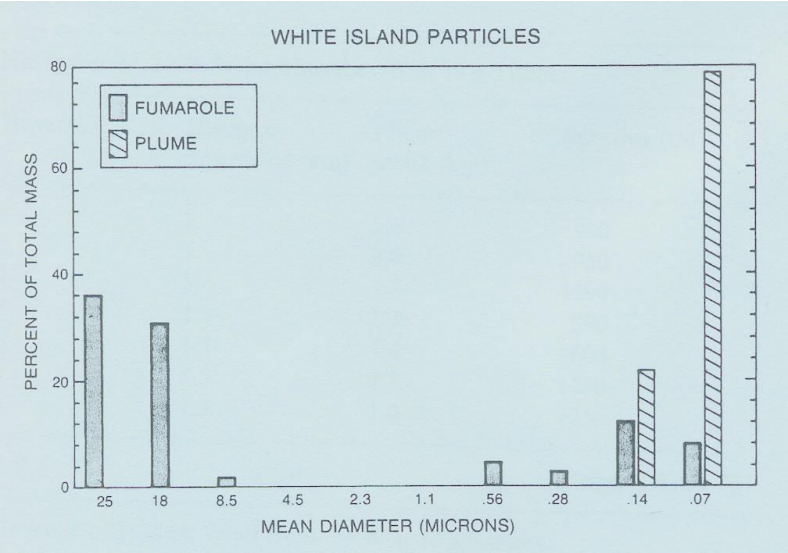

Figure 3. 3
Size distributions of particles collected at fumaroles in the Donald Mound area on 23 November 1983 and from plume measurements on 27 November 1983.
Figure from Rose et al. [1986].

Airborne aerosol sampling was performed on 23 and 27 November 1983. The QMC was operated aboard of an aircraft flying perpendicular to and through the volcanic plume [Rose et al. 1986]. The average aerosol mass concentration in the plume measured during the survey on 27 November was determined to be 19 µg/m^3 and considered only to be three times higher than the aerosol concentration of the ambient air. The size distribution of collected aerosols was unimodal, containing particles of <0.2 µm in diameter (Figure 3. 3). The particle flux was calculated with 1.3 Mg d^{-1} [Rose et al. 1996]. The same sampling method was used at Colima volcano (Mexico) in 1982, where nearly all particles were finer than 3 µm and a particle flux of 24 Mg d^{-1} was determined [Rose et al. 1996, Casadevall et al. 1984].

The collected particles on White Island volcano from 27 November 1983 varied in grain size and composition [Rose et al. 1986]. The largest individual aerosol particles with grain sizes between 20-5 μm represented about 1% of the total particle mass. They were analysed as calcium and calcium-magnesium carbonates (?) as well as silica, possibly quartz. The particles with a size range of 4-0.5 μm in diameter also made up a total mass of c. 1%. They were determined to consist of NaCl and much S-rich liquid, possibly H_2SO_4. The small size particles (<0.5 μm) represented more than 95% of the total mass and included chemical species of H_2SO_4, SiO_2, $FeCl_3$, NaCl, a Fe-Mg-Al-Si phase (possibly chlorite) and a K-Al-Si phase (possibly illite or smectite). The chlorite and clay species were probably derived from altered rocks of the fumarole field, whereas the halide species are likely to have been formed by condensation of the volcanic gases [Rose et al. 1986].

3. 2. 4. Weather station on White Island

An automatic weather station was installed on 10 November 2004 on the crater rim at the NW-side of White Island (Figure 3. 4). The station is battery powered with solar charging. The data collected daily are telemetered via cellphone to the Institute of Geological & Nuclear Sciences (IGNS), Wairakei Research Centre, Taupo, who operate the station. The weather station was assembled by the National Institute of Water and Atmospheric Research (NIWA) and is designed to measure solar radiation, air temperature, relative humidity, rainfall and wind speed & direction.

The station is fitted with a RM Young Wind Monitor that measures wind speed and direction. The output signal for wind speed is an AC voltage with a frequency proportional to the wind speed (1 Hz = 0.098 ms^{-1}). Wind direction is measured using a precision potentiometer that has a 5deg dead-band centred at 360deg (North) [White Island Met Station – Operator Manual 2004].

Daily-recorded data is important for calculating the SO_2 emission rate. For the present project, data of wind speed, wind direction, ambient temperature and relative humidity, recorded in 2005, were used for the meteorological evaluation of the pollution dispersion modelling.

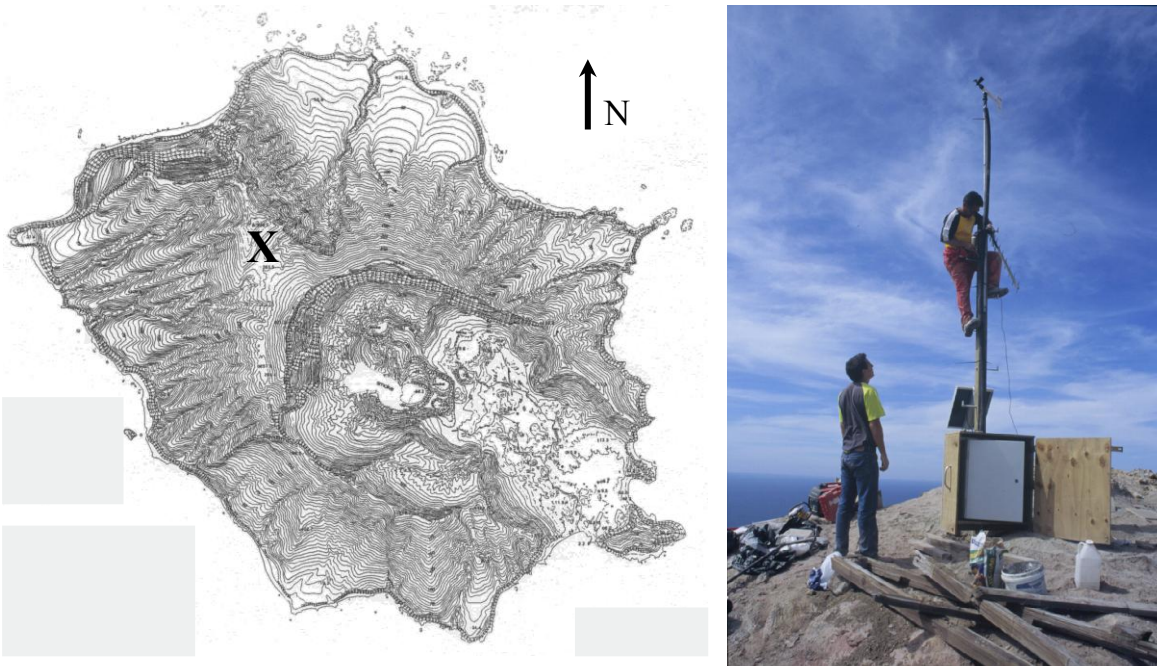

Figure 3. 4 The meteorological monitoring site was set up on the north-west rim (X) on White Island (a). The upper right photo (b) shows the installation of the weather station.

3. 3. Ruapehu volcano

Ruapehu volcano is located in the central North Island of New Zealand, at the southern end of TVZ and represents the highest (2797 m a.s.l.) and largest (approx. 110 km^3 of volcanic cone and c. 100 km^3 of surrounding pyroclastic and epiclastic deposits) andesitic stratovolcano in this area [Latter 1986, Hackett & Houghton 1989, Cronin et al. 2003]. The formation of Ruapehu volcano started about 300 ka ago with four cone-building eruption episodes: Te Herenga Formation (c. 120 ka), Wahianoa Formation (c. 120-60 ka), Mangawhero Formation (60-15 ka) and Whakapa Formation (c. 15-0 ka). During all periods took place both central (summit) and flank eruptions [Hackett & Houghton 1989]. The volcanic edifice of Ruapehu is divided into the central volcanic cone and a surrounding ring plain. The former is composed of sheet lavas and autobreccias, whereas the latter is consists of reworked material [Cole et al. 1986, Hackett & Houghton 1989].

Ruapehu is one of the most active volcanoes in New Zealand and has experiences numerous eruptions in historical time [e.g. Hackett & Houghton 1989, Christenson & Wood 1993, Werner et al. 2006]. The latest period of volcanic activity occurred in 1995-96. The majority of volcanic activity of Ruapehu volcano is characterised by phreatic and phreatomagmatic eruptions [Werner et al. 2006], such as the eruptions in September 1995 [Gamble et al. 1999, Cronin et al. 2003]. Other styles of volcanic activity were also reported, such as lava dome-forming eruption during 1945-46 [Gamble et al. 1999], strombolian activity, for example, in July 1996 [Cronin et al. 2003] and sub-plinian eruption events in October 1996 [Christenson 2000]. Petrological investigations indicate magma mixing as trigger for historical (>10,000 years) as well as recent (1995-96) volcanic activity [Nakagawa et al. 1999, 2002].

At crater lake at the summit of Ruapehu volcano has covered the active vent periodically probably since c. 3000 years B.P. [Donoghue et al. 1997]. Variations in lake temperature between 10-60 °C and its chemical compositions is caused by variable rates of gas input [Hurst et al. 1991, Cronin et al. 2003].

3. 3. 1. Geophysical monitoring

Geophysical monitoring of Ruapehu volcano is mainly seismic, which has been employed since the 1940s [Sherburn et al. 1999]. Currently, the permanent seismic network consists of five seismographs that are located at the summit, the flanks and surrounding Ruapehu at a distance of 12 km and 30 km. All seismic stations have an identical, vertical, 1-Hz seismometer [Sherburn et al. 1999, Bryan & Sherburn 1999]. There was little change in the style of seismicity at Ruapehu between 1971-1995, probably due to relatively low eruptive activity and consequent long-term stability within the vent system. Volcanic earthquakes and volcanic tremor both occurred predominantly with a frequency of about 2 Hz [Sherburn et al. 1999]. The style of seismicity was significantly different during the 1995-96 eruptive activity. The differences are the results of processes, which include the intrusion of magmatic melt into shallow depths of the volcanic edifice, its subsequent eruption and changes in the volcanic plumbing system due to the eruption [Sherburn et al. 1999, Bryan & Sherburn 1999].

In addition to the seismic network, an acoustic microphone was installed on 22 September 1995 at the unmanned Chateau observatory [Bryan & Sherburn 1999].

Other studies and measurements at Ruapehu volcano include visual observation of the crater and deformation measurements across the lake [Otway 1986], depth and temperature profiles of the lake [Hurst 1980, Scott 1991, Hurst & Vandemeulebrouck 1996] as well as geochemical studies of the crater lake and modelling the chemical and physical dynamics of the magmatic-hydrothermal system beneath the crater lake [Christenson & Wood 1993, Christenson 2000].

Variation in the Ruapehu crater lake temperature between 10-60 °C has been observed since the 1960s and the cyclic behaviour of the heating cycle is thought to last between 6 and 12 months [Hurst et al. 1991]. Only one entire cycle was studied in detail by Hurst & Vandemeulebrouck [1996], which indicated that an increase in the crater lake temperature followed a few days after recordings of seismic and acoustic signals, which are associated with the onset of a heat transfer process. Hurst et al. [1991] had previously suggested a heat pipe model, involving water and steam, which represents the source of energy to the crater lake. This heat pipe model is characterised by degassing magma at depth and steam condensing into water underneath the lake, producing acoustic and seismic noise due to collapsing bubbles and resonance [Leet 1988, Hurst & Vandemeulebrouck 1996].

3. 3. 2. Gas monitoring

Giggenbach & Goguel [1989] published the results of the first gas measurements on Ruapehu, using direct sampling method at several locations within the crater area, when the crater lake disappeared and safe access could be guaranteed during the activity phase in 1995-96. Christenson [2000] published the results of the analyses from several gas samplings between December 1995 and February 1997, where the fumarole temperature of the different sites varied between 91.5 and 281 °C.

Airborne SO_2 measurements using COSPEC instrument at Ruapehu commenced on 25 September 1995. The SO_2 emission rates of 21 flights until December 1996 were calculated between 300 and 15,800 Mg d^{-1} [Christenson 2000]. The highest emission rates were measured on 13 and 17 October 1995 (>14,000 Mg d^{-1}) and 24 July 1996 (>10,000 Mg d^{-1}). These values coincided with peaks of the eruptive episode. Two sub-plinian eruption events took place on 11-12 October and 14 October with eruption columns between 8-10 and 10-11 km, respectively, whereas on 20 July 1996 intense tremor activity occurred,

accompanied with ash and bomb eruptions and eruption columns between 6-10 km [Christenson 2000].

Werner et al. [2006] published the results of concurrently collected measurements of SO_2, H_2S and CO_2 that commenced in 2003/04. These gas measurements were carried out from an airborne platform at a constant distance downwind of the summit. Several traverses were flown perpendicular to the wind direction in approximately 30 m vertical intervals (usually at a height between 2500-3200 m), resulting in a spatial resolution of c. 50 m in vertical and horizontal direction [Werner et al. 2006]. The variability of emission rates of CO_2 and SO_2 ranged from not detectable to 900 Mg d^{-1} and 35 Mg d^{-1}, respectively.

The emission rate of H_2S was measured with less than 1 Mg d^{-1} during two flights in April and May 2004. On the basis of the results of their study, Werner et al. [2006] suggest a cyclic behaviour during quiescent degassing of Ruapehu volcano, which had previously been observed with lake temperatures and seismicity. A 2-month delay between the peaks of crater lake heating and seismic activity and the peak of gas emission was observed, which led Werner et al. [2006] to the assumption that the source of the gas anomaly is located at a significant depth.

Chapter 4: Aerosol sampling on White Island volcano

4. 1. Introduction

Volcanoes represent a natural source of particulate matter that is emitted into the atmosphere, both during phases of volcanic eruptions, as well as periods of quiescent degassing. Strong emissions of aerosols during large eruptions are considered to cause strong perturbations to atmospheric chemistry and Earth's energy balance [Robock 2000, Mather et al. 2003b], but such large volcanic events are rare. On the other hand, smaller eruptions and sustained volcanic degassing are widespread and the time-averaged magnitude of such emissions exceeds that of large eruptive events [Mather et al. 2003b].

Tropospheric volcanic aerosols also affect atmospheric radiation by absorbing and backscattering short-wave radiation, as well as by acting as cloud condensation nuclei (CCN), and consequently, the modification of cloud cover and cloud radiative properties [Hobbs et al. 1982, Albrecht 1989, Kaufman et al. 2002]. Emissions of particulate matter into the troposphere also influence the terrestrial ecosystems and can cause human health problems on local to regional scales [Mannino et al. 1996, Allen et al. 2000, Grattan et al. 2003].

Aerosol-sampling sessions in the present study are focused on White Island volcano (WIV). Although the gas emission was low in 2005, WIV currently represents the most active volcano in New Zealand. There are several fumarolic vents distributed over the crater floor, which are characterised by varying but continuous degassing. The objectives of this study are (1) to get a general overview of the chemical composition of near-source collected non-silicate volcanic particles and (2) to compare these results with those of previous measurements on White Island by Rose et al. [1986] and other volcanoes with the same tectonic settings and similar chemical composition, such as Soufriere Hills volcano (Montserrat) by Allen et al. [2000] and La Fossa (Vulcano, Italy) by Mather et al. [2004b].

4. 2. Sampling method

It was not possible to carry out aerosol sampling with the same high-cost instruments as used by Rose et al. [1986], who had a 10-stage cascade impactor

with quartz crystal microbalance impactor plates, which is able to separate airborne particles into ten aerodynamic size groups. Instead, two *MiniVol Portable Air Samplers* were used for the collection of particulate matter from plumes of the fumaroles (Figure 4. 1). The following description of this aerosol-sampling instrument is based on the description of the instrument handbook, the AIRmetrics MiniVol Users Guide.

The major part of the instrument is the sampler body that is plugged-in to a battery pack during sampling (Figure 4. 1a). The flow control device maintains the programmed flow rate and the programmable timer controls the operation of the sampler. The volumetric flow rate, recommended by the company AIRmetrics, is 5 litres per minute at ambient conditions. The MiniVol Portable Air Sampler is designed to collect particulate matter and non-reactive gases from the ambient air. In this method, air is drawn at ambient conditions through a particle size pre-separator and then through a 47-mm filter medium (Figure 4. 1b). For the present study, particle size pre-separation was achieved using an impactor with 10-µm cut-off point. Within the sampler body all components necessary for aerosol sampling are installed, such as the flowmeter and the programmable timer (Figure 4. 1c).

Two aerosol-sampling sessions (9 February and 6 April 2005) were carried out for the present study. Figures 4. 2a-d, 4. 3 and 4. 4 show the locations of fumaroles and aerosol-sampling sites, which were chosen after consideration of the dispersion of individual plumes from the fumarolic vents, as well as their smell and acidity. Additionally, positioning of the two instruments had to be chosen carefully, since parts of these instruments react easily with the acidic gases.

Figure 4. 1a
MiniVol instrument and its three main components.

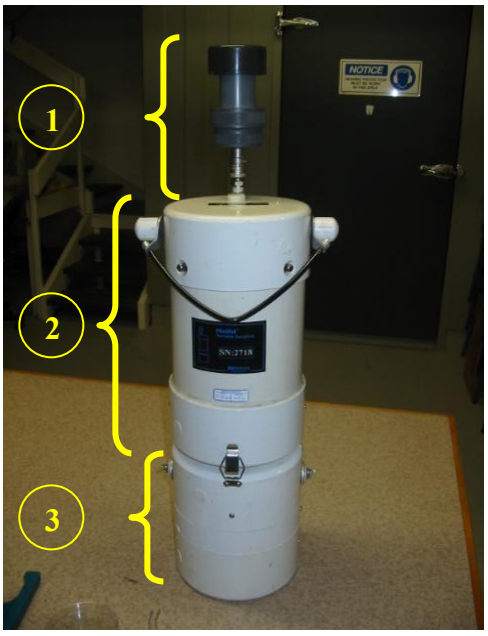

1 Pre-separator and filter holder assembly

2 Sampler body with sampling controls and adjustments

3 Battery pack

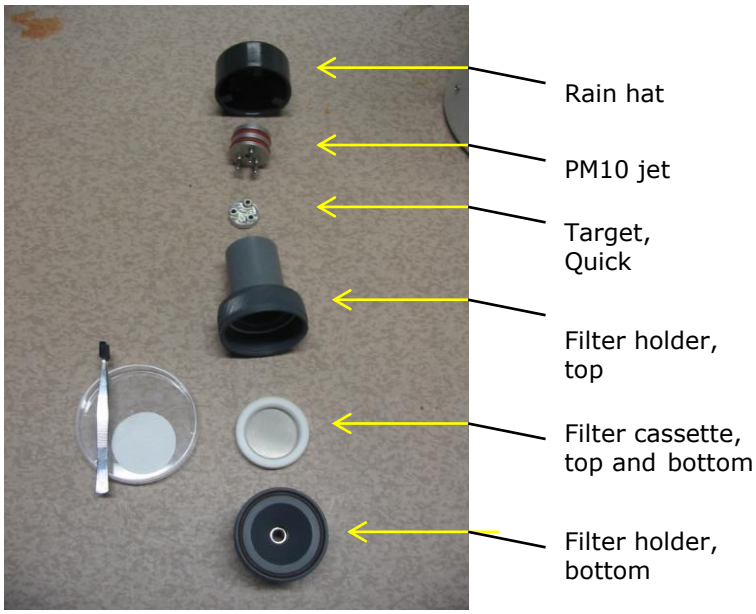

Figure 4. 1 b
PM_{10} Pre-separator and filter holder assembly

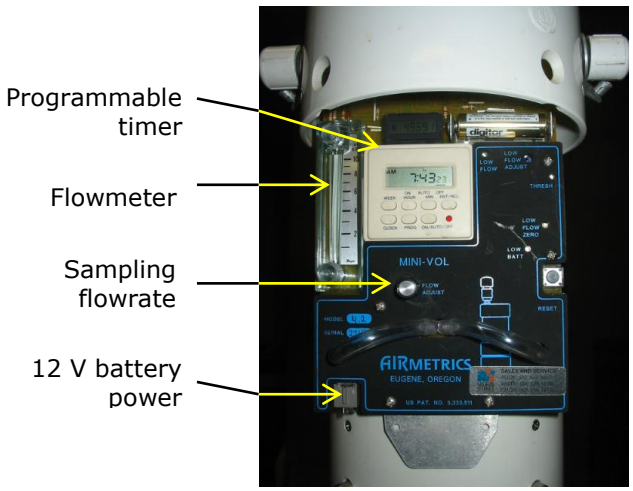

Figure 4. 1 c
Sampler control and adjustments

The weather during the two sampling sessions was generally fine, with sunny days and very few clouds. According to the weather station on White Island, the mean temperature during sampling (between 11am and 3pm) was ~23 °C in February and ~18 °C (between 10 am and 3 pm) in April. Only light wind was recorded from the monitoring site with wind speeds between 0.6 and 3.5 m s^{-1} during first sampling and 2.3-3.5 m s^{-1} on the second sampling day.

For sampling, the recommended flow rate of 5 L min^{-1} was chosen and the manual timer was used to start and stop the sampling operations. The duration of sampling time was chosen to be consistent with those used during previous sampling sessions and reported by other authors, such as Allen et al. [2000] and Mather et al. [2003a], who measured between 30 minutes and a few hours at different locations near their studied volcanic vent. Aerosol sampling on White Island was carried out on the crater floor at distances of a few tens of metres. Therefore, low exposure times of 20-40 minutes were chosen. Details of the individual sampling runs are listed in Table 4. 1.

The aim of the first sampling session was to obtain a general overview of emitted aerosols in fumarole plumes. Two fumarolic plumes were chosen and glass microfibre filters (Gm) of 1.6 µm pore size were used for aerosol collection. During the second sampling only one plume was chosen, which was then sampled using different filters. Glass microfibre filters of 1.6 µm pore size were used again, but additionally, polycarbonate filters (Pc) with different pore sizes (5.0, 2.0 and 0.2 µm) were also used. All runs of the second sampling session had the same exposure time of 30 minutes. During the second aerosol sampling, the influence of two factors were tested: (1) the variation of the aerosol concentration collected using filters of different pore sizes at the same sampling time and, (2) the variation in the sample collected due to the positioning of the samplers at different distances from the vent. While the first instrument was positioned close to the source, the second sampler was located at a distance of c. 60 meters. It was assumed that the plume had been diluted during dispersion by the background atmosphere. Particulate matter from the background atmosphere was also sampled and was carried out at the north-east side of White Island (Figure 4. 2b).

After sampling, each exposed filter was sealed in one plastic bag, which in turn was put into another plastic bag containing previously prepared lab tissues soaked with ascorbic acid, in order to diminish acid neutralisation. All plastic bags were packed in an icebox and a cool bag, where the samples were covered and sheltered from heat and sunlight. All filters, including blank filters, were analysed for the cations and anions of H^+, Ca^{2+}, Mg^{2+}, Na^+, K^+, NH_4^+ Br^-, Cl^-, F^-, NO_3^-, NO_2^-, SO_4^{2-} and PO_4^{3-}, in which the resulting concentrations of the background and blank filters are used for reference and to see what ion concentrations come from the fumarolic plumes by subtracting these levels from the filters exposed in the plume.

The SO_2 emission rates on the days of aerosol sampling are unknown, since no airborne gas measurements were carried out. On 28 January and 15 March 2005, scientists from GNS measured SO_2 emissions of 138 and 140 Mg d^{-1}. After the activity declined, and an emission rate 73 Mg d^{-1} was measured on 26 April.

Table 4. 1 Detailed information of aerosol-sampling runs on White Island.

Date	Run	Position		Sampling site	Filter type	Pore size	Start Time	Exposure time
		Easting	Northing					
9 February 2005	01	2880203	6400193	1	Glass fibre	1.5	11:40	20 min
9 February 2005	02	2880203	6400193	1	Glass fibre	1.5	12:10	30 min
9 February 2005	03	2880203	6400193	1	Glass fibre	1.5	12:50	45 min
9 February 2005	04	2880203	6400193	1	Glass fibre	1.5	13:05	45 min
9 February 2005	05	2880400	6400311	2	Glass fibre	1.5	14:30	45 min
9 February 2005	06	2880400	6400311	2	Glass fibre	1.5	14:35	45 min
6 April 2005	07	2879823	6401577	Background	Polycarbonate	0.2	10:40	30 min
6 April 2005	08	2879823	6401577	Background	Polycarbonate	0.2	10:40	30 min
6 April 2005	09	2880275	6400104	3 (proximal)	Polycarbonate	5.0	12:15	30 min
6 April 2005	10	2880275	6400104	3 (proximal)	Polycarbonate	2.0	12:15	30 min
6 April 2005	11	2880275	6400104	3 (proximal)	Polycarbonate	0.2	13:05	30 min
6 April 2005	12	2880275	6400104	3 (proximal)	Glass fibre	1.5	13:05	30 min
6 April 2005	13	2880218	6400122	3 (distal)	Polycarbonate	5.0	14:00	30 min
6 April 2005	14	2880218	6400122	3 (distal)	Polycarbonate	2.0	14:00	30 min
6 April 2005	15	2880218	6400122	3 (distal)	Polycarbonate	0.2	14:50	30 min

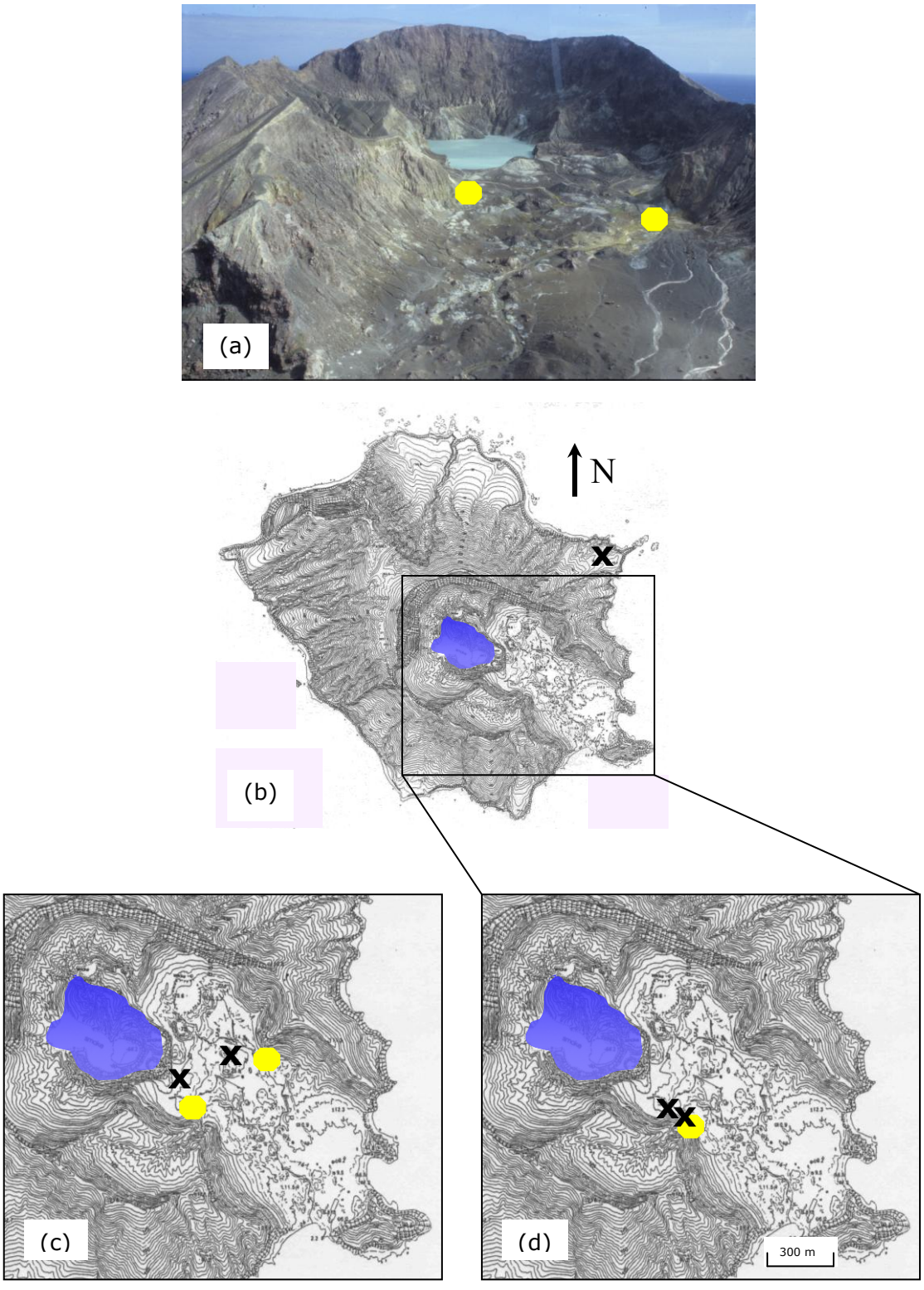

Figure 4. 2 The photograph (a) shows an aerial view into the crater area of White Island volcano. In the background can be seen the crater lake. The yellow-coloured points represent areas of strong fumarolic activity, where aerosol sampling was performed. Figure (b) shows a map of the whole volcanic island. The x-sign is the location where sampling of background aerosols was carried out. A the image (c) and (d) is the detail of the crater area. The yellow points are the fumarolic vents and the x-signs represent the positions of the MiniVol instruments during sampling sessions 1 (c) and 2 (d).

Figure 4. 3 The two photographs show the aerosol sampling site 1 (photo left) and site 2 (photo right) during the first session on 9 February 2005. Aerosol sampling at the first site was carried out using different exposure times (between 20-45 minutes), whereas at the two the filters were all exposed for 45 minutes.

Figure 4. 4 Aerosol sampling at fumarole site 3 during the second campaign on 6 April 2005. Two locations at different distances to the source for aerosol sampling were chosen. One instrument were positioned close to the fumaroles (left photo), the second instrument at a distance of c. 60 m (arrow on the right photo). The exposure times of all sampling runs were 30 minutes. During sampling were used different filters with diverse pore size. The aim was to see correlations between collected and distance to the source and/or pore size of the used filters.

4. 3. Analyses of aerosol samplings

Landcare Research in Palmerston North carried out the analyses of the exposed filters. The filters were put into plastic bottles with 20 mL of de-ionised water, which were shaken for one hour to remove the salts from the filters. After this, the solutions were analysed using three methods of analysis: ion chromatography (F^-, Cl^- and Br^- and SO_4^{2-}), atom absorption spectroscopy (Ca^{2+}, Mg^{2+}, Na^+ and K^+) and flow injection analysis (NH_4^+, NO_3^-, NO_2^-, PO_4^{3-}) in order to obtain information about the concentration of the individual ions.

Solution pH, and hence the concentration of H^+, was measured with a glass electrode attached to a radiometer pH meter (Brian Daly 2006, *pers. comm.*). Based on previous work [e.g. Mather et al. 2003a], the chemical constituents of main interest are Ca^{2+}, Mg^{2+}, H^+, Na^+, K^+, NH_4^+, F^-, Cl^-, NO_3^- and SO_4^{2-}, but the analyses of the other ions (Br^-, NO_2^- and PO_4^{3-}) were included.

Table 4. 2 summarises the concentrations of all analysed ions from each sampling run, in which the concentration unit after analysing is given in µg/filter. Since µmoles m^{-3} is a more commonly used unit to describe the molar concentration of aerosol in volcanic plumes [e.g. Mather et al. 2003a, 2004b], all values were converted into this unit. First the concentration values of the blank filters were subtracted from the exposed filters. Afterwards, the particle mass concentrations (c_P) in the sampled plume-affected air were calculated using the formula in Equation 4. 1. The resulting unit is µg m^{-3}.

$$c_P = \frac{m}{(FT)/1000} \qquad (4.\ 1)$$

where m is mass of analysed ion [µg/filter], F is the flow rate of the aerosol sampler (5 L min^{-1}) and T is the exposure time of the filter [min]. The results are listed in Table 4. 2. Finally, these results were divided by the molar weight (M) of the specific ion (Equation 4. 2). The concentration values of the blank filters chosen for subtraction and the calculated molar concentrations [µmol m^{-3}] are shown in Table 4. 3.

$$c_{mol} = \frac{c_P}{M} \qquad (4.\ 2)$$

4. 4. Results and discussion

It can be seen from Table 4. 2 that the concentrations of Br^- and NO_2^- are below their limit of detection, both in the blank and in the exposed filters. The concentration values of the blank filter analyses are quite similar, although there are a few minor differences between concentrations for the ions of Na^+, F^- and SO_4^{2-} for the glass microfibre filter analyses. Larger discrepancies are found for NH_4^+ for the glass microfibre filters as well as Na^+ and K^+ for the polycarbonate filters. Further, there is a large and concerning difference for the F^- concentration of the two Pc

blank filters. These differences were probably caused by contamination during production, transport or analysis of the filters.

Many analysed ions from Table 4. 2 are not listed in Tables 4. 3 and 4. 4. This is because the concentrations are below their limit of detection, perhaps because of too short exposure times. The detected concentration values of some ions from the filters exposed to the fumaroles reached lower values than those of the corresponding blank filters. This applies particularly for the ions of K^+ and F^-.

Ions of Ca^{2+}, Mg^{2+}, Na^+, Cl^-, NO_3^- and SO_4^{2-} are found onto all filters from of the first run and some correlation can be found between those ions. The highest concentrations of all ions are found for Na^+ and Cl^-, which also show a very good correlation (Figure 4. 5a). This finding suggests the deposition of NaCl onto the filters. A weak correlation can be found between Ca^{2+} and Mg^{2+}, which can be caused by deposition of fine silicate dust onto the filters (Figure 4. 5b). Rose et al. [1986] studied collected aerosols by scanning electron microscopy (SEM) and energy dispersive spectroscopy (EDS) and found particles with Ca and Mg peaks, which they assumed to be dolomite. Concentrations of Ca^{2+} also show good correlation with PO_4^{3-} (Figure 4. 5c), which is also evidence of silicate dust onto the filters. Phosphorus is commonly found by XRF analyses of volcanic products from White Island volcano, as shown in publications of Cole et al. [2000] and Wardell et al. [2001]. Additionally, Ca^{2+} is more abundant than Mg^{2+}. This reflects their concentration in nearly all known rock analyses. Sulphate (SO_4^{2-}) was detected on all filters during the first sampling session. There is an inverse correlation between detected concentration and exposure time for sampling site 1. The SO_4^{2-} concentration collected at fumarole site 2 is about twice as much as at site 1 beside of the same exposure times. However, no cation can be correlated with SO_4^{2-}, which is maybe due to missing hydrogen ions.

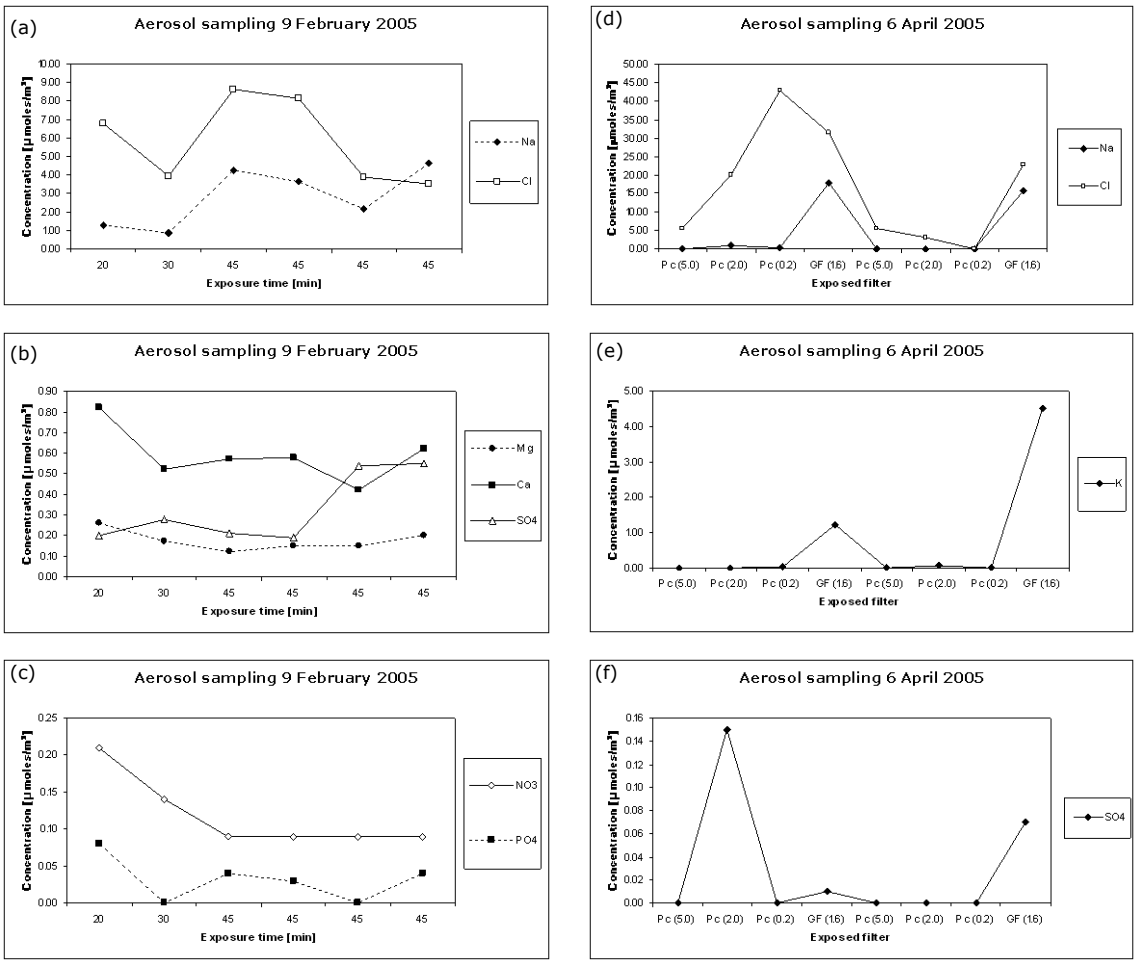

Figure 4. 5 Variations of molar concentrations of detected cations and anions from aerosol-sampling sessions on 9 February (a-c) and 6 April 2005 (d-f) at fumaroles of White Island volcano. Best temporal trends are found for Na^+ and Cl^- from both sampling days (Figures a and d). At the first sampling session, some dust from eroded pyroclastic deposits was probably collected, which is characterised by a weak relationship of Mg^{2+}, Ca^{2+} and PO_4^{3-} (Figure b, c). The detection of NO_3^- (Figure c) is possibly due to nitric acid (HNO_3). A rather speculative relationship is thought for the detection of SO_4^{2-} (Figure e) and K^+ (Figure f).

Table 4. 2. Results of filter analyses from the aerosol sampling on White Island, in µg/filter. The first four rows are the results of blank filter analyses. The results of runs 7 and 8 show the concentration values of the background runs. The hydrogen ions were not analysed after the first sampling.

Date	Run	Filter	H^+	Ca^{2+}	Mg^{2+}	Na^+	K^+	NH_4^+	Br^-	Cl^-	F^-	NO_3^-	NO_2^-	SO_4^{2-}	PO_4^{3-}
		Gf_bl (1.5)	6.2	0.0	0.0	84.7	12.6	2.0	<0.1	46	3.3	<0.1	<0.04	3.3	<0.2
		Gf_bl (1.5)	6.2	0.0	0.0	86.1	12.8	0.9	<0.1	49	3.6	<0.1	<0.04	2.7	<0.2
		Pc_bl (5.0)	5.6	0.0	0.0	1.1	4.1	<0.1	<0.1	10	0.5	<0.1	<0.04	<1.0	<0.2
		Pc_bl (2.0)	5.4	0.0	0.1	2.1	3.3	<0.1	<0.1	10	7.9	<0.1	<0.04	<1.0	<0.2
9 Feb 05	01	Gf (1.5)		3.26	0.64	88	7.8	0.15	<0.1	72	2.9	1.30	<0.02	4.9	0.8
9 Feb 05	02	Gf (1.5)		3.15	0.61	88	7.9	0.18	<0.1	69	2.7	1.30	<0.02	7.1	<0.2
9 Feb 05	03	Gf (1.5)		5.15	0.68	107	9.6	0.48	<0.1	117	3.3	1.28	<0.02	7.5	0.9
9 Feb 05	04	Gf (1.5)		5.18	0.80	104	10.6	0.41	<0.1	113	3.0	1.32	<0.02	7.2	0.7
9 Feb 05	05	Gf (1.5)		3.78	0.80	96	8.6	<0.04	<0.1	79	2.9	1.28	<0.02	14.6	<0.2
9 Feb 05	06	Gf (1.5)		5.56	1.07	109	20.0	0.51	<0.1	76	3.5	1.26	<0.02	14.8	0.8
6 Apr 05	07	Pc_Bg_1 (0.2)	6.9	0.0	0.2	2.5	3.1	<0.1	<0.1	8	<0.1	1.9	<0.04	3.4	<0.2
6 Apr 05	08	Pc_Bg_2 (0.2)	5.3	0.0	0.2	3.3	4.6	<0.1	<0.1	11	7.2	<0.1	<0.04	<1.0	<0.2
6 Apr 05	09	Pc (5.0)	4.2	0.0	0.0	2.0	2.3	0.17	<0.1	39	11.9	<0.1	<0.04	<1.0	<0.2
6 Apr 05	10	Pc (2.0)	4.0	0.7	0.2	4.3	2.1	<0.1	<0.1	116	<0.1	<0.1	<0.04	2.1	<0.2
6 Apr 05	11	Pc (0.2)	3.7	0.0	0.0	2.3	3.9	0.3	<0.1	238	<0.1	<0.1	<0.04	<1.0	<0.2
6 Apr 05	12	Gf (1.5)	5.6	0.0	0.8	147	19.9	0.7	<0.1	215	2.4	<0.1	<0.04	3.1	<0.2
6 Apr 05	13	Pc (5.0)	4.2	0.0	0.0	0.3	2.7	<0.1	<0.1	39	7.0	<0.1	<0.04	<1.0	<0.2
6 Apr 05	14	Pc (2.0)	4.5	0.0	0.0	0.8	4.1	<0.1	<0.1	27	7.5	<0.1	<0.04	<1.0	<0.2
6 Apr 05	15	Pc (0.2)							SEM						
6 Apr 05	16	Gf (1.5)	5.7	0.0	0.6	139	39.2	1.3	<0.1	170	2.4	<0.1	<0.04	4.0	<0.2

Table 4. 3. Particle mass concentration of all detected ions from the aerosol-sampling sessions on White Island, in µg m^{-3}. The results of runs 7 and 8 show the concentration values of the background runs. The hydrogen ions were not analysed after the first sampling on 9 February 2005. The letters p and d indicate proximal and distal distance of the MiniVol instruments to the fumaroles.

Date	Run	Filter	Exposure time [min]	H^+	Ca^{2+}	Mg^{2+}	Na^+	K^+	NH_4^+	Cl^-	F^-	NO_3^-	SO_4^{2-}	PO_4^{3-}	Total
9 Feb 05	01	Gf (1.5)	20		33	6	30			240		13	19	8	349
9 Feb 05	02	Gf (1.5)	30		21	4	20			140		9	27		221
9 Feb 05	03	Gf (1.5)	45		23	3	98			307		6	20	4	461
9 Feb 05	04	Gf (1.5)	45		23	4	84			289		6	18	3	427
9 Feb 05	05	Gf (1.5)	45		17	4	49			138		6	52		266
9 Feb 05	06	Gf (1.5)	45		25	5	107	32		124		6	53	4	356
6 Apr 05	07	Pc_Bg_1 (0.2)	30	9		1	6					13	23		52
6 Apr 05	08	Pc_Bg_2 (0.2)	30			1	11	6		7					25
6 Apr 05	09	Pc (5.0)	30 (p)				3		1	193	27				224
6 Apr 05	10	Pc (2.0)	30 (p)		5	1	18			707			14		745
6 Apr 05	11	Pc (0.2)	30 (p)				5	1	2	1520					1528
6 Apr 05	12	Gf (1.5)	30 (p)			9	413	48	5	1113			1		1589
6 Apr 05	13	Pc (5.0)	30 (d)							193					193
6 Apr 05	14	Pc (2.0)	30 (d)					3		113					116
6 Apr 05	15	Pc (0.2)	30 (d)							SEM					
6 Apr 05	16	Gf (1.5)	30 (d)			4	360	176		813			7		1360

Table 4. 4. Molar concentration of all detected ions after unit conversion, where the unit is µmoles m^{-3}. The first two rows are the average values from the blank filter analyses, where the unit is µg/filter. These values were first subtracted from the analysed ions of the exposed filters. Due to the large difference of F^- concentration at the blank filters, both values were used to calculate its molar concentration at the exposed filters. The results of runs 7 and 8 show the concentration values of the background runs. The hydrogen ions were not analysed after the first sampling. The letters p and d indicate proximal and distal distance of the MiniVol instruments to the fumaroles.

Date	Run	Filter	Exposure time [min]	H^+	Ca^{2+}	Mg^{2+}	Na^+	K^+	NH_4^+	Cl^-	F^-	NO_3^-	SO_4^{2-}	PO_4^{3-}
		Qz_blank		6.20	0.00	0.00	85.00	12.70	2.00	48.00	0.18	0.00	3.00	0.00
		Pc_blank		5.50	0.00	0.10	1.60	3.70	0.00	10.00	7.9 (0.5)	0.00	0.00	0.00
9 Feb 05	01	Gf (1.5)	20		0.82	0.26	1.30			6.77		0.21	0.20	0.08
9 Feb 05	02	Gf (1.5)	30		0.52	0.17	0.87			3.95		0.14	0.28	
9 Feb 05	03	Gf (1.5)	45		0.57	0.12	4.25			8.65		0.09	0.21	0.04
9 Feb 05	04	Gf (1.5)	45		0.58	0.15	3.67			8.14		0.09	0.19	0.03
9 Feb 05	05	Gf (1.5)	45		0.42	0.15	2.13			3.89		0.09	0.54	
9 Feb 05	06	Gf (1.5)	45		0.62	0.2	4.64	0.83		3.51		0.09	0.55	0.04
6 Apr 05	07	Pc_Bg_1 (0.2)	30	9.33		0.03	0.26					0.2	0.24	
6 Apr 05	08	Pc_Bg_2 (0.2)	30			0.03	0.49	0.15		0.19	(2.35)			
6 Apr 05	09	Pc (5.0)	30 (p)				0.12		0.06	5.45	1.40 (4.00)			
6 Apr 05	10	Pc (2.0)	30 (p)		0.12	0.03	0.78			19.93			0.15	
6 Apr 05	11	Pc (0.2)	30 (p)				0.2	0.03	0.11	42.88				
6 Apr 05	12	Gf (1.5)	30 (p)			0.22	17.97	1.23	0.26	31.4			0.01	
6 Apr 05	13	Pc (5.0)	30 (d)							5.45	(2.28)			
6 Apr 05	14	Pc (2.0)	30 (d)					0.07		3.2	(2.46)			
6 Apr 05	15	Pc (0.2)	30 (d)						SEM					
6 Apr 05	16	Gf (1.5)	30 (d)			0.16	15.65	4.52		22.94			0.07	

Potassium (K^+) was only found on the filter of run 6 of the first sampling session. As mentioned before, the other analysed K^+ concentrations had even lower values than those of the two blank filters (Table 4. 4). Some nitrate (NO_3^-) was also detected on the glass microfibre filters from the first sampling. As mentioned in e.g. Mather et al. [2003a], NO_3^- is an ion of nitric acid (HNO_3) that dissolves easily via the following equilibria:

$$HNO_3\ (g) \Leftrightarrow HNO_3\ (aq) \Leftrightarrow H^+\ (aq) + NO_3^-\ (aq) \qquad (4.\ 3)$$

Unfortunately, H^+ ions were not determined after aerosol sampling on 9 February 2005. The filters from the second aerosol-sampling session on 6 April 2005 were analysed for both, H^+ and NO_3^-, but the two ions were only detected on one Pc filter exposed for sampling of background concentration (Table 4. 4, run 7). This result is comparable with observations of Allen et al. [2000] who reported no detection of HNO_3 at the summit of the Soufriere Hills volcano (Montserrat) but at other distal locations. Nitric acid is unlikely to become discharged out of volcanic vents, since it is largely a product of atmospheric oxidation [Allen et al. 2000]. Additionally, SO_4^{2-} was found on the same filter and an enormous concentration of H^+, whereas no hydrogen has been detected on the other background filter, although the two MiniVol instruments stand next to each other and were sampling at the same time. The detection of H^+ together with NO_3^- and SO_4^{2-} onto the one filter is perhaps caused by the deposition of HNO_3 and H_2SO_4.

The distribution of detected ions from the second aerosol-sampling session appears random. A good argument can again be found for relationship between the ions of Na^+ and Cl^- (Table 4. 4, Figure 4. 5d). K^+ was only detected on the glass microfibre filters, in which the distal exposed filter had a threefold higher molar concentration than the proximal exposed filter (Figure 4. 5e). The detection of Na^+, K^+ and Cl^- ions suggests the deposition of NaCl and KCl, respectively. While chloride was the only halide ion that was detected on the filters from the first sampling session, there is one filter from the second sampling session where F^- could be detected (Table 4. 4, run 9). However, as mentioned earlier, the blank Pc filter analyses show an enormous difference of F^- concentration (0.5 and 7.9 µg/filter). Assuming the lower value, the calculated molar concentration is shown in brackets (Table 4. 4). No relationship can be seen with any cation, which is maybe also due to low exposure times. Concentration of Mg^{2+} and Ca^{2+} analysed from the second sampling session show much lower concentration values than those from the first analysis and they were only detected on very few filters (Table 4. 4).

On three filters from the second sampling session NH_4^+ was detected. They were exposed close to the fumaroles, which strongly indicates that the detected NH_4^+ comes from the fumaroles. This finding is supported by previous work, such as Giggenbach [1983], Rose et al. [1986] and Giggenbach & Sheppard [1989], who mentioned the presence of gaseous ammonia (NH_3) in fumarolic plumes from White Island volcano. In two filters (runs 11 and 12) where NH_4^+ was detected, the highest concentrations of Cl^- ions were also found. It is possible that this relationship is caused by the occurrence of ammonium chloride (NH_4Cl). Mather et al. [2004b] showed a tight correlation of NH_4^+ and Cl^- ions in particles with diameters between 0.8 and 1.5 µm at Solfatara (Italy). The reaction of gaseous ammonia (NH_3) and hydrogen chloride (HCl) to form solid NH_4Cl (Equation 4. 4) is common and known to occur under atmospheric conditions [Seinfeld 1986].

$$NH_3\ (g) + HCl\ (g) \Rightarrow NH_4Cl\ (s) \qquad (4.\ 4)$$

Ammonium chloride is a white crystalline salt that dissolves easily in water. Ammonia is easily liquefied as well and dissolves via the following equilibria:

$$NH_3\ (g) \Leftrightarrow NH_3\ (aq) + H^+ \Leftrightarrow NH_4^+\ (aq) \qquad (4.\ 5)$$

On the filters from runs 10, 12 and 16, sulphate ions were detected, though concentrations were much lower than those from the first filter analyses (Figure 4. 5f). Two of these filters (runs 10 and 12) were exposed close to the fumaroles. The third filter is also a glass microfibre filter. It is noted that the concentration of the two Gm filters shows (similar to K^+ ions) a negative relationship with the distance to the source. However, the relationship of SO_4^{2-} is only based on its detection on two filters. On the other hand, the detection of SO_4^{2-} on the proximal exposed quartz filter is quite speculative as the concentration after analysis is 3.1 µg/filter. This is only 0.1 µm more than the average value of the two blank filters (3.3 and 2.7 µg/filter).

The expectation during this sampling of finding differences in the aerosol concentration due to the different pore sizes of the filters was only found for NH_4^- and Cl^-, which is may be due to the exposure times being too short and hence, insufficient quantities of the ions being collected for detection. A relationship between the different distances from the source was only found confidently for Na^+ and Cl^-. Ions of NO_3^- and PO_4^{3-} were not detected on the filters from the second aerosol-sampling session.

One Pc filter of 0.2 µm, which was exposed at site 4, was retained for laboratory analysis of particle morphology by scanning electron microscopy (SEM). Images of particles <2 µm that were caught by the exposed filters are shown in Figure 4. 6a-d. At least one particle (>1µm) of distinctive cubic shape indicates the presence of sodium chloride (NaCl), proving the correlating concentration values of these ions. The occurrence of halite particles in fumarolic plumes on White Island was also observed by Rose et al. [1986].

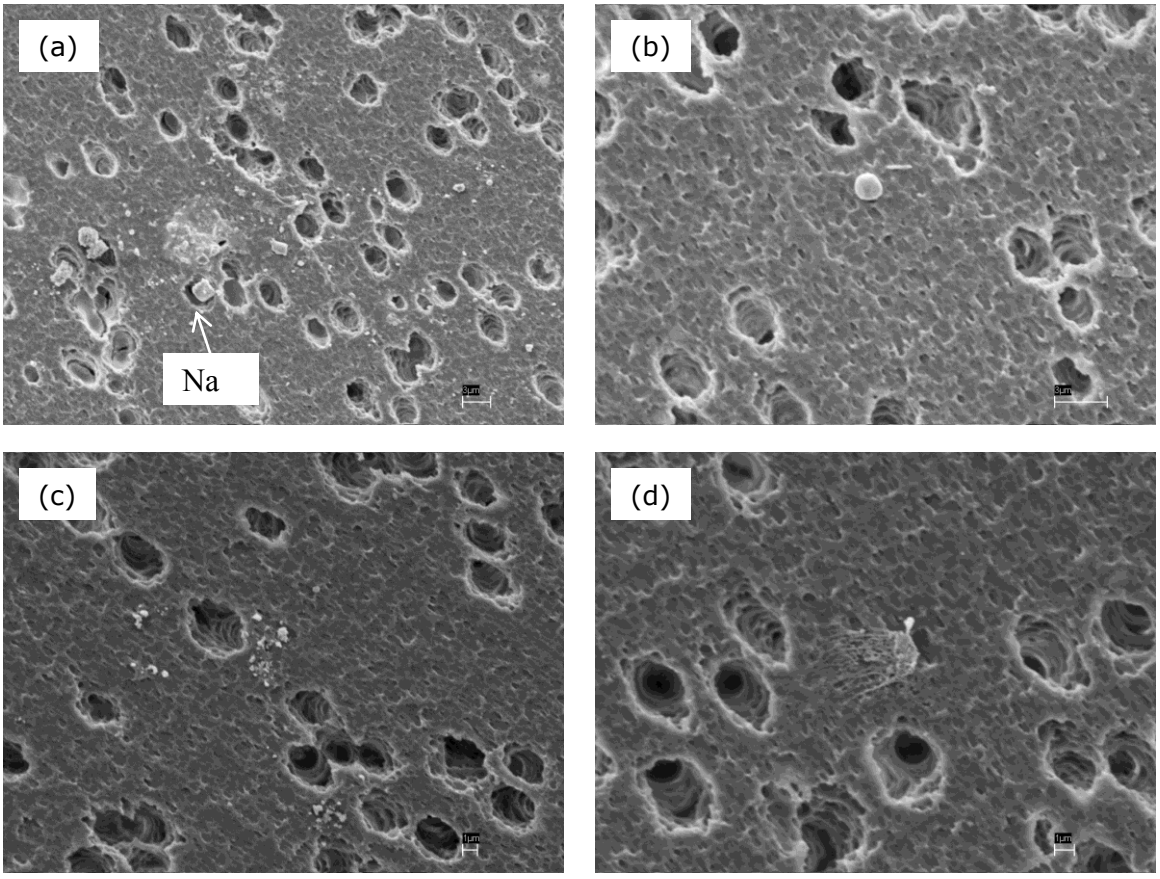

Figure 4. 6 SEM images of particles collected onto a polycarbonate filter during second sampling on 6 April 2005. Only very few particles have been collected, which is may be due to low exposure times.

There are some other particles that may be NaCl particles too but Figure 4. 6b shows clearly an image with a single spherical-shaped particle. Rose et al. [1986] found very similar looking particles, which showed primarily Ti and S in the EDS (energy dispersive spectroscopy) spectrum. They assumed that these are non-volcanic particles but are derived from the titanium gas sampling tube. Figure 4. 6c presents particles of different and irregular shapes that may represent silicate dust. An impression can be seen in Figure 4. 6d, which may be a deposited liquid particle. However, this description is speculative and a confident explanation cannot be

given. EDS study for elemental composition, as carried out by Rose et al. [1986], was not performed. Thus, the particles on the SEM images cannot be specified more precisely.

Extensive research over the last few years about aerosols in tropospheric volcanic plumes has been carried out by Allen et al. [2000, 2002] and Mather et al. [2003a, 2004b, c 2006]. They report the concentration of many ions and chemical compounds that are released from their studied volcanic vents. Of particular interest for the present results is the comparison of data from aerosol sampling at the Soufriere Hills volcano on Montserrat [Allen et al. 2000] and La Fossa (Vulcano) in Italy [Mather et al. 2004b], since they represent subduction-related volcanic edifices whose magma compositions are as similar as that of White Island volcano. Allen et al. [2000] described three different techniques for sampling of particles with an aerodynamic diameter of ≤10 µm (PM_{10}) as well as total suspending particles (TSP). They carried out aerosol sampling at different locations on the island of Montserrat during a high level of activity, which was characterised by intensified degassing and increasing growth of the lava dome [Allen et al. 2000]. The exact SO_2 emission rate in that time is not known, since no measurements were carried out (Vicky Hards 2006, *pers. comm.*). Mather and co-workers used a 10-stage (plus inlet and outlet stages) deposit impactor with PTFE filters at all stages and performed aerosol measurements at a flow rate of 30 L min^{-1}. They all reported exposure times from 30 minutes to several hours, depending on the location of their sampler. During the sampling on Vulcano, SO_2 emission was determined at 17 Mg d^{-1} [McGonigle et al. 2003, Mather et al. 2004b].

Some results from aerosol sampling by Allen et al. [2000] and Mather et al. [2004b] and the data from the present study are summarised in Table 4. 5. Besides the fact that during the present study not all ions have been found, the order of magnitude of detected ions are similar to concentrations reported by Allen et al. [2000] and Mather et al. [2004b].

The data from Montserrat are shown in two rows, in which the upper row includes the detected ions that were collected at Castle Peak, approximately 1 m from the active vent. The second sampling site, Chances Peak, is at a distance of c. 100 m from the vent [Allen et al. 2000]. As mentioned above, Allen and co-workers performed aerosol sampling in March 1996 during a period of increased volcanic activity. Therefore the concentration data in the upper row show very high values (e.g. H^+, Cl^- and SO_4^{2-}). However, the data of Chances Peak are approximately in the same range as the data of White Island and Vulcano.

Table 4. 5 Comparison of molecular concentrations from aerosol sampling on White Island with concentration values of Soufriere Hills volcano from Allen et al. [2000] and La Fossa (Vulcano) from Mather et al. [2004b]. The unit is µmoles m^{-3}. The results from Allen and co-workers include only the data from two locations: Castle Peak and Chances Peak. Since they measured at a period of increased volcanic activity, their results are quite high and, therefore, were splitted into two rows. The upper row shows the data of Castle Peak, which represent the active vent. The location of Chances Peak is about 100 m to the west from Castle Peak. Their results are shown in the lower row. Allen and co-workers published their results in µm m^{-3}. Thus these data were further calculated into the unit µmoles m^{-3}.

Authors	Volcano	Exposure time	Location	F^-	Cl^-	NO_3^-	SO_4^{2-}	PO_4^{3-}
Present study	White Island volcano	20 – 45 min	Crater floor	0.00 – 1.40 (4.00)	3.20 – 42.88	0.00 – 0.21	0.00 – 0.55	0.00 – 0.08
Allen et al. [2000]	Soufriere Hills volcano	c. 30 min	Castle Peak	1.12	245.31	0.38	65.21	n/a
			Chances Peak	0.004	0.09	0.00	0.31	
Mather et al. [2004b]	La Fossa, Vulcano	2 hr 50-53 min	Crater rim of La Fossa	0.15 – 0.38	0.17 – 0.46	0.05 – 0.10	0.07 – 0.13	n/a

Authors	Volcano	Exposure time	Mg^{2+}	Ca^{2+}	Na^+	K^+	H^+	NH_4^+
Present study	White Island volcano	20 – 45 min	0.00 – 0.26	0.00 – 0.82	0.00 – 17.97	0.00 – 4.52	0.00	0.00 – 0.26
Allen et al. [2000]	Soufriere Hills volcano	c. 30 min	n/a	n/a	5.08	n/a	40.43	0.48
					0.23		0.34	0.1
Mather et al. [2004b]	La Fossa, Vulcano	2 hr 50-53 min	0.02 – 0.05	0.35 – 0.44	0.15 – 0.18	0.01	0.04 – 0.12	0.19 – 0.47

In hindsight longer exposure times should have been used. However, the aerosol-sampling instruments used for the present study are quite sensitive to acidity. The two instruments used for the second sampling session had to be cleaned with utmost care. Increased activity of White Island volcano with higher gas emission rates provided a good opportunity for more aerosol-sampling sessions, but it was too risky to expose the previously used instruments for subsequent sampling with the same or longer exposure times, as it could cause damage to the instruments. Other aerosol samplers, such as filter packs, which are not as sensitive to the acidity, were not available. Hence, further aerosol-sampling sessions were abandoned.

4. 5. Summary

This chapter presents the results of two aerosol-sampling sessions, which were carried out at four locations on the crater floor of White Island volcano. Analyses of the exposed filters were carried out to determine the molar concentration of Mg^{2+}, Ca^{2+}, H^+, Na^+, K^+ and NH_4^+ as well as the anions of F^-, Cl^-, Br^-, NO_2^-, NO_3^-, SO_4^{2-} and PO_4^{3-}. Several suggestions about the relationship of detected ions have been made, although many of them are uncertain. Best correlations from the two sampling sessions are found for Na^+ and Cl^-, which also have the highest concentrations. A correlation is assumed for Ca^{2+} and PO_4^{3-} and partly Mg^{2+} from the first aerosol sampling. This relationship as well as the higher concentration of calcium with respect to magnesium suggests the deposition of silicate dust, eroded and dispersed from the surrounding volcanic deposits. Another compound collected during the first aerosol-sampling is probably HNO_3. On three filters from the second sampling NH_4 was detected, which is maybe due to the collection of NH_4Cl particles. A last and very weak correlation is suggested for K^+ and SO_4^{2-}, which would result from the deposition of K_2SO_4 onto two filters. SEM study was conducted for one exposed filter and the particles found are the same or show similar shape as images from a previous study.

More discussion about any correlations between detected ions would be very speculative and is not useful, since aerosol sampling with the MiniVol instruments were carried out to collect all particles ≤10 µm with one impactor and filter medium per run. A more detailed study of particulate matter, as performed by other authors would be useful but this requires other instruments. Other researchers such as Rose et al. [1986], Mather et al. [2004b] and Allen et al. [2000] used size-resolving instruments with which it is easier to correlate analysed cations and anions to suggest which compounds are present.

CHAPTER 5: The Air Pollution Model (TAPM)

5. 1. Introduction

Estimating the concentration of pollutants in the atmosphere under different meteorological conditions and emission rates from natural or anthropogenic sources is necessary for the evaluation of the hazard posed to public health. Numerical modelling represents an important tool used to describe the dispersion of pollutants in the air. The computer software *The Air Pollution Model (TAPM) Version 3.0.7* was used for the present project to model the dispersion of sulphur dioxide (SO_2) and particulate matter (PM_{10}) from White Island and Ruapehu volcanoes. This chapter provides some general information about TAPM itself, the meteorology and the pollution module of the model program and describes the input parameters that were chosen to model the different scenarios of SO_2 and PM_{10} dispersion.

5. 2. General information to TAPM

TAPM represents an Integrated Meteorological-Emission (IEM) Model [Wilson & Zawar-Reza 2006]. Such models are also called *mesoscale* models, referring to their capability to simulate sub-synoptic scale atmospheric processes [e.g. Pielke 2002]. Mesoscale systems are concerned with weather and atmospheric circulation systems with horizontal scales between 5 and 1000 km [Arya 1999]. Mesoscale models take into account the air pollution dispersion depending on daily weather cycles as well as the airflow caused by variation in landscape, such as sea breezes or mountain flows [Whiteman 1990, Wilson & Zawar-Reza 2006].

TAPM is a PC-based 3-D, nestable, prognostic model for air pollution studies and consists of coupled meteorological and air pollution concentration components. The program computes a complete set of mathematical calculations in fluid dynamics and scalar transport equations to predict and visualise meteorology and dispersion for a range of pollutants [e.g. Hurley et al. 2001, Luhar & Hurley 2003, Hurley 2005a]. For detailed mathematical and technical descriptions of TAPM the reader is referred to publications of Hurley et al. [2003], Luhar & Hurley [2003] and Hurley [2005a].

As a replacement for the required site-specific meteorological observation data, the model predicts the flows important to local-scale air pollution, such as sea

breezes and terrain-induced flows, against a large-scale background meteorology based on synoptic analyses [Hurley 2005a].

Various global databases are available for work with TAPM that include terrain height (where resolution is dependent on working area), land use, sea surface temperature and synoptic scale meteorology. TAPM is driven by a graphical user interface (GUI). GUI is linked to all database information and selects all model input and configuration options for the modelling process. GUI also processes the analysis of outputs and visualisation of the model [e.g. Hurley et al. 2001, Hibberd et al. 2005, Wilson & Zawar-Reza 2006].

5. 3. Meteorological component

The meteorological component of TAPM represents an incompressible, optionally non-hydrostatic, simple equation model that includes a terrain-following vertical coordinate for three-dimensional simulations [e.g. Hurley 2005a]. The model uses parameterisations to solve cloud/rain/snow microphysical processes. Further mathematical equations are used for other factors, such as turbulence, urban land use, vegetation and soil at the surface as well as radiative fluxes at the surface and at upper levels [Hurley et al. 2001, Hurley 2005a].

Large-scale weather information (synoptic analysis or, potentially, weather forecasts) is used for the meteorological module of TAPM. This information is obtained from the Bureau of Meteorology LAPS (Limited Area Prediction System) or GASP (Global Analysis and Prediction). The analyses are calculated for a horizontal grid spacing of c. 100 km and at 6-hourly intervals as boundary conditions for the model outer grid [Hibberd et al. 2005].

The synoptic data are for the horizontal wind components (wind direction and wind speed), temperature and moisture. They are gained from the output of meteorological model(s) of the Bureau of Meteorology, which incorporates meteorological observations from a network of stations [Hibberd et al. 2005].

Hurley [2005a] emphasises that the horizontal part of TAPM is restricted to an extension of less than 1500 x 1500 km, as the model equations do not take into account the curvature of the earth. Additionally, the model equations assume uniform distance grid spacing across the domain [Hurley 2005a].

5. 4. Air pollution component

The air pollution component of TAPM, which uses the predicted meteorology and turbulence from the meteorological component for calculations, consists of four modules: the Eulerian Grid Mode (EGM), the Lagrangian Particle Mode (LPM), the Plume Rise Module and the Building Wake Module [Hurley 2005a].

The *Eulerian Grid Mode* uses prognostic equations, calculating the mean and variance of pollutant concentration as well as the cross-correlation of pollutant concentration, representing counter-gradient fluxes. The *Lagrangian Particle Mode* can be used to determine the near-source dispersion more accurately [e.g. Hurley et al. 2001, Hurley et al. 2003, Hurley 2005a]. The *Plume Rise Module* is used to determine plume momentum and buoyancy effects of point sources, while the *Building Wake Module* allows plume rise and dispersion to comprise wake effects on meteorology and turbulence [Hurley 2005a].

The air pollution component of TAPM runs either using a *tracer* or *chemistry mode*. The former mode is used for dispersion modelling of particulate matter in four particle sizes ($PM_{2.5}$, PM_{10}, PM_{20} and PM_{30}). The chemistry mode includes semi-empirical gas-phase photochemical reactions for major species of interest, such as sulphur dioxide, nitrogen oxide, ozone and particles. Particle settling and dry deposition processes are calculated in both tracer and chemistry mode, whereas wet depositional processes are considered in TAPM only for some soluble gas and aerosol species [Hurley et al. 2001, Hurley 2005a].

5. 5. TAPM for the present modelling study

For the present project, TAPM was applied to simulate the dispersion of SO_2 and PM_{10} that are emitted from White Island and Ruapehu volcanoes. The vents of these two volcanoes, which are sources for emitting pollutants into the atmosphere, are located at different elevations. The crater area of White Island is nearly at sea level, whereas the vent of Ruapehu volcano is located at almost 2800 m above sea level. Consequently, the gases and aerosols from WIV are emitted into the boundary layer, whereas emissions from Ruapehu are into the free atmosphere. However, these effects are automatically taken into account via the prognostic turbulence scheme equations that are linked to both the meteorology and dispersion equations in TAPM (Peter Hurley 2006, *pers. comm.*). Different scenarios are modelled, using changing parameters of emission rates, gas exit velocity and gas

exit temperature. Modelling is divided into two parts. Firstly, annual plume dispersion modelling of SO_2 and PM_{10} from the two volcanic vents using synoptic weather data of the year 2005 was undertaken, in which modelling was performed in quarterly periods. The midpoint for all grids during all models was at longitude (37° 31' S) and latitude (177° 10' E) for White Island volcano and longitude (39° 17' S) and latitude (175° 34' E) for Ruapehu volcano, respectively. This part of modelling was performed to see which areas in the North Island are most affected by the plumes. Secondly, SO_2 dispersion modelling was performed for 22 November 2006 when proximal and distal airborne plume measurements on White Island were carried out. This phase of modelling has mainly been done to evaluate the air pollution component of TAPM. Detailed information of chosen input parameters are described in the corresponding chapters, where the model results are presented.

Three menu options can be selected and processed from the main window menu bar of TAPM for analysing outputs: GIS visualisation, Meteorology and Pollution (Figure 5. 1). GIS visualisation processes the two-dimensional simulation of meteorology and pollution using the Graphical Information System (GIS). The menu options 'Meteorology' or 'Pollution' are chosen to extract time series, profiles and summary statistics of meteorological or pollution data, respectively [Hurley 2005b].

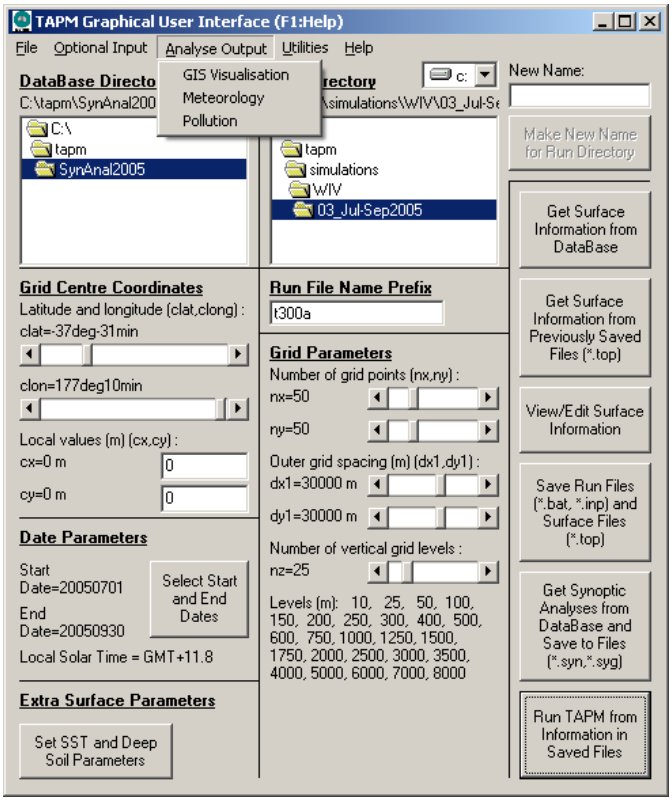

Figure 5. 1
TAPM main window and possible analysing output options.

Chapter 6: Evaluation of meteorological data from annual modelling

6. 1. Introduction

Dispersion and concentration of air pollutants is governed by regional meteorological conditions, such as wind speed, wind direction, temperature and relative humidity. Thus, it is always necessary to perform statistical analysis of the meteorological data to evaluate the accuracy of air pollution models. While the previous chapter provided a general summary about The Air Pollution Model (TAPM), this chapter analyses the output data of the meteorological component from annual modelling of the year 2005.

The weather situation in New Zealand is variable and can differ widely between different locations. Thus, the recorded data of six weather stations (White Island, Whakatane airport, Auckland airport, Wellington airport, Rotorua airport and Ruapehu Chateau) were chosen (Table 6. 1) to evaluate the accuracy of the annual dispersion modelling. The selection of the weather stations was influenced primarily by their location. The weather stations of White Island and Mt. Ruapehu are in the direct vicinity of the volcanic centres, whereas the monitoring sites of Whakatane and Rotorua are located in towns within a few tens of kilometres from the emission sources. Auckland and Wellington represent two main urban centres and are among the most important cities in New Zealand. All these weather stations are distributed throughout the North Island and the comparison of the recorded observation data with the modelled data provides a good opportunity to show the accuracy of the models.

Table 6. 1 Weather stations (including their geographic coordinates and height above sea level), which are distributed in the North Island and from where weather data are used.

Weather station	Northing	Easting	Height (a.s.l.)
White Island	37° 31′ S	177° 10′ E	c. 300 m
Whakatane airport	37° 00′ S	174° 48′ E	7 m
Auckland airport	37° 55′ S	176° 55′ E	6 m
Wellington airport	41° 19′ S	174° 48′ E	4 m
Rotorua airport	38° 07′ S	176° 19′ E	285 m
Ruapehu Chateau	39° 20′ S	175° 50′ E	1097 m

6. 2. Validation of TAPM by statistical analyses

6. 2. 1. TAPM synoptic output data

For the present study, TAPM was used to model the hour-by-hour meteorology of New Zealand (mainly the North Island) in 2005. In order to evaluate the meteorology of the present modelling study, the synoptic hourly data of wind speed, wind direction, temperature and relative humidity at 10 m above the ground were extracted at the nearest grid point of the best available grid spacing to each of the monitoring sites (Table 6. 2). After extraction of the model data, TAPM performance is evaluated against locally observed meteorological data using an internationally accepted set of statistical calculations. This is done by comparing the model predictions using the best available grid spacing with the recorded observation data from the available near surface weather stations in the North Island. For model evaluation and statistical calculations, the output data of all four quarterly models were summarised for the period of one year. The data extracted from the grid points of the six locations is saved on the CD-ROM attached to this thesis.

Table 6. 2 To evaluate the modelled weather data with recorded data from the weather stations, the synoptic weather data from the models need to be extracted. This was done at the nearest grid point using the best available grid spacing.

Locality	Grid	Grid spacing [m]
White Island	3	3500
Whakatane	3	3500
Ruapehu	3	3500
Rotorua	3	3500
Auckland	2	10,000
Wellington	2	10,000

The wind modelled for White Island is changing all year, although the prevailing wind direction for most of the year is to east (Figure 6. 1). This is particularly valid for the periods from January to March and October to December. From April to June and July to September, the wind direction modelled is more variable and frequently blows to the south-west. From April to June the modelled wind is blowing to the north and west, whereas from July to September it blows to the east, south and west.

As can be seen in Figure 6. 2, the wind modelled for Auckland usually blows to the east. This is particularly recognisable from January to March, April to June and October to December. From July to September the wind also blows to the south-western. The wind modelled for Whakatane is much more variable, although there are prevailing winds to the north and south (Figure 6. 3). Most variability can be seen for the period from October to December. Similar high variability in prevailing wind direction occurs for the period from April to June in Wellington. The rest of the year the wind is mainly blowing to the south-west (Figure 6. 4). The wind at Ruapehu blows in all directions throughout the year and no prevailing wind can be recognised (Figure 6. 5). However, it can be seen that wind frequently blows to the west. The wind modelled for Rotorua is mostly to the east throughout the year (Figure 6. 6). Additional prevailing winds occur to the north-west from January to March and to the south from July to September.

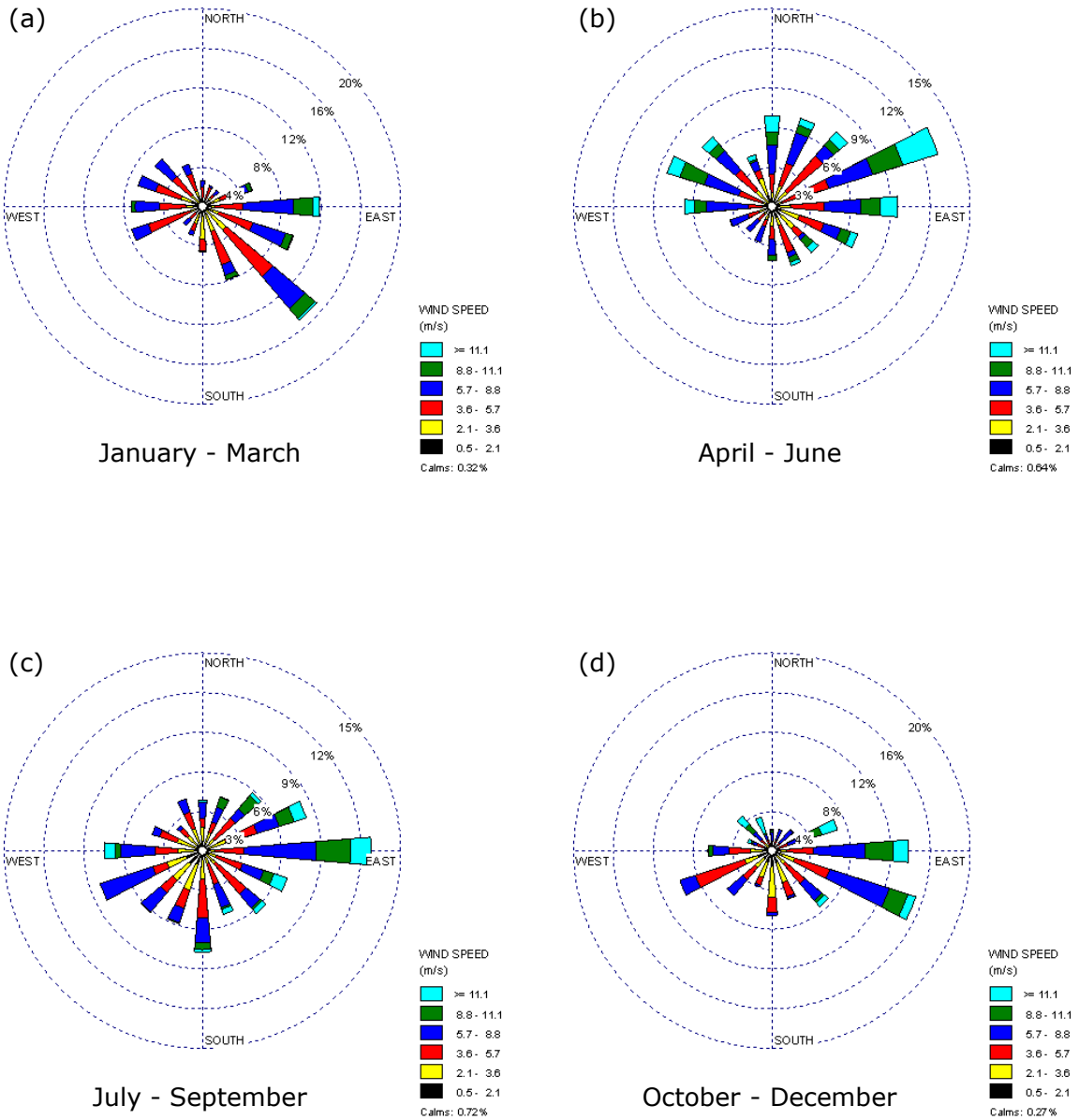

Figure 6. 1 2005 wind roses for White Island, derived from modelled wind data

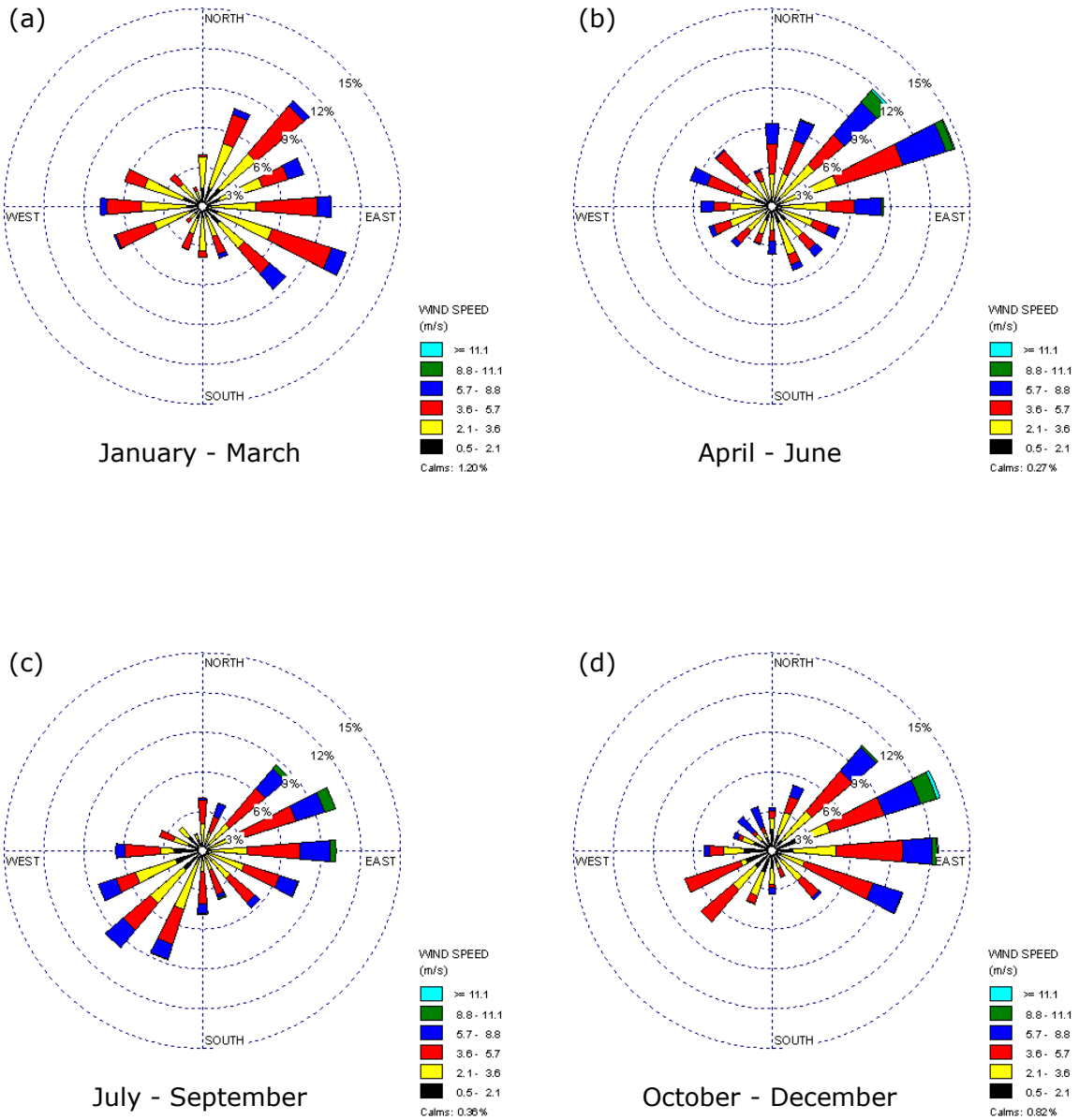

Figure 6. 2 2005 wind roses for Auckland, derived from modelled wind data

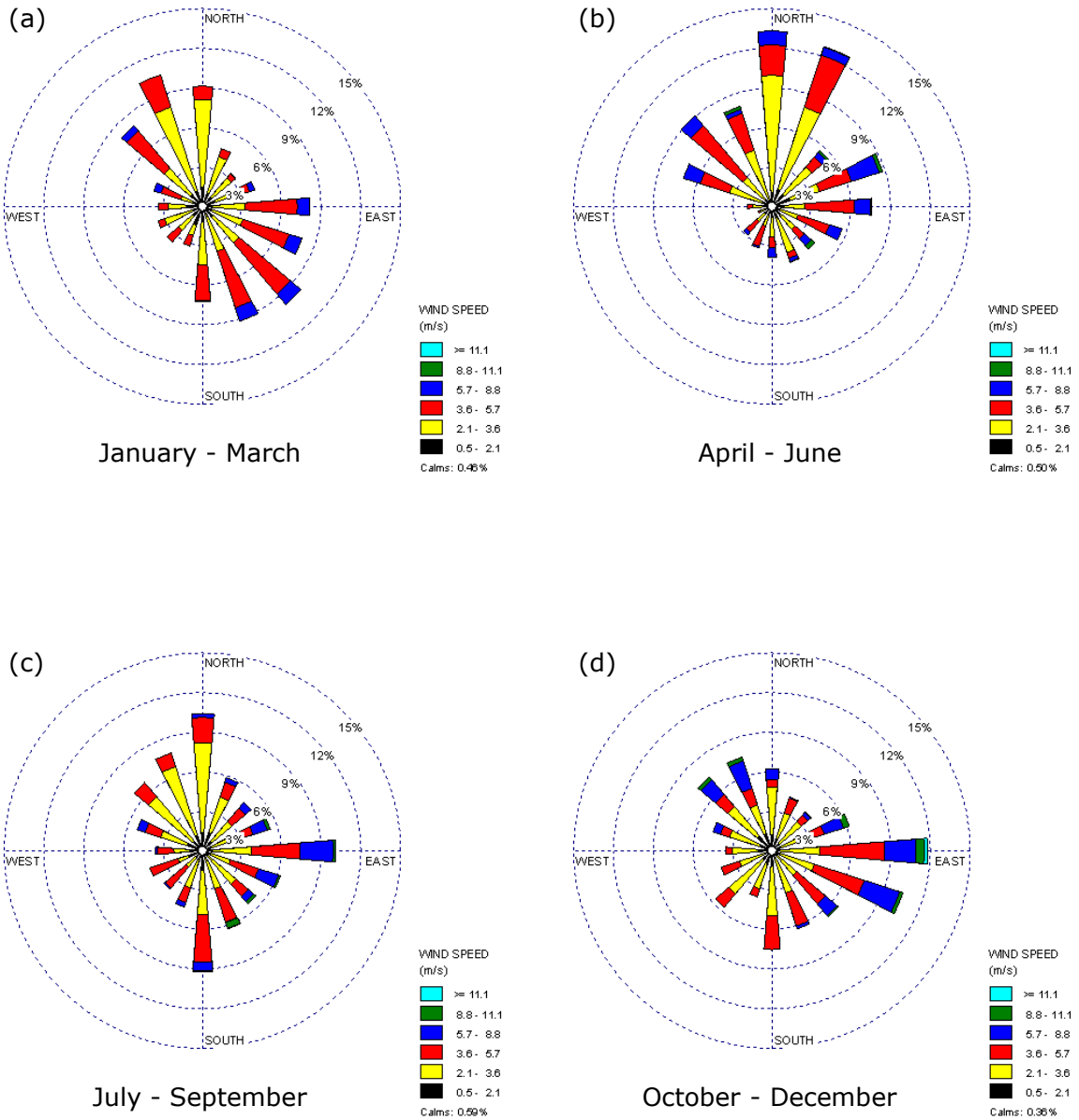

Figure 6. 3 2005 wind roses for Whakatane, derived from modelled wind data

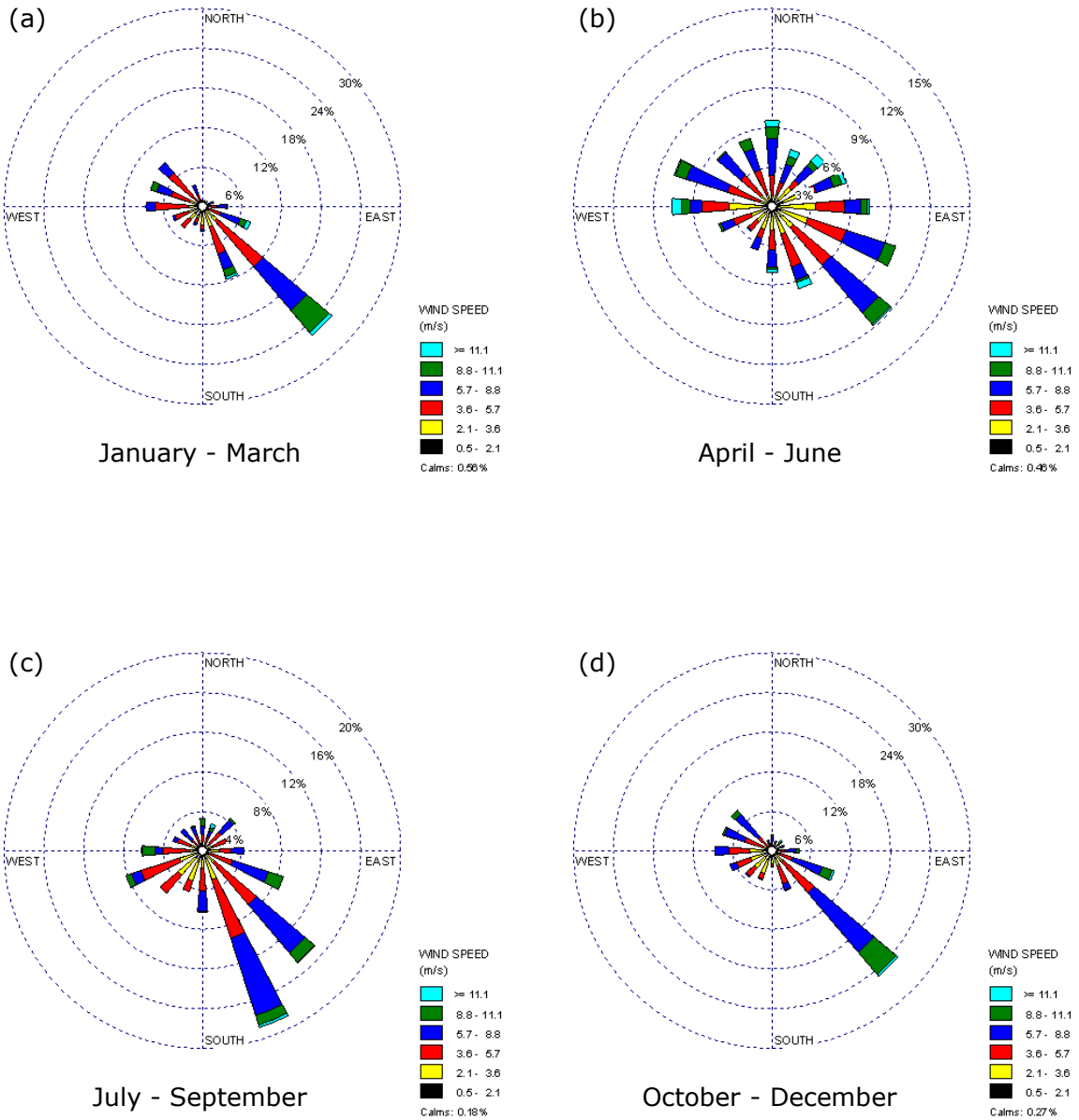

Figure 6. 4 2005 wind roses for Wellington, derived from modelled wind data

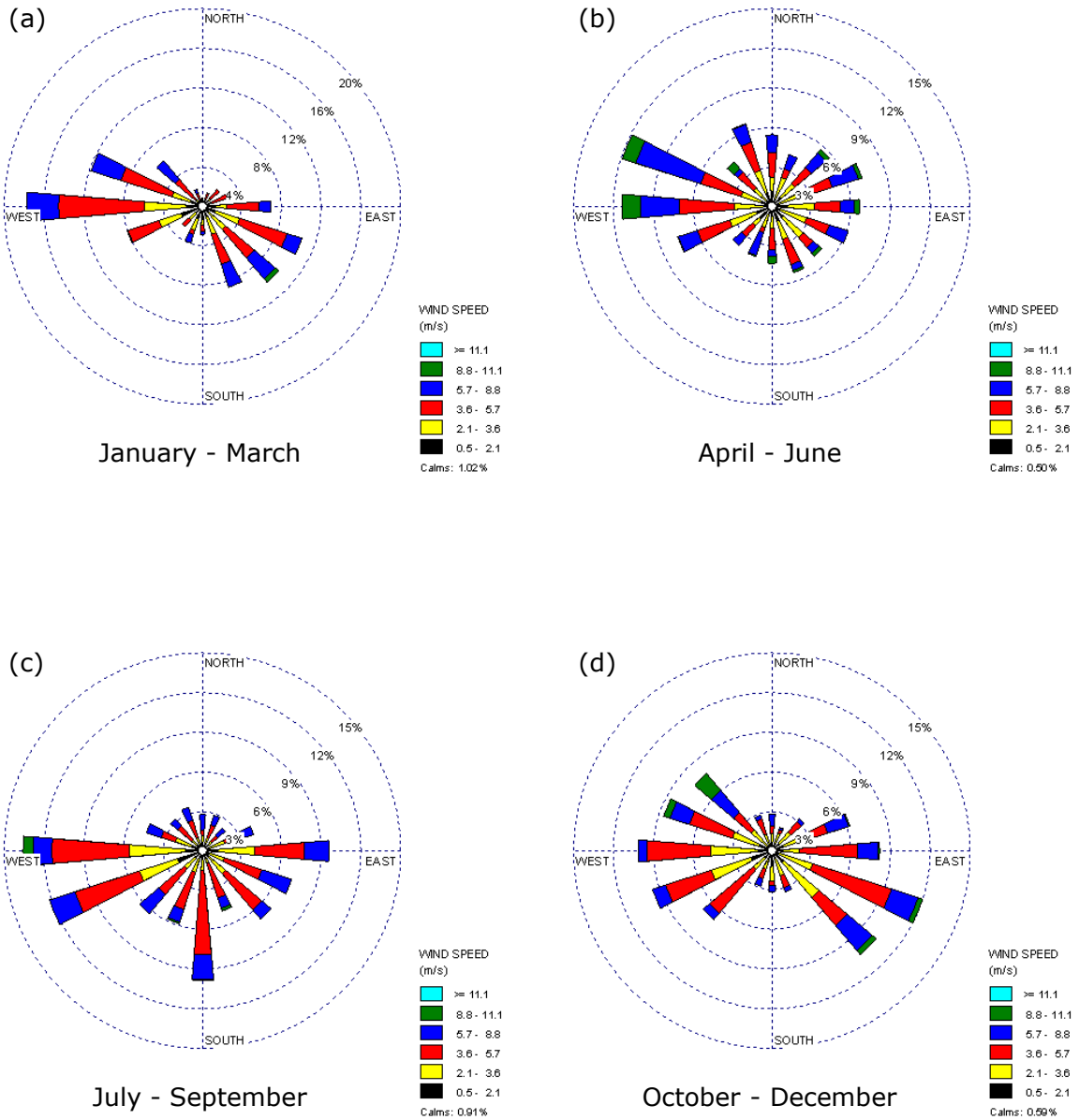

Figure 6. 5 2005 wind roses for Ruapehu, derived from modelled wind data

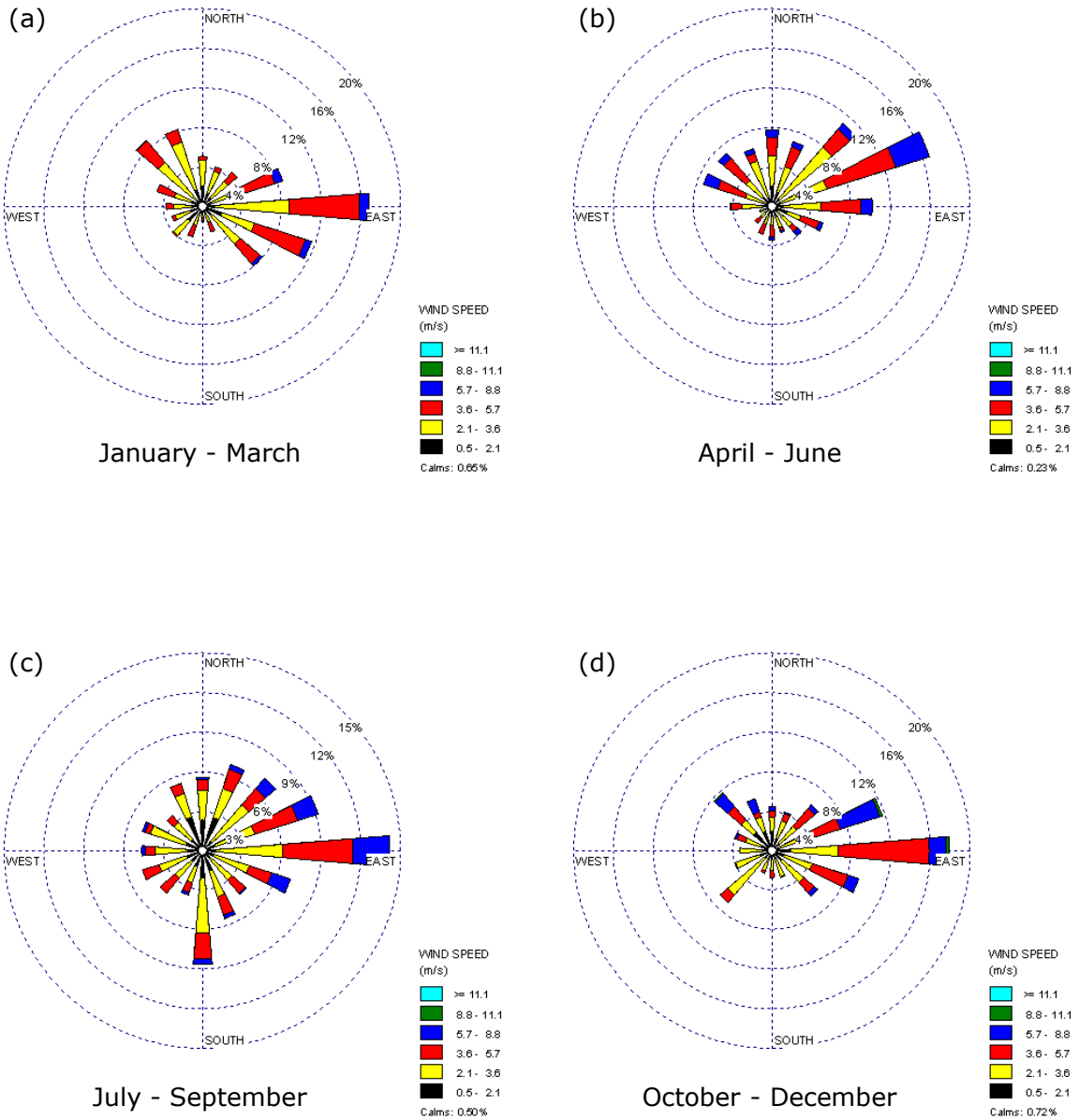

Figure 6. 6 2005 wind roses for Rotorua, derived from modelled wind data

6. 2. 2. Statistical methods used

There are several standardised coefficients of agreement to provide informed evaluations and to validate the accuracy of models. In order to verify the present models, statistical calculations were performed for all weather components based on recommendation of Willmott [1981] and previous TAPM evaluations as reported by Hurley et al. [2001, 2002], Luhar & Hurley [2003] and Luhar et al. [2004]. However, according to Stull [1995] and Luhar et al. [2004], the wind direction values cannot be used directly for statistical calculations due to the discontinuity at north. Therefore the wind components (U, V) are used instead and were calculated using Equations 6. 1 and 6. 2, respectively.

$$U = -M * \sin(\alpha) \tag{6. 1}$$

$$V = -M * \cos(\alpha) \tag{6. 2}$$

A positive U-Value indicates a westerly wind component, whereas a negative value of U means an easterly wind component. In the same way, positive or negative values of V indicate southerly or northerly wind components [Stull 1995, Luhar et al. 2004].

The simplest way is to compare the mean values (O_{mean} and P_{mean}) of observed (O_i) and predicted (P_i) data (Equation 6. 3 and 6. 4). The term N is the number of observations or predictions, respectively.

$$O_{mean} = \sum_{i=1}^{N} O_i \tag{6. 3}$$

$$P_{mean} = \sum_{i=1}^{N} P_i \tag{6. 4}$$

Another regularly used statistical value to verify a model is the standard deviation of observed and predicted data (O_{Std} and P_{Std}), respectively [Willmott 1981, Hurley et al. 2002]. It indicates how much the values vary from the mean value of observed and predicted data (Equations 6. 5 and 6. 6).

$$O_{Std} = \sqrt{\frac{1}{N}\sum_{i=1}^{N}\left(\mathrm{O_i} - \mathrm{O_{mean}}\right)^2} \tag{6. 5}$$

$$P_{Std} = \sqrt{\frac{1}{N}\sum_{i=1}^{N}\left(\mathrm{P_i} - \mathrm{P_{mean}}\right)^2} \tag{6. 6}$$

According to Willmott [1981], Pearson's Correlation Coefficient (r) is another common value to confirm the validation of models. It describes colinearity of a linear relationship between predicted modelled and observed values. Hurley et al. [2002] and Luhar et al. [2004] also used this coefficient while performing statistic calculations to verify TAPM (Equation 6. 7). The resulting values range from –1.0 to 1.0 inclusive, in which '0' means no correlation and '-1.0' and '1.0' indicate perfect negative and positive correlations, respectively [Luhar et al. 2004].

$$r = \frac{N\left(\sum_{i=1}^{N} O_i P_i\right) - \left(\sum_{i=1}^{N} O_i\right)\left(\sum_{i=1}^{N} P_i\right)}{\sqrt{\left[N\left(\sum_{i=1}^{N} O_i^{\,2}\right) - \left(\sum_{i=1}^{N} O_i\right)^2\right]\left[N\left(\sum_{i=1}^{N} P_i^{\,2}\right) - \left(\sum_{i=1}^{N} P_i\right)^2\right]}} \tag{6. 7}$$

A further statistical model evaluation is the determination of the root mean squared error (RMSE). It is an average error produced by the model, which exemplifies the size of the miscalculation [Willmott 1981]. RMSE is calculated as:

$$RMSE = \sqrt{\frac{1}{N}\sum_{i=1}^{N}\left(\mathrm{P_i} - \mathrm{O_i}\right)^2} \tag{6. 8}$$

RMSE is divided into $RMSE_S$ (systematic Root Mean Square Error) and $RMSE_U$ (unsystematic Root Mean Square Error). In a good model application, $RMSE_U$ should be larger than $RMSE_S$. Furthermore, $RMSE_S$ should approach zero while $RMSE_U$ should be close to RMSE.

From a mathematical point of view, $RMSE_S$ determines whether the model errors are predictable, whereas $RMSE_U$ calculates the errors that are not predictable mathematically [Luhar et al. 2004]. $RMSE_S$ and $RMSE_U$ are calculated using Equations 6. 9 and 6. 10. As noted in other reports [e.g. Hurley 2000, Luhar et al. 2004], the term $\hat{P}_i = a + bO_i$ is the linear regression fitted formula with intercept (a) and slope (b).

$$RMSE_S = \sqrt{\frac{1}{N}\sum_{i=1}^{N}\left(\hat{P}_i - O_i\right)^2} \tag{6. 9}$$

$$RMSE_U = \sqrt{\frac{1}{N}\sum_{i=1}^{N}\left(\hat{P}_i - P_i\right)^2} \tag{6. 10}$$

Another statistical value is the index of agreement (IOA) that Willmott [1981] described as a statistical method to illuminate the degree to which the modelled predictions are error free (Equation 6. 11). The values for the IOA range between 0 and 1, where '1' stands for perfect agreement. Values greater than 0.5 represent good results for modelling the meteorology [Hurley et al. 2002, Hibberd et al. 2005].

$$IOA = 1 - \frac{\sum_{i=1}^{N}\left(P_i - O_i\right)^2}{\sum_{i=1}^{N}\left(\left|P_i - O_{mean}\right| + \left|O_i - O_{mean}\right|\right)^2} \tag{6. 11}$$

Finally, there are three values ($SKILL_V$, $SKILL_E$ and $SKILL_R$) in which the relationships of previous statistical measures are involved. They are used to show the expressiveness and to make additional statements about the *skill* of the model. The letters V, E and R are notations, which distinguish between these skill measures: 'V' refers to the use of the '**V**ariance' (standard deviation), 'E' refers to the use of RMS**E**$_U$ in the numerator of the formula and 'R' refers to the use of **R**MSE (Peter Hurley, *pers. comm.*). According to Hurley et al. [2000, 2002] and Luhar et

al. [2004], good models predict the meteorology with skill if the values of modelled and observed standard deviations are approximately the same, and consequently the result value should be near to '1' (Equation 6. 12). The values of RMSE and $RMSE_U$ ought to be smaller than the observed standard deviation. Hence, the results for good predicted models should be less than 1 (Equations 6. 13 and 6. 14).

$$SKILL_V = \frac{P_{Std}}{O_{Std}} \quad (6.\ 12)$$

$$SKILL_E = \frac{RMSE_U}{O_{Std}} \quad (6.\ 13)$$

$$SKILL_R = \frac{RMSE}{O_{Std}} \quad (6.\ 14)$$

6. 2. 3. Comparison of model results with observed meteorological data

Tables 6. 3 shows the results of model evaluation statistics for wind speed (WS), wind components (U, V), temperature (T) and relative humidity (RH) for each of the monitoring sites. Additionally, Figures 6. 7 to 6. 12 present scatter plots of observed data vs. model predictions of the recorded weather factors for all weather stations. In the following descriptions of the results from the statistical evaluation for each individual location are given.

6. 2. 3. 1. White Island

The scatter plots of observed vs. modelled data for wind speed, wind direction, temperature and relative humidity are presented in Figures 6. 7a-d. TAPM predicts a mean wind speed of 5.7 ms^{-1}, which is slightly stronger than the observation of 5.3 ms^{-1}. The model also has a tendency to predict a weaker mean (1.2 ms^{-1} vs. 2.6 ms^{-1}) west-east component (U) and (0.3 ms^{-1} vs. 0 ms^{-1}) south-north component of the horizontal wind vector. This implies that the model is predicting weaker and/or less frequent easterly and northerly winds than the observed data suggest. The values for predicted standard deviations (P_{std} and O_{std}) vary but the overall predictions are reasonable. Wind speed, ambient temperature

and relative humidity are smaller, whereas the U and V-components are larger for the modelled data. The correlation coefficient (r) is good (≥0.63) for all weather components, particularly for the temperature (0.91). For all variables besides temperature, $RMSE_S$ is smaller than $RMSE_U$, which is a characteristic of good models. The index of agreement (IOA) indicates good modelling results for all variables (≥0.77), in which the highest value is 0.88 for temperature.

The measures of skill show that the standard deviations of all weather components were successfully predicted. The ratio of $SKILL_V$ is between 0.74 for temperature and 1.19 for the V-component. The other two variables ($SKILL_E$ and $SKILL_R$) show that unsystematic and total RMSE values are always less than the standard deviation of the observations (SKILL values less than one), which indicates good modelling results.

6. 2. 3. 2. Whakatane

The scatter plots of observed vs. modelled data for wind speed, wind direction, temperature and relative humidity are shown in Figure 6. 8a-d. Similar to White Island, the model calculates a slightly stronger mean wind speed (3.7 m s^{-1} vs. 3.4 m s^{-1}) for Whakatane. The predicted mean U-component is also weaker but only slightly (0.6 m s^{-1} vs. 0.7 m s^{-1}). The observed and modelled mean V-components have different signs again, although the difference is negligible. While the observation shows a more northerly wind component (-0.3 m s^{-1}), TAPM predicted a southerly wind component (0.3 m s^{-1}). The predicted standard deviations (P_{std}) are smaller than the observed values (O_{std}) for all weather components except the U-component. Overall, the calculated values for the correlation coefficient (r) are good to very good, in which temperature has the highest value (0.91). The results for the wind components are better than for the wind speed, which suggests that the data of modelled wind directions have a stronger correlation than the wind speed data. Another similar result to White Island is that all $RMSE_S$ values but temperature are smaller than $RMSE_U$, as it should be for an unbiased simulation. The values of IOA are good to very good (0.75–0.92) for all variables. The measures of $SKILL_V$ show that the standard deviations for all weather components were predicted well with values between 0.70 for temperature and 1.09 for the V-component. The values for $SKILL_E$ and $SKILL_R$ are all smaller than one, which indicate skill.

Table 6. 3 Meteorology statistics (WS = wind speed [ms^{-1}], U = west-east component [ms^{-1}], V = south-north component [ms^{-1}], T = ambient temperature [°C], RH = relative humidity [%]) for TAPM simulation of 2005.

Site: White Island													
Variable	**N**	**O_{mean}**	**P_{mean}**	**O_{Std}**	**P_{Std}**	**r**	**RMSE**	**$RMSE_S$**	**$RMSE_U$**	**IOA**	**$SKILL_V$**	**$SKILL_E$**	**$SKILL_R$**
WS	8760	5.3	5.7	3.5	3.0	0.63	2.91	1.69	2.37	0.78	0.86	0.67	0.82
U	8760	2.6	1.2	4.9	5.1	0.76	3.71	1.68	3.30	0.85	1.05	0.68	0.76
V	8760	0.3	0.0	3.1	3.7	0.63	3.01	0.84	2.89	0.78	1.19	0.93	0.96
T	8760	14.1	15.6	3.4	2.5	0.91	2.11	1.85	1.02	0.88	0.74	0.30	0.62
RH	8760	81.0	79.1	13.6	10.4	0.63	10.85	7.26	8.06	0.77	0.77	0.59	0.80

Site: Whakatane													
Variable	**N**	**O_{mean}**	**P_{mean}**	**O_{Std}**	**P_{Std}**	**r**	**RMSE**	**$RMSE_S$**	**$RMSE_U$**	**IOA**	**$SKILL_V$**	**$SKILL_E$**	**$SKILL_R$**
WS	8684	3.4	3.7	2.2	1.7	0.59	1.82	1.21	1.37	0.75	0.78	0.63	0.84
U	8533	0.7	0.6	2.6	2.9	0.69	2.19	0.66	2.09	0.82	1.09	0.80	0.83
V	8533	-0.3	0.3	3.0	2.8	0.72	2.23	1.17	1.90	0.84	0.90	0.63	0.73
T	8684	14.3	14.5	5.4	3.8	0.91	2.57	2.02	1.58	0.92	0.70	0.29	0.47
RH	8684	80.4	76.5	13.7	12.0	0.66	11.44	6.96	9.08	0.79	0.88	0.66	0.84

Table 6. 3 continued.

Site: Auckland													
Variable	**N**	**O_{mean}**	**P_{mean}**	**O_{Std}**	**P_{Std}**	**r**	**RMSE**	**$RMSE_S$**	**$RMSE_U$**	**IOA**	**$SKILL_V$**	**$SKILL_E$**	**$SKILL_R$**
WS	8753	4.4	3.9	2.8	1.9	0.70	2.08	1.58	1.35	0.79	0.67	0.48	0.74
U	8537	1.3	1.0	3.9	3.3	0.79	2.42	1.34	2.02	0.88	0.84	0.52	0.62
V	8537	0.5	0.2	3.3	2.6	0.81	1.95	1.19	1.54	0.89	0.80	0.47	0.59
T	8109	15.3	15.5	4.3	2.8	0.88	2.37	1.91	1.40	0.88	0.65	0.32	0.55
RH	8749	78.9	80.9	11.7	11.9	0.68	9.70	4.19	8.74	0.81	1.02	0.75	0.83

Site: Wellington													
Variable	**N**	**O_{mean}**	**P_{mean}**	**O_{Std}**	**P_{Std}**	**r**	**RMSE**	**$RMSE_S$**	**$RMSE_U$**	**IOA**	**$SKILL_V$**	**$SKILL_E$**	**$SKILL_R$**
WS	8747	6.7	4.7	3.5	2.2	0.56	3.46	2.95	1.81	0.65	0.63	0.52	1.00
U	8611	-0.1	0.7	2.2	3.6	0.35	3.60	1.24	3.38	0.58	1.63	1.52	1.62
V	8611	-1.7	-1.2	7.0	3.5	0.85	4.47	4.06	1.88	0.81	0.50	0.27	0.64
T	8747	13.9	13.3	3.6	3.4	0.90	1.72	0.85	1.50	0.94	0.94	0.42	0.48
RH	8747	76.7	80.3	10.5	11.3	0.61	10.37	5.18	8.98	0.75	1.08	0.86	0.99

Table 6. 3 continued.

Site: Ruapehu													
Variable	**N**	**O_{mean}**	**P_{mean}**	**O_{Std}**	**P_{Std}**	**r**	**RMSE**	**$RMSE_S$**	**$RMSE_U$**	**IOA**	**$SKILL_V$**	**$SKILL_E$**	**$SKILL_R$**
WS	8760	4.0	4.3	2.3	2.1	0.60	2.03	1.12	1.70	0.77	0.91	0.73	0.87
U	8760	0.6	-0.3	3.9	3.5	0.86	2.15	1.19	1.78	0.91	0.91	0.46	0.56
V	8760	0.4	0.7	2.4	3.2	0.61	2.60	0.53	2.55	0.76	1.34	1.06	1.09
T	8760	7.7	6.7	5.1	4.2	0.90	2.51	1.67	1.87	0.93	0.83	0.37	0.49
RH	8760	84.8	81.1	15.9	21.8	0.34	22.42	9.17	20.46	0.58	1.37	1.29	1.41

Site: Rotorua													
Variable	**N**	**O_{mean}**	**P_{mean}**	**O_{Std}**	**P_{Std}**	**r**	**RMSE**	**$RMSE_S$**	**$RMSE_U$**	**IOA**	**$SKILL_V$**	**$SKILL_E$**	**$SKILL_R$**
WS	8751	3.3	3.4	2.2	1.6	0.62	1.76	1.26	1.23	0.76	0.70	0.55	0.79
U	8330	0.7	1.0	2.8	2.8	0.66	2.36	0.98	2.15	0.81	1.01	0.77	0.85
V	8330	0.1	0.4	2.9	2.2	0.79	1.79	1.17	1.35	0.87	0.76	0.47	0.62
T	8751	13.0	11.0	5.1	4.2	0.92	2.81	2.28	1.64	0.91	0.83	0.32	0.56
RH	8751	81.7	85.3	12.9	13.9	0.75	10.18	4.20	9.27	0.84	1.11	0.74	0.81

KEY: O = observation, P = model prediction, mean = arithmetic mean, Std = standard deviation, r = Pearson correlation coefficient (0 = no correlation, 1 = exact correlation), RMSE = root mean square error, $RMSE_S$ = systematic root mean square error, $RMSE_U$ = unsystematic root mean square error, IOA = index of agreement (0 = no agreement, 1 = perfect agreement), $SKILL_V$ = (P_{Std}/O_{Std}) (near to 1 shows skill), $SKILL_E$ = ($RMSE_U/O_{Std}$) (<1 shows skill), $SKILL_R$ = ($RMSE/O_{Std}$) (<1 shows skill).

6. 2. 3. 3. Auckland

The scatter plots of observed vs. modelled data for wind speed, wind direction, temperature and relative humidity are presented in Figure 6. 9a-d. TAPM predicts a slightly weaker mean wind speed (3.9 m s^{-1} vs. 4.4 m s^{-1}) and smaller U (1.0 m s^{-1} vs. 1.3 m s^{-1}) and V (0.2 m s^{-1} vs. 0.5 m s^{-1}) components than the observation. The mean observed and modelled U- and V-components have the same sign, suggesting that the winds (in terms of strength and frequency) are from the same quadrant (south-west) for both observation and prediction. Correlation coefficient (r) and index of agreement (IOA) for all weather components are well to very good (0.70–0.88 and 0.79–0.89). The correlation coefficient (r) for the wind components (U, V) is better than for the wind speed. Consequently, the prediction of wind direction is more accurate than for wind speed. The systematic part of RMSE for wind speed and temperature are larger than the unsystematic part, which is not a good characteristic. The measures of skill show that the standard deviations of all weather components were predicted well with their ratio ($SKILL_V$) between 0.65 for the ambient temperature and 1.02 for the relative humidity. The other two variables ($SKILL_E$ and $SKILL_R$) show that unsystematic and total RMSE values are all less than the standard deviation of the observations (SKILL values less than one), which indicates good modelling results.

6. 2. 3. 4. Wellington

The scatter plots of observed vs. modelled data for wind speed, wind direction, temperature and relative humidity are shown in Figure 6. 10a-d. TAPM calculates a strong underestimation (4.7 m s^{-1}) for the mean wind speed against the observation (6.7 m s^{-1}) at Wellington. The mean observed and predicted west-east components (U) have a different sign. While the model predicts a westerly wind component (0.7 m s^{-1}), the observation data shows a slight easterly wind component (-0.1 m s^{-1}). The results for the south-north (V) wind component are a little better. There is a slightly lower value for the V-component of the model (-1.2 m s^{-1} vs. -1.7 m s^{-1}), which means that the model is predicting weaker and less frequent northerly winds than suggested by the observation data. The correlation coefficient (r) of the U-component (0.35) is not satisfactory, since the value is closer to zero than to one. The r-values for wind speed (0.56) and relative humidity (0.61) are satisfactory, whereas the values for the U- and V-component (0.85 and 0.90) indicate good model results.

The values for the index of agreement (IOA) of all components are well to very good and are between 0.58 for the U-component and 0.94 for temperature. For all variables other than wind speed and V-component, $RMSE_S$ is smaller than $RMSE_U$, which represent good values for model results. The values of $SKILL_V$ vary between 0.50 for the V-component and 1.63 for the U-component, compared to the ideal value of 1.0. The best results are temperature (0.94) and relative humidity (1.08). Although the majority of the other two skill variables ($SKILL_E$ and $SKILL_R$) show values less than zero, there are some values equal to or larger than one.

6. 2. 3. 5. Ruapehu

The scatter plots of observed vs. modelled data for wind speed, wind direction, temperature and relative humidity are presented in Figure 6. 11a-d. TAPM predicts a slighter stronger wind speed (4.3 m s^{-1}) and V-component (0.7 m s^{-1}) than the observations (4.0 m s^{-1} vs. 0.4 m s^{-1}). The observed (0.6 m s^{-1}) and predicted (-0.3 m s^{-1}) west-east (U) wind components have different signs, indicating that the model predicted a more easterly wind component, while the observation recorded more westerly winds. The correlation coefficient (r) indicates well to very good model results (0.60–0.90) for most weather components. The value for the relative humidity of 0.34, however, is not considered to be a good result. The values for index of agreement (IOA) are between 0.76 for the V-component and 0.93 for temperature, which represent good to very good results for predictions. All values of $RMSE_S$ are smaller than $RMSE_U$, which, as mentioned earlier, is a good characteristic feature of models. The measures of skill show that the standard deviations of all weather components were predicted well with their ratio ($SKILL_V$) between 0.83 for temperature and 1.37 for the relative humidity. The two other variables ($SKILL_E$ and $SKILL_R$) show that unsystematic and total RMSE values are on the whole less than the standard deviation of the observations (SKILL values less than one), which indicates good modelling results. The values for the V-component and the relative humidity are larger than one.

6. 2. 3. 6. Rotorua

The scatter plots of observed vs. modelled data for wind speed, wind direction, temperature and relative humidity are presented in Figure 6. 12a-d. The predicted means for wind speed (3.4 m s^{-1}), as well as the two wind components (U=1.0 m s^{-1}, V=0.4 m s^{-1}), are slightly overestimated in comparison to the observed data (WS=3.3 m s^{-1}, U=0.7 m s^{-1}, V=0.1 m s^{-1}). The two components U and V for the measurements and the model have the same sign, which suggest that overall the winds come from the same quadrant (south-west). The correlation coefficient (r) reached good and very good values (0.62–0.92) for all variables. The values of $RMSE_S$ are smaller than $RMSE_U$ for the two wind components U and V, as well as for the relative humidity. For wind speed, $RMSE_S$ is slightly larger than the $RMSE_U$ value, whereas the difference for the ambient temperature is much larger. The values of IOA show good and very good results for all components (0.76-0.91). All measures of skill show good to very good results. The values for $SKILL_V$ vary between 0.70 for wind speed and 1.08 for the relative humidity, compared to the ideal value of 1.0. As was expected, the values for the other two skill variables are all less than zero and indicate skill.

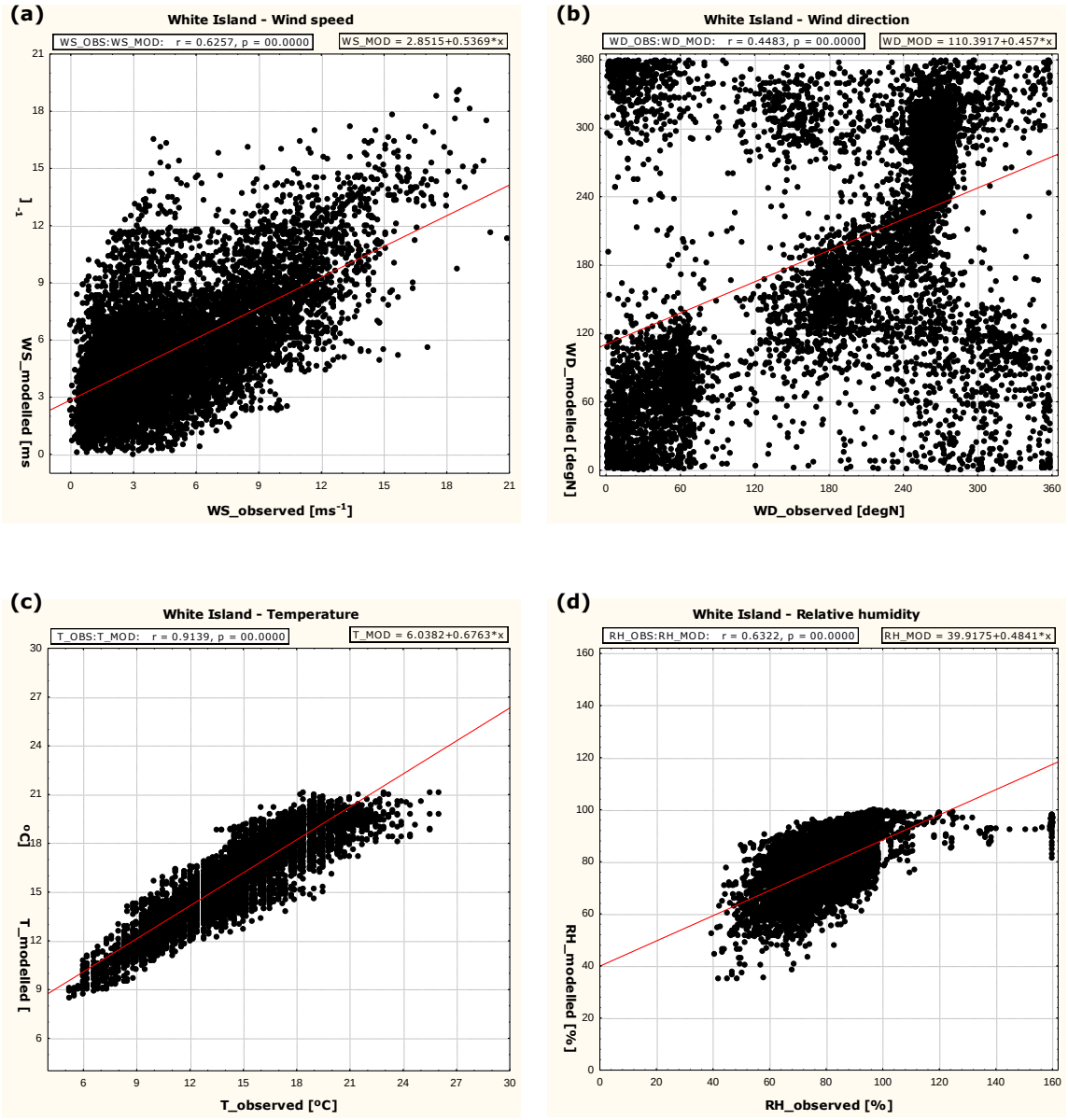

Figure 6. 7 Scatter plots of model predictions vs. observed data for wind speed (a), wind direction (b), temperature (c) and relative humidity (d) for White Island.

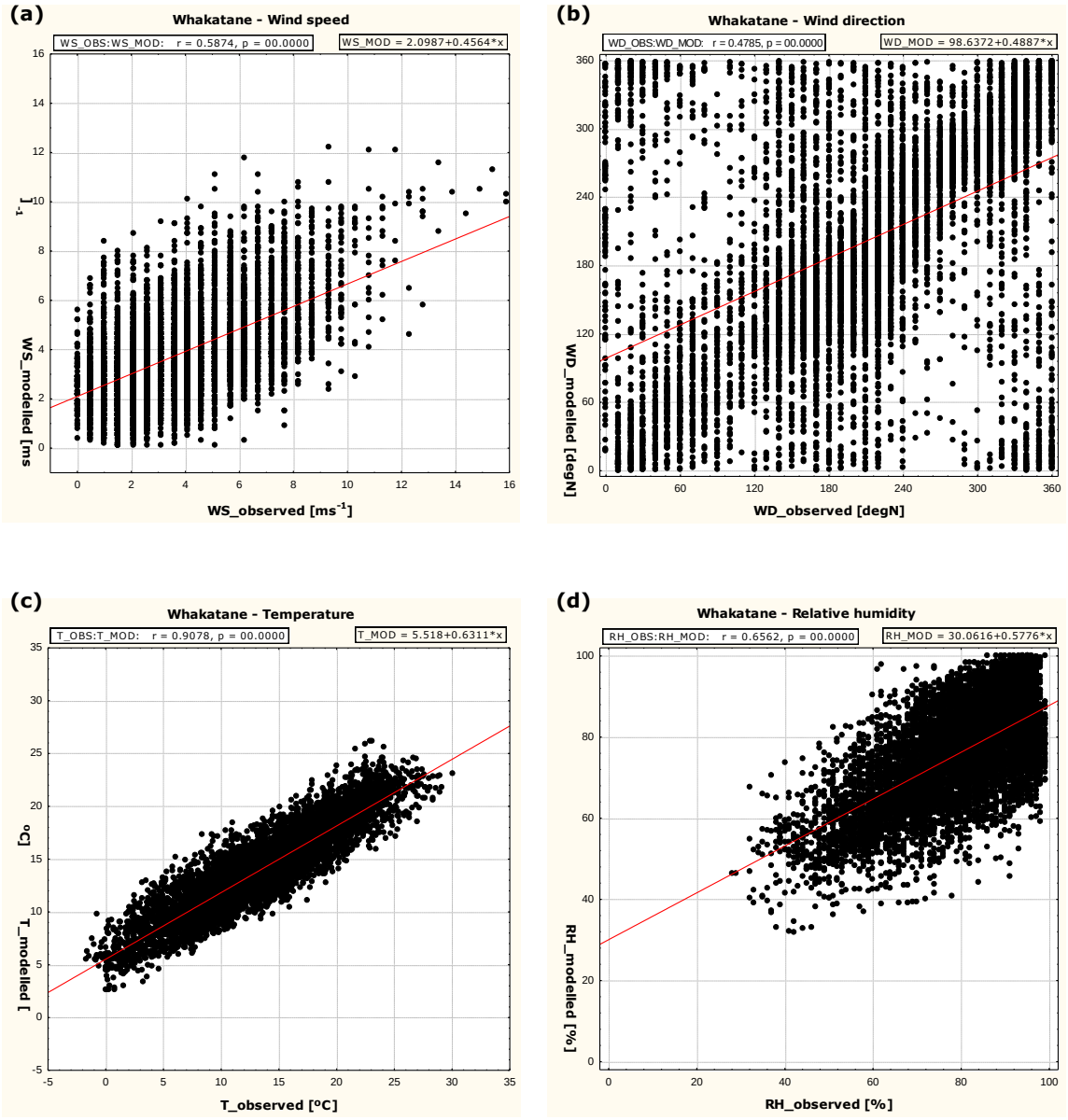

Figure 6. 8 Scatter plots of model predictions vs. observed data for wind speed (a), wind direction (b), temperature (c) and relative humidity (d) for Whakatane.

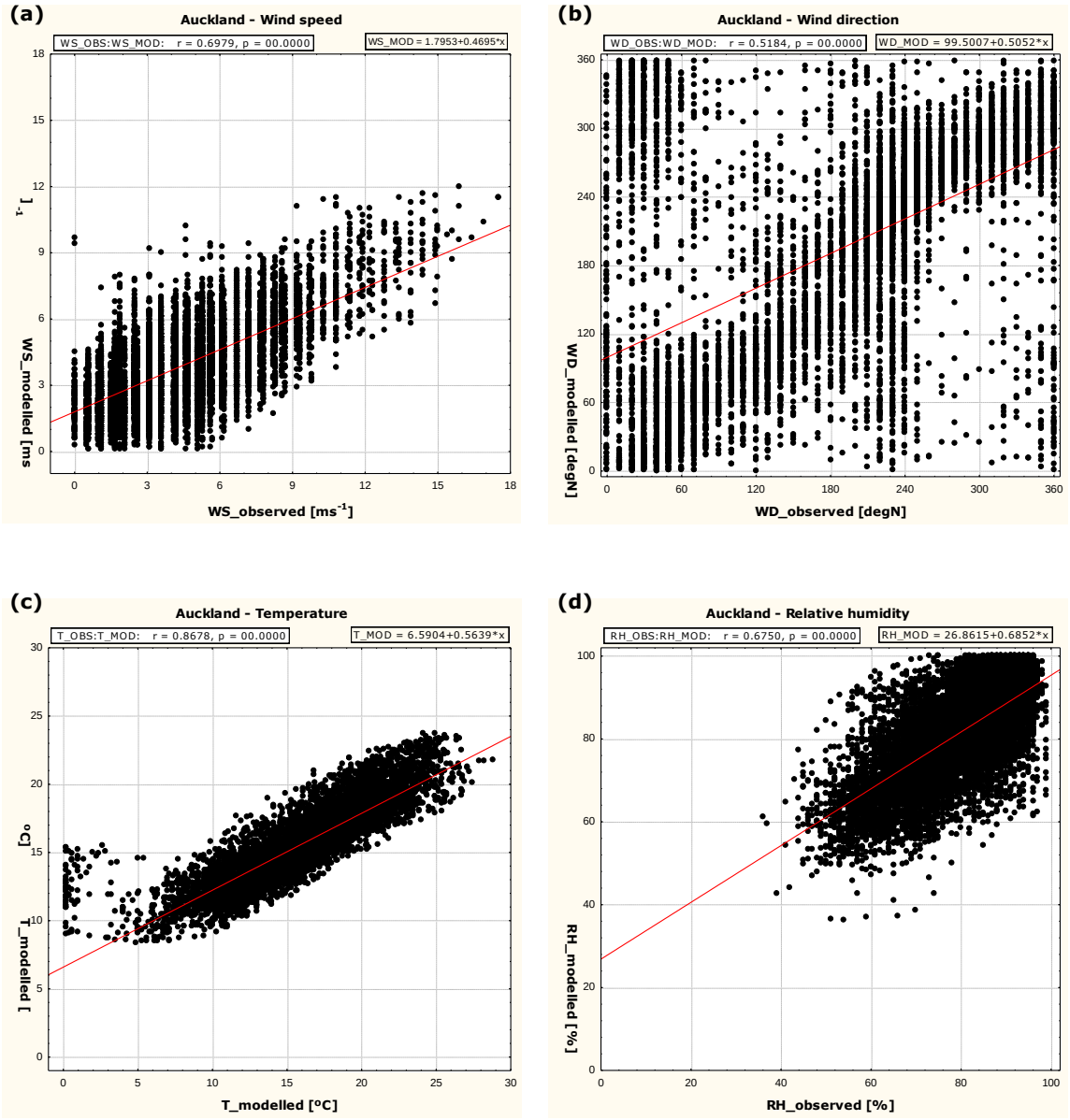

Figure 6. 9 Scatter plots of model predictions vs. observed data for wind speed (a), wind direction (b), temperature (c) and relative humidity (d) for Auckland.

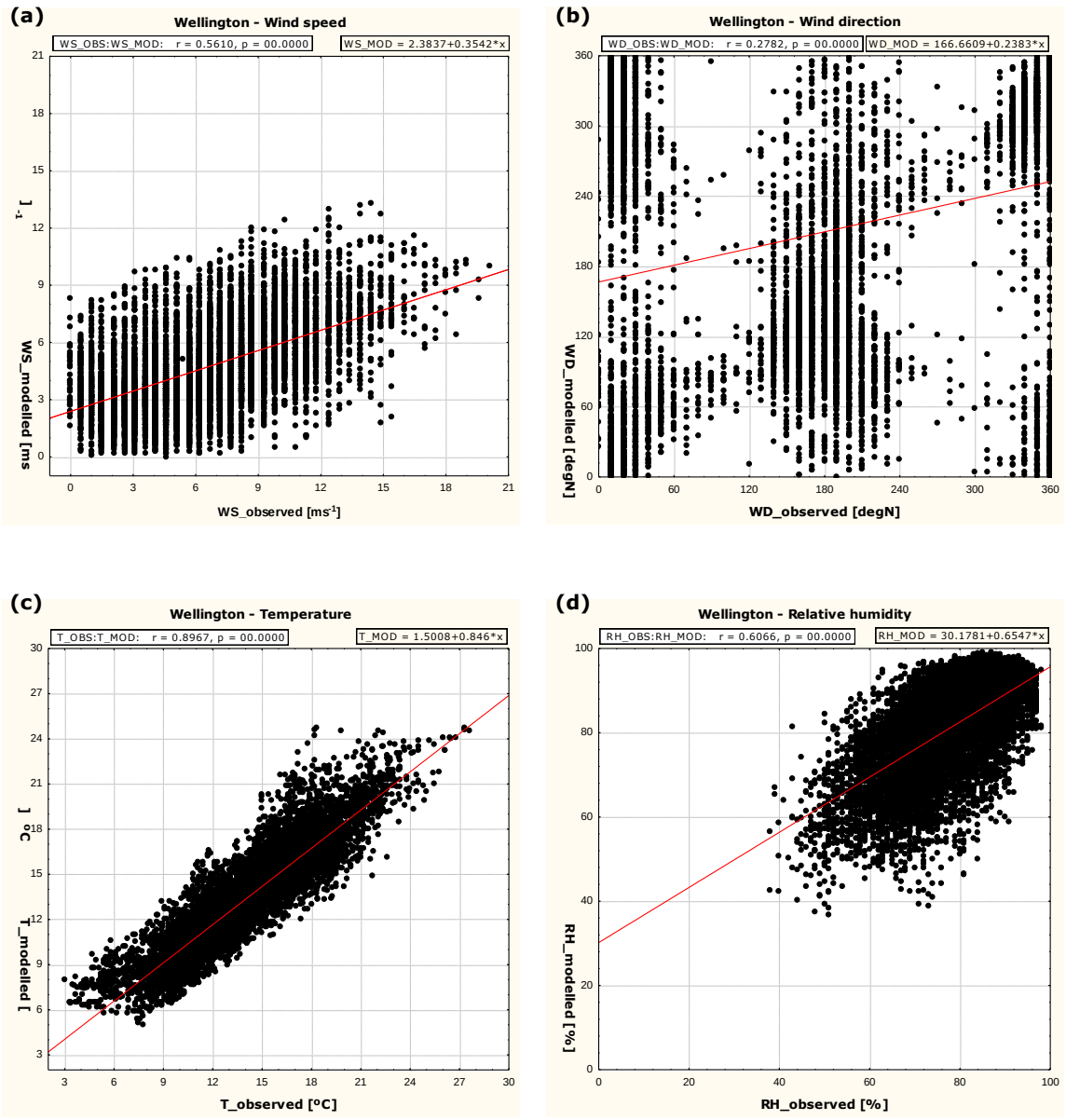

Figure 6. 10 Scatter plots of model predictions vs. observed data for wind speed (a), wind direction (b), temperature (c) and relative humidity (d) for Wellington.

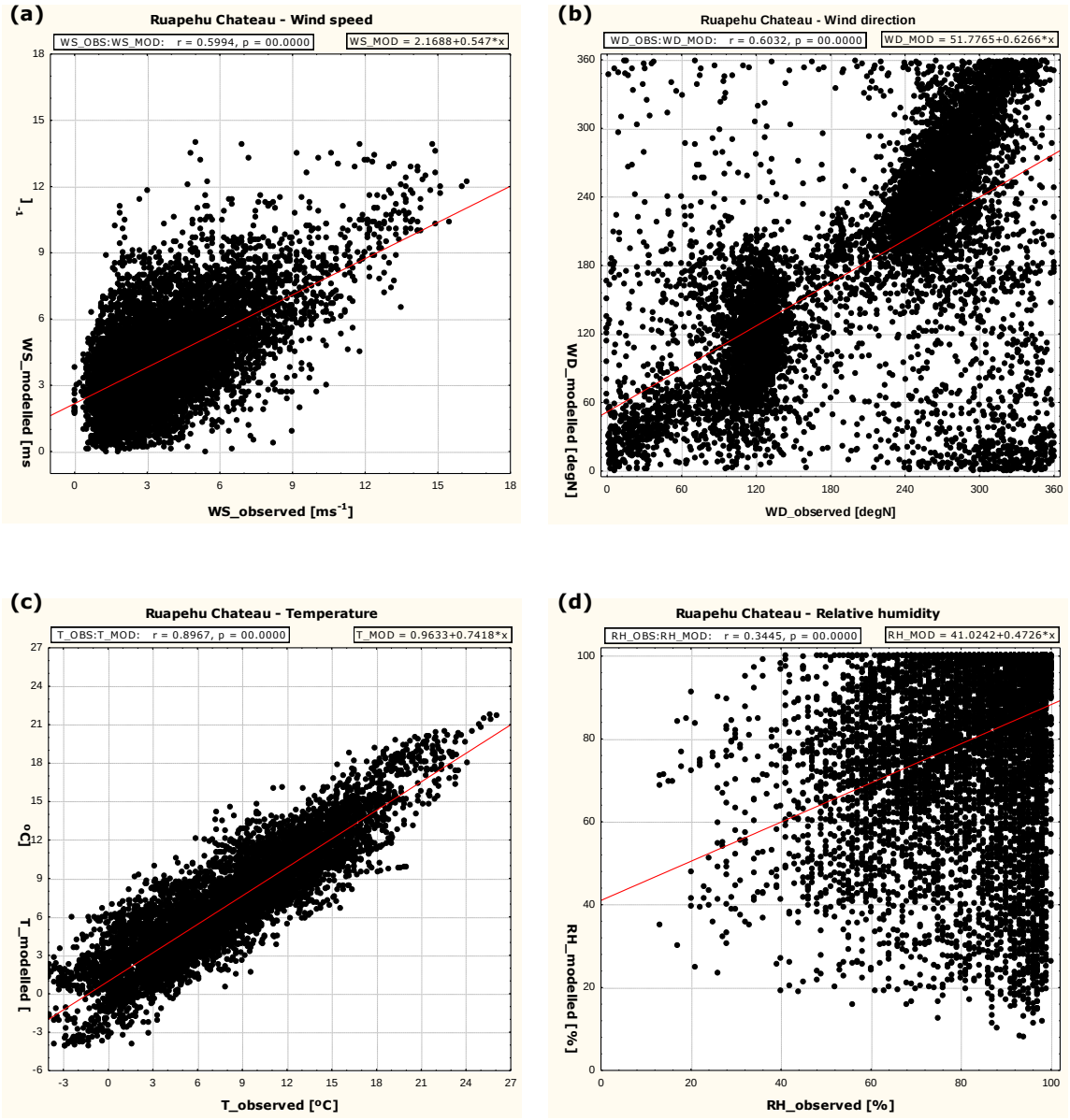

Figure 6. 11 Scatter plots of model predictions vs. observed data for wind speed (a), wind direction (b), temperature (c) and relative humidity (d) for Ruapehu.

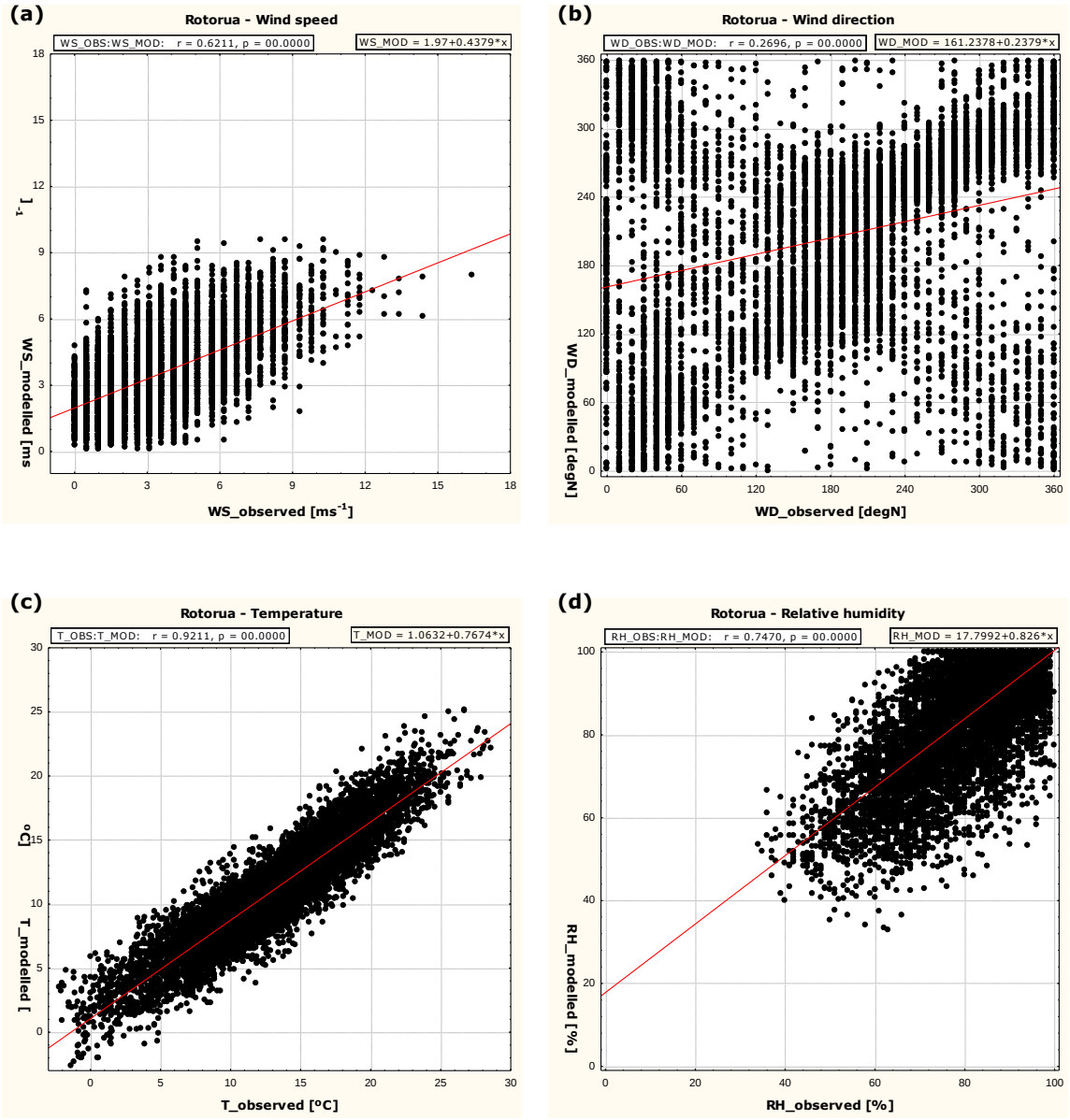

Figure 6. 12 Scatter plots of model predictions vs. observed data for wind speed (a), wind direction (b), temperature (c) and relative humidity (d) for Rotorua.

6. 3. Comparison of model results with previous TAPM studies

Several meteorological models have been used and model evaluations have been given during the last two decades, such as the Colorado State University (CSU) model, the MM5 model and the Regional Atmospheric Meteorological System (RAMS). Luhar et al. [2004] presented a short summary of comparison between some other modelling studies and TAPM. The statistical measures in this summary indicate that TAPM reached on average better values than any other model. The main focus of the model comparison was given to the index of agreement (IOA). IOA is the key performance statistics [Hurley et al. 2001], which verifies how closely the model's prediction matches field observations [Luhar et al. 2004]. Models with IOA values greater than 0.5 indicate good results for meteorology predictions [e.g. Hurley et al. 2001, 2002, Luhar et al. 2004].

There are several publications where TAPM was used to predict meteorology and air pollution in various regions in Australia, such as Kwinana [Hurley et al. 2001], Melbourne [Hurley et al. 2003] and Christchurch in New Zealand [Wilson & Zawar-Reza 2006]. In order for this study to evaluate TAPM performance, it is useful to compare the present calculated statistical measures with results of previous published TAPM verification studies. The main focus here is also on IOA. Table 6. 4 provides the average IOA values for all weather variables of the present study as well as for other TAPM studies. As can be seen, TAPM predicted the meteorology quite well for the North Island of New Zealand. The IOA ranged between 0.65–0.79 for the wind speed, 0.58–0.91 for the west-east component (U), 0.76–0.89 for the south-north wind components (V), 0.88–0.94 for the ambient temperature and 0.58–0.84 for the relative humidity. Regarding the high variability and fluctuations of wind data, predictions of meteorology by TAPM for 2005 compare quite well with the observed data at each of the weather stations over the North Island.

Table 6. 4 Averaged index of agreement (IOA) values for near-surface (10 m above the ground) meteorology from various TAPM studies.

TAPM version	Location	Duration	Variable	IOA	Reference
TAPM (v2.0)	Kwinana, West Australia (6 sites)	One year (1997)	WS U V T	0.67 0.88 0.80 0.96	Hurley et al. [2001, 2002]
TAPM (v2.0)	Cape Grim, Tasmania, Australia (1 site)	Dec 1997–Feb 1998	WS U V T RH	0.71 0.89 0.82 0.92 0.70	Hurley et al. [2002]
TAPM (v2.0)	Melbourne, Australia (11 sites)	July 1998	WS U V T	0.89 0.85 0.87 0.84	Hurley et al. [2002]
TAPM (v2.0)	Melbourne, Australia (11 sites)	December 1998	WS U V T	0.82 0.90 0.88 0.95	Hurley et al. [2002]
TAPM (v2.0) without meteorological data assimilation	Melbourne, Australia (8 sites)	Jul 1996–Jun 1997	WS U V T	0.85 0.86 0.92 0.95	Hurley et al. [2002]

Table 6. 4 continued. It is noted that the IOA values of Luhar et al. [2004] represent data calculated 30 m above the ground.

TAPM version	Location	Duration	Variable	IOA	Reference
TAPM (v2.0)	Perth, Australia (3 sites)	One year (1999)	WS U V T	0.78 0.91 0.90 0.95	Hurley et al. [2002]
TAPM (v2.0)	Dampier, West Australia (1 site)	One year (1999)	WS U V T RH	0.68 0.90 0.85 0.94 0.86	Hurley et al. [2002]
TAPM (v2.0)	Karratha, West Australia (1 site)	One Year (1999)	WS U V T RH	0.79 0.92 0.86 0.90 0.87	Hurley et al. [2002]
TAPM (v2.6)	Wagerup Refinery, West Australia (2 sites)	One year, Apr 2003–Mar 2004	WS U V T RH	0.65 0.79 0.92 0.97 0.87	Luhar et al. [2004]
TAPM (v3.0)	**North Island, New Zealand (6 sites)**	**One year (2005)**	**WS U V T RH**	**0.75 0.81 0.83 0.91 0.76**	**Present study**

6. 4. Summary

The Air Pollution Model (TAPM) was used to model the meteorology and the dispersion of pollutants, in which this chapter reports the results of the meteorological module of the model. The model predictions of near-surface (≤10 m) weather data, including wind speed, wind direction, ambient temperature and relative humidity) were extracted from various grid points, representing the area with meteorological monitoring sites, where weather data were available. The results of modelling were subsequently compared with recorded observations.

The period of January to December 2005 was selected as the period of model performance and model evaluation, as it encompasses a complete year with all seasons and existing weather conditions throughout the year. Additionally, this year was chosen to use the recorded weather data of the newly installed (November 2004) meteorological monitoring site on White Island. The individual localities were selected using the following factors:

(1) close proximity to point sources (White Island, Ruapehu)

(2) medium distance to the point sources (Whakatane, Rotorua)

(3) long distance to the point sources (Auckland, Wellington)

It was also important to evaluate the model results to see the accuracy of meteorology predictions distributed over a large region of the North Island or the total area modelled, respectively. These localities, among others, were later also chosen for pollution predictions and health hazard assessment for the population, particularly for the main urban areas.

The model results were extracted from the two innermost grid domains (10,000 and 3500 m grid spacing), depending on the distance of extracted grid point to the grid centre. Model evaluation was performed using various statistical measures, including arithmetic means and standard deviations of observed and modelled data, Pearson's Correlation Coefficient (r), root mean square error (RMSE), systematic RMSE, unsystematic RMSE, the index of agreement (IOA) and three SKILL values. The results of the statistical calculation are clearly arranged in Table 6. 3 and are presented in form of scatter plots.

The results of the present models are also compared with the results of previous TAPM performances. The comparison of results presented here and those of previous TAPM studies suggests a good TAPM performance for the present work and the marks are comparable to other near-surface meteorology predictions by TAPM.

As noted by Luhar et al. [2004], the model performance depends partly on the complexity of the studied area. It is emphasised that the published reports of previous TAPM results comprise much smaller areas, whereas TAPM performance presented here includes a large region and the individual localities have characteristic and different complexities. The comparison of the individual localities in this work with other TAPM studies, however, indicates good modelling and equivalent results.

Chapter 7: Results of annual SO_2 and PM_{10} dispersion modelling

7. 1. Introduction

As introduced in chapter 5, different input data for emission rate, gas exit velocity and gas exit temperature were used for dispersion modelling of sulphur dioxide (SO_2) and particulate matter (PM_{10}) from White Island and Ruapehu volcanoes. The different dispersion scenarios were performed for the entire year of 2005. Due to computer capacity, each model was run over a period of three months: January-March, April-June, July-September and October-December. This chapter gives detailed information on chosen input parameters, explains the calculations used for unit conversion and presents and discusses the results of the modelled plume dispersion scenarios.

7. 2. Summary of TAPM input parameters for modelled scenarios

Three nested grid domains of 50 x 50 x 25 points with horizontal grid spacing of 30,000 m (Grid 1), 10,000 m (Grid 2) and 3500 m (Grid 3) were used for annual modelling. Images of the three grids for White Island and for Ruapehu modelling are shown in Figures 7. 1. The 25 vertical levels in both parts are: 10, 25, 50, 100, 150, 200, 250, 300, 400, 500, 600, 750, 1000, 1250, 1500, 1750, 2000, 2500, 3000, 3500, 4000, 5000, 6000, 7000 and 8000 m. The model scenarios 1-3 correspond to quiescent degassing of SO_2, in which the input value for the emission rate in three of four model scenarios is 15,000 g s^{-1}, which is equivalent to the highest known emission rate of 1300 Mg d^{-1} measured on White Island in November 1983 by Rose et al. [1986]. Similar and even higher emission rates were calculated several times during the last phase of activity on Ruapehu in 1995-96 [Christenson 2000]. This input value was chosen to see the possible spreading of the plumes dispersion during phases of increased volcanic activity and to compare the amplified related hazard of SO_2 dispersion to cities and environment surrounding the volcanic vents. Lower values were used during previously performed test modelling and are considered to be non-relevant for distal plume concentrations from the outset.

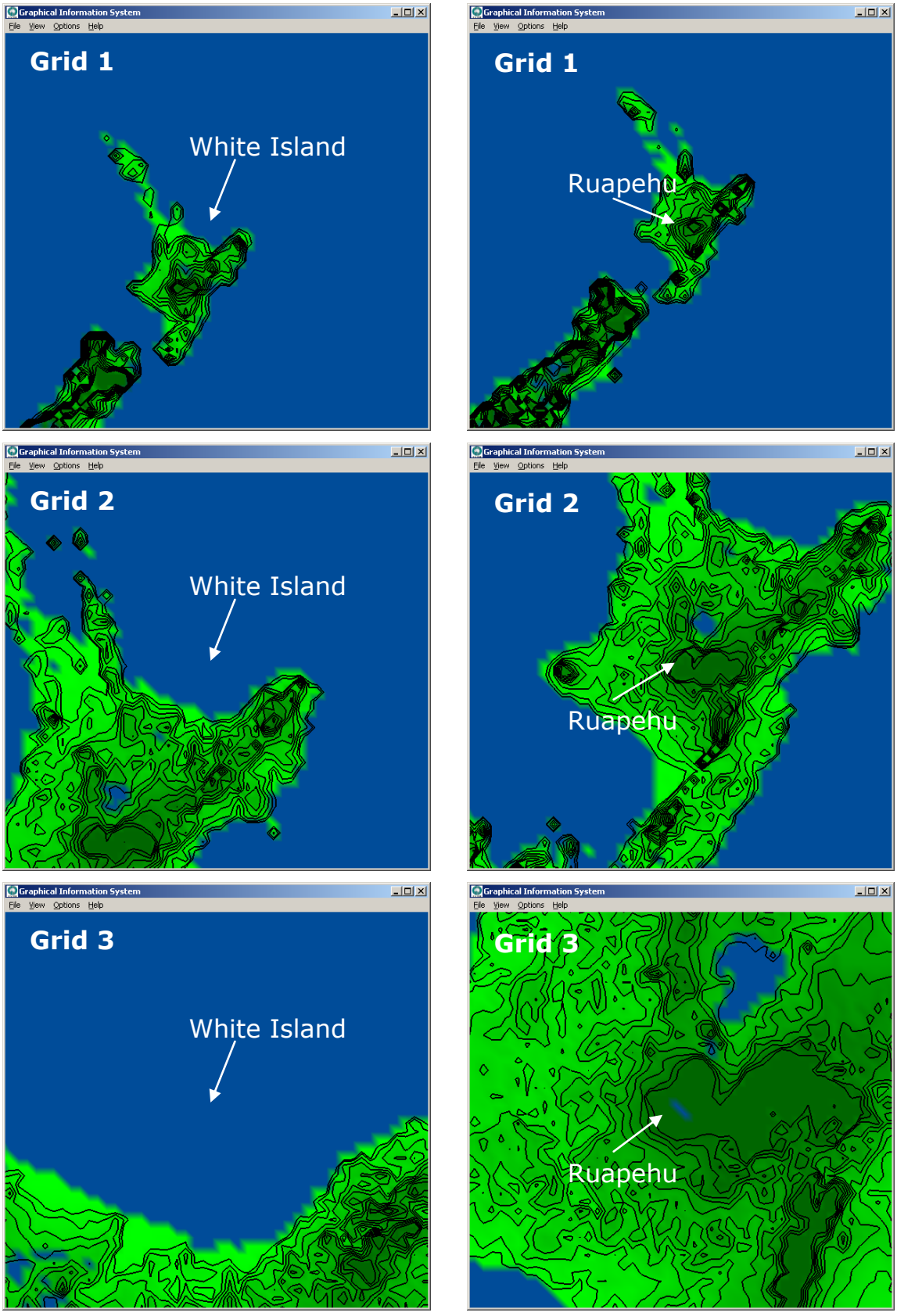

Figure 7. 1 The annual dispersion of SO2 and PM10 from White Island and Ruapehu volcanoes was modelled with a tripled nested grid of 50 x 50 with horizontal grid spacings of 30,000 m (Grid 1), 10,000 m (Grid 2) and 3500 m (Grid 3).

Different gas exit velocities and gas exit temperatures were chosen to see differences in modelled plume dispersion. Gas temperature at fumarolic vents is measured regularly, and the input parameters of 373 and 773 K for modelling are used from published data [e.g. Rose et al. 1986, Giggenbach & Sheppard 1989, Christenson 2000]. The chosen input parameters of the gas exit velocities of model scenarios 1-3 are based on personal assumptions and visual observations. Since the gas exit velocity may vary, two different input parameters were chosen. A gas exit velocity of 1 m s^{-1} was chosen for models 1, 2 and 5 and 0.1 m s^{-1} was used in model 3. The selection of the latter parameter was also chosen, because plume rise in the modelled scenario of 21/22 November 2006 (chapter 9) was very high, reaching elevations of more than 1000 metres, which is more than twofold the height as determined during airborne plume measurements with the contouring method.

Scenario 4 was chosen to model a situation of high volcanic activity, in which puffs are released from the vent. The input parameter for the emission rate is used from observations and reports of the explosive activity phases of Ruapehu volcano in 1995/96. The SO_2 emission rate was defined as 170,000 g s^{-1}, which corresponds to an emission rate of c. 14,700 Mg d^{-1}. Such enormous amounts of SO_2 emission were also reported from the last activity phase of Ruapehu volcano on 13 October 1995 (15,800 Mg d^{-1}) and 17 October 1995 (14,000 Mg d^{-1}) by Christenson [2000]. It is not expected that such enormous emission rates of 15,000 Mg d^{-1} can be released continuously from volcanic vents, but at intervals of several hours. Cronin et al. [2003] reported that dry-magmatic eruptions probably took place between 13 and 17 October 1995. Therefore, intervals of five hours were chosen for model 4. The generation of puffs from the volcanic crater do not originate from the whole crater but from a smaller single vent along the crater floor. Therefore the input parameter for the crater radius was changed from 300 m (models 1-3 and 5) to 50 m. The input parameter chosen for the gas exit velocity was 5 m s^{-1}.

Models 5 and 6 were performed to see the dispersion of particulate matter with a maximum aerodynamic diameter of 10 µm (PM_{10}). Model 5 corresponds to a quiescent degassing scenario, where an input value of 20 g s^{-1} was chosen and which is equivalent to an emission rate of 1.7 Mg d^{-1}. During particle measurements on White Island in November 1983 a value of 1.3 Mg d^{-1} was calculated Rose et al. [1986]. These authors also summarised the particle emission rate from other volcanoes and under reference of Casadevall et al. [1984] the highest measured

emission rate was determined to be 24 Mg d^{-1} at the Colima volcano in Mexico. Therefore, the equivalent value of 280 g s^{-1} was used as input parameter for the emission rate in model 6. However, release of the particles in model 6 occurs in form of puffs at intervals of five hours. All detailed information about input parameters used to model the different scenarios of plume dispersion of SO_2 and PM_{10} from White Island and Ruapehu volcanoes is summarised in Table 7.1.

Table 7. 1. Model configuration for annual meteorological and dispersion modelling

	Model version	TAPM V3.0.7	
Databases	Terrain data		
	Modelled period	• from 01/01/2005 to 31/03/2005 • from 01/04/2005 to 30/06/2005 • from 01/07/2005 to 30/09/2005 • from 01/10/2005 to 31/12/2005	
	Grid centre coordinates	• Latitude and Longitude - Lat. 37° 31' S - Long. 177° 10' E ⇒ World Geodetic System 1984 Equivalent Easting and Northing - 6400974 mN - 2878459 mE ⇒ NZ Map Grid 1949	
Meteorological Grid Parameters	Number of grid points	50 x 50	
	Outer grid resolution [m]	30,000	30,000
	Grid 2 resolution [m]	10,000	10,000
	Grid 3 resolution [m]	3,500	3,500
	Number of vertical levels (levels in italics are not included in output files)	25 (10, 25, 50, 75, 100, 150, 200, 250, 300, 400, 500, 600, 750, 1000, 1250, 1500*, 1750, 2000, 2500, 3000, 3500, 4000, 5000, 6000, 7000 and 8000 m*)	
Pollution Grid	Number of grid points	50 x 50	
	Outer grid resolution [m]	30,000	30,000
	Grid 2 resolution [m]	10,000	10,000
	Grid 3 resolution [m]	3500	3500
	Pollution Mode	• Chemistry mode with SO_2 • Tracer 2 for PM_{10} • Output 3-d concentration files • Point source • Use of EGM + LPM (Eulerian grid + Lagrangian near-source particle mode	

Table 7. 1. continued.

	Source Characterisations	Number of point sources	1
		Emission rate_ SO_2 *Model scenario 1* *Model scenario 2* *Model scenario 3* *Model scenario 4* Emission rate_ PM_{10} *Model scenario 5* *Model scenario 6*	 *15,000 g s^{-1}* *15,000 g s^{-1}* *15,000 g s^{-1}* *170,000 g s^{-1}* *20 g s^{-1}* *280 g s^{-1}*
		Source radius *Model scenario 1* *Model scenario 2* *Model scenario 3* *Model scenario 4* *Model scenario 5* *Model scenario 6*	 *300 m* *300 m* *300 m* *50 m* *300 m* *50 m*
		Emission rate_time *Model scenario 1* *Model scenario 2* *Model scenario 3* *Model scenario 4* *Model scenario 5* *Model scenario 6*	 *Constant* *Constant* *Constant* *Intervals of 5 hours* *Constant* *Intervals of 5 hours*
		Exit velocity *Model scenario 1* *Model scenario 2* *Model scenario 3* *Model scenario 4* *Model scenario 5* *Model scenario 6*	 *1 m s^{-1}* *1 m s^{-1}* *0.1 m s^{-1}* *5 m s^{-1}* *1 m s^{-1}* *5 m s^{-1}*
		Exit temperature *Model scenario 1* *Model scenario 2* *Model scenario 3* *Model scenario 4* *Model scenario 5* *Model scenario 6*	 *373 K* *773 K* *773 K* *773 K* *373 K* *773 K*

7. 3. Extraction and calculations of the SO_2 data

During post-processing of a simulation, after each model run, there were two forms of pollution data extracted that are important for the present study: gridded summary statistic and time series files. The gridded summary statistic files, contain the averaged and the maximum concentrations at ground level (≤10 m) of all grid points of each modelled grid domain for the entire period of modelling. Examples of each gridded summary statistic file, showing the average and maximum values, can be seen in Figure 7. 2. The complete set of these files is presented on the CD-ROM attached to this thesis. Although all modelling was performed with 25 vertical grid levels (see Table 7. 1), it must be emphasised that the gridded summary statistic files only show the concentration values at ground level (≤10 metres). They play the major part of present modelling results, as they represent the most important data regarding hazards to human health and most of the environment.

Additionally, the time series of individual grid points within the two innermost grid domains were extracted. These files contain information on the date, hour of the day, hourly model run time, the average concentration of the selected grid point, the maximum concentration on the entire grid field and the local maximum concentration for a 5x5 sub-grid region surrounding the selected grid point [Hurley 2005b]. The individual grid points represent certain locations in the North Island, including the sources of emission (White Island and Ruapehu volcanoes), all main urban areas in the North Island, two independent urban communities and one rural/remote area. The number of all grid points of each grid domain and the name of the corresponding location in the North Island are listed in Table 7. 2. These grid points are also marked in the analysed gridded statistic files. The relationship between the number of the grid points in the grid domain and the gridded summary statistic files from output data is explained in Figure 7. 3. The time series files only play a minor role in this chapter but some of these files are used for detailed pollution analysis in chapter 8. Due to the large size of the extracted files, there are only given in the CD-ROM attached to the thesis.

Finally, to see the vertical distribution of pollutants (up to 1500 m), the process of creating 3-d concentration files by TAPM were chosen and the corresponding files from the individual grid points were extracted as well. However, this data is not analysed further and the data are saved on the attached CD-ROM.

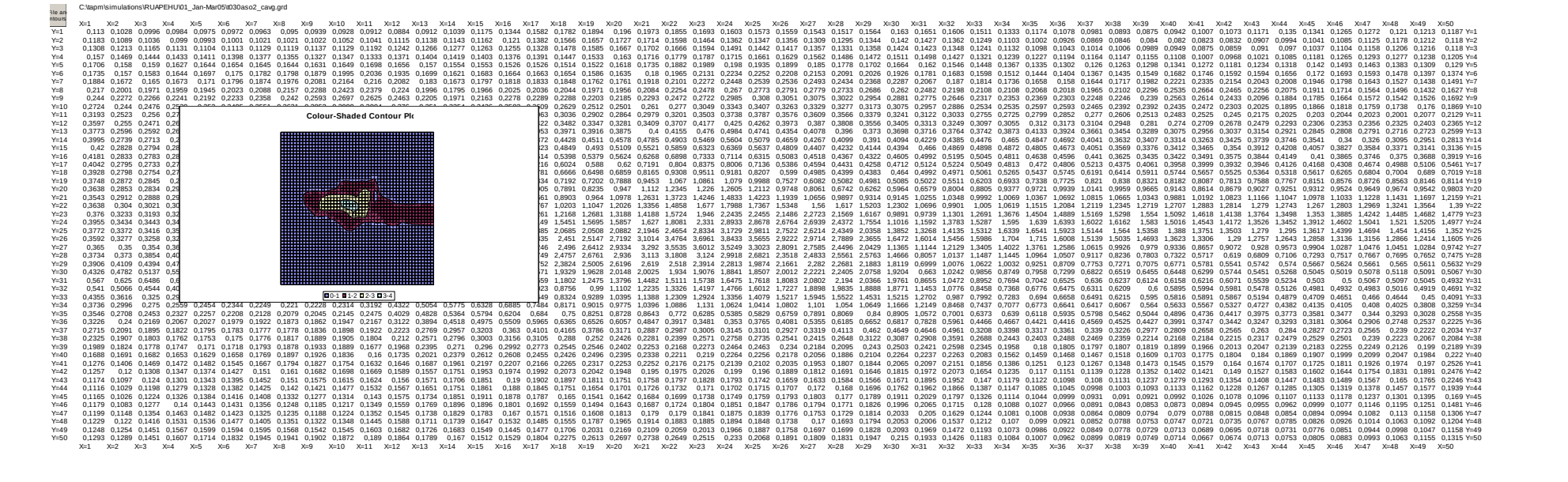

Figure 7. 2 Examples of gridded summary statistic files. The data show the average (upper image) and maximum concentration data (lower image) of model 3 from Ruapehu volcano during the period of January-March 2005.

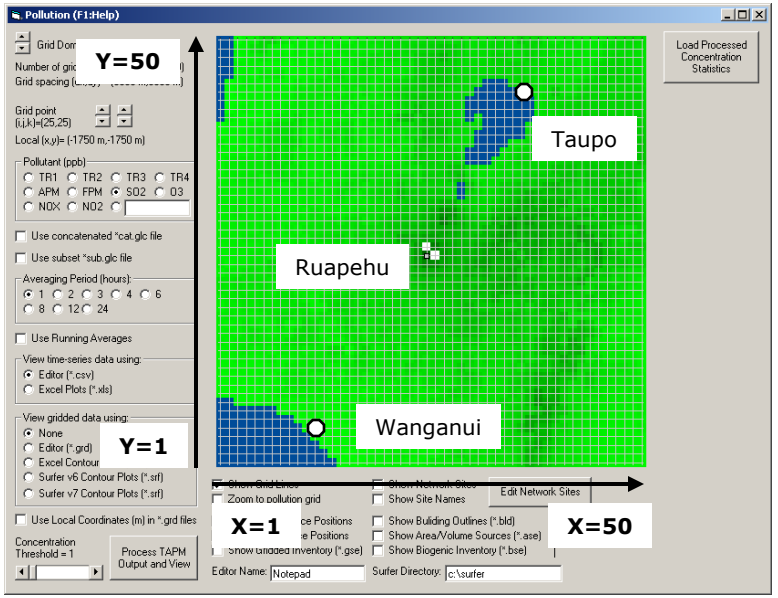

Figure 7. 3
The left image shows the 'Analyse Output - Pollution' window, whereas the image below is an example of a gridded summary statistic file, extracted from the Output-Pollution window. The two images show the same grid domain (Ruapehu, Grid 3).
The arrows on both images indicate the directions of the local coordinate system and the number of the horizontal grid points (X=west-east; Y=south-north). Thus, each grid point is defined by one X- and Y-value (X/Y). It is noted that the image of the gridded summary statistic file is a mirror image from the image in the 'Analyse Output - Pollution' window. There are shown the two examples for Taupo (37/44) and Wanganui (11/05).

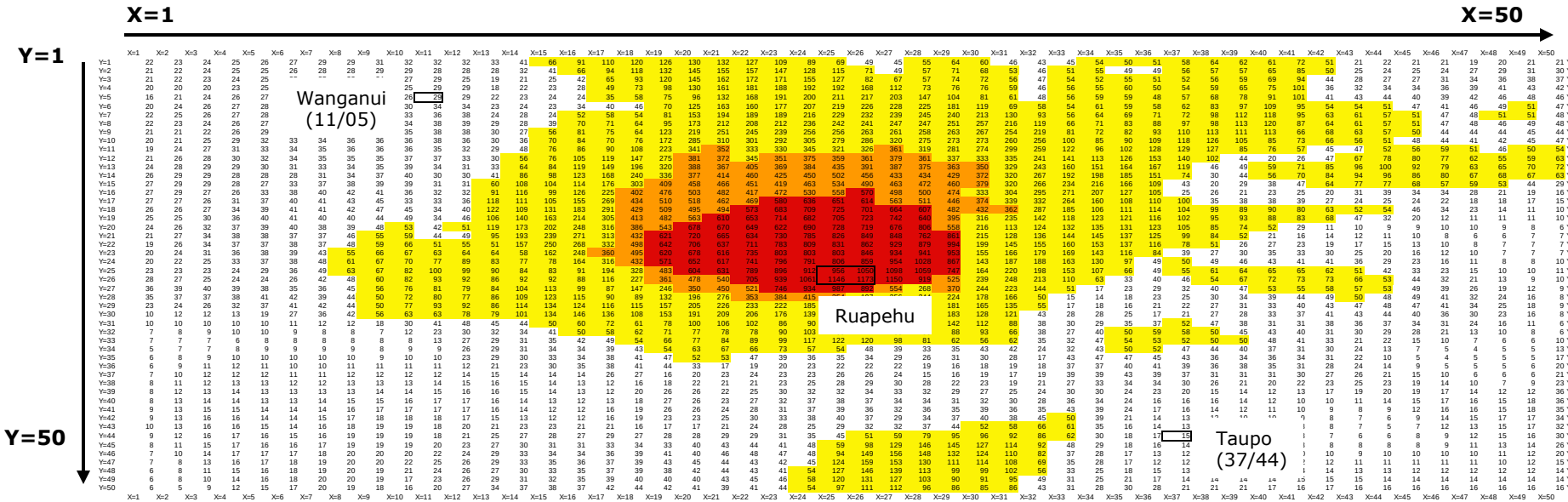

While three grid domains were used for annual modelling, the following results represent data from only the two innermost grids with a resolution (grid widths) of 10,000 and 3500 m, respectively. The resolution of the outermost grid (30,000 m grid width) is considered to be too low and is only included in the attached CD-ROM. In addition the areas covered by the two innermost grids are large enough for hazard assessment from present dispersion modelling. Generally, it can be said the higher the resolution, the better the modelled predictions [e.g. Luhar et al. 2004].

Table 7. 2. Grid points and corresponding locations in the North Island. The locations of White Island and Ruapehu volcanoes are not listed. They include four grid points in the centre of each grid domain: 25/25, 25/26, 26/25 and 26/26.

White Island volcano		**Ruapehu volcano**		**Location (North Island)**
Grid points Grid 2	**Grid point Grid 3**	**Grid point Grid 2**	**Grid point Grid 3**	
23/21	20/12	38/40		Whakatane
04/32				Auckland
		19/04		Wellington
15/13		29/32	37/44	Taupo
19/17	06/02	31/38		Rotorua
24/01		37/22		Napier
08/22		23/41		Hamilton
18/23	02/20	31/42		Tauranga
35/24	50/24	47/44		Hicks Bay
		25/14		Palmerston North
33/13		45/33		Gisborne
01/45		12/27		New Plymouth
				Whangarei
		21/18	11/05	Wanganui

The concentration units of the output data depend on the pollutant mode used for modelling. While the unit [µg m^{-3}] is given for the tracer mode (modelling for PM_{10}), the output unit from modelling for SO_2 concentration is given in parts per billion by volume (ppbv). Since this is not a SI unit, the output data are presented in [µg m^{-3}].

According to Seinfeld & Pandis [1998], the formula for conversion from a mixing ratio [ppbv] of a gas species into a gas concentration [µg m^{-3}] at any point in the atmosphere is based on the formula from the ideal gas law (Equation 7. 1), where p is the pressure, M_i is the molecular weight of gas species i, T is the temperature and R is the universal gas constant, which is defined to be 8.314 J K^{-1} mol^{-1}.

$$Concentration\ [\mu g\ \ m^{-3}] = \frac{pM_i}{RT} * Mixing\ \ ratio\ [ppm] \qquad (7.\ 1)$$

As mentioned earlier, the gridded summary statistic files of all three modelled grid domains with their average and maximum concentration data were extracted. The files of grid domains 2 and 3 were coloured according to defined concentration levels and are also saved on the CD-ROM. To get a better view of pollution-affected areas in the North Island, fairly accurate plume dispersions of all models and all periods, including the average and maximum concentration values, were projected onto DEM images. The size of the DEM images corresponds approximately to the extension of the two innermost grids used for modelling (Figure 7. 4 for White Island and Figure 7. 21 for Ruapehu).

7. 4. Results of SO_2 dispersion modelling from White Island volcano

7. 4. 1. Results of model 1 (373 K, 1 m s^{-1})

Figure 7. 5 to 7. 8 show the average and maximum SO_2 distribution of model 1 at grids 2 and 3. The average SO_2 concentration does not exceed 1.0 µg m^{-3} for most of the year. It only exceeds this concentration level during the October to December quarter along the east coast between Hicks Bay and Gisborne. A concentration of 5.0 µg m^{-3} is not reached. The maximum concentration shows similar results. While no concentration larger than 50 µg m^{-3} was found during the period from January to March 2005, the SO_2 ground concentration exceeded this value during the other three quarters in very few locations.

Main areas affected are between Hicks Bay Gisborne and Whakatane as well as Whakatane, Gisborne and Taupo. Two smaller regions, on Coromandel Peninsula and north-west of Rotorua, were affected between July and September. Additionally, the model results show two plume fans travelling north (April-June) and west (October-December) from White Island. A concentration of 350 µg m^{-3} is not reached during this model scenario.

The model output of grid 3 shows similar results. The average SO_2 concentration level of 1.0 µg m^{-3} is only exceeded in a small area in the south-east part of the grid domain and only during the period of October to December 2005. The main affected area of maximum concentration is a region in the south-east part of the grid domain, between Hicks Bay, Whakatane and Gisborne. Another affected location is the region around Rotorua in the south-west part of the grid domain. The concentration level of 5.0 µg m^{-3} for average concentrations and 350 µg m^{-3} for maximum concentrations was not reached in any of the four time periods.

7. 4. 2. Results of model 2 (773 K, 1 m s^{-1})

The results of model 2 are presented in Figures 7. 9 to 7. 12. Ground level concentrations for SO_2 of model 2 are the lowest among all modelled scenarios. The average concentrations at grid 2 did not reach the value of 1.0 µg m^{-3} during the year. The maximum ground level concentration of 50 µg m^{-3} was only exceeded at locations on the east-side of the North Island between Hicks Bay, Gisborne and Whakatane and only during the period of July to December. A SO_2 concentrations of 350 µg m^{-3} were not reached at all during the year.

The concentration distribution of grid 3 is similar to grid 2. While the average concentrations were less than 1.0 µg m^{-3} throughout all four modelled periods, the maximum SO_2 concentration only exceeded the value of 50 µg m^{-3} between April and December in the region south-east of White Island, between Hicks Bay, Gisborne and Whakatane. A concentration of 350 µg m^{-3} was never reached during this model scenario.

7. 4. 3. Results of model 3 (773 K, 0.1 m s^{-1})

Figure 7. 13 to 7. 16 show the average and maximum concentrations of SO_2 dispersion of model 3. TAPM calculated the highest SO_2 ground level concentrations

for scenario 3, however, the concentration levels of 5.0 µg m^{-3} and 350 µg m^{-3} for the calculated average and maximum concentrations were not reached during this model.

The main area affected during the period of January to March is the entire north-east side of the North Island between Hicks Bay and Gisborne. Another region that was influenced by the plume from White Island is the area west of White Island, between Coromandel Peninsula, Auckland and Hamilton. During the period of April to June the plume is found in the large region north of White Island, yet affects only the sea. From July to September the plume mostly reached ground concentrations of ≥50 µg m^{-3} in a large fan east of White Island and two smaller regions just south of Hamilton and west of Rotorua. Two small fans north and east of White Island as well as a larger region north of Gisborne were affected by ground level SO_2 concentrations of higher than 50 µg m^{-3} during the last quarter of the year.

The main area that is affected by modelled maximum SO_2 concentrations at ground level all year but April to June is again between Hicks Bay, Gisborne and Whakatane. Other regions, which are less affected, are located between Rotorua, Tauranga and Hamilton. During the period from April to June, the SO_2 plume is at ground level mainly over the sea, north and east of White Island. The largest part on land is found between Hamilton and Auckland. Large parts of the Coromandel Peninsula are affected during the months of July to September. During the same period the SO_2 plume hit the sea north-east, and particularly east of White Island. Besides of the fact that the SO_2 affects almost the whole north-east side of the North Island during the period of October to December, another distinctive feature are four distinctive plumes, which disperse in all four directions from White Island.

The average SO_2 concentration modelled in grid 3 rarely reached the ground level throughout the year. During the quarters of January to March and October to December, the plume affected an area in the south-east part of the grid domain, whereas from April to June, the plume is found north of White Island. No plume was modelled at ground level for the period of July to September.

The maximum ground concentrations affect large parts of the Bay of Plenty region for most of the year. Most affected area is the south-east side of the grid domain between Hicks Bay, Gisborne and Whakatane, but also areas between Whakatane, Rotorua and Tauranga are affected with changing expansions. The plume from White Island volcano travelled also north and reached ground level over the sea mainly between April and June and smaller areas during the second half of the year.

7. 4. 4. Results of model 4 (773 K, 5 m s^{-1})

Figure 7. 17 to 7. 20 show the average and maximum SO_2 distribution of model 4 at grid domains 2 and 3. The average SO_2 concentration exceeds the threshold value of 1.0 µg m^{-3} in grid 2 all year. The plumes in all periods show a distinctive west-east dispersion. The plumes usually form several fans, which disperse over different areas of the grid domain and also affect large parts of the North Island. The plume in the period from April to June is characterised by its covering of almost the whole region north of White Island. A concentration level of 5.0 µg m^{-3} is never reached in grid domain 2.

In grid 3, the modelled plumes cover different areas far away from the source. Apart from the period between April and June where most of the plumes cover an area north of White Island, the plumes reached ground level in the south-eastern and south-western part of the grid domain. The threshold value of 5.0 µg m^{-3} was only exceeded at two small areas south of Hicks Bay in the period of October to December.

The individual plumes of grid 2, containing the maximum SO_2 concentration, are characterised by covering most parts of the grid domain with concentrations of ≥50 µg m^{-3}. Consequently, the plume affects nearly all urban communities throughout the entire year. A concentration of 350 µg m^{-3} is exceeded in all periods apart January to March. However, these parts of the plumes do not reach the coast but affect small areas over the sea. The largest fan of ≥350 µg m^{-3} is found north of White Island during the period of April to June. In addition the next threshold value of 570 µg m^{-3} is exceeded during two periods (April-June and October-December), affecting very small areas near White Island.

The maximum concentration of SO_2 exceeding 50 µg m^{-3} covers large areas in grid domain 3 all year. The plumes in the individual periods formed several fans, which disperse over the entire modelled region. The most affected areas are found south of Whakatane, where the ground level concentrations exceed the threshold values of 350 and 570 µg m^{-3}.

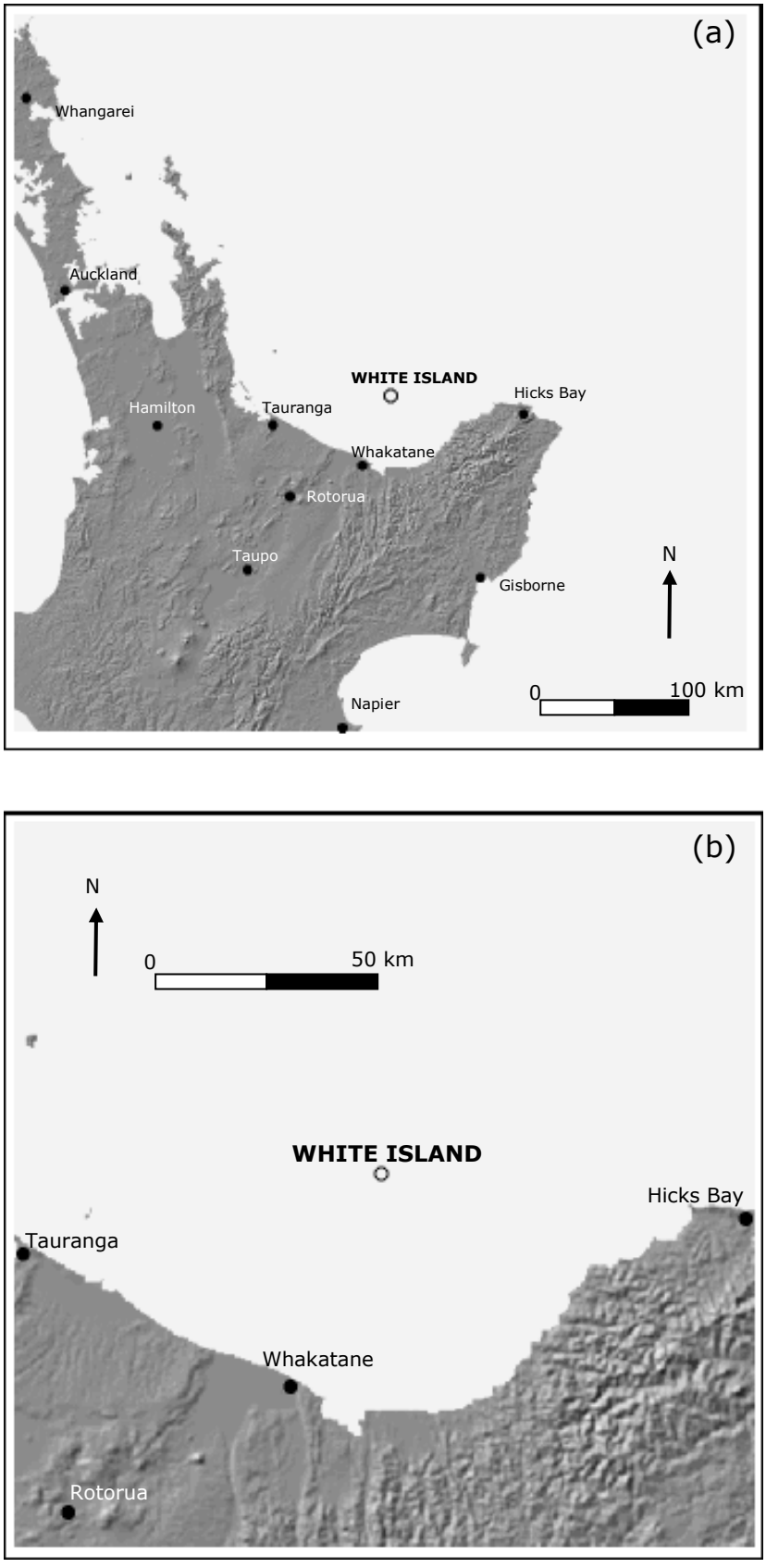

Figure 7. 4 DEM images of parts of the North Island. They correspond to two innermost grids of dispersion modelling from White Island volcano (Figure a = Grid 2 and Figure b = Grid 3).

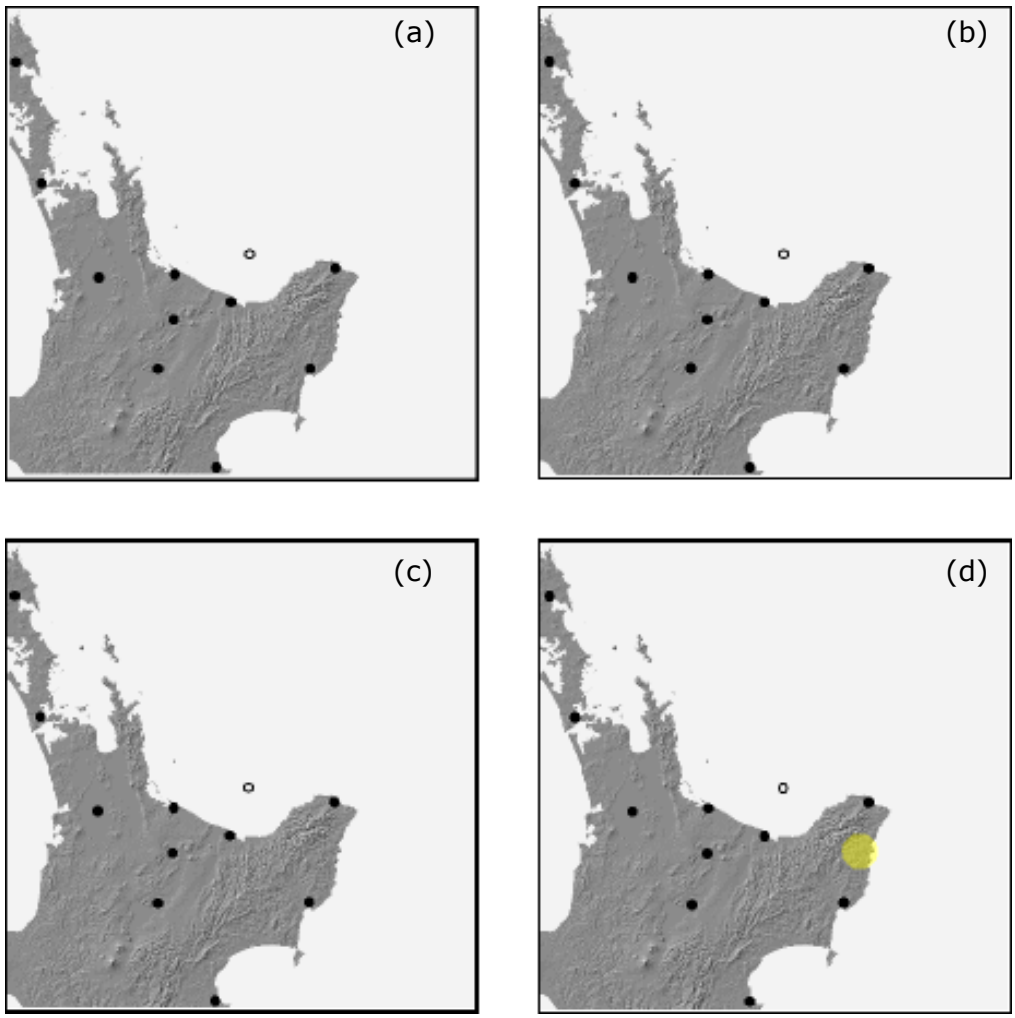

Figure 7. 5 White Island volcano - Model 1, Grid 2, SO_2 average

a) January - March 2005
b) April - June 2005
c) July - September 2005
d) October - December 2005

1.0 - 4.9 µg m^{-3}
5.0 - 9.9 µg m^{-3}
≥10.0 µg m^{-3}

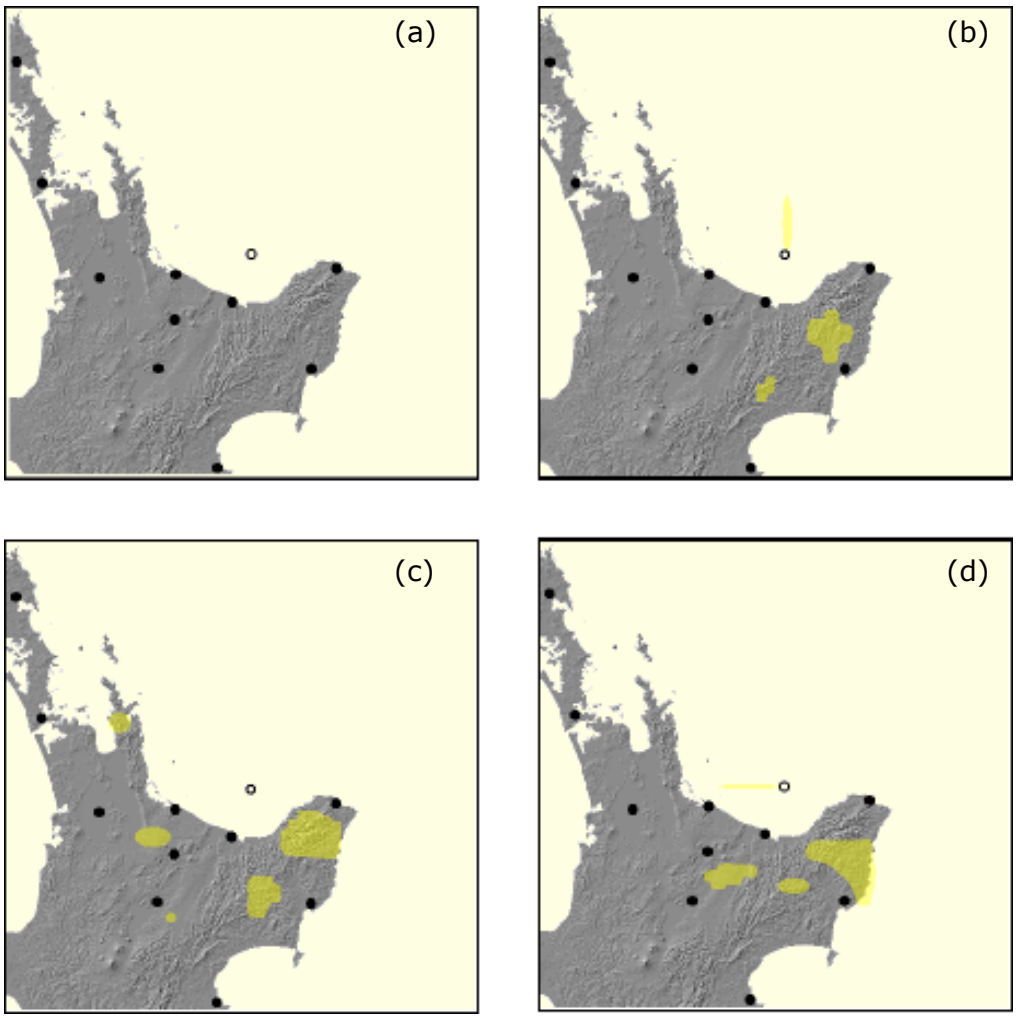

Figure 7. 6 White Island volcano - Model 1, Grid 2, SO_2 maximum

a) January - March 2005
b) April - June 2005
c) July - September 2005
d) October - December 2005

50 - 349 µg m^{-3}
350 - 569 µg m^{-3}
≥570 µg m^{-3}

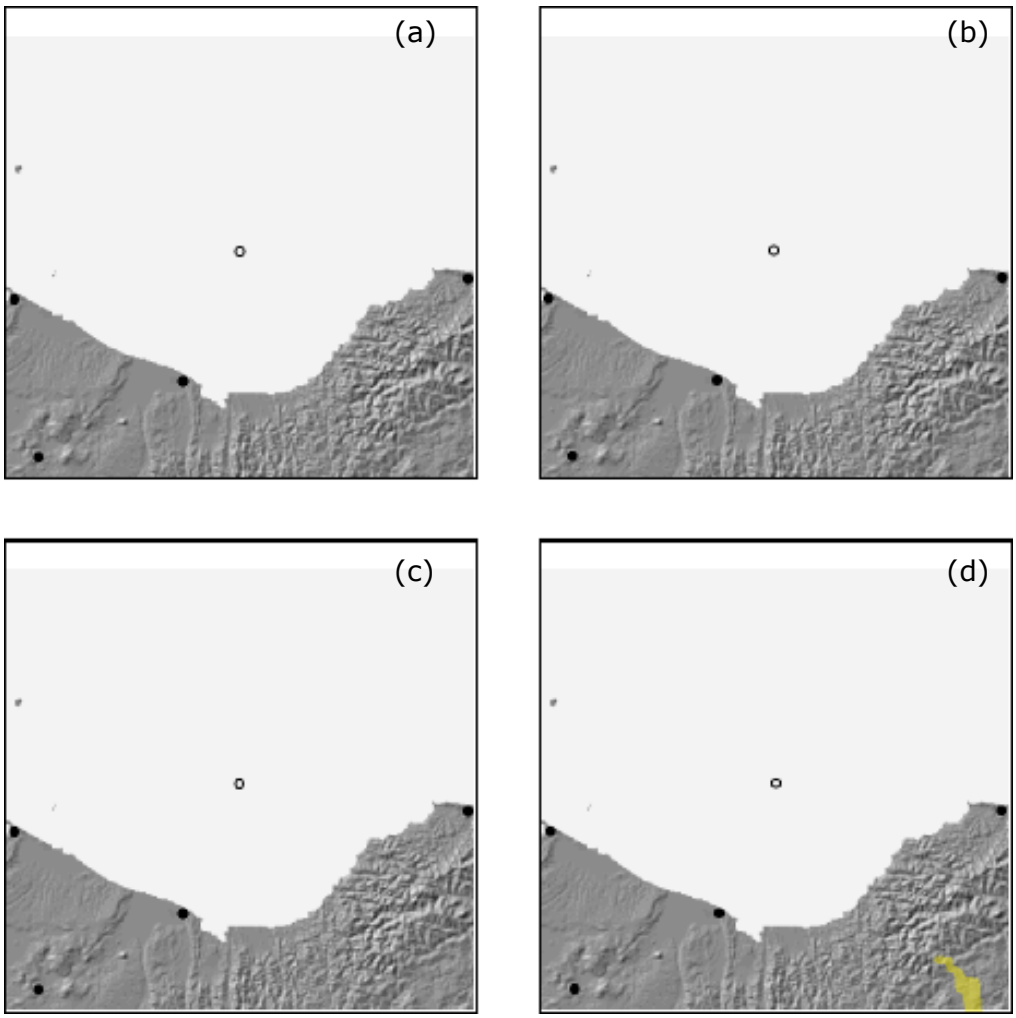

Figure 7. 7 White Island volcano - Model 1, Grid 3, SO_2 average

a) January - March 2005
b) April - June 2005
c) July - September 2005
d) October - December 2005

1.0 - 4.9 µg m^{-3}
5.0 - 9.9 µg m^{-3}
≥10.0 µg m^{-3}

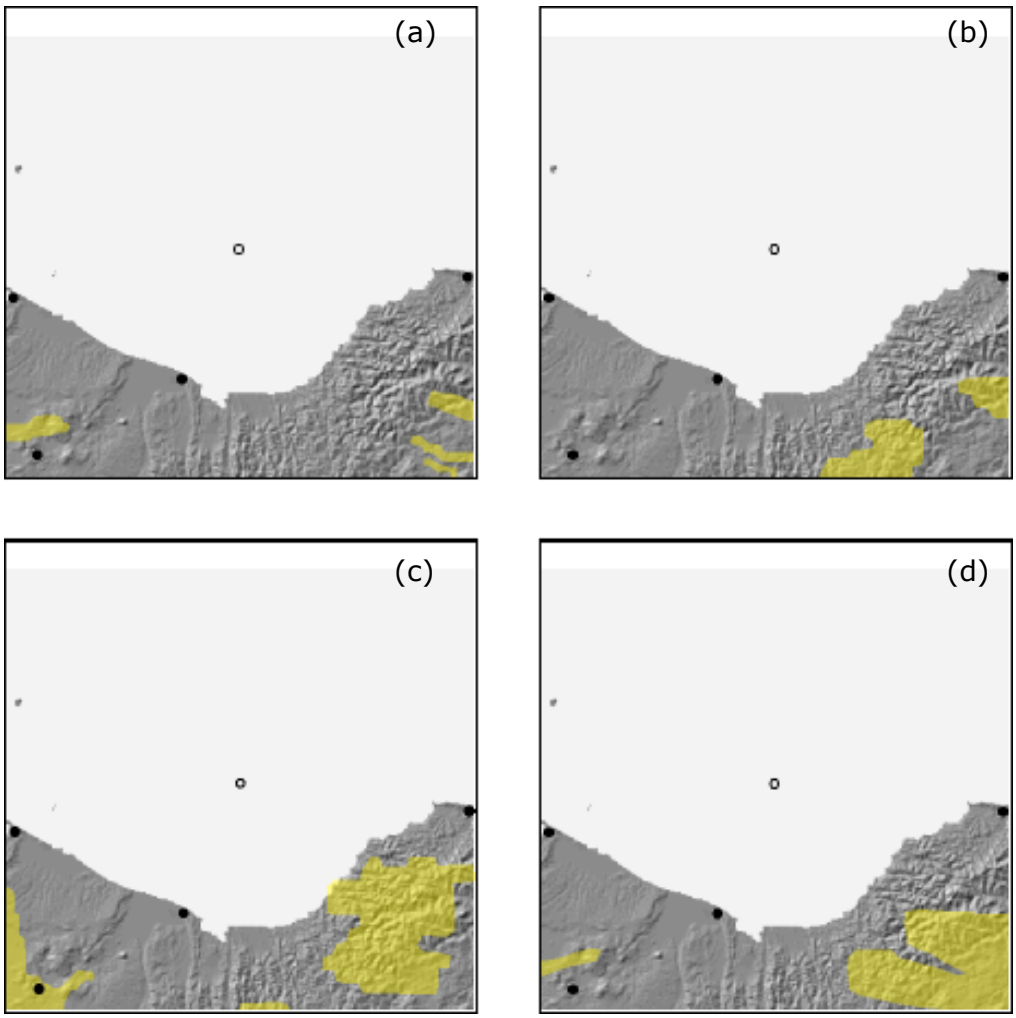

Figure 7. 8 White Island volcano - Model 1, Grid 3, SO_2 maximum

a) January - March 2005
b) April - June 2005
c) July - September 2005
d) October - December 2005

50 - 349 µg m^{-3}
350 - 569 µg m^{-3}
≥570 µg m^{-3}

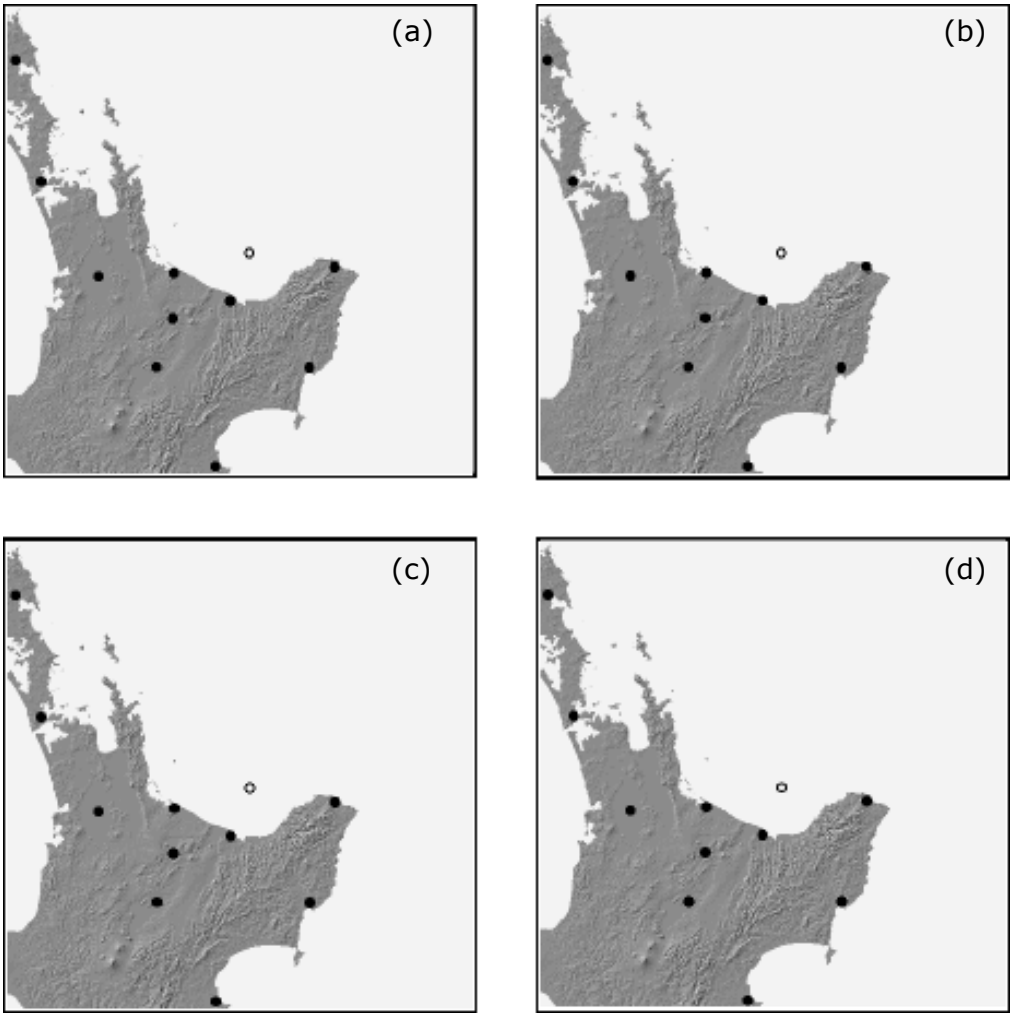

Figure 7. 9 White Island volcano - Model 2, Grid 2, SO_2 average

a) January - March 2005
b) April - June 2005
c) July - September 2005
d) October - December 2005

1.0 - 4.9 µg m^{-3}
5.0 - 9.9 µg m^{-3}
≥10.0 µg m^{-3}

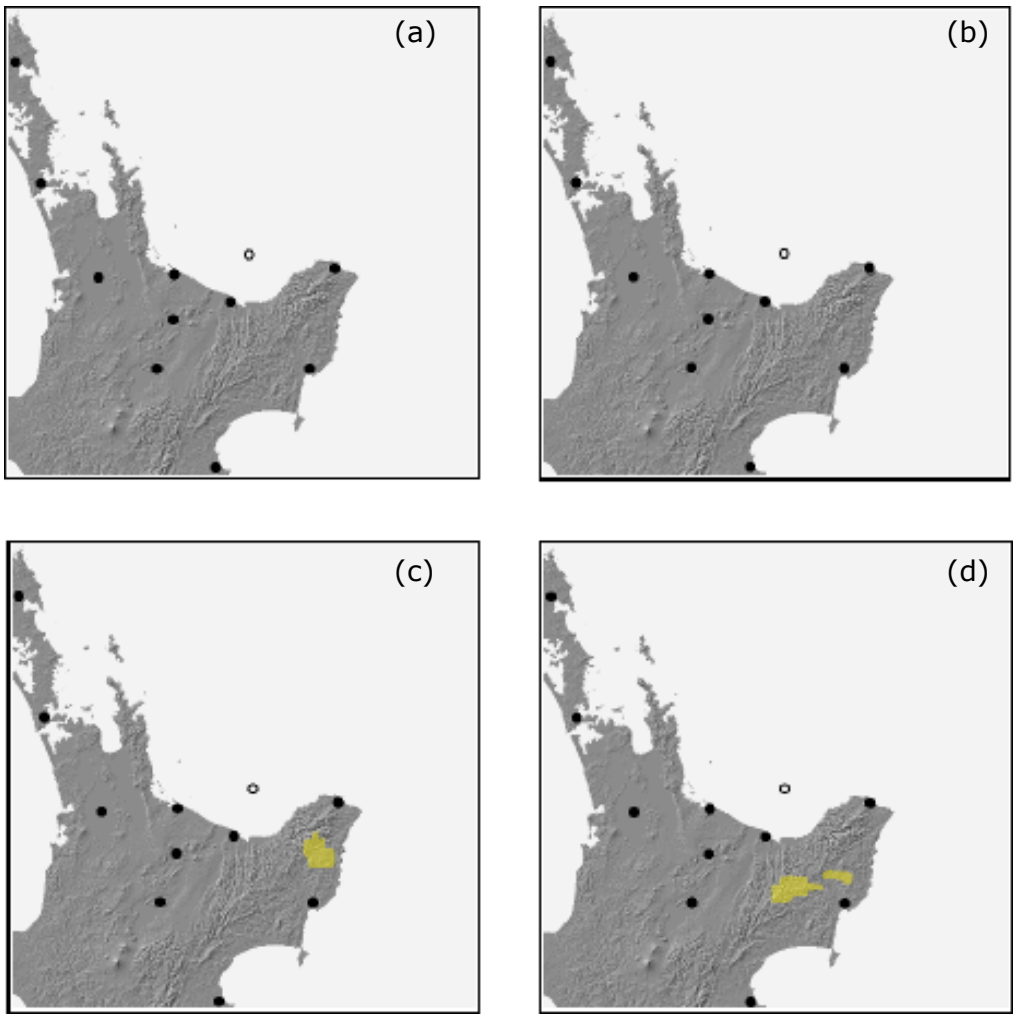

Figure 7. 10 White Island volcano - Model 2, Grid 2, SO_2 maximum

a) January - March 2005
b) April - June 2005
c) July - September 2005
d) October - December 2005

50 - 349 µg m^{-3}
350 - 569 µg m^{-3}
≥570 µg m^{-3}

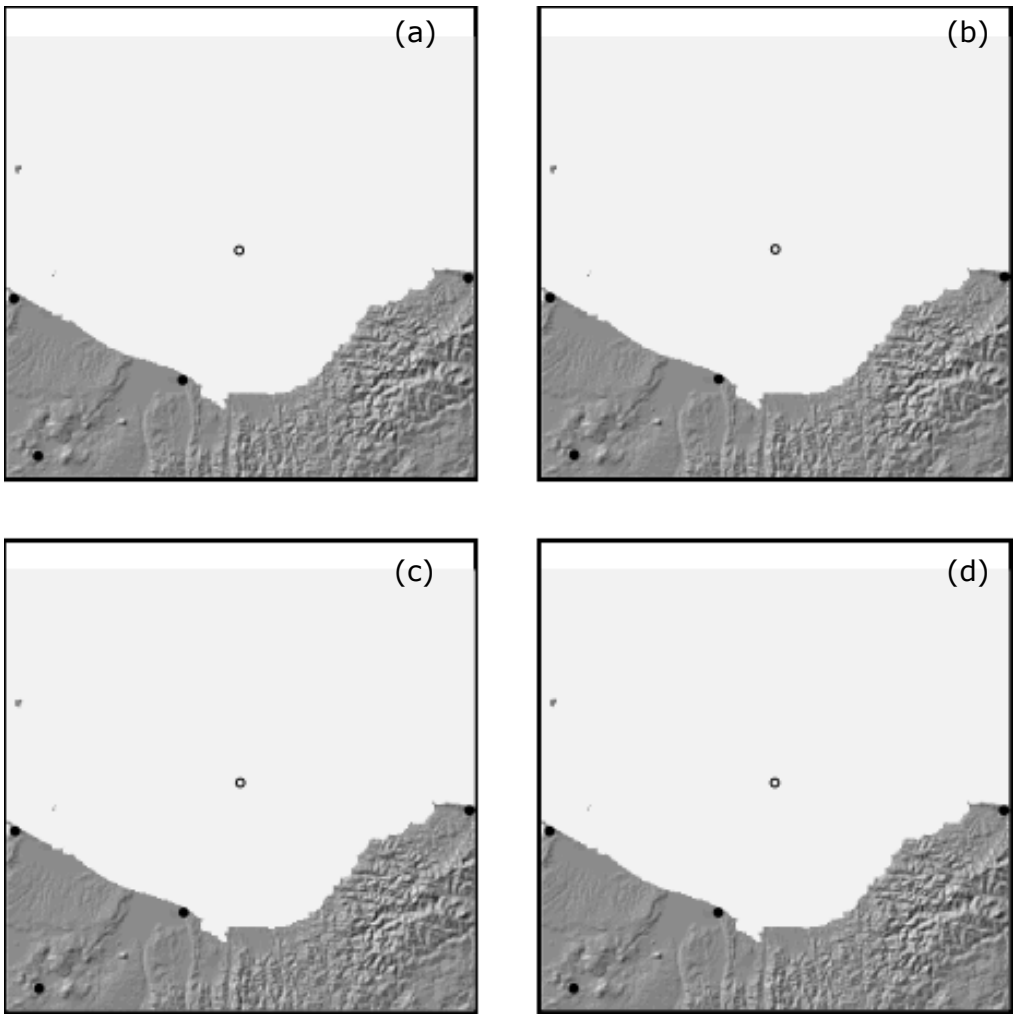

Figure 7. 11 White Island volcano - Model 2, Grid 3, SO_2 average

a) January - March 2005
b) April - June 2005
c) July - September 2005
d) October - December 2005

1.0 - 4.9 µg m^{-3}
5.0 - 9.9 µg m^{-3}
≥10.0 µg m^{-3}

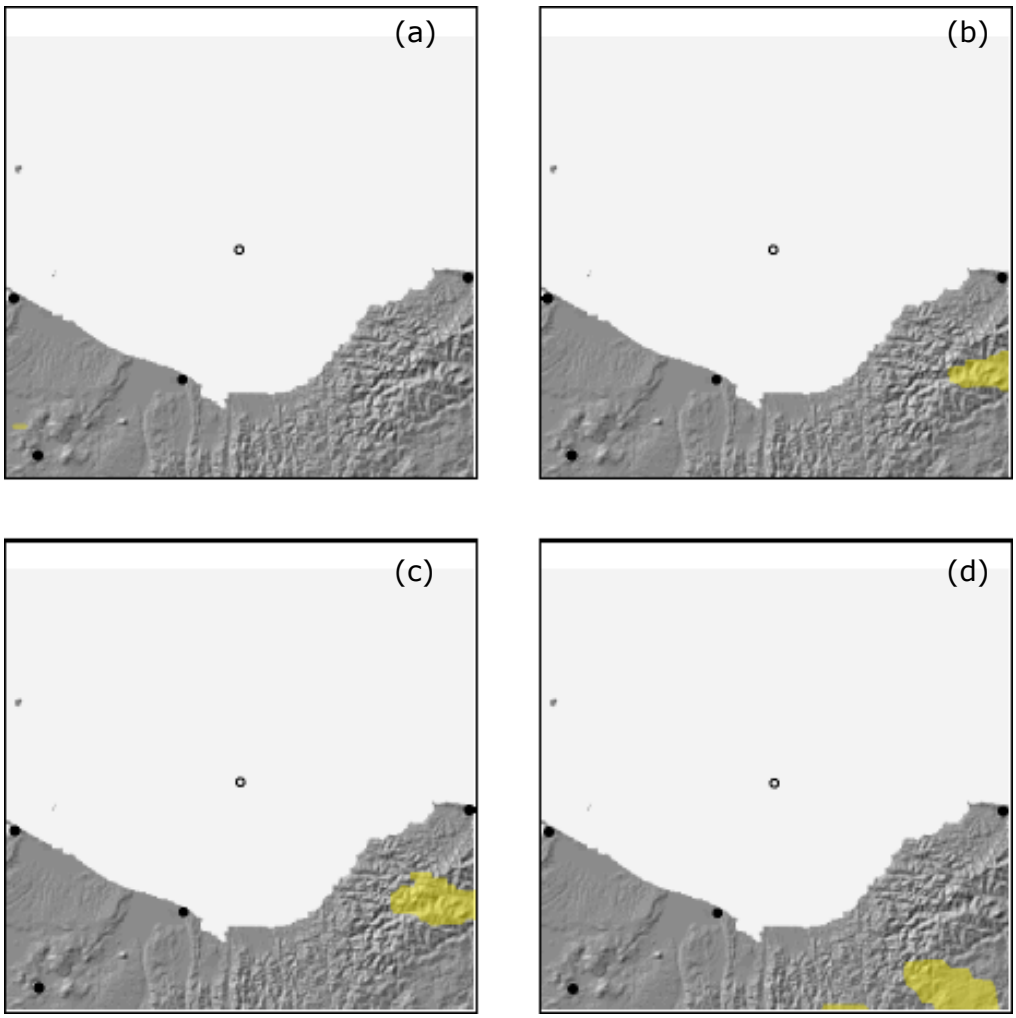

Figure 7. 12 White Island volcano - Model 2, Grid 3, SO_2 maximum

a) January - March 2005
b) April - June 2005
c) July - September 2005
d) October - December 2005

50 - 349 µg m^{-3}
350 - 569 µg m^{-3}
≥570 µg m^{-3}

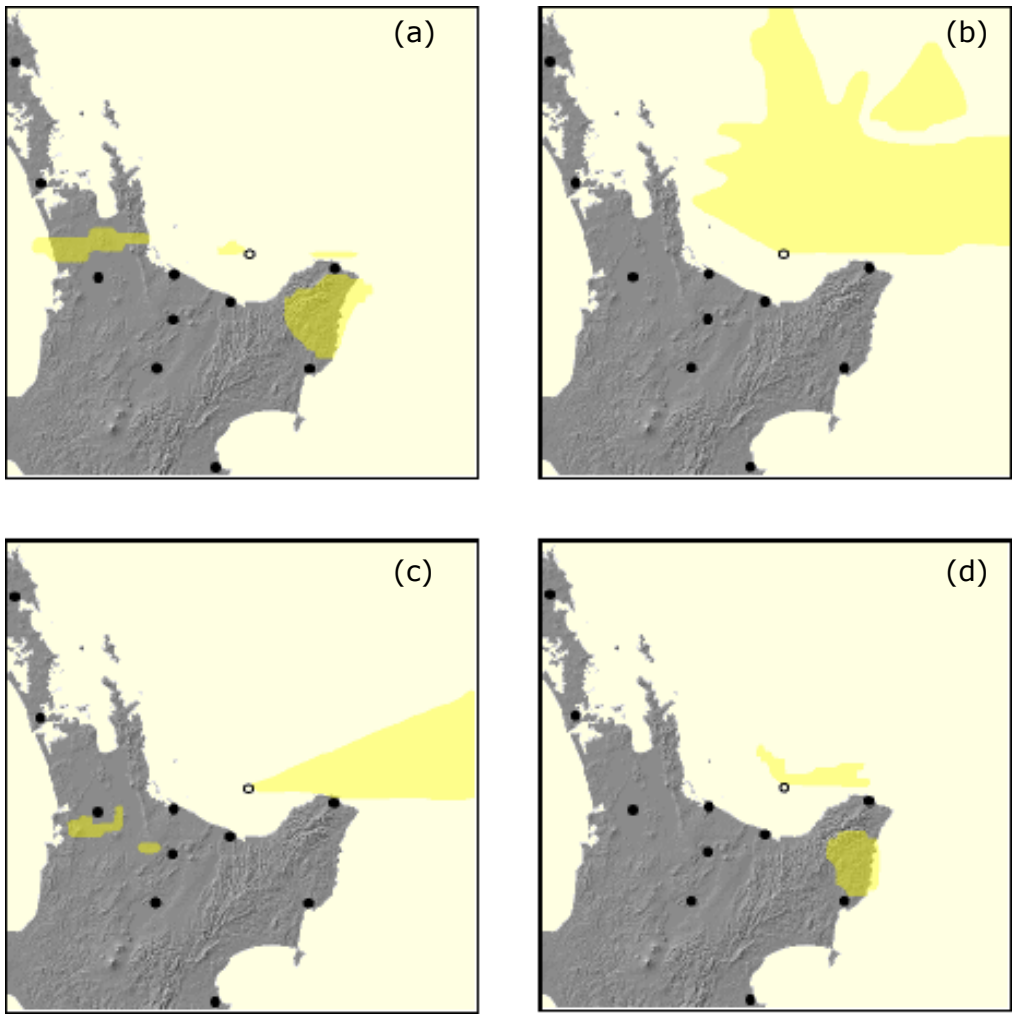

Figure 7. 13 White Island volcano - Model 3, Grid 2, SO_2 average

a) January - March 2005
b) April - June 2005
c) July - September 2005
d) October - December 2005

1.0 - 4.9 µg m^{-3}
5.0 - 9.9 µg m^{-3}
≥10.0 µg m^{-3}

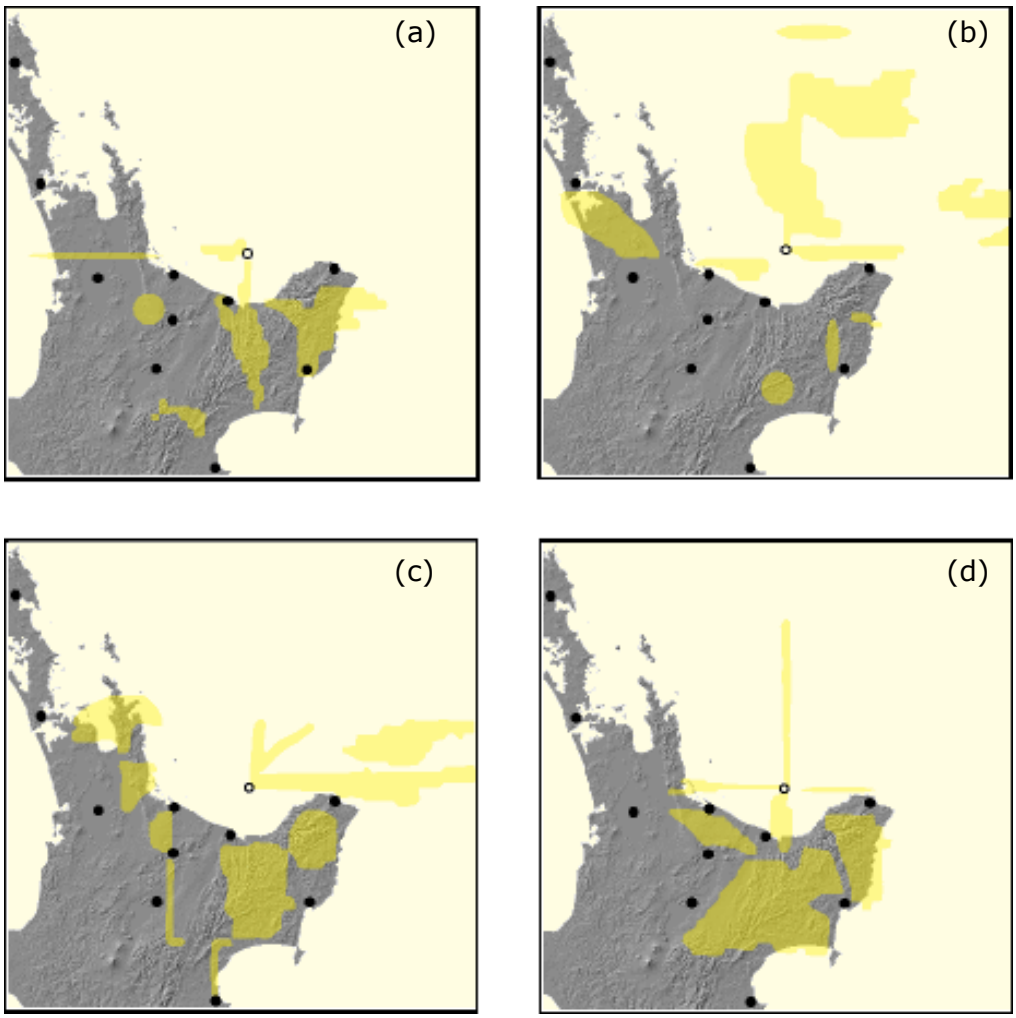

Figure 7. 14 White Island volcano - Model 3, Grid 2, SO_2 maximum

a) January - March 2005
b) April - June 2005
c) July - September 2005
d) October - December 2005

50 - 349 µg m^{-3}
350 - 569 µg m^{-3}
≥570 µg m^{-3}

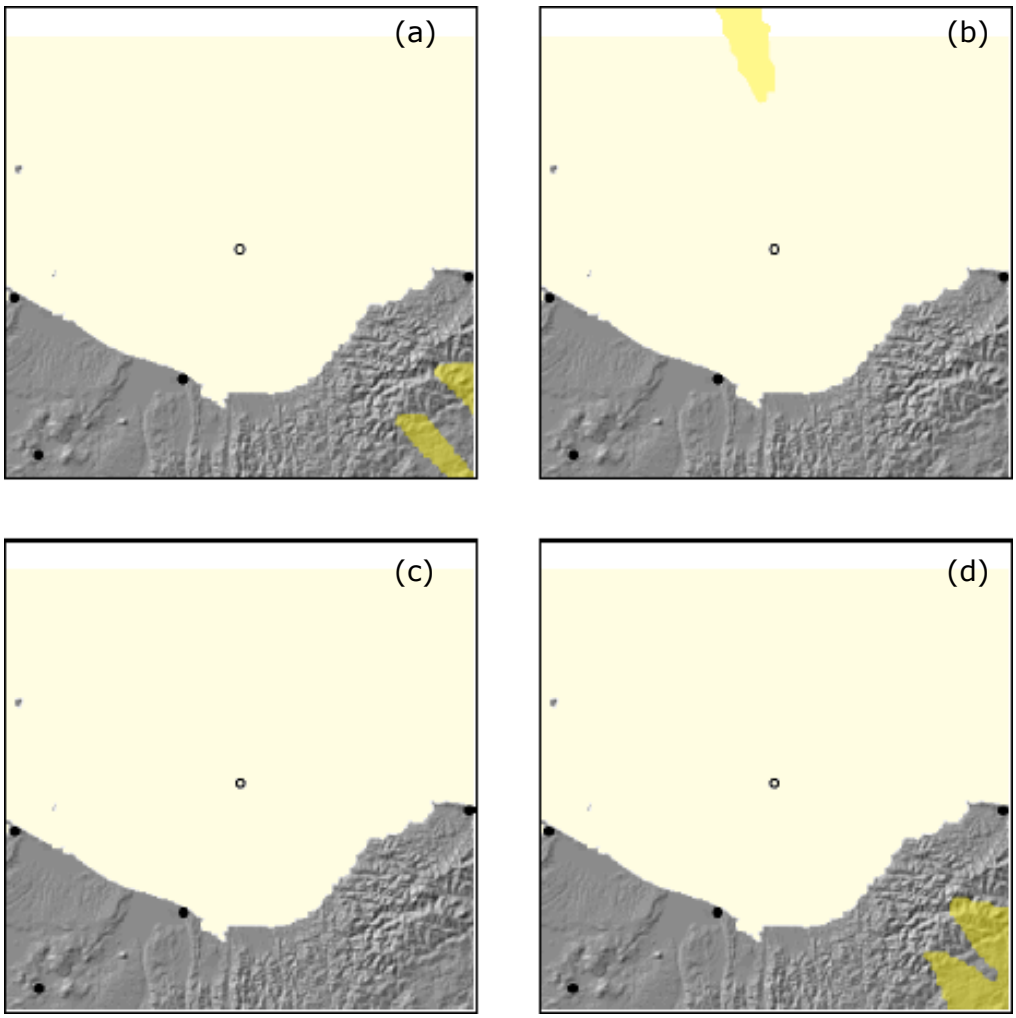

Figure 7. 15 White Island volcano - Model 3, Grid 3, SO_2 average

a) January - March 2005
b) April - June 2005
c) July - September 2005
d) October - December 2005

1.0 - 4.9 µg m^{-3}
5.0 - 9.9 µg m^{-3}
≥10.0 µg m^{-3}

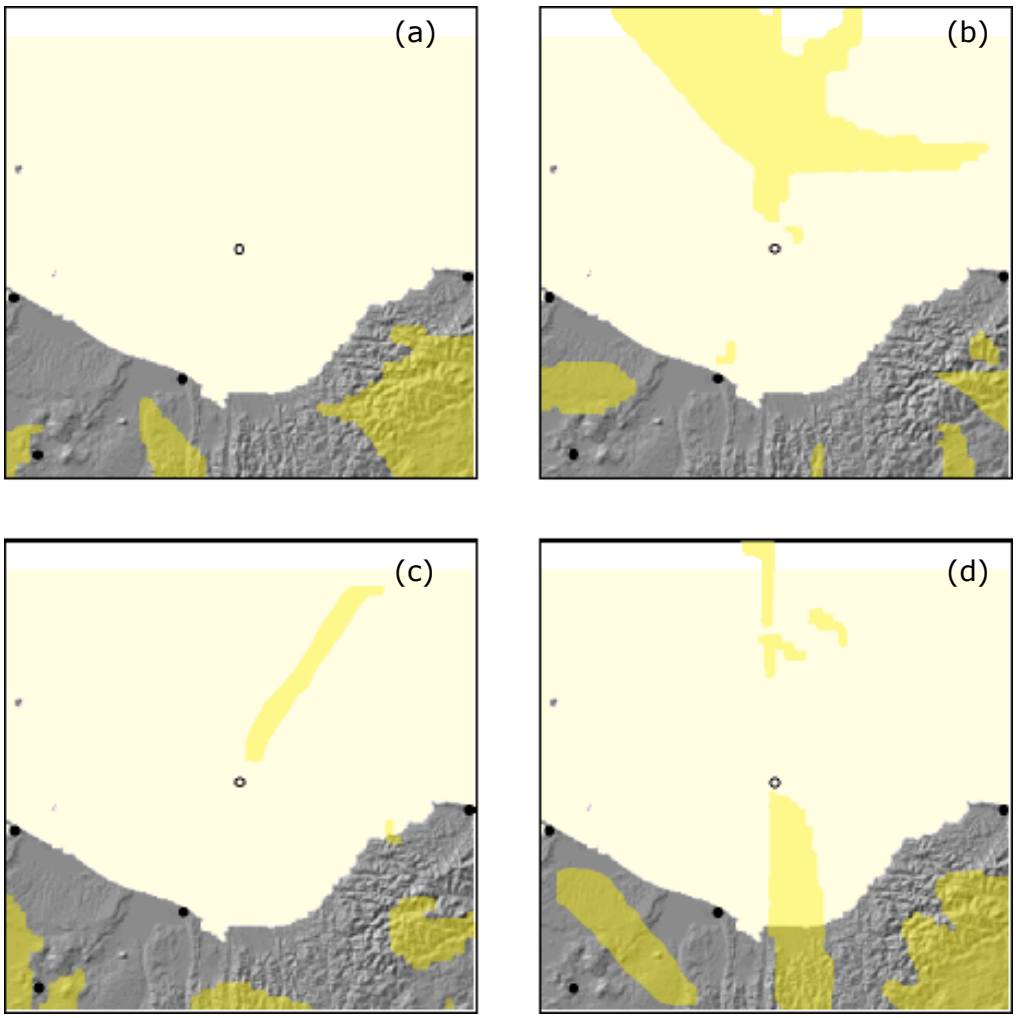

Figure 7. 16 White Island volcano - Model 3, Grid 3, SO_2 maximum

a) January - March 2005
b) April - June 2005
c) July - September 2005
d) October - December 2005

50 - 349 µg m^{-3}
350 - 569 µg m^{-3}
≥570 µg m^{-3}

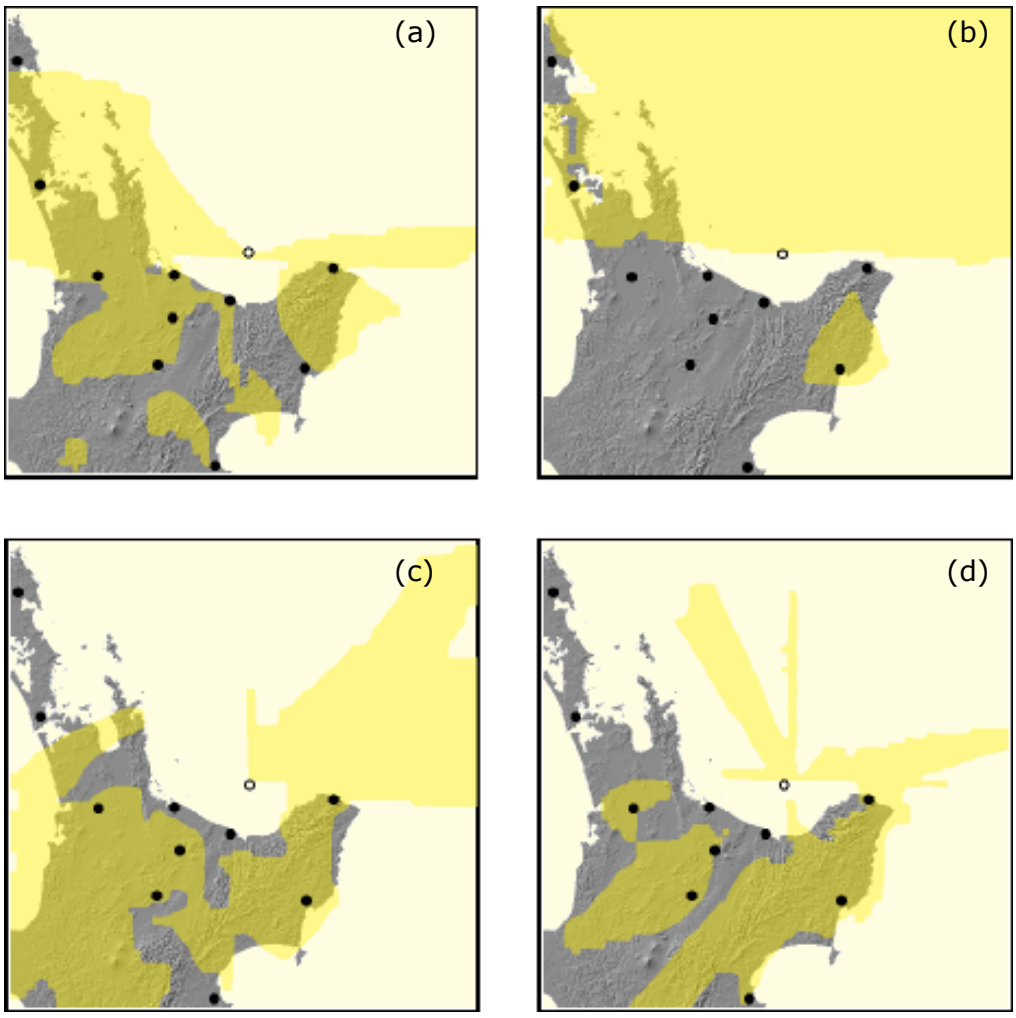

Figure 7. 17 White Island volcano - Model 4, Grid 2, SO_2 average

a) January - March 2005
b) April - June 2005
c) July - September 2005
d) October - December 2005

1.0 - 4.9 µg m^{-3}
5.0 - 9.9 µg m^{-3}
≥10.0 µg m^{-3}

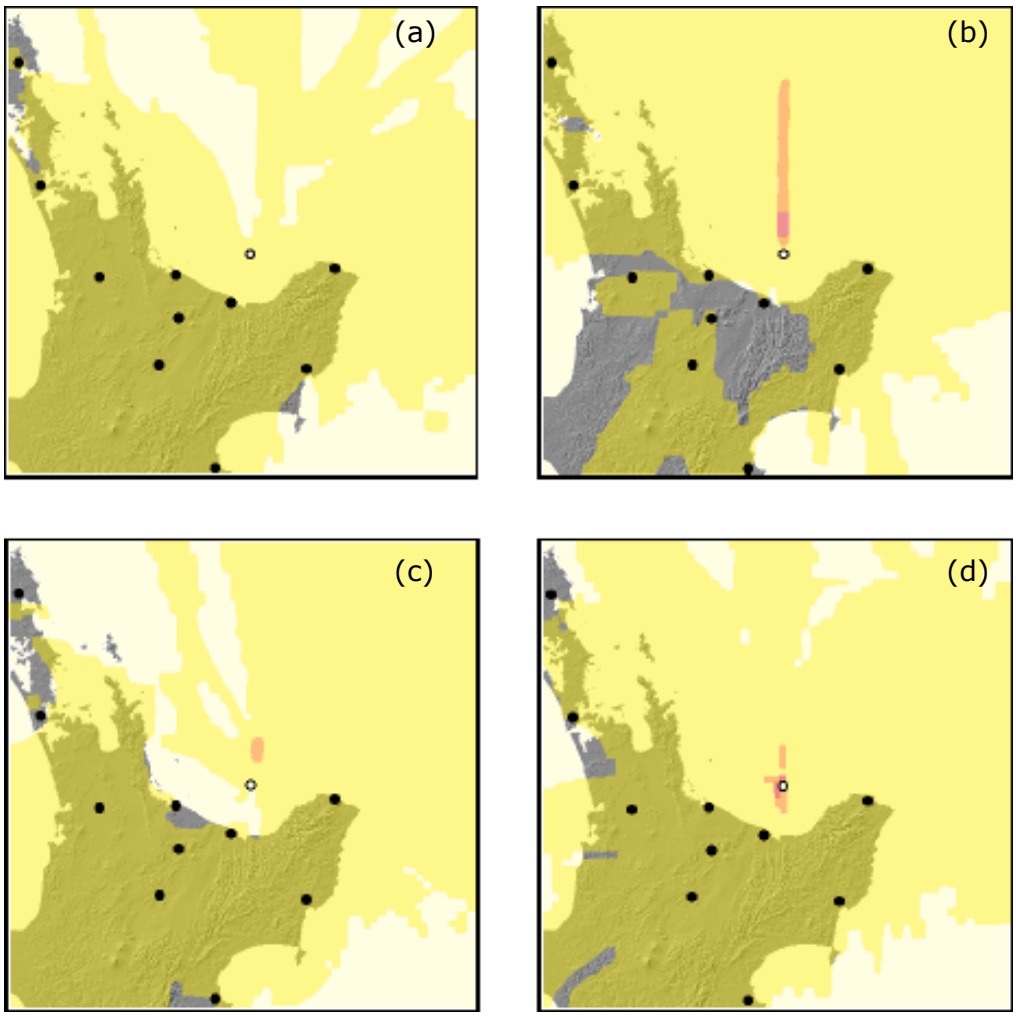

Figure 7. 18 White Island volcano - Model 4, Grid 2, SO_2 maximum

a) January - March 2005
b) April - June 2005
c) July - September 2005
d) October - December 2005

50 - 349 µg m^{-3}
350 - 569 µg m^{-3}
≥570 µg m^{-3}

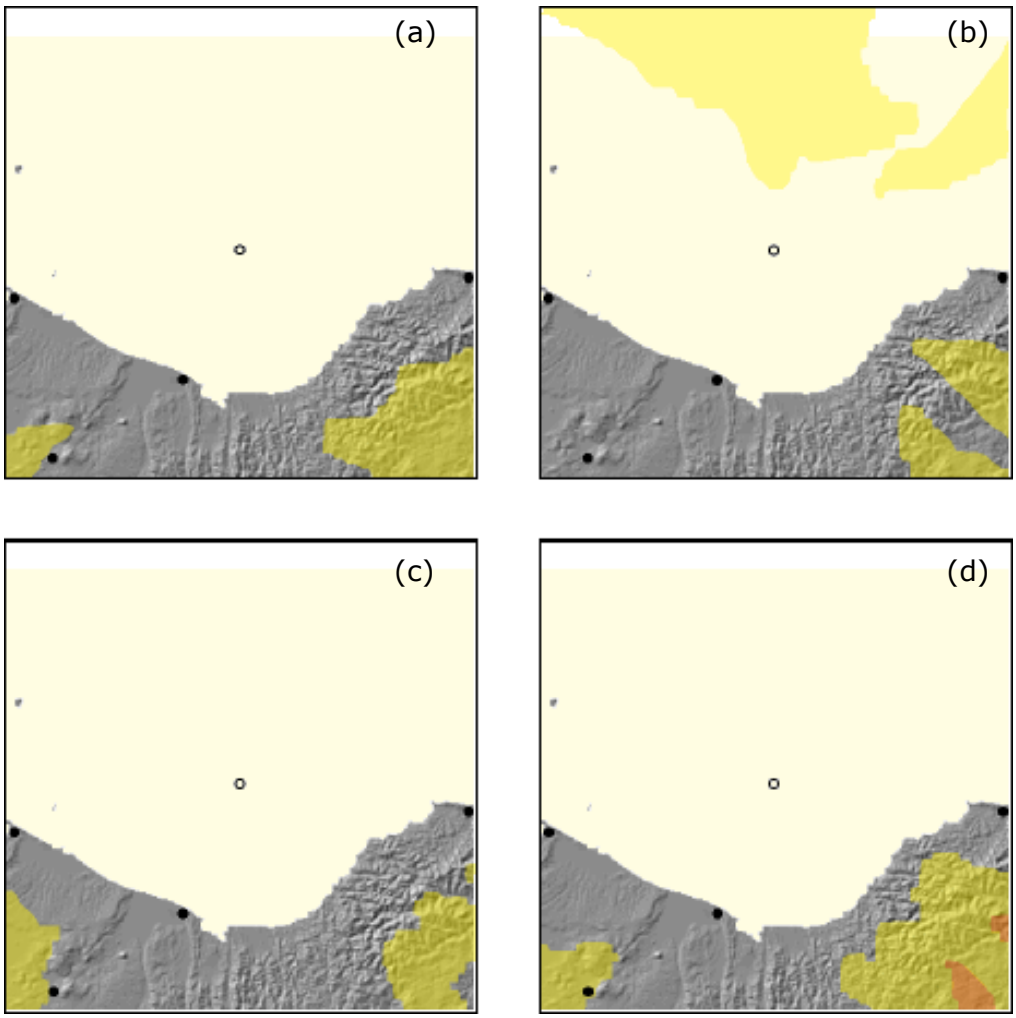

Figure 7. 19 White Island volcano - Model 4, Grid 3, SO_2 average

a) January - March 2005
b) April - June 2005
c) July - September 2005
d) October - December 2005

1.0 - 4.9 µg m^{-3}
5.0 - 9.9 µg m^{-3}
≥10.0 µg m^{-3}

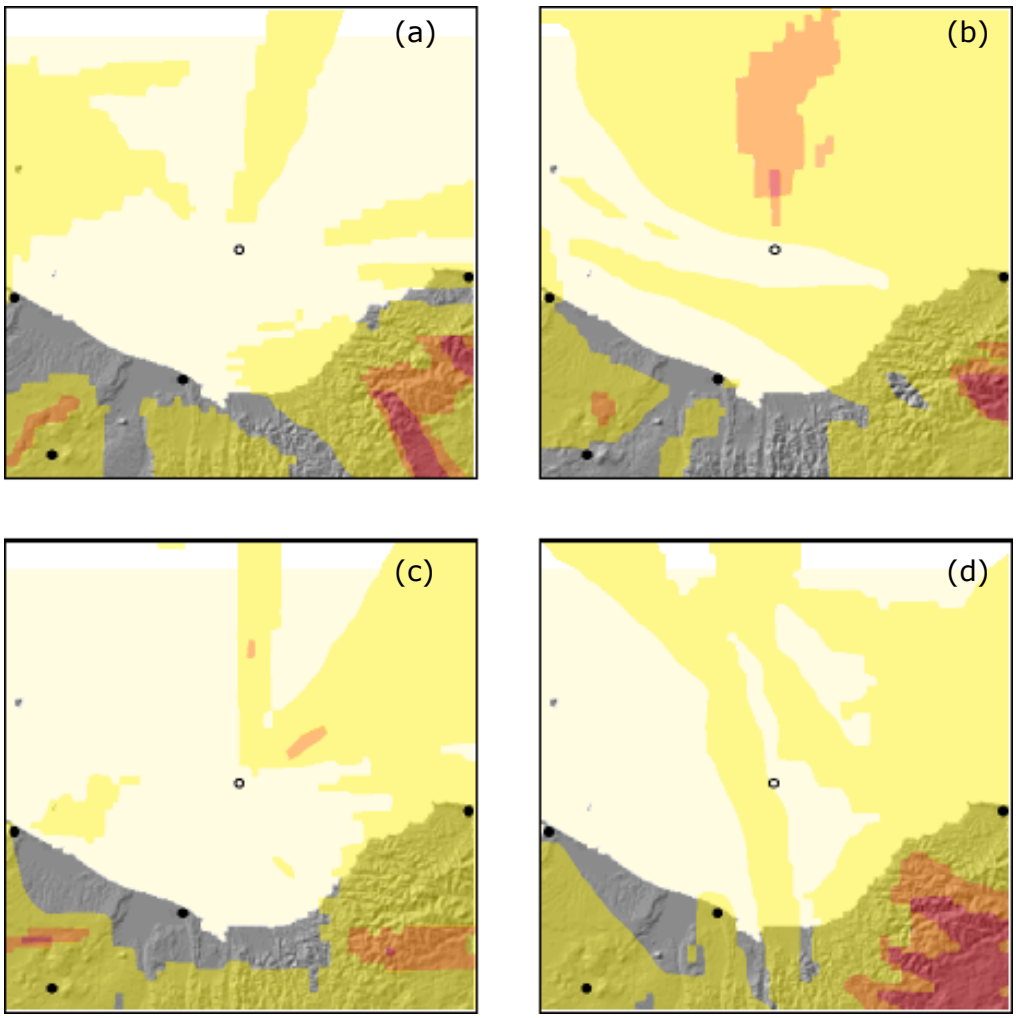

Figure 7. 20 White Island volcano - Model 4, Grid 3, SO_2 maximum

a) January - March 2005
b) April - June 2005
c) July - September 2005
d) October - December 2005

50 - 349 µg m^{-3}
350 - 569 µg m^{-3}
≥570 µg m^{-3}

7. 5. Results of SO_2 dispersion modelling from Ruapehu volcano

7. 5. 1. Results of model 1 (373 K, 1 m s^{-1})

Figure 7. 22 to 7. 25 show the average and maximum SO_2 distribution of model 1 at grids 2 and 3. The average SO_2 concentration in grid domain 2 exceeds the ground concentration value of 1.0 µg m^{-3} throughout the year and it covers a large area surrounding the pollution source. An east-west expansion of the gas plume, affecting urban areas several hundred of kilometres away from the volcano occurs all year. The largest plume dispersion was modelled between April and June, travelling west out of the grid domain. Other smaller plume fans also travel in other directions. The main affected urban areas are the cities of Napier and Gisborne on the east coast of the North Island. Other cities temporarily affected are New Plymouth in the west, as well as Wanganui and Palmerston North in the south. Most of these urban areas are only affected by the outer parts of the dispersed plumes, consequently, the concentrations are close to 1.0 µg m^{-3}. The concentration level of 5.0 µg m^{-3} is exceeded all the year in the inner parts of the plume and cover larger regions, particularly during the periods of January to March and October to December. This plume concentration, however, is found only in rural areas and does not affect areas with high population densities. Additionally, two small areas with average ground level concentration of ≥10 µg m^{-3} are found during the period of January to March. One is located just west of the crater, the other area is in eastern direction.

The plume dispersion showing the maximum concentration values with a lower limit of 50 µg m^{-3} is also widespread throughout the entire year. The plumes disperse mainly in N-S and E-W direction. The maximum concentration affects urban areas, but only with the outer zones of the plumes. The cities of Napier, Palmerston North, Wanganui and Taupo are affected in all four modelling periods. The urban areas of New Plymouth, Hamilton and Gisborne and the independent urban community of Whakatane are less affected. A concentration of 350 µg m^{-3} was not calculated at any time during the year.

The average concentration (>1 µg m^{-3}) in grid domain 3 is less widespread than in grid 2. Although the plume fans still cover large areas throughout the year, they do not reach the two urban communities of Wanganui and Taupo. The concentration of 5.0 µg m^{-3} is exceeded all year, apart from the period of April to June. This part of the plume modelled, however, is only found a few tens of kilometres away from the source. Most widespread plume was modelled during the period of October to December, when ground level concentrations exceeded a value of 10.0 µg m^{-3}. However, this part of the plume just covers the area surrounding the volcanic edifice of Ruapehu.

The four modelled plumes showing the maximum concentration are very widespread, covering large parts of the grid domain. Although they do not affect the urban community of Taupo, the outer parts of the plumes reach the urban area of Wanganui. TAPM also calculated higher ground level concentrations of 350 µg m^{-3} and 570 µg m^{-3}, but they only affect smaller regions within a few tens of kilometres near the volcanic source.

7. 5. 2. Results of model 2 (773 K, 1 m s^{-1})

The modelling results of scenario 2 are shown in Figures 7. 26 – 7. 29. The ground level concentrations for SO_2 of model 2 are the lowest of the three modelled scenarios. The dispersed plumes during all modelled periods reach average concentration values of ≥1 µg m^{-3} and cover mainly rural areas. The urban communities of Napier, Wanganui, Taupo and Gisborne are only intermittently affected. The most widespread plume was modelled during the quarter from January to March, affecting Napier and Taupo at its outer zones. During this period, TAPM also calculated an area exceeding a concentration of 5.0 µg m^{-3}. This area, however, is a small and narrow area north of Napier.

The plume dispersion with the maximum concentration values for all four periods was widespread and reaches ground level concentrations of ≥50 µg m^{-3}. Similar to model 1, a plume dispersion can be recognised in N-S and E-W directions. Although the plumes cover large areas, they have a minimal affect on any of the urban communities. If populated areas are affected, it is only from the outer zones of the plumes: Taupo (January-June), Wanganui and Palmerston North (April-June), New Plymouth (July-December) and Napier and Hamilton (October-December). A concentration of 350 µg m^{-3} is not reached in this grid domain.

The dispersing plumes in grid domain 3, containing the average concentration, exceed the value of 1.0 µg m^{-3} in all four periods but they are less

widespread than in grid 2 and cover only an area surrounding the volcanic edifice. The populated areas of Wanganui and Taupo are not affected. The dispersing plumes containing the maximum concentration of ≥50 µg m^{-3} are more widespread and cover mainly areas south-east of the source. While Taupo is not affected at any time, the urban area of Wanganui is more affected by the outer zones of the plumes. The concentration values of 350 and 570 µg m^{-3} are only exceeded during parts of the year but cover only a small area near the volcanic edifice.

7. 5. 3. Results of model 3 (773 K, 0.1 m s^{-1})

Figures 7. 30 - 7. 33 show the results of plume dispersion modelling of model 3. The plumes with an average concentration of 1.0 µg m^{-3} disperse widely and cover large areas during all modelled periods of grid domain 2. There are a number of cities that are affected by the plume, including Napier, Palmerston North, Wanganui, New Plymouth, Taupo and Gisborne. In this instance, these cities are not affected by the outer zone of the plumes. Individual plumes travel as far as Tauranga and Hicks Bay (April-June) and Wellington (October-December). Large parts in the interior of the plumes also exceed the ground level concentration of 5.0 and 10.0 µg m^{-3}. However, these higher concentrations (>10.0 µg m^{-3}) cover rural and remote areas, while the plumes with concentration values between 5.0 and <10.0 µg m^{-3} also affect the urban communities of Napier (January-March, October-December) and Wanganui (July-September).

Individual plume fans of the four modelled periods with maximum concentration value of 50 µg m^{-3} also cover large areas of the North Island. All urban communities are affected at least once during the modelled year. The most affected cities are Napier, Palmerston North, Wanganui, New Plymouth, Hamilton and Gisborne. The ground level concentration of 350 µg m^{-3} is also exceeded during all modelled periods, however, the affected area is only in the close vicinity of the Ruapehu volcano.

The modelled plumes with the average concentration data of grid 3 are less widespread than in grid 2. Although covering large regions, they mainly affect rural areas. The only period when Wanganui is affected by the plume is between July and September. For all four modelling periods, TAPM calculated localised parts of the plumes that exceed concentration values of 5.0 µg m^{-3} and cover regions several tens of kilometres away from the source. During all quarters besides April to June, the volcanic plumes also cover regions, exceeding a concentration of 10.0 µg m^{-3}. However, these areas are very small and near the volcanic edifice.

The plumes with the maximum concentration data are widespread and cover most parts of the grid domain throughout the entire year. While the city of Wanganui is affected during all four modelled periods, the urban community of Taupo is affected only between July and September. The ground level concentrations exceed the values of 350 and 570 μg m^{-3} during all four models but cover only in the rural and remote regions of the grid domain.

7. 5. 4. Results of model 4 (773 K, 5 m s^{-1})

Figure 7. 34 to 7. 37 show the average and maximum SO_2 distribution of model 4 at grid domains 2 and 3. The individual plumes in all grids and during every period exceed all defined threshold values for the average (1.0, 5.0 and 10.0 μg m^{-3}) and maximum (50, 350 and 570 μg m^{-3}) concentrations. Due to the location of the vent in the central part of the North Island, the plumes mainly affect areas over land. The plumes of grid 2, that exceed the values of 1.0 μg m^{-3} (average concentration) and 50 μg m^{-3} (maximum concentration) cover nearly the whole area of the North Island, whereas the same plumes of grid 3 cover nearly the whole grid domain. Those parts of the dispersing plumes of grid 2, which exceed the concentration values of 5.0 μg m^{-3} (average concentration) and 350 μg m^{-3} (maximum concentration), cover smaller areas but still reach the urban communities of Napier, Gisborne, Wanganui and Palmerston North. The core of the modelled plumes with concentrations of ≥10.0 μg m^{-3} (average concentration) and ≥570 μg m^{-3} cover only a slightly smaller areas, reaching the urban areas of Napier and Wanganui.

The plumes of grid 3, exceeding the lowest threshold values of 1.0 μg m^{-3} (average concentration) and 50 μg m^{-3} (maximum concentration), cover nearly the whole grid domain. The plumes with average SO_2 concentrations of ≥5 μg m^{-3} cover large areas surrounding the volcanic edifice but they do not reach any urban community. On the other hand, the plumes with maximum SO_2 concentrations of ≥570 μg m^{-3} cover areas north-west of Taupo and affect the urban area of Wanganui nearly the entire year.

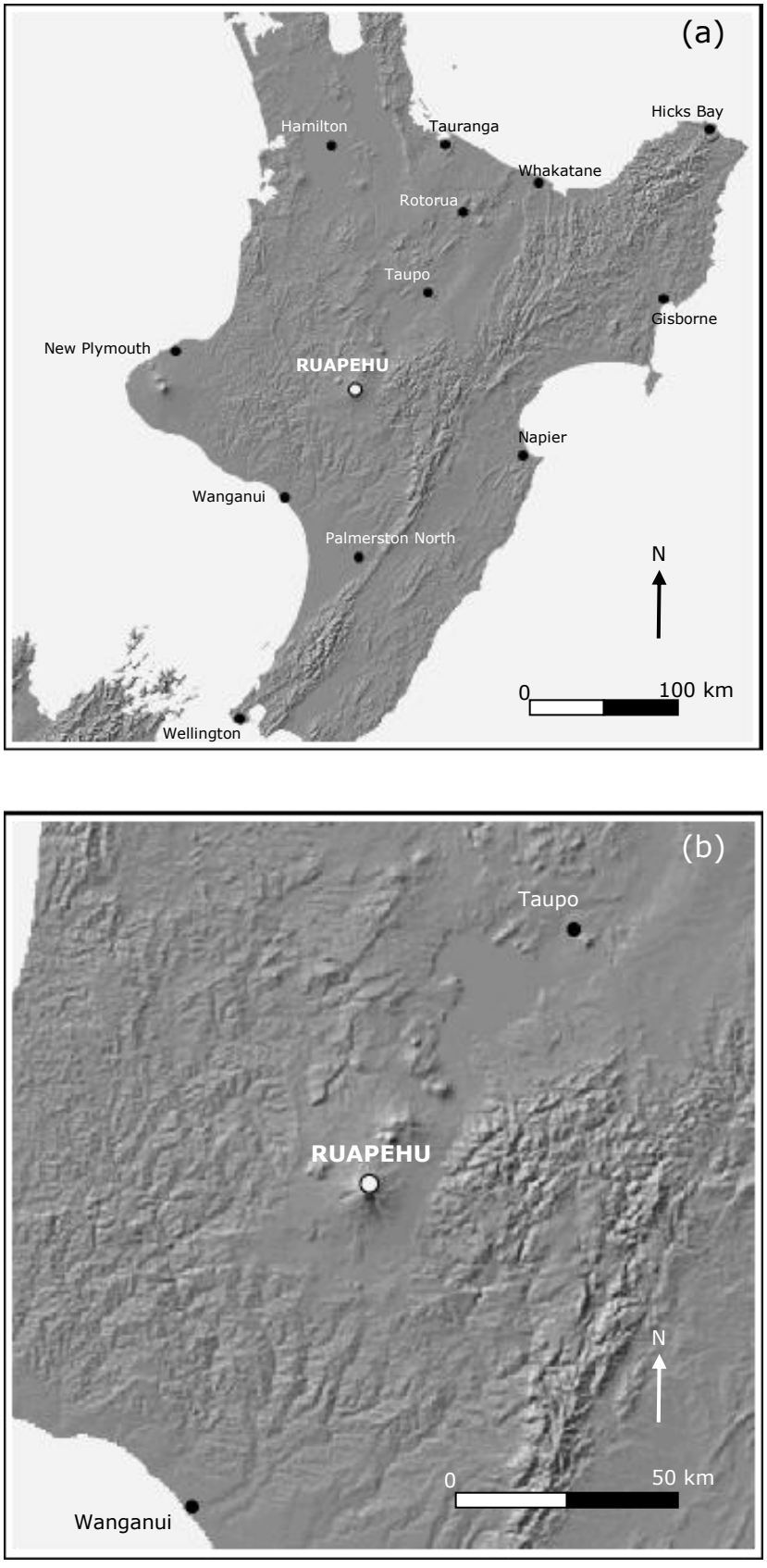

Figure 7. 21 DEM images of parts of the North Island. They correspond to two innermost grids of dispersion modelling from Ruapehu volcano (Figure a = Grid 2 and Figure b = Grid 3).

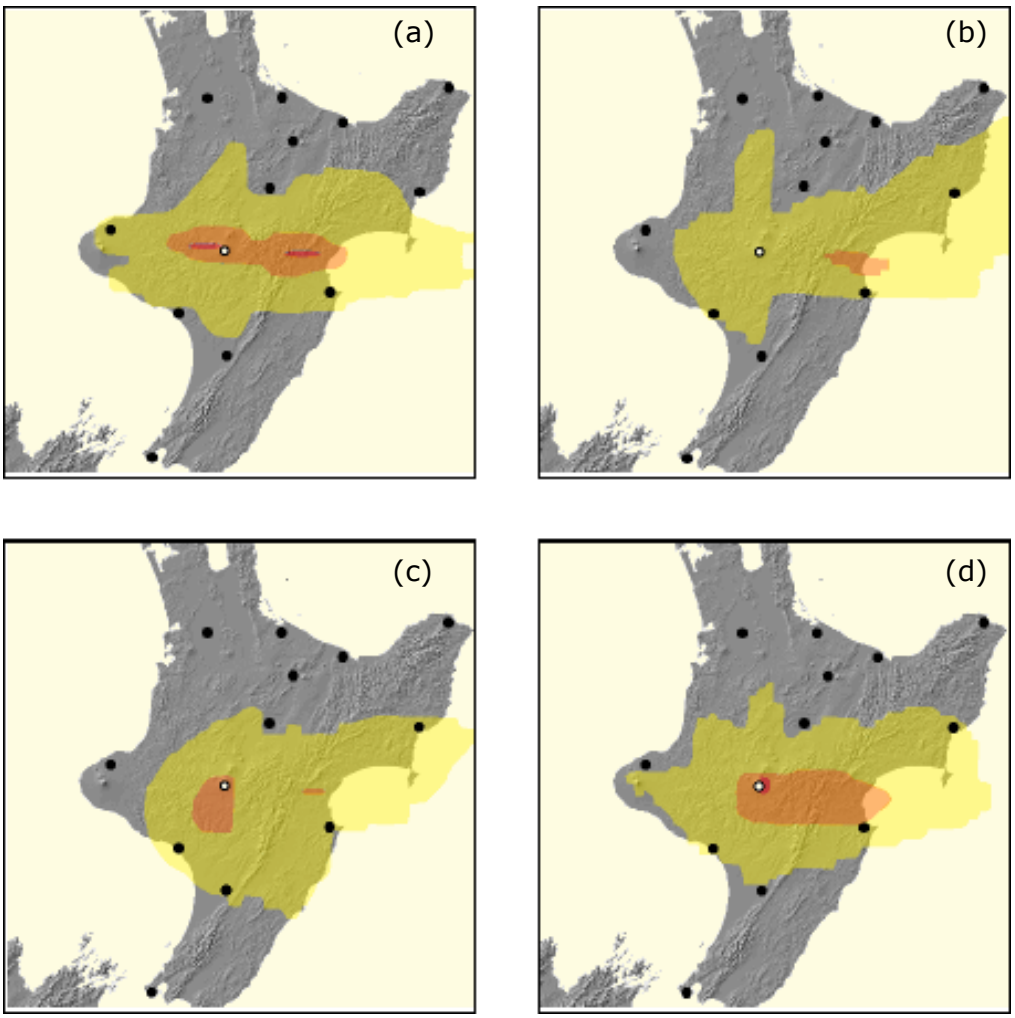

Figure 7. 22 Ruapehu volcano - Model 1, Grid 2, SO_2 average

a) January - March 2005
b) April - June 2005
c) July - September 2005
d) October - December 2005

1.0 - 4.9 µg m^{-3}
5.0 - 9.9 µg m^{-3}
≥10.0 µg m^{-3}

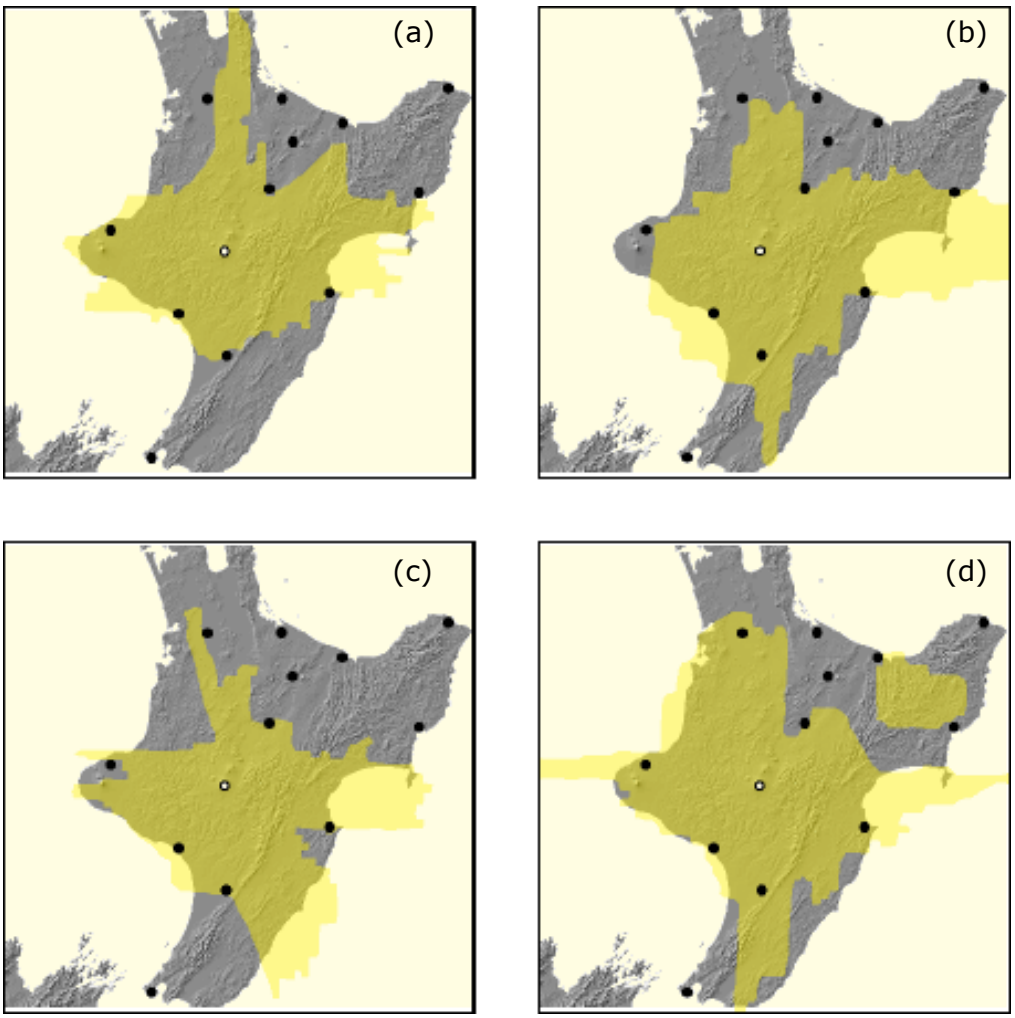

Figure 7. 23 Ruapehu volcano - Model 1, Grid 2, SO_2 maximum

a) January - March 2005
b) April - June 2005
c) July - September 2005
d) October - December 2005

50 - 349 µg m^{-3}
350 - 569 µg m^{-3}
≥570 µg m^{-3}

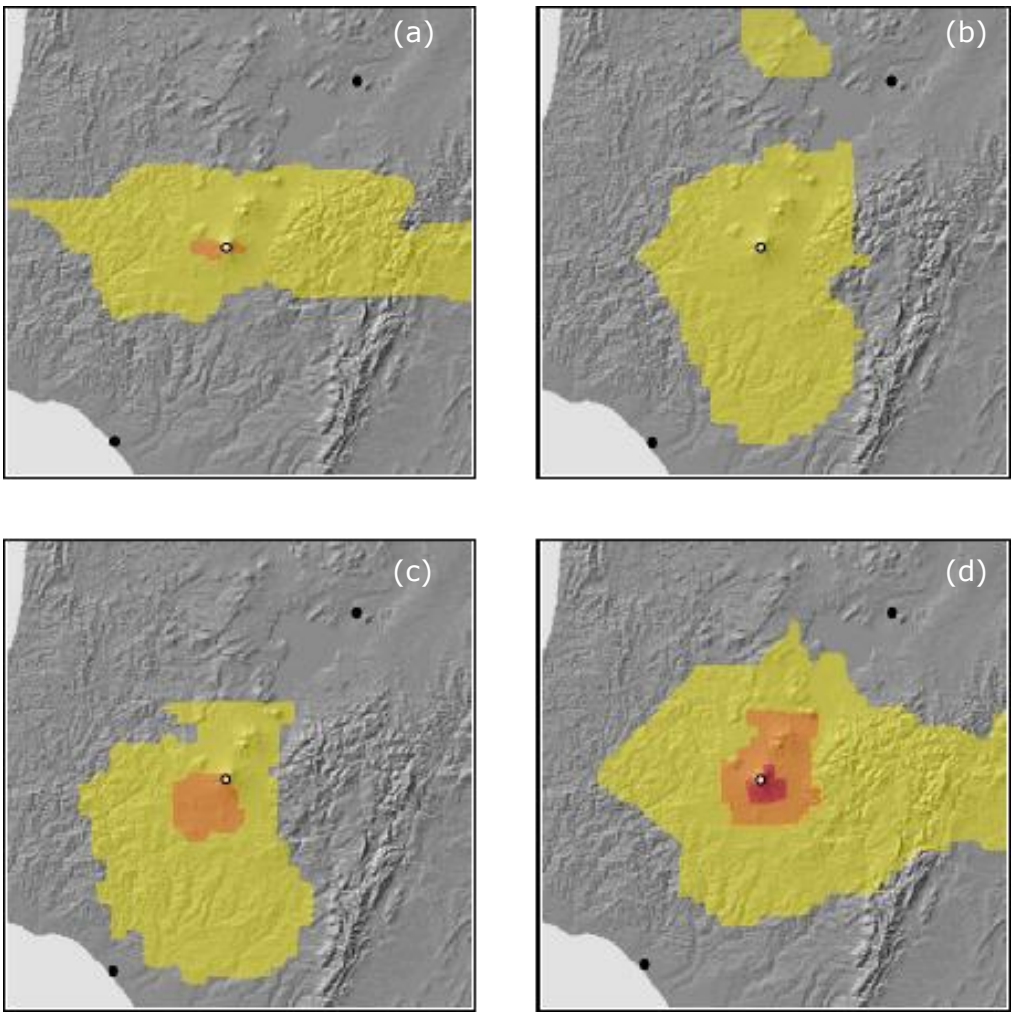

Figure 7. 24 Ruapehu volcano - Model 1, Grid 3, SO_2 average

a) January - March 2005
b) April - June 2005
c) July - September 2005
d) October - December 2005

1.0 - 4.9 µg m^{-3}
5.0 - 9.9 µg m^{-3}
≥10.0 µg m^{-3}

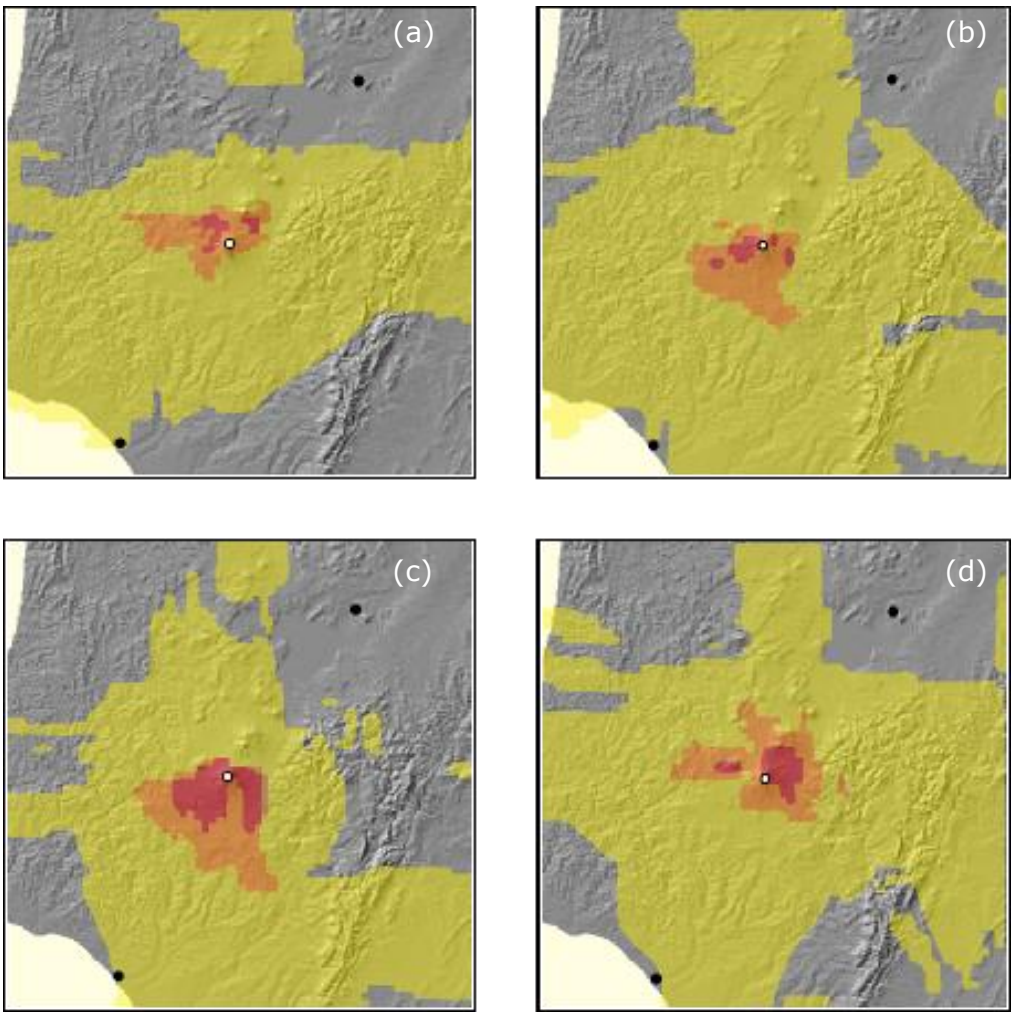

Figure 7. 25 Ruapehu volcano - Model 1, Grid 3, SO_2 maximum

a) January - March 2005
b) April - June 2005
c) July - September 2005
d) October - December 2005

50 - 349 µg m^{-3}
350 - 569 µg m^{-3}
≥570 µg m^{-3}

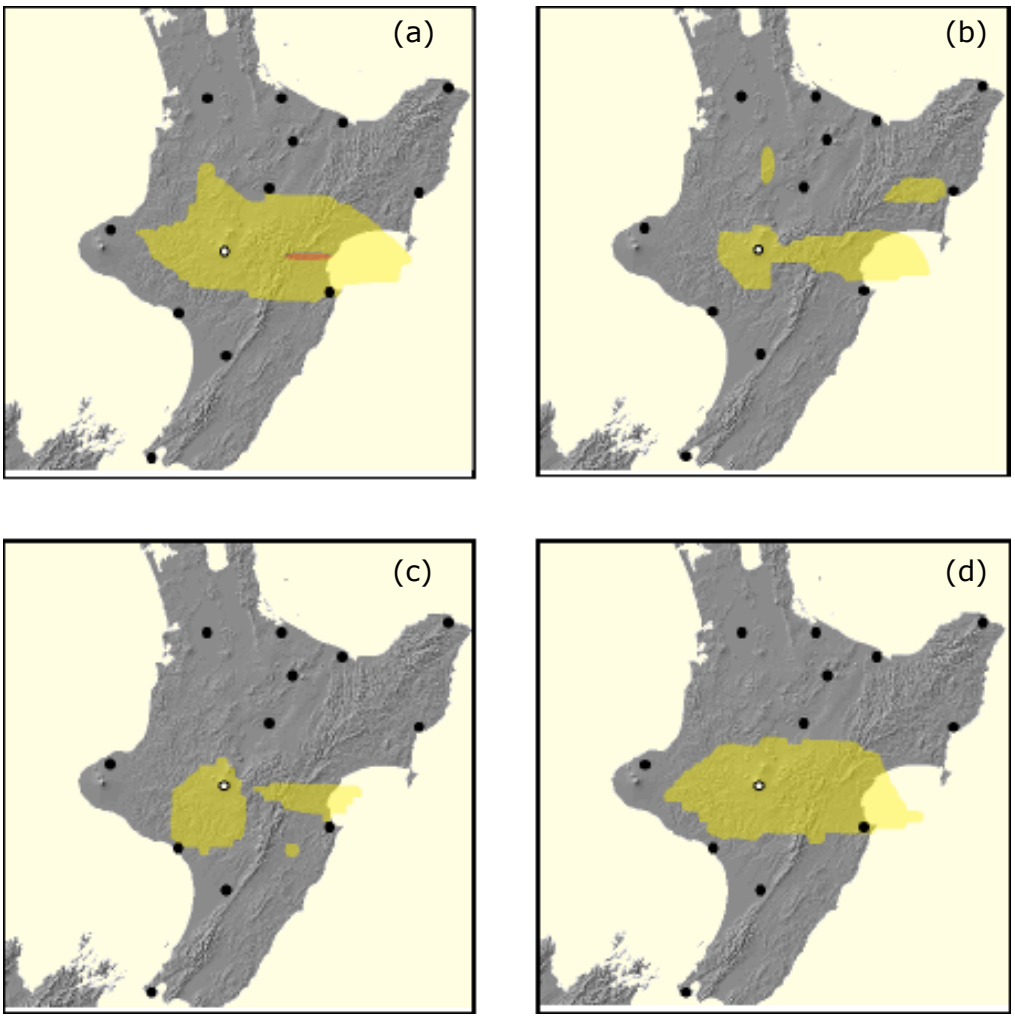

Figure 7. 26 Ruapehu volcano - Model 2, Grid 2, SO_2 average

a) January - March 2005
b) April - June 2005
c) July - September 2005
d) October - December 2005

1.0 - 4.9 µg m^{-3}
5.0 - 9.9 µg m^{-3}
≥10.0 µg m^{-3}

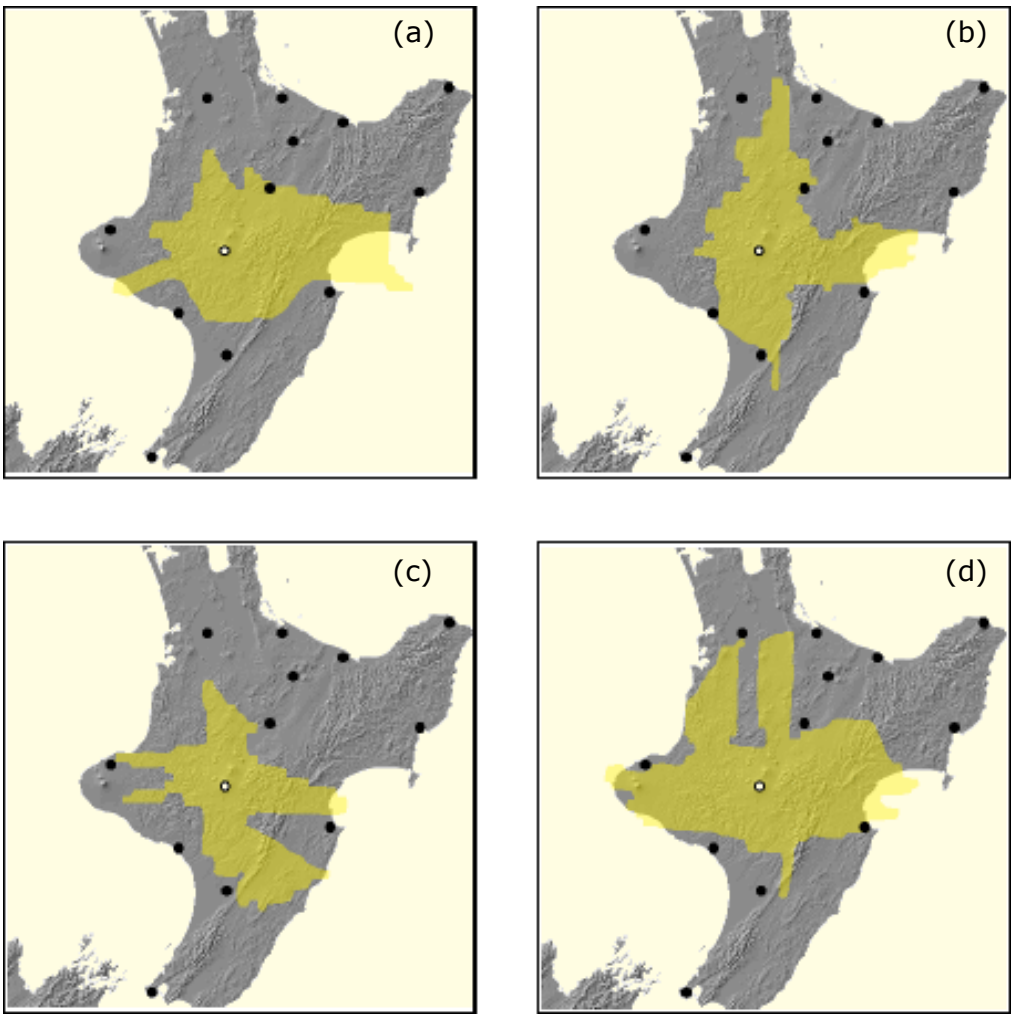

Figure 7. 27 Ruapehu volcano - Model 2, Grid 2, SO_2 maximum

a) January - March 2005
b) April - June 2005
c) July - September 2005
d) October - December 2005

50 - 349 µg m^{-3}
350 - 569 µg m^{-3}
≥570 µg m^{-3}

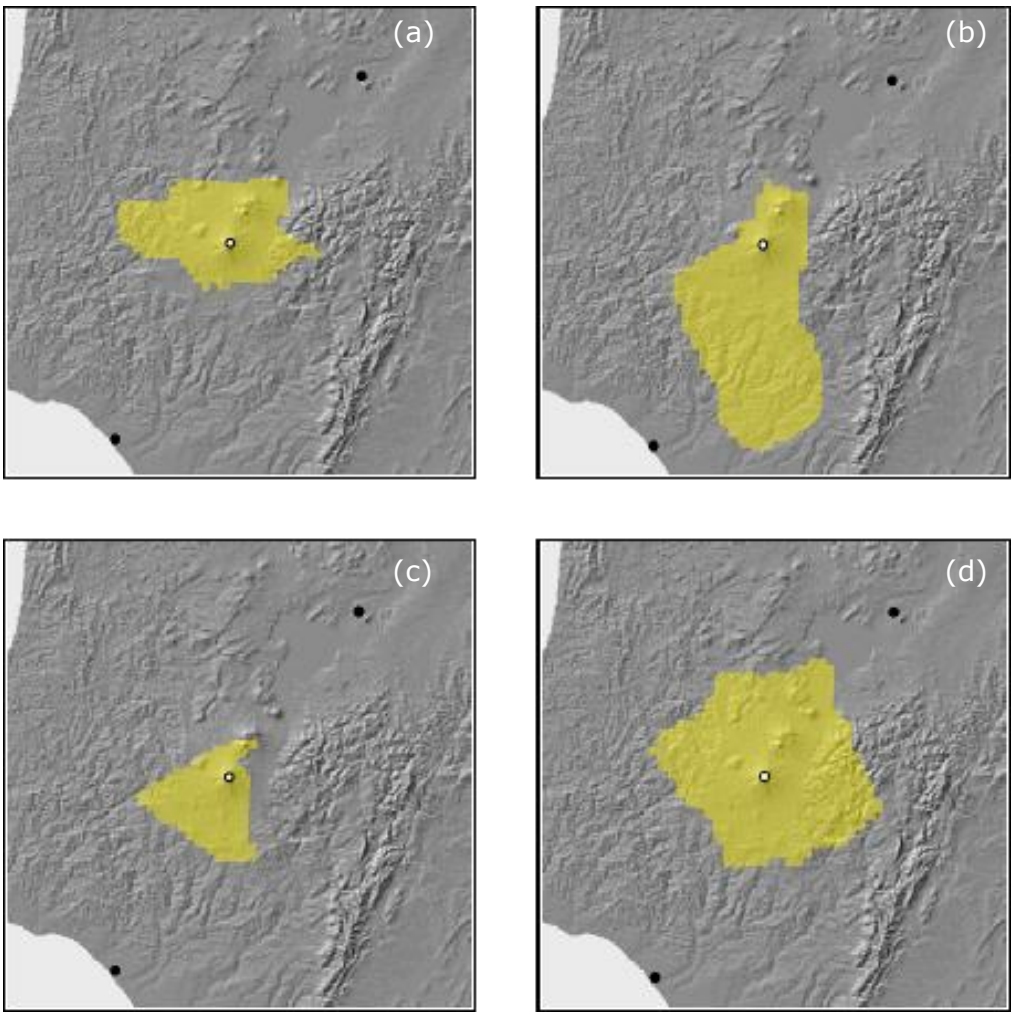

Figure 7. 28 Ruapehu volcano - Model 2, Grid 3, SO_2 average

a) January - March 2005
b) April - June 2005
c) July - September 2005
d) October - December 2005

1.0 - 4.9 µg m^{-3}
5.0 - 9.9 µg m^{-3}
≥10.0 µg m^{-3}

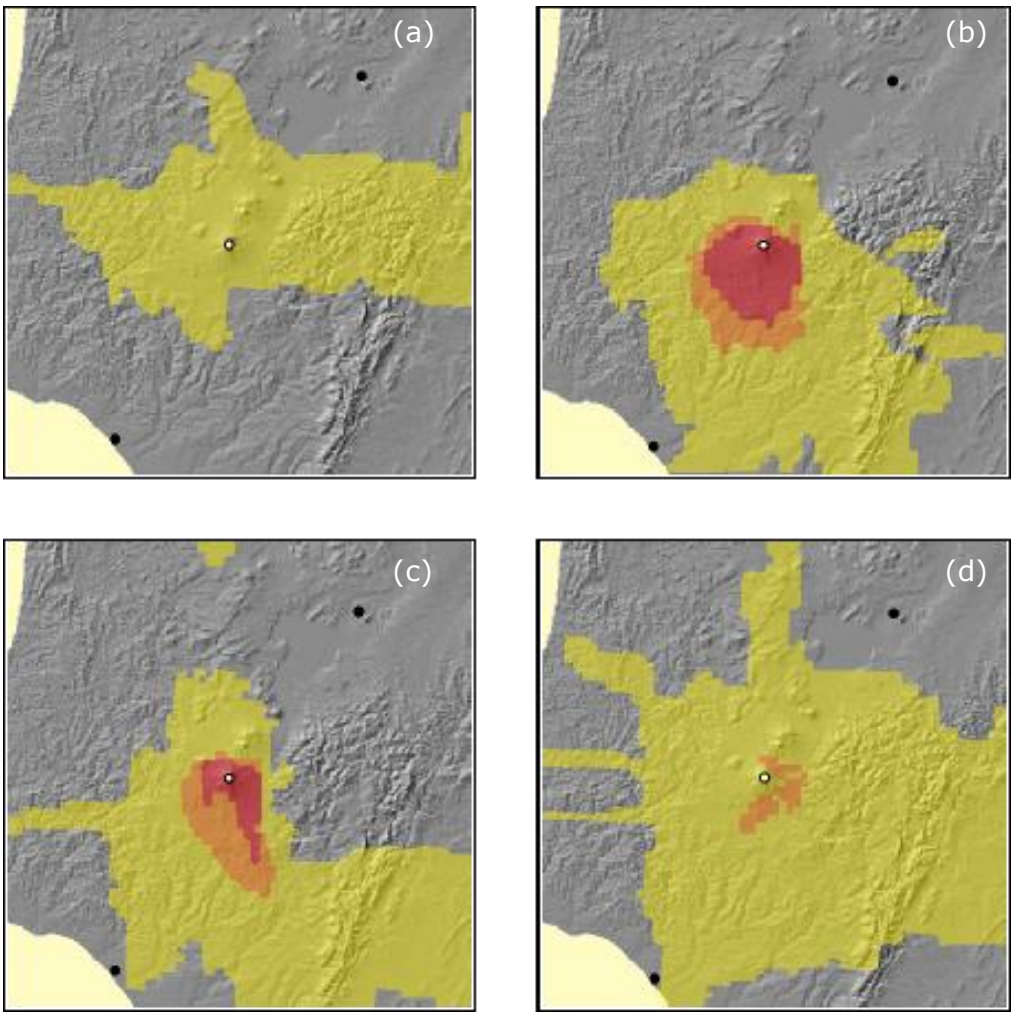

Figure 7. 29 Ruapehu volcano - Model 2, Grid 3, SO_2 maximum

a) January - March 2005
b) April - June 2005
c) July - September 2005
d) October - December 2005

50 - 349 µg m^{-3}
350 - 569 µg m^{-3}
≥570 µg m^{-3}

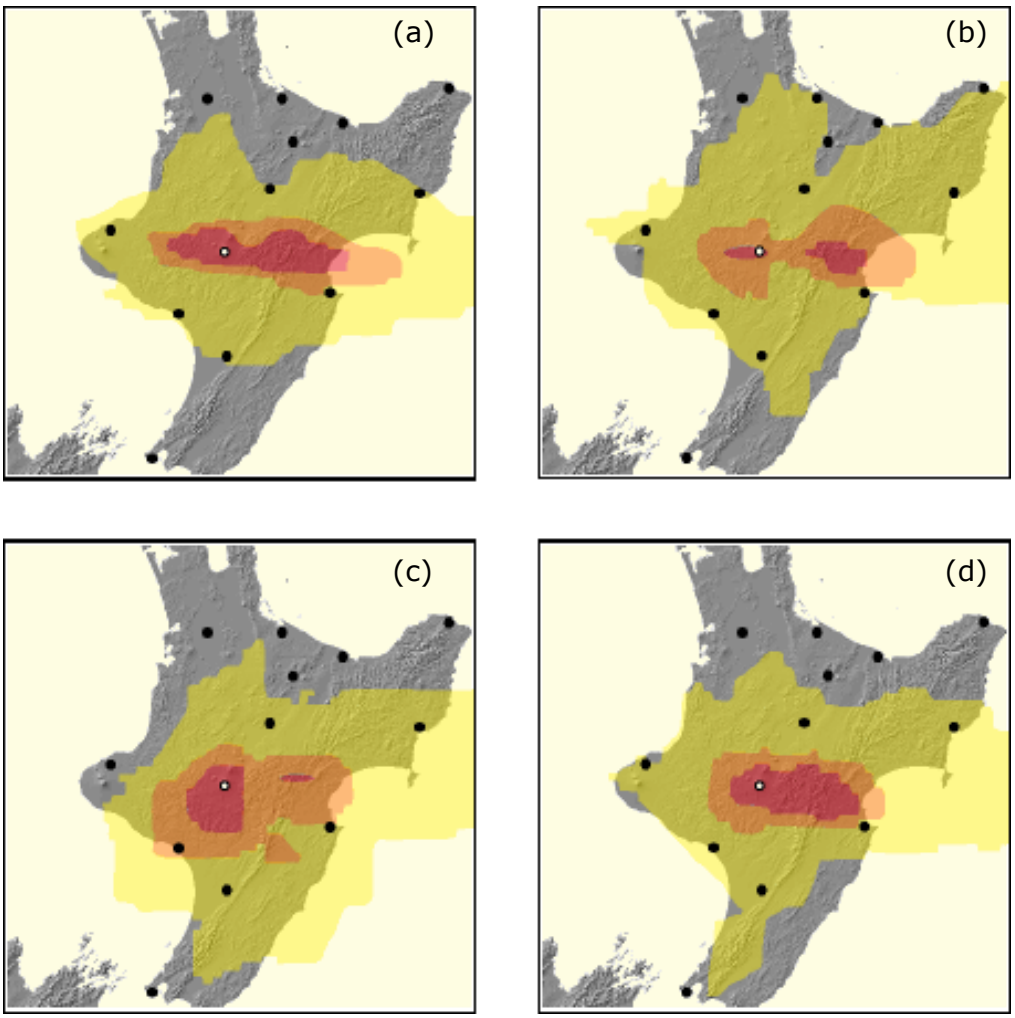

Figure 7. 30 Ruapehu volcano - Model 3, Grid 2, SO_2 average

a) January - March 2005
b) April - June 2005
c) July - September 2005
d) October - December 2005

1.0 - 4.9 µg m^{-3}
5.0 - 9.9 µg m^{-3}
≥10.0 µg m^{-3}

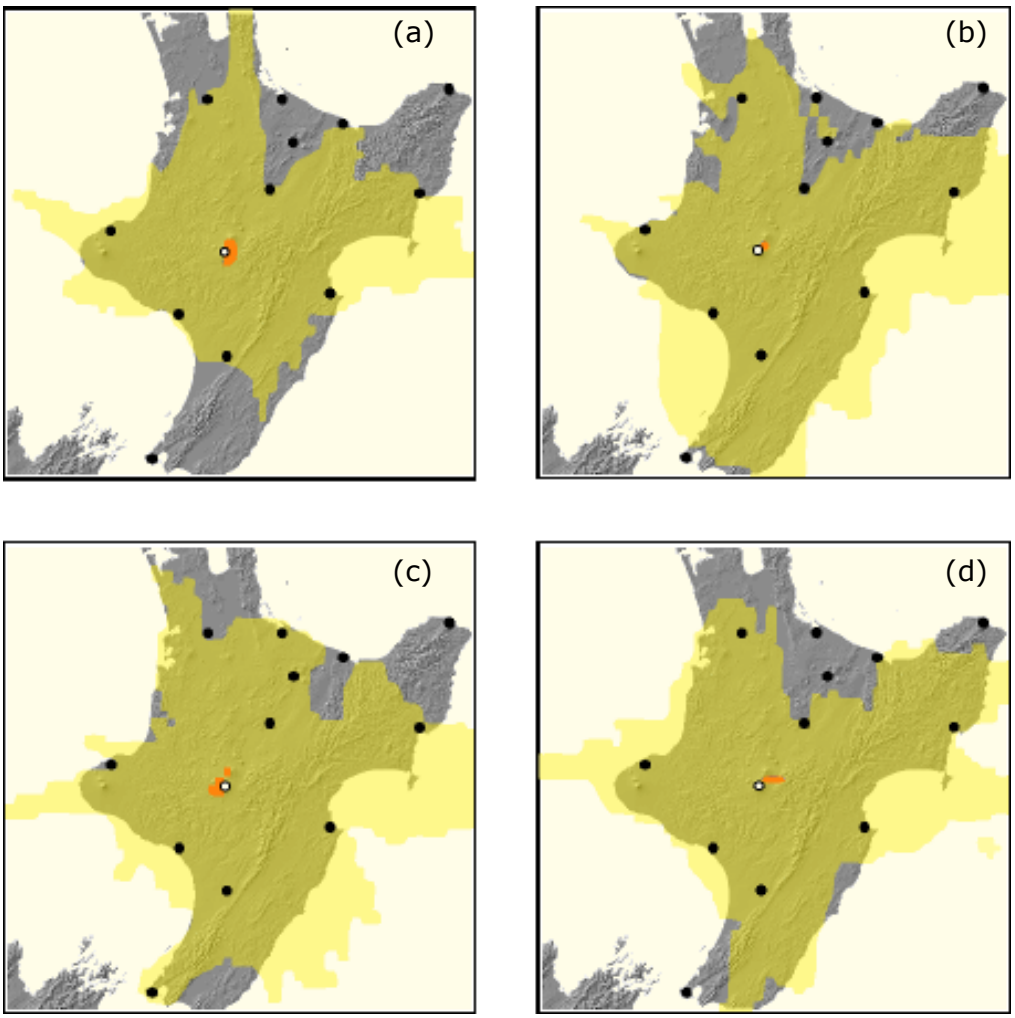

Figure 7. 31 Ruapehu volcano - Model 3, Grid 2, SO_2 maximum

a) January - March 2005
b) April - June 2005
c) July - September 2005
d) October - December 2005

50 - 349 µg m^{-3}
350 - 569 µg m^{-3}
≥570 µg m^{-3}

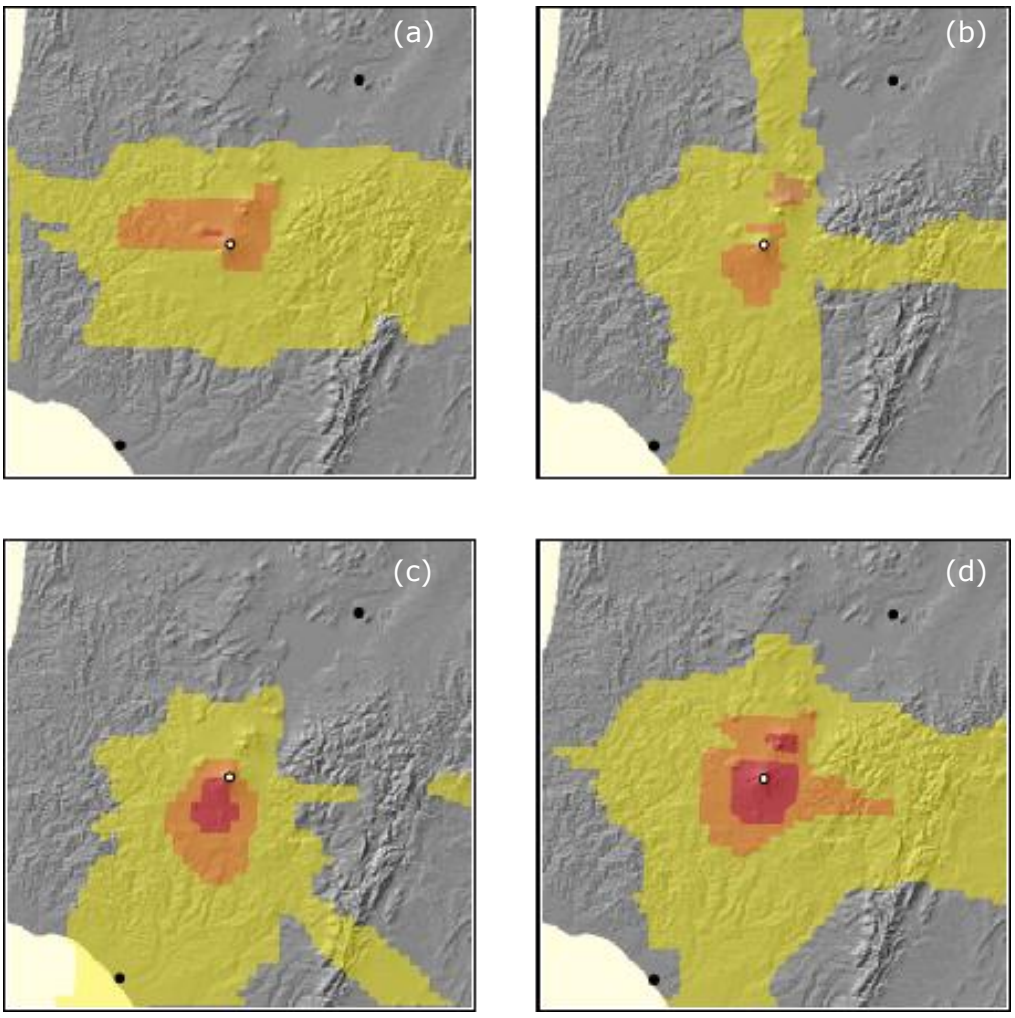

Figure 7. 32 Ruapehu volcano - Model 3, Grid 3, SO_2 average

a) January - March 2005
b) April - June 2005
c) July - September 2005
d) October - December 2005

1.0 - 4.9 µg m^{-3}
5.0 - 9.9 µg m^{-3}
≥10.0 µg m^{-3}

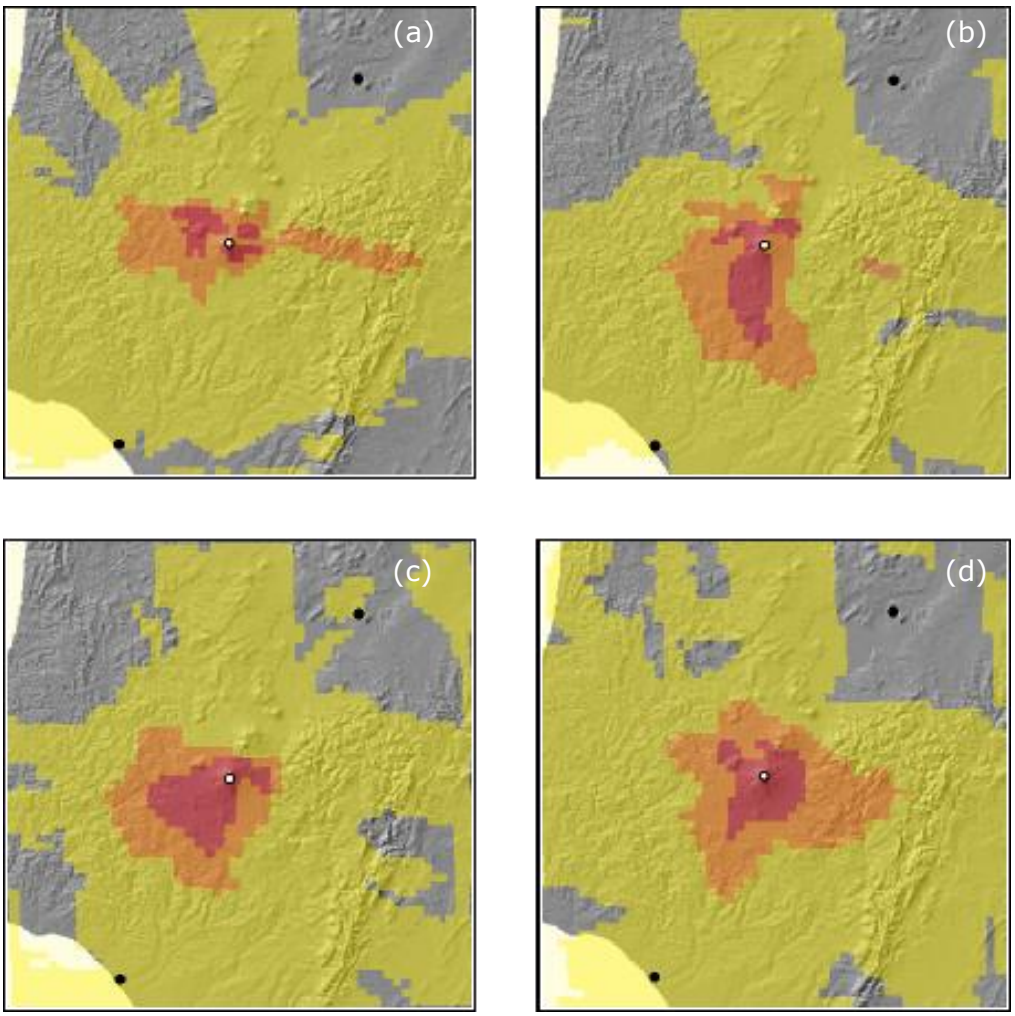

Figure 7. 33 Ruapehu volcano - Model 3, Grid 3, SO_2 maximum

a) January - March 2005
b) April - June 2005
c) July - September 2005
d) October - December 2005

50 - 349 µg m^{-3}
350 - 569 µg m^{-3}
≥570 µg m^{-3}

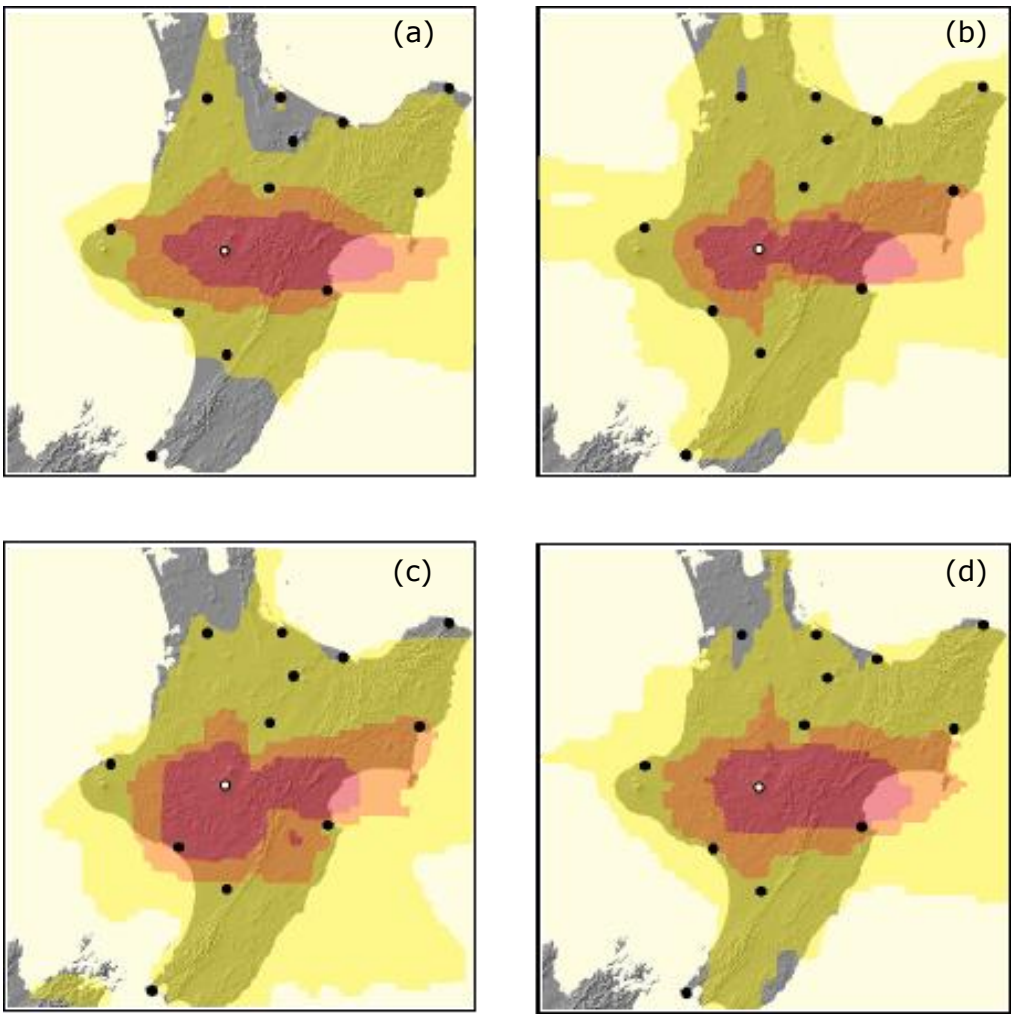

Figure 7. 34 Ruapehu volcano - Model 4, Grid 2, SO_2 average

a) January - March 2005
b) April - June 2005
c) July - September 2005
d) October - December 2005

1.0 - 4.9 µg m^{-3}
5.0 - 9.9 µg m^{-3}
≥10.0 µg m^{-3}

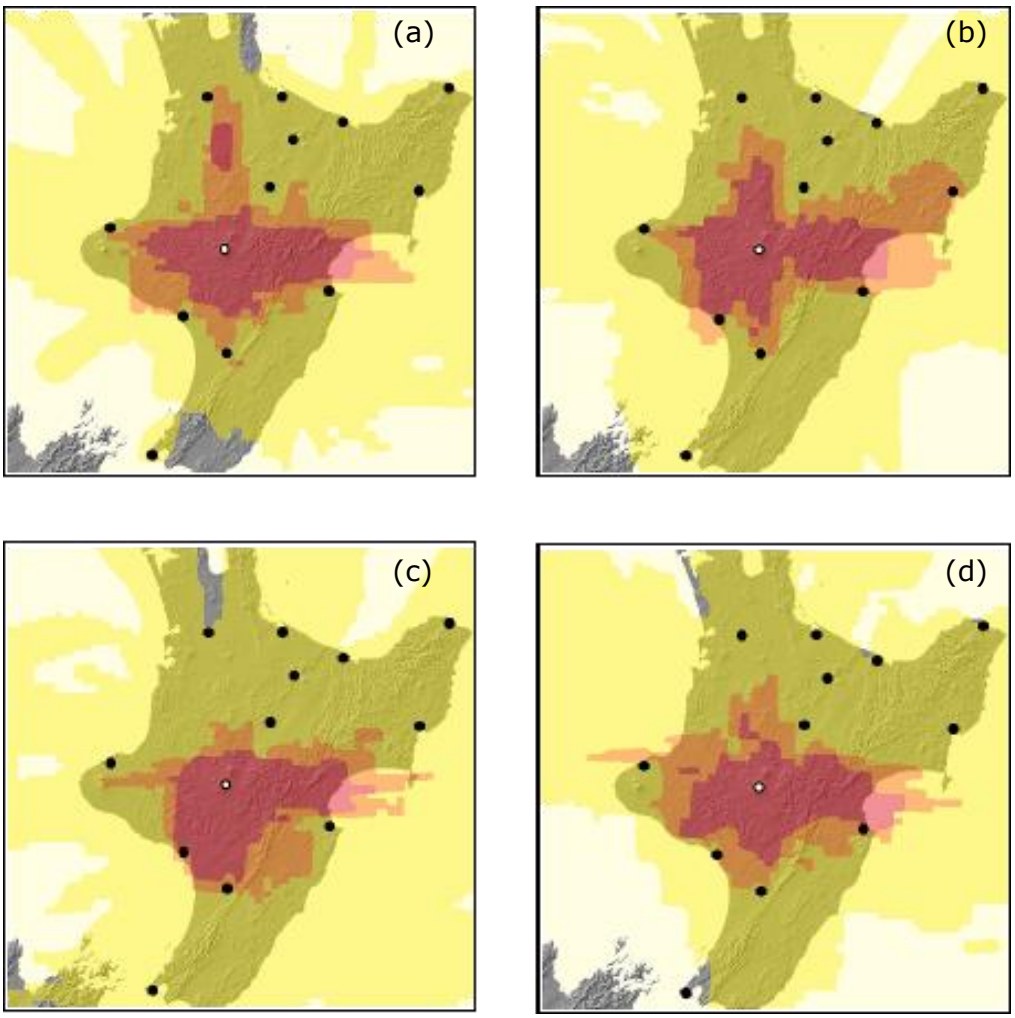

Figure 7. 35 Ruapehu volcano - Model 4, Grid 2, SO_2 maximum

a) January - March 2005
b) April - June 2005
c) July - September 2005
d) October - December 2005

50 - 349 µg m^{-3}
350 - 569 µg m^{-3}
≥570 µg m^{-3}

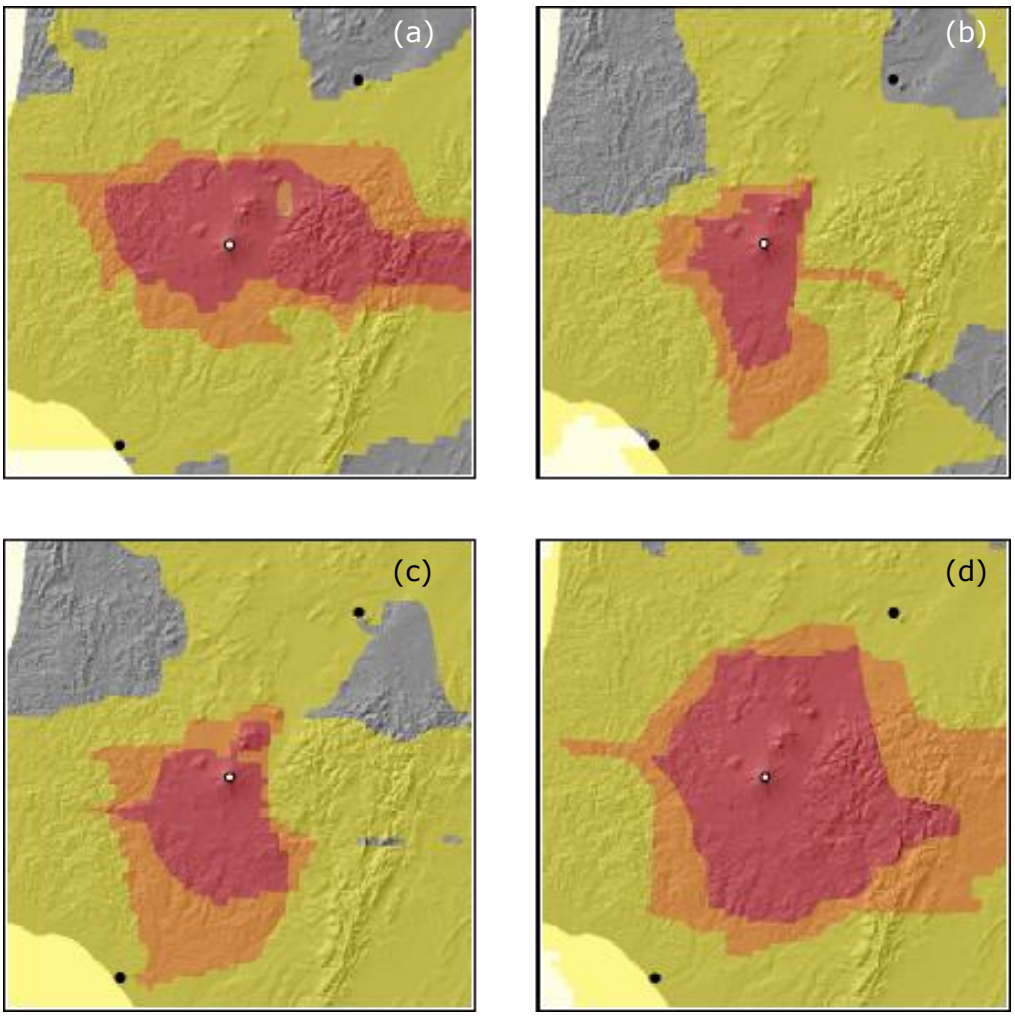

Figure 7. 36 Ruapehu volcano - Model 4, Grid 3, SO_2 average

a) January - March 2005
b) April - June 2005
c) July - September 2005
d) October - December 2005

1.0 - 4.9 µg m^{-3}
5.0 - 9.9 µg m^{-3}
≥10.0 µg m^{-3}

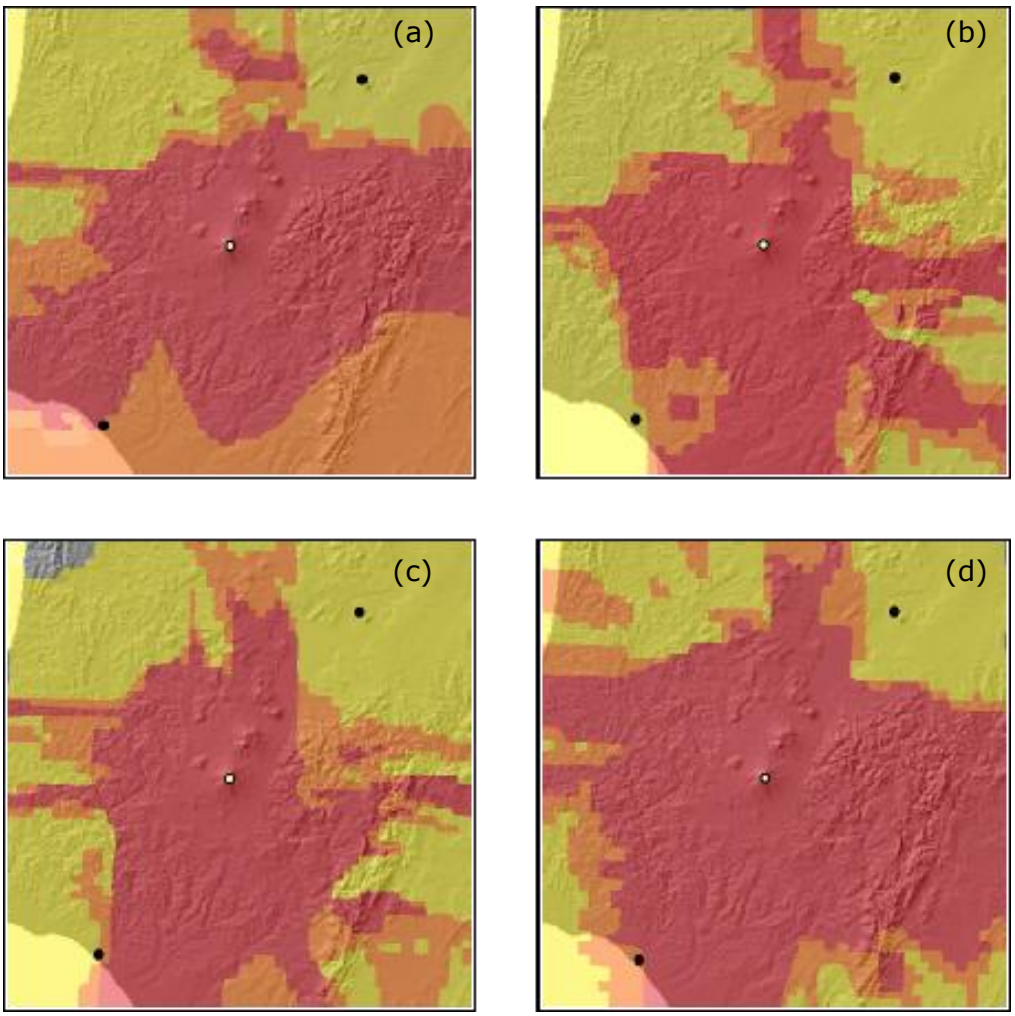

Figure 7. 37 Ruapehu volcano - Model 4, Grid 3, SO_2 maximum

a) January - March 2005
b) April - June 2005
c) July - September 2005
d) October - December 2005

50 - 349 µg m^{-3}
350 - 569 µg m^{-3}
≥570 µg m^{-3}

7. 6. Results of PM_{10} dispersion modelling from White Island volcano

7. 6. 1. Results of model 5 (373 K, 1 m s^{-1})

Figures 7. 38 to 7. 41 show the results of continuous emission of PM_{10} (model 5) with a defined emission rate of 20 g s^{-1}, which is equivalent to an emission rate of 1.7 Mg d^{-1}. In both grid domains, 2 and 3, all grid points reached average concentrations below 0.00 µg m^{-3}.

The maximum concentration values in grid 2 are all below 1.0 µg m^{-3}. TAPM calculated the highest values of 0.5 µg m^{-3} in the period of January to March for a single grid point west of Hicks Bay. The highest concentration value at ground level in grid 3 is 0.3 µg m^{-3}, which is located south-west of Hicks Bay and between White Island and Whakatane (January-March), as well as in a larger area between White Island and Tauranga (October-December). Since the resulted concentrations are too low, no plume fan was projected onto the DEM images. Instead the distribution of these low concentration values can be viewed from the gridded summary statistic files, which are saved on the CD-ROM.

7. 6. 2. Results of model 6 (773 K, 5 m s^{-1})

Figures 7. 42 to 7. 45 present the results from plume dispersion using a PM_{10} emission rate of 280 g s^{-1} (c. 24 Mg d^{-1}) at intervals of five hours (model 6). The highest average concentration in both grid domains 2 and 3 is 0.01 µg m^{-3}. These low concentrations are found in different regions throughout the year. Like model 5, the dispersion of the low concentration plumes is not shown on the DEM images but, as mentioned above, the corresponding files are saved on the CD-ROM.

The maximum concentration reached reasonable values to project those parts of plume fans exceeding a value 1.0 µg m^{-3} onto DEM images. The maximum concentrations at ground level in grid 2 only cover very small areas near White Island and a few other locations. The highest value of 2.1 µg m^{-3} is found at a single grid point west of Hicks Bay during the January to March period. The plumes in grid 3 cover much larger areas than in grid 2. While the plumes in the period of January to September are characterised by covering numerous, yet smaller areas, there can be found one large plume east of White Island for the period of October to

December. The highest value was calculated at 4.2 µg m^{-3} for a single grid point south of Whakatane during the period January to March.

7. 7. Results of PM_{10} dispersion modelling from Ruapehu volcano

7. 7. 1. Results of model 5 (373 K, 1 m s^{-1})

Figures 7. 46 to 7. 49 show the results of continuous emission of PM_{10} (model 5) with a defined emission rate of 20 g s^{-1}, which is equivalent to an emission rate of 1.7 Mg d^{-1}. Similar to the results from White Island volcano, the average concentrations in both grids 2 and 3 are extremely low, reaching values up to 0.02 µg m^{-3}. In grid domain 2, this highest value is found near the vent during the period of January to March, as well as at a single point from October to December, whereas in grid domain 3, this value is only found at a single point at the source in the period between October and December.

The maximum concentration values in grid 2 are all below 1.0 µg m^{-3}. TAPM calculated the highest values of 0.5 µg m^{-3} in the period of October to December for two grid points at the source. The calculated values for the average concentration in grids 2 and 3, and the maximum concentration in grid 2 are too low to project a plume fan onto the DEM images. The distribution of these low concentration values can be viewed from the gridded summary statistic on the CD-ROM.

The highest ground concentration in grid domain 3 is 1.4 µg m^{-3} and it is found c. 15 km east of the vent during the periods of July to September and October to December. The ground level concentrations higher than 1.0 µg m^{-3} only cover a small region near the source.

7. 7. 2. Results of model 6 (773 K, 5 m s^{-1})

Figures 7. 50 to 7. 53 present the results from plume dispersion using a PM_{10} emission rate of 280 g s^{-1} (c. 24 Mg d^{-1}) at intervals of five hours (model 6). Generally, the average concentrations are very low. The highest value in grid domain 2 is 0.08 µg m^{-3}, which is found at fee grid points near the vent in the periods of January to March and October to December. The highest concentration in

grid domain 3 is 0.16 µg m^{-3}, and was only calculated for the period of October to December. Like in previous results, the dispersion of the low concentration plumes is not shown on the DEM images but can be seen from the gridded summary statistic files, which are saved on the CD-ROM.

The maximum concentration in grid domains 2 and 3 reached higher values, exceeding 1.0 µg m^{-3}. Hence, those parts of the plume fans are projected onto DEM images. In contrast to White Island where the plumes covered several small areas, the plumes from Ruapehu volcano cover a single larger region surrounding the vent. A characteristic feature of the plumes in all four modelled periods is a distinctive dispersion in an east-west direction, travelling several tens of kilometres, predominantly in a western direction, and extending toward the urban area of Napier. The only urban area affected by the plumes between April to September is Wanganui. The highest concentration value of 3.2 µg m^{-3} was calculated for the period of July to September at the source.

The volcanic plumes from Ruapehu in grid 3, containing the maximum concentrations, are characterised by covering large regions in that grid domain. In all four periods, the concentration exceeds the threshold value of 10.0 µg m^{-3}, in which the highest value is 26.9 µg m^{-3}. Like the results in grid 2, the individual plumes show a distinctive east-west expansion, though there is also some dispersion in northern and southern directions. Wanganui is the only urban area affected during the period of October to December.

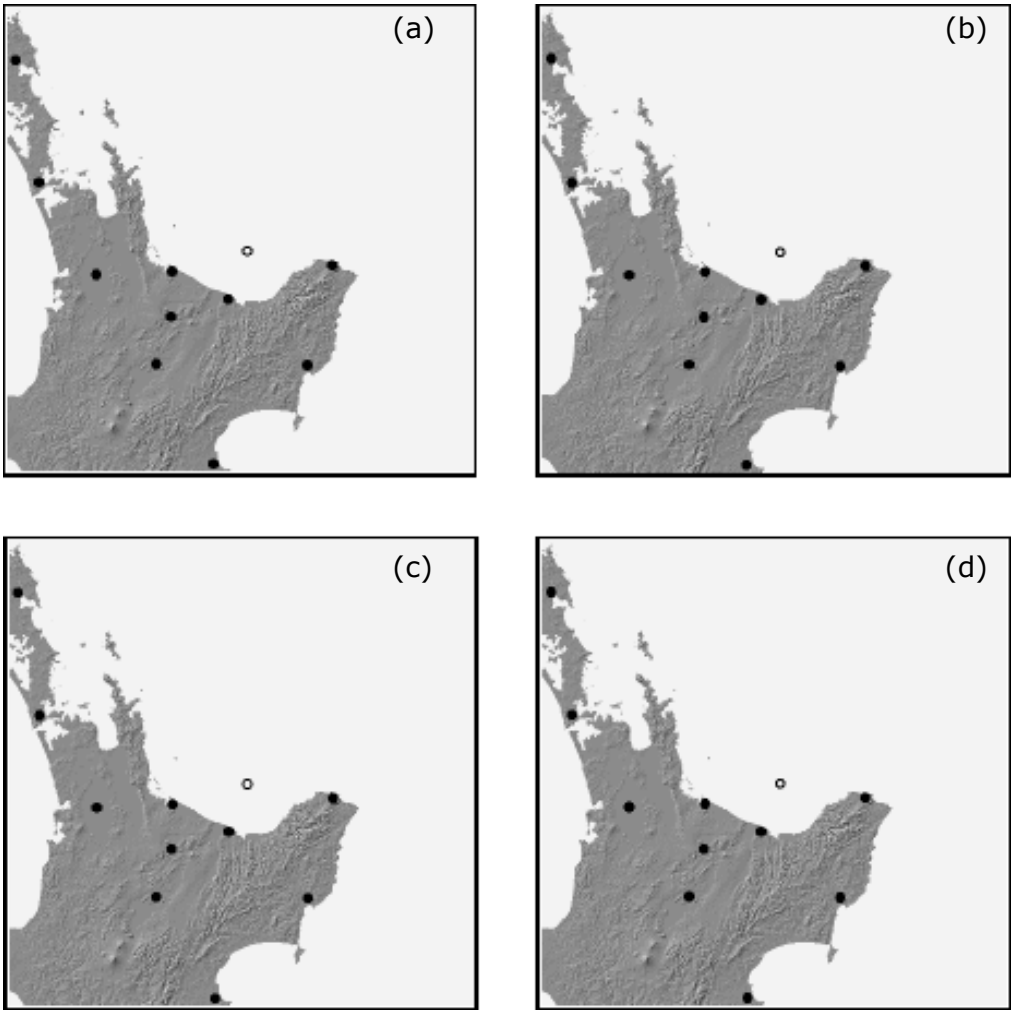

Figure 7. 38 White Island volcano - Model 5, Grid 2, PM_{10} average

a) January - March 2005
b) April - June 2005
c) July - September 2005
d) October - December 2005

1.0 - 4.9 µg m^{-3}
5.0 - 9.9 µg m^{-3}
≥10.0 µg m^{-3}

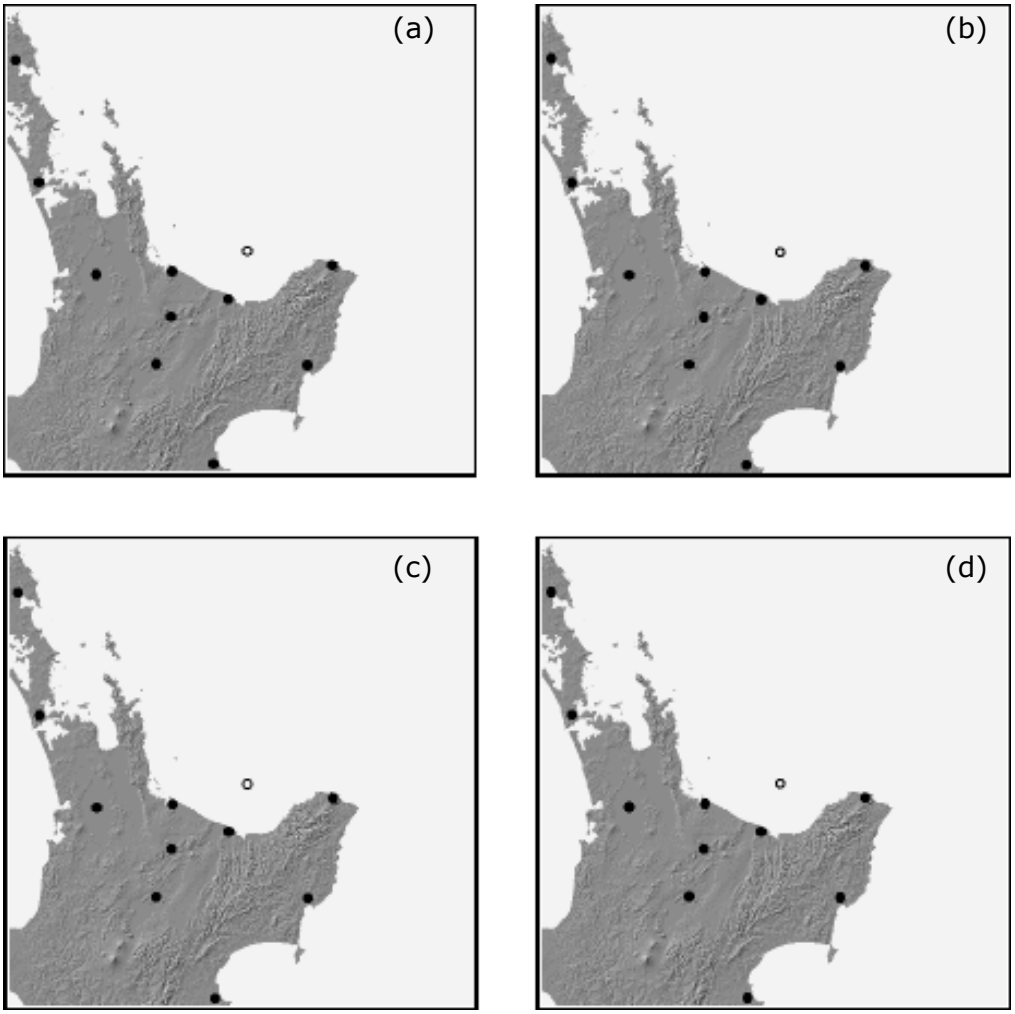

Figure 7. 39 White Island volcano - Model 5, Grid 2, PM_{10} maximum

a) January - March 2005
b) April - June 2005
c) July - September 2005
d) October - December 2005

1.0 - 4.9 µg m^{-3}
5.0 - 9.9 µg m^{-3}
≥10.0 µg m^{-3}

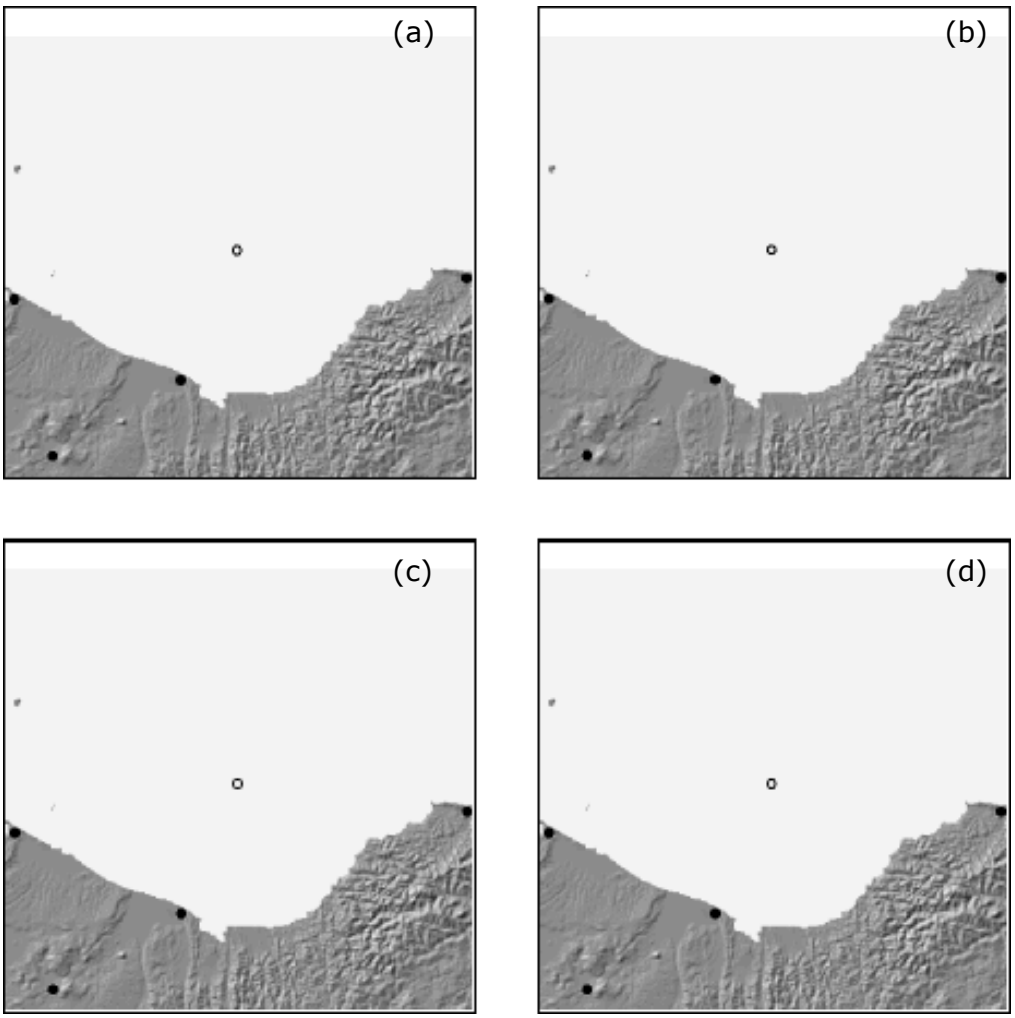

Figure 7. 40 White Island volcano - Model 5, Grid 3, PM_{10} average

a) January - March 2005
b) April - June 2005
c) July - September 2005
d) October - December 2005

1.0 - 4.9 µg m^{-3}
5.0 - 9.9 µg m^{-3}
≥10.0 µg m^{-3}

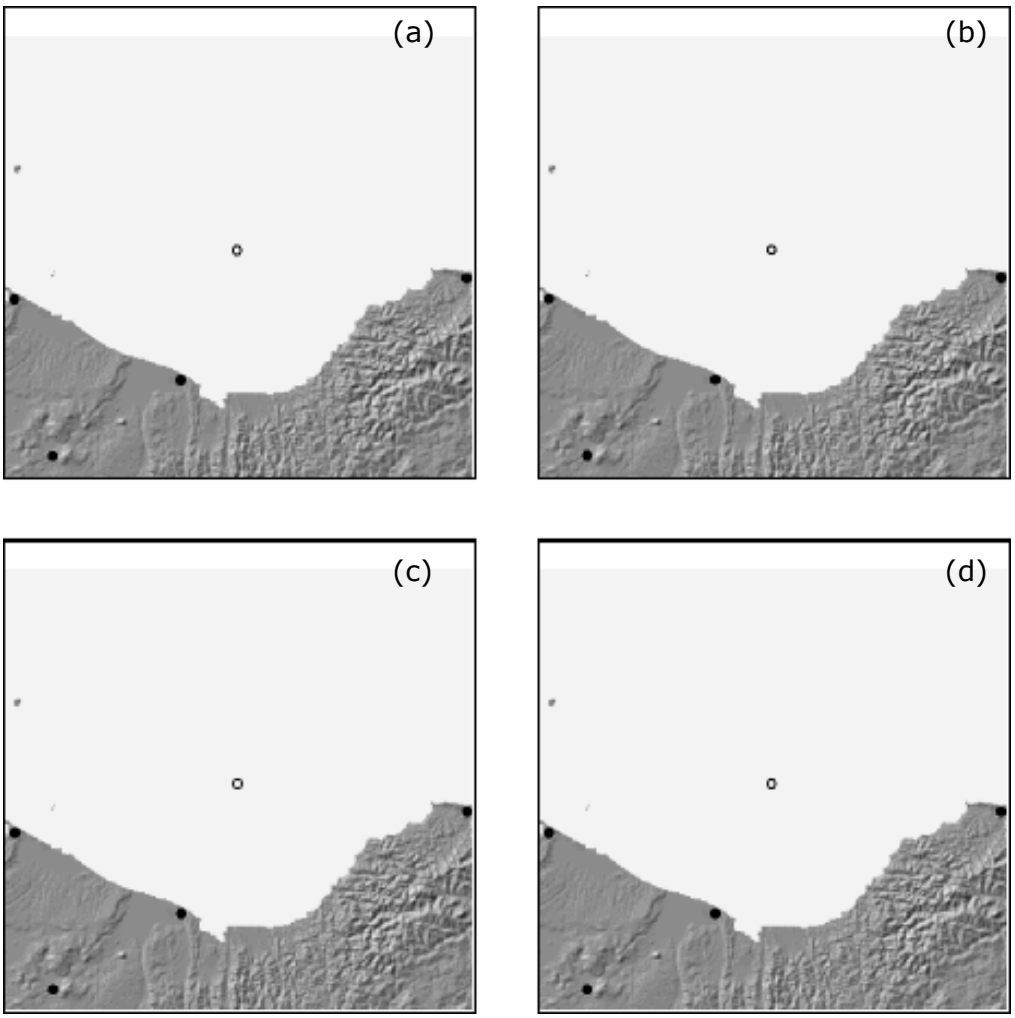

Figure 7. 41 White Island volcano - Model 5, Grid 3, PM_{10} maximum

a) January - March 2005
b) April - June 2005
c) July - September 2005
d) October - December 2005

1.0 - 4.9 µg m^{-3}
5.0 - 9.9 µg m^{-3}
≥10.0 µg m^{-3}

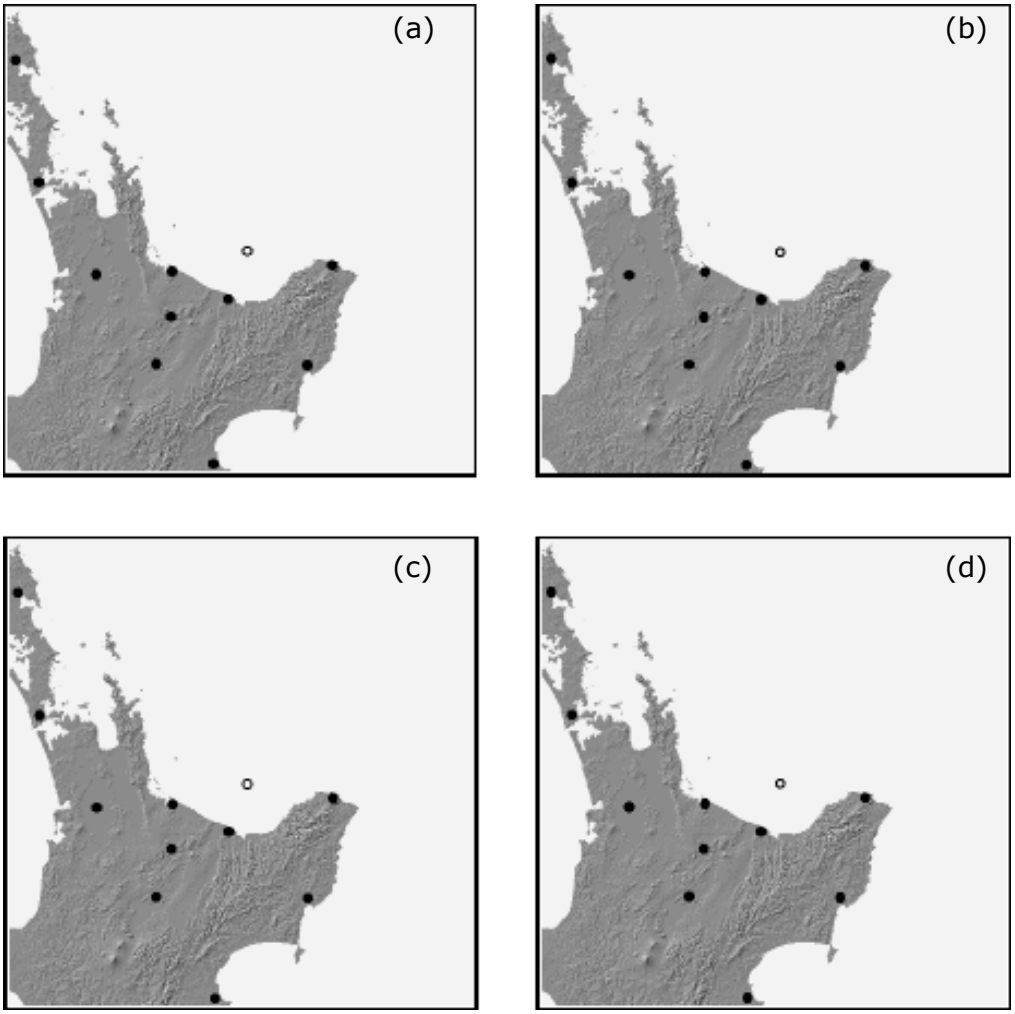

Figure 7. 42 White Island volcano - Model 6, Grid 2, PM_{10} average

a) January - March 2005
b) April - June 2005
c) July - September 2005
d) October - December 2005

1.0 - 4.9 µg m^{-3}
5.0 - 9.9 µg m^{-3}
≥10.0 µg m^{-3}

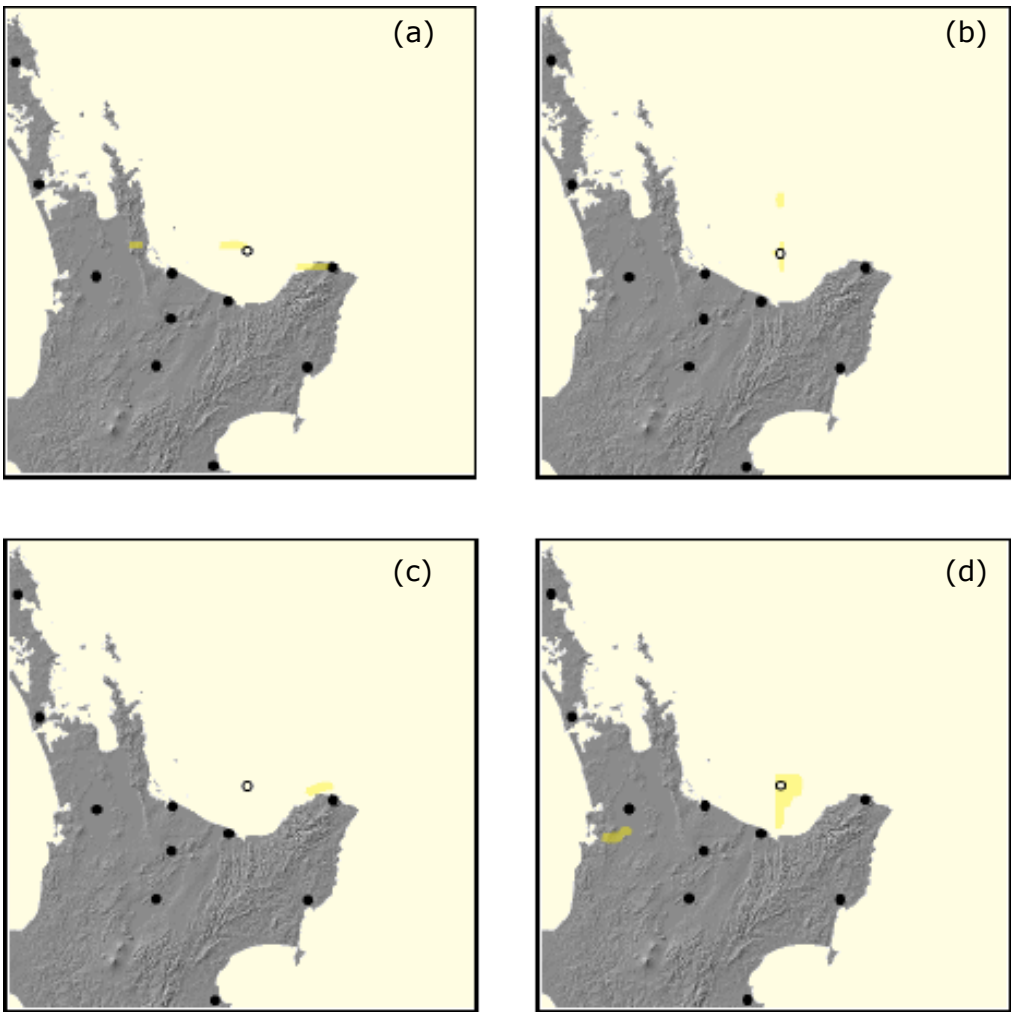

Figure 7. 43 White Island volcano - Model 6, Grid 2, PM_{10} maximum

a) January - March 2005
b) April - June 2005
c) July - September 2005
d) October - December 2005

1.0 - 4.9 µg m^{-3}
5.0 - 9.9 µg m^{-3}
≥10.0 µg m^{-3}

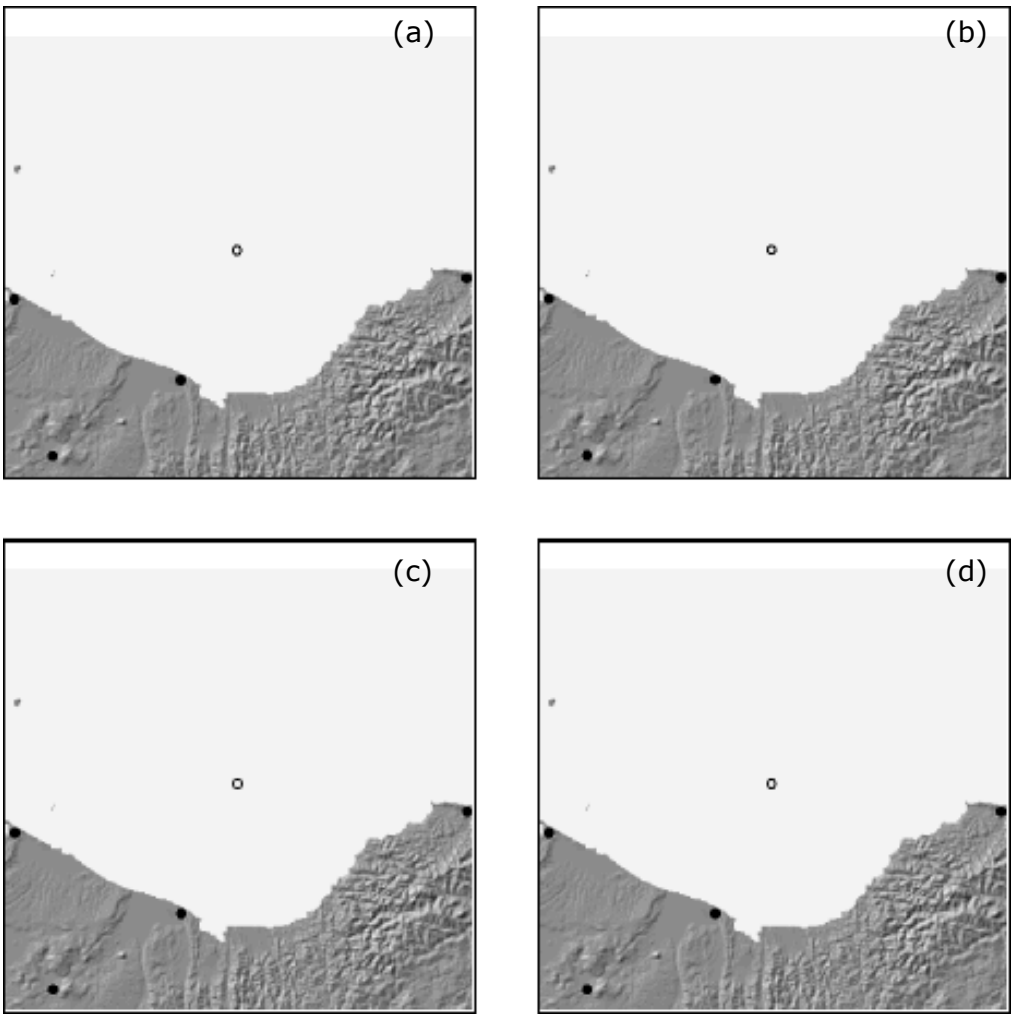

Figure 7. 44 White Island volcano - Model 6, Grid 3, PM_{10} average

a) January - March 2005
b) April - June 2005
c) July - September 2005
d) October - December 2005

1.0 - 4.9 µg m^{-3}
5.0 - 9.9 µg m^{-3}
≥10.0 µg m^{-3}

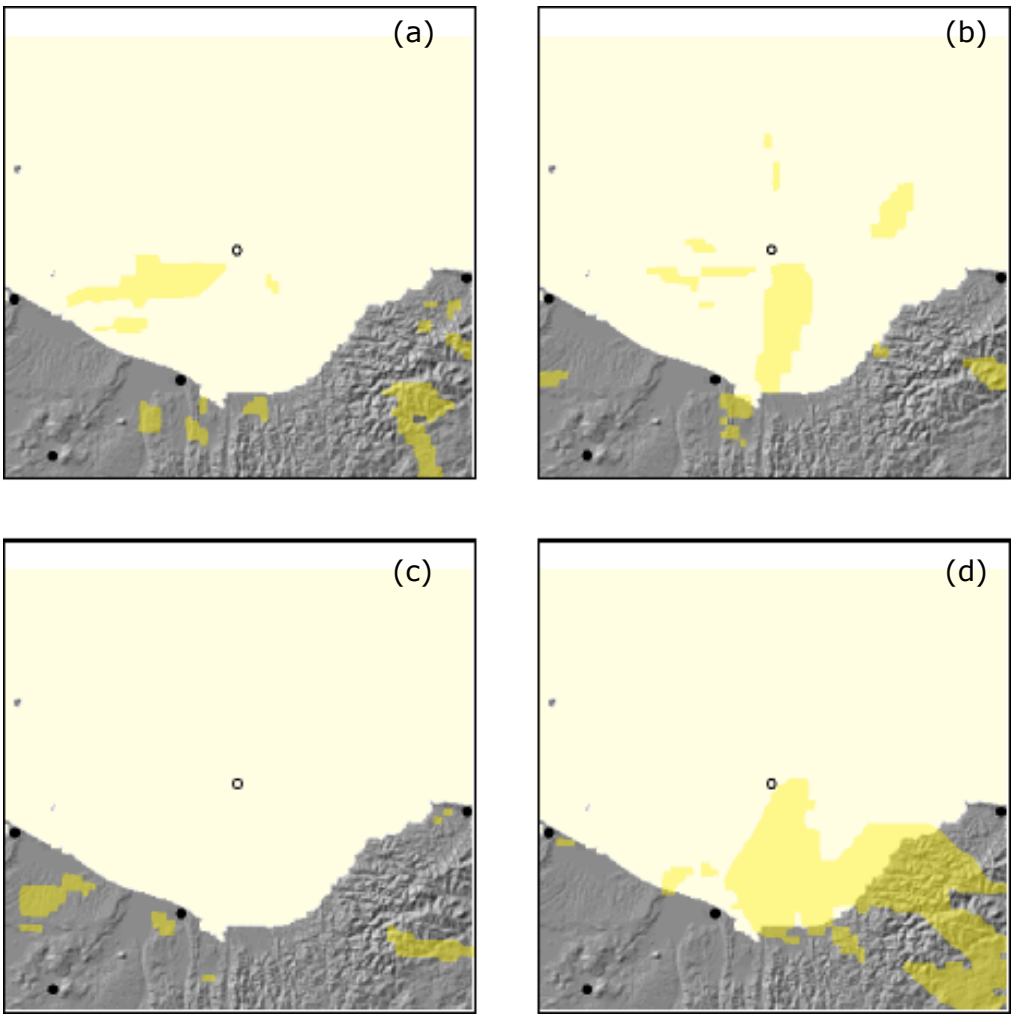

Figure 7. 45 White Island volcano - Model 6, Grid 3, PM_{10} maximum

a) January - March 2005
b) April - June 2005
c) July - September 2005
d) October - December 2005

1.0 - 4.9 µg m^{-3}
5.0 - 9.9 µg m^{-3}
≥10.0 µg m^{-3}

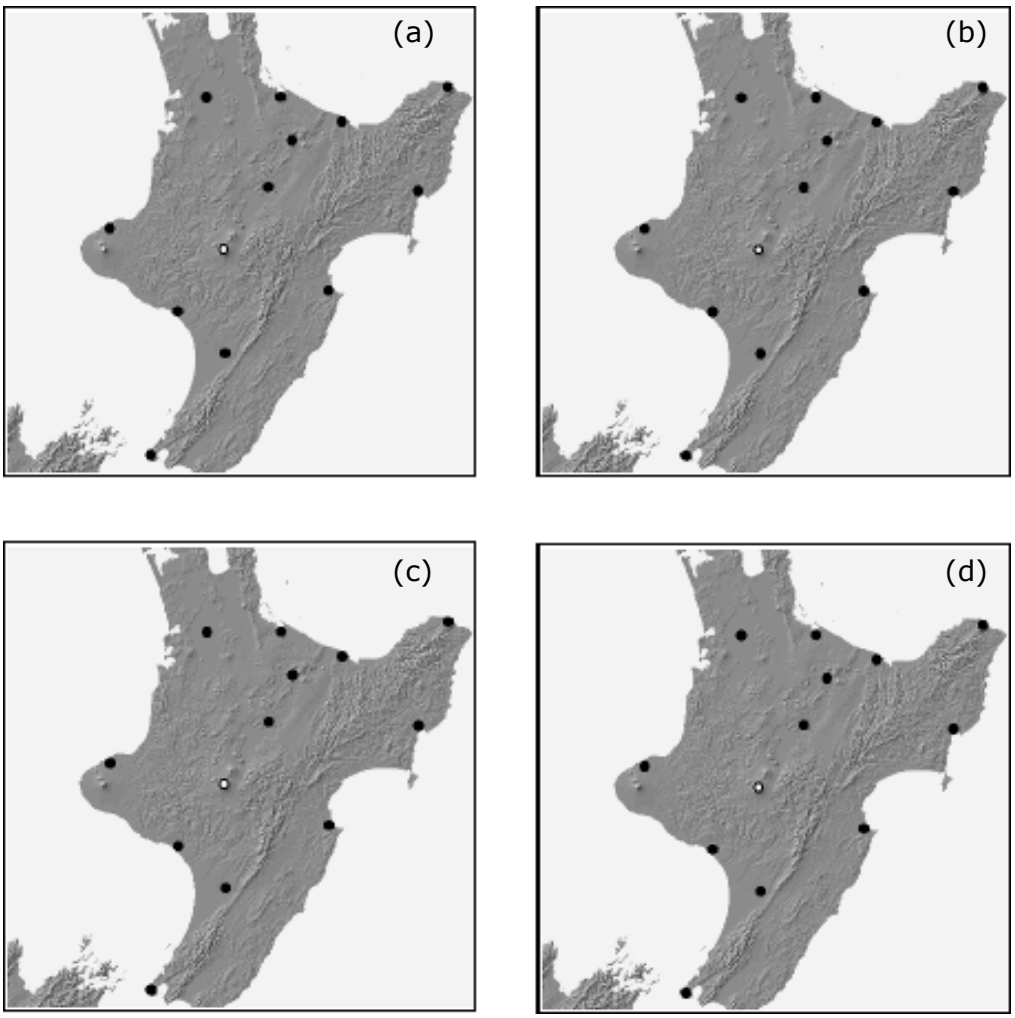

Figure 7. 46 Ruapehu volcano - Model 5, Grid 2, PM_{10} average

a) January - March 2005
b) April - June 2005
c) July - September 2005
d) October - December 2005

1.0 - 4.9 µg m^{-3}
5.0 - 9.9 µg m^{-3}
≥10.0 µg m^{-3}

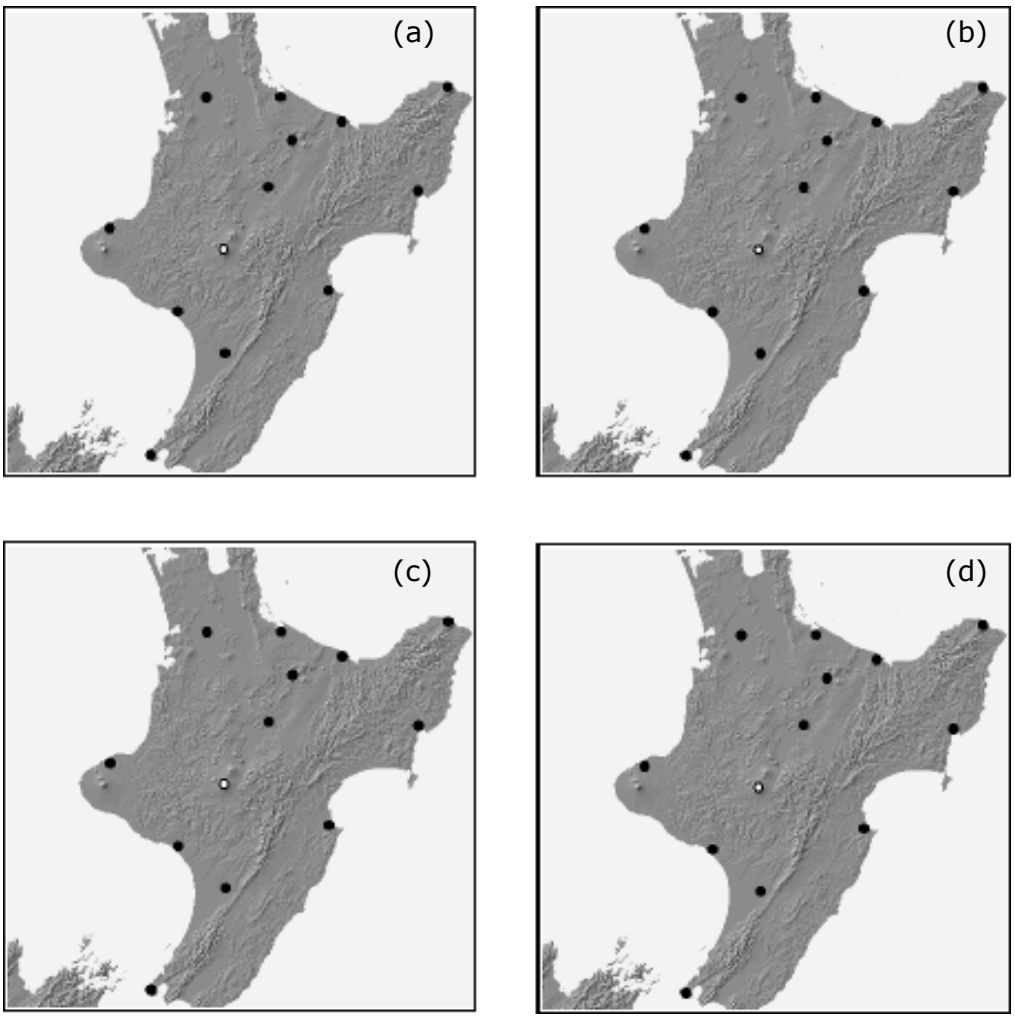

Figure 7. 47 Ruapehu volcano - Model 5, Grid 2, PM_{10} maximum

a) January - March 2005
b) April - June 2005
c) July - September 2005
d) October - December 2005

1.0 - 4.9 µg m^{-3}
5.0 - 9.9 µg m^{-3}
≥10.0 µg m^{-3}

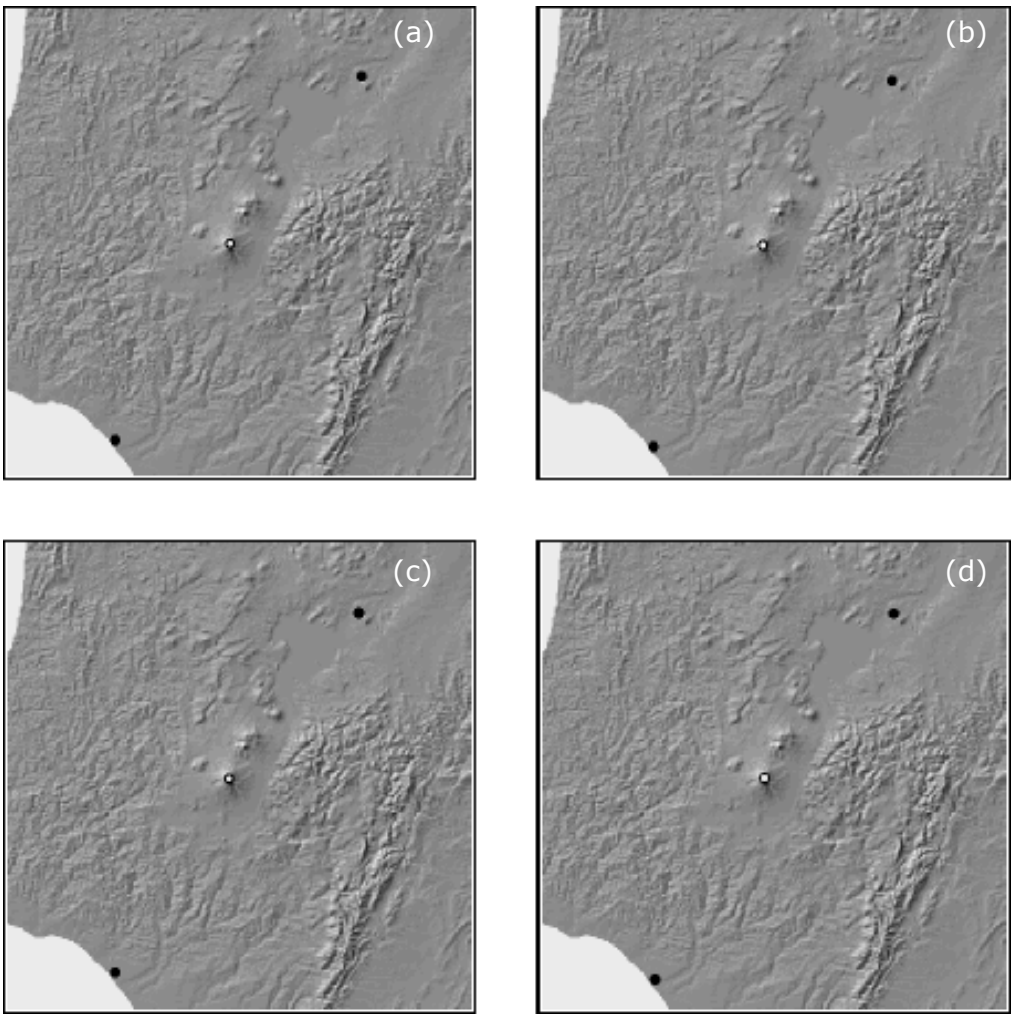

Figure 7. 48 Ruapehu volcano - Model 5, Grid 3, PM_{10} average

a) January - March 2005
b) April - June 2005
c) July - September 2005
d) October - December 2005

1.0 - 4.9 µg m^{-3}
5.0 - 9.9 µg m^{-3}
≥10.0 µg m^{-3}

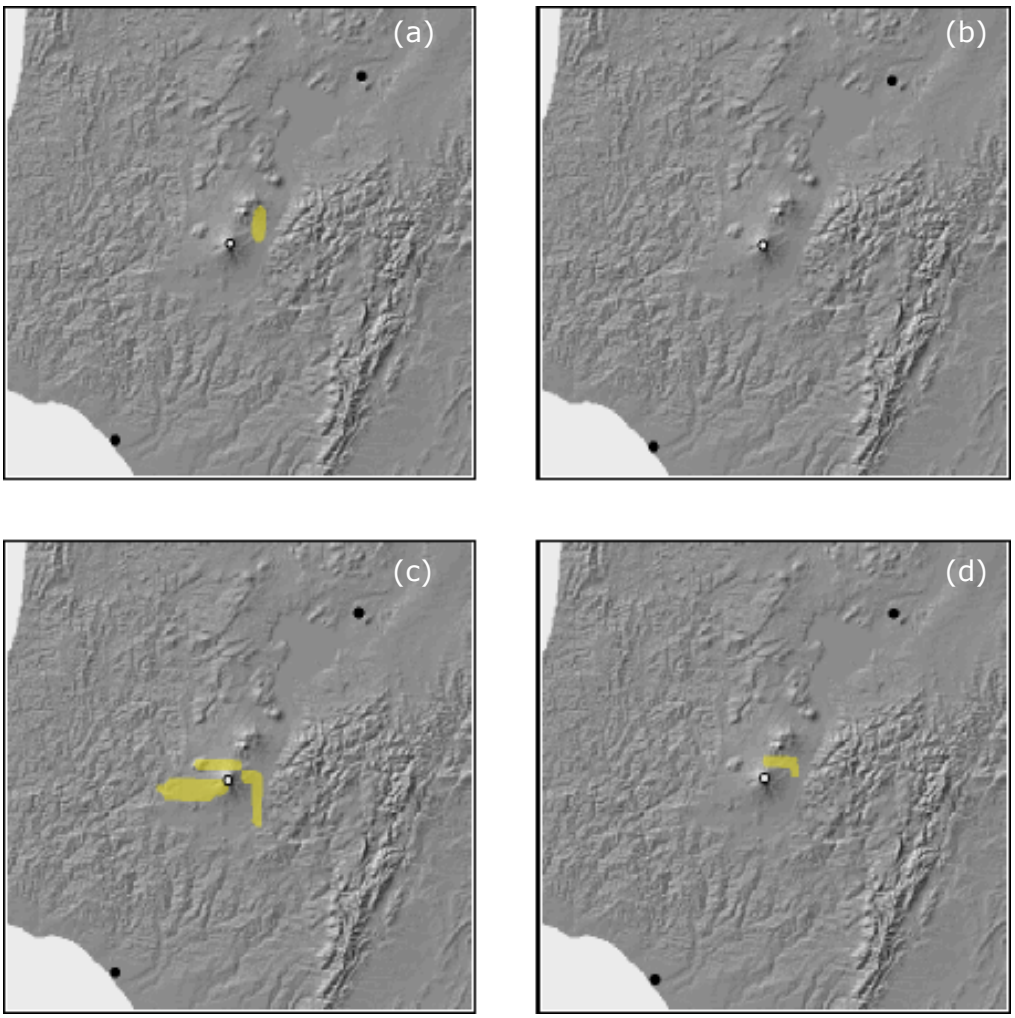

Figure 7. 49 Ruapehu volcano - Model 5, Grid 3, PM_{10} maximum

a) January - March 2005
b) April - June 2005
c) July - September 2005
d) October - December 2005

1.0 - 4.9 µg m^{-3}
5.0 - 9.9 µg m^{-3}
≥10.0 µg m^{-3}

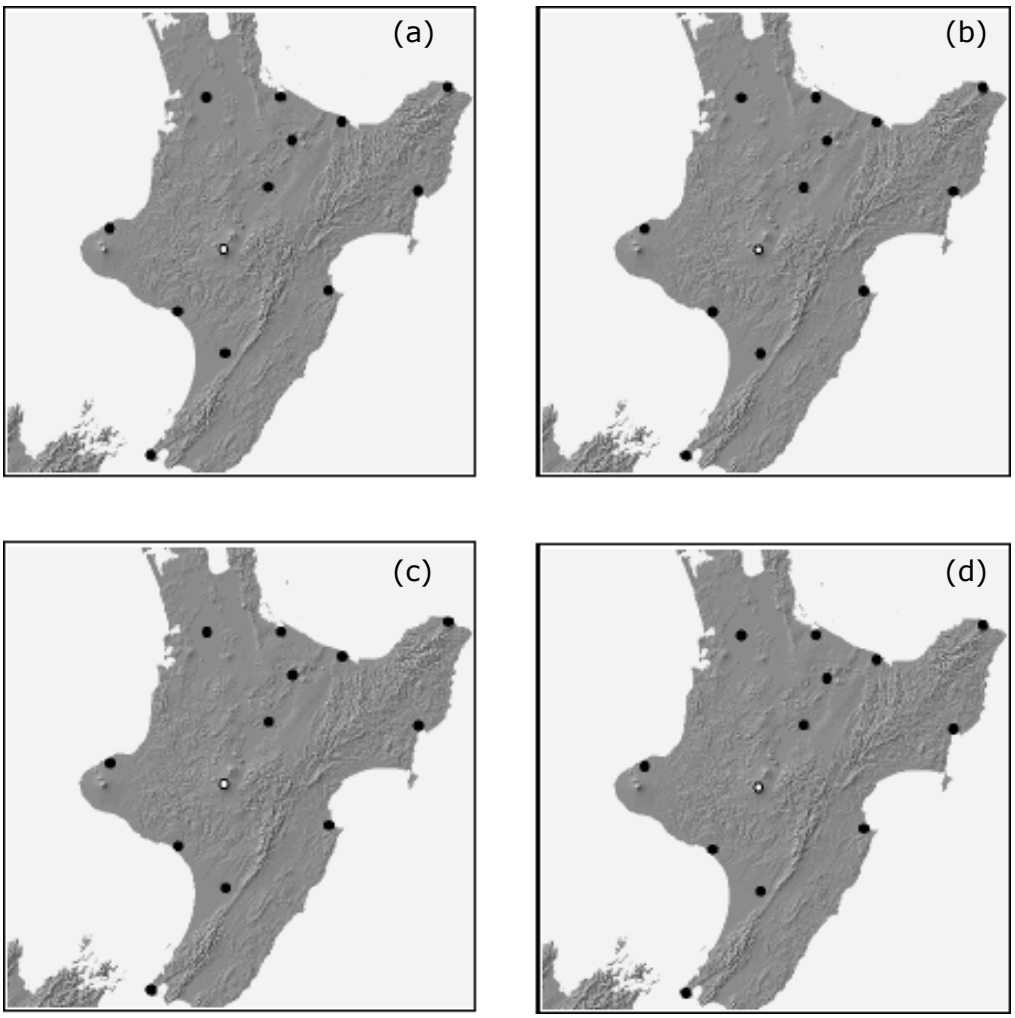

Figure 7. 50 Ruapehu volcano - Model 6, Grid 2, PM_{10} average

a) January - March 2005
b) April - June 2005
c) July - September 2005
d) October - December 2005

1.0 - 4.9 µg m^{-3}
5.0 - 9.9 µg m^{-3}
≥10.0 µg m^{-3}

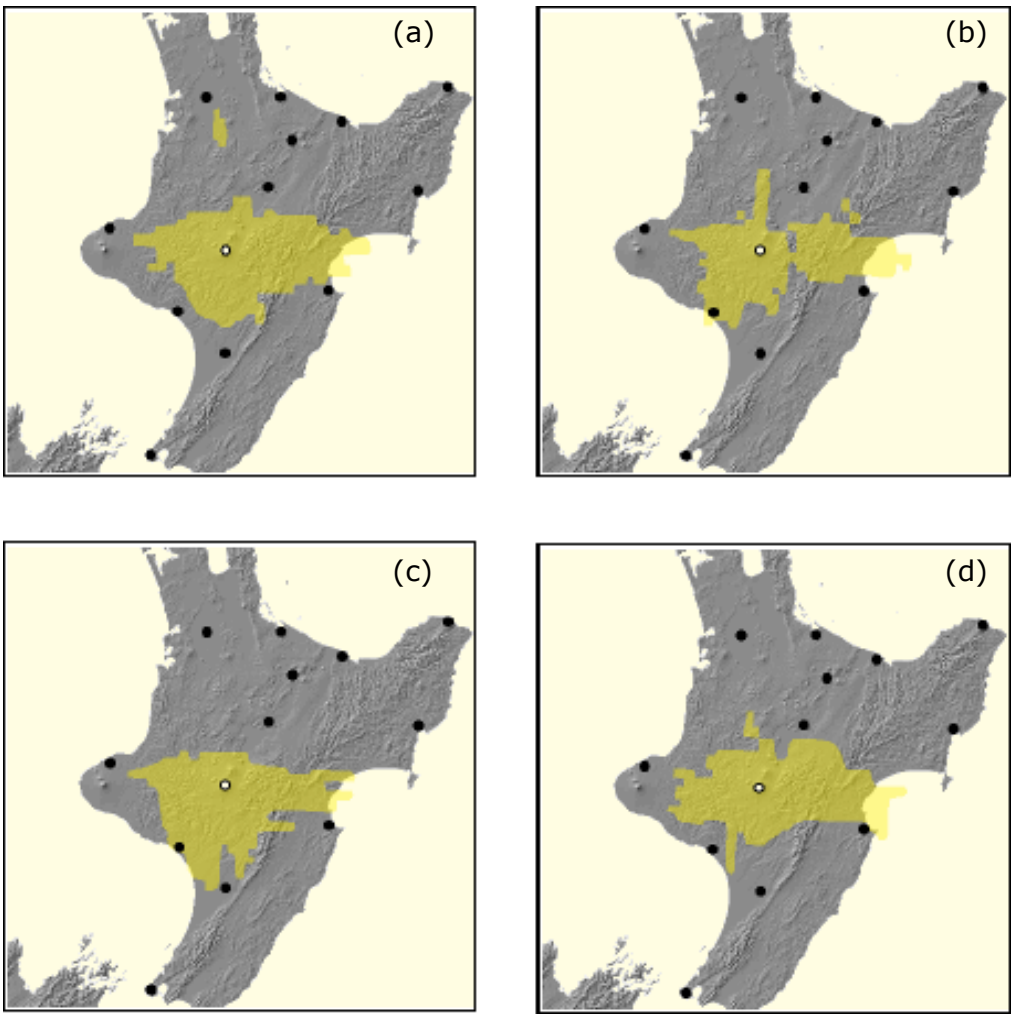

Figure 7. 51 Ruapehu volcano - Model 6, Grid 2, PM_{10} maximum

a) January - March 2005
b) April - June 2005
c) July - September 2005
d) October - December 2005

1.0 - 4.9 µg m^{-3}
5.0 - 9.9 µg m^{-3}
≥10.0 µg m^{-3}

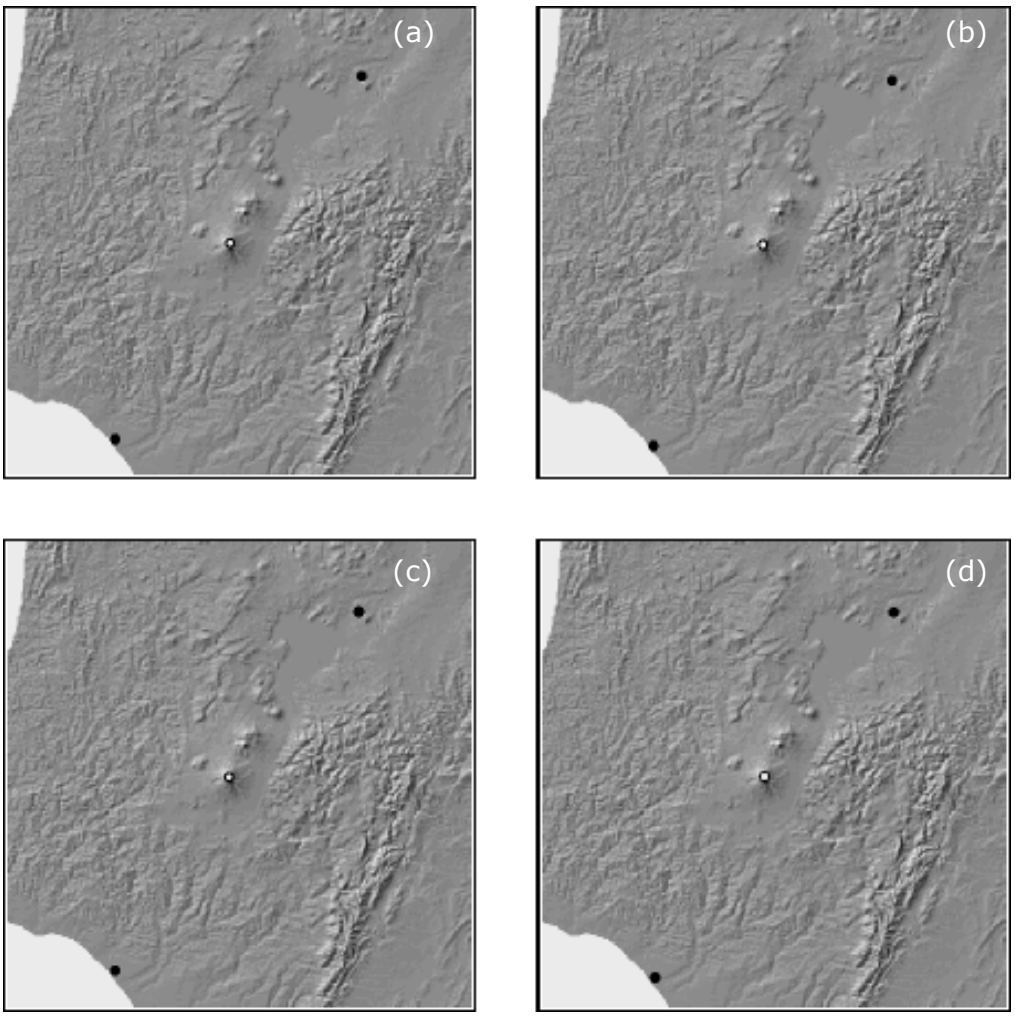

Figure 7. 52 Ruapehu volcano - Model 6, Grid 3, PM_{10} average

a) January - March 2005
b) April - June 2005
c) July - September 2005
d) October - December 2005

1.0 - 4.9 µg m^{-3}
5.0 - 9.9 µg m^{-3}
≥10.0 µg m^{-3}

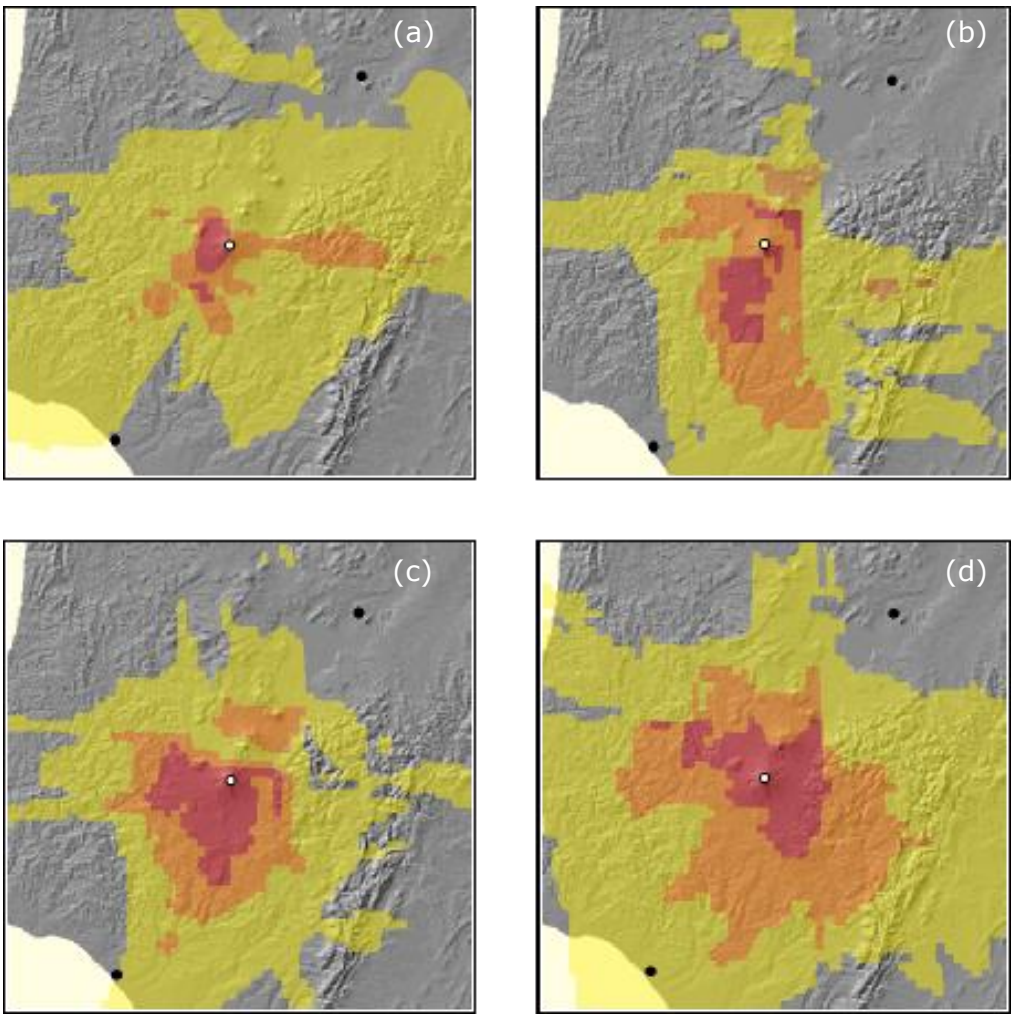

Figure 7. 53 Ruapehu volcano - Model 6, Grid 3, PM_{10} maximum

a) January - March 2005
b) April - June 2005
c) July - September 2005
d) October - December 2005

1.0 - 4.9 µg m^{-3}
5.0 - 9.9 µg m^{-3}
≥10.0 µg m^{-3}

7. 8. Summary and discussion

Depending on input parameters used, the modelling of the volcanic plumes from White Island show that the dispersion of SO_2 are partly widespread but the ground level concentrations are generally low. This is particularly valid for the scenarios of quiescent degassing from White Island volcano, where the average and maximum concentrations do not exceed the value of 5.0 and 350 µg m^{-3} at all during the modelled periods. During model 4, the plumes from White Island volcano are much more widespread than in models 1-3 and cover larger areas at ground level. The ground level concentration, however, hardly exceeds the threshold values of 350 and 570 µg m^{-3} and do not affect any urban communities. But the results of model 4 also suggest higher plume concentrations (≥350 µg m^{-3}) at the proximity of White Island.

The results of SO_2 dispersion modelling (models 1-3) from Ruapehu volcano show higher plume concentrations at ground level and cover large areas over land than the results from White Island. However, since the central part of the North Island is not highly populated, the modelled plumes affect the rural region rather than any urban areas. The widespread plumes from Ruapehu are also characterised by low average and maximum concentrations of 1.0 and 50 µg m^{-3}, respectively. The next concentration levels of 5.0 and 350 µg m^{-3} mainly affect the close surroundings of the volcanic source. The only highly populated area affected by the quiescent degassing plume with concentrations of ≥350 µg m^{-3} is Napier at the east coast, which is due to the preferable westerly winds. The dispersing plumes in model 4, with average and maximum concentrations of 1.0 and 50 µg m^{-3}, are even more widespread and cover most of the North Island. Those parts of the plume with higher concentrations (≥5 µg m^{-3} and ≥350 µg m^{-3}) are also more widespread than in models 1-3 but they are mainly affect the central part of the North Island, including the urban communities of Napier, Gisborne, Wanganui, Palmerston North and New Plymouth. For Napier was even modelled a maximum SO_2 concentration of ≥570 µg m^{-3}.

The results of PM_{10} dispersion modelling from White Island volcano show very low ground level concentrations. A concentration of 1.0 µg m^{-3} is not exceeded at all in model 5 and the plumes in model 6 cover only small areas, mainly south-west of White Island and south of Hicks Bay.

The results of model 5 with Ruapehu as a point source are similar the results from White Island. Only very small areas near the vent exceed a concentration of 1.0 µg m^{-3} during most of the year. The plumes in model 6 are more widespread and cover large parts of the North Island. While the plume exceeding a concentration of 1.0 µg m^{-3} also reaches the urban communities of Napier and Wanganui, the inner parts of the individual plumes with concentrations of ≥5 µg m^{-3} only affect the rural area surrounding the volcanic edifice.

While the results of modelling from Ruapehu volcano suggest a more gradual deposition of SO_2 from proximal to the distal areas, the White Island model indicates that the pollution concentration at the urban areas of Whakatane and Tauranga, located at the coast of the Bay of Plenty, are less than the urban areas more inland, such as Hamilton and Taupo. This result is probably caused by the characteristic features of the boundary layer. According to Stull [1989] and Arya [1999], the marine boundary layer shows little variation of depth in time and space. On the other hand, the boundary layer over land experiences more turbulence due to more temperature variations.

Output data from meteorological modelling include information of the boundary layer depth at any point in the modelled grid domains. Therefore data were extracted at the grid centres (White Island and Ruapehu), at four random locations near the North Island (over sea) and four random locations in the North Island (over land) to see differences of the boundary layer depth (Figure 7. 54). The minimum, maximum and average values of the depth of the boundary layer are listed in Table 7. 3 and line graphs in Figures 7. 55a-l show the variation of depth of the boundary layer at all locations for the period of January-March 2005, where data was extracted. The meteorological output data of all locations in Figure 7. 55 is saved on the CD-ROM.

Comparison of the wind roses from meteorological modelling with the individual figures from pollution dispersion modelling shows that there are similarities between the results of SO_2 ground pollution with prevailing wind direction modelled. As mentioned in chapter 6, the prevailing wind direction from January to March on White Island is SE (Figure 6. 1a). In Figures 7. 16a it can be seen that the largest area of SO_2 ground pollution is found SE of White Island, corresponding with the prevailing wind direction. A parallel situation can be recognised in Figure 7. 20a that shows a more wide spread plume with higher ground concentrations, particularly SE of White Island.

Similar characteristic is found from April to June where to highest concentration of ground pollution in north of White Island (e.g. Figures 7. 16b and 7. 20b). This confirms the prevailing wind direction modelled (Figure 6. 1b).

The wind direction and dispersion of particulate matter (PM_{10}) of models 5 and 6 with White Island as point source are different. However, this may be due to the very low emission rate chosen and the resulting low ground pollution in the models.

The models with Ruapehu as point source show that the wind is blowing in all direction throughout the year (Figure 6. 5). The results of pollution modelling (SO_2 and PM_{10}) confirms also indicate equally pollution dispersion in 2005 (e.g. Figures 7. 33 and 7. 51). This characteristic is valid for the proximal pollution dispersion but not valid for distal pollution dispersion. For example, Figure 7. 51b (April to June) shows a wider plume dispersion of PM_{10} to the east than to the west. As shown in Figure 6. 5, the wind rose for the period from April to June indicates prevailing wind direction to the west.

Table 7. 3 Minimum, average and maximum values of depth of the boundary layer at various locations in and around the North Island for the period from January to March 2005.

Location over sea (Grid point)	Depth of the boundary layer			Location over land (Grid point)	Depth of boundary layer		
	Min	Avg	Max		Min	Avg	Max
White Island (Grid 2) (25/25)	25	226	2633	Ruapehu (Grid 2) (25/25)	22	243	2925
White Island (Grid 3) (25/25)	25	241	2515	Ruapehu (Grid 3) (25/25)	20	81	472
Bay of Plenty (North) (39/46)	25	237	3869	North of Ruapehu (27/38)	24	353	2294
Pacific Ocean (East) (46/20)	25	245	4899	East of Ruapehu (30/25)	22	259	2518
Tasman Sea (West) (06/36)	25	246	2238	West of Ruapehu (22/33)	24	356	1622
Cook Strait (South) (17/12)	25	254	6725	South of Ruapehu (24/21)	24	352	1522

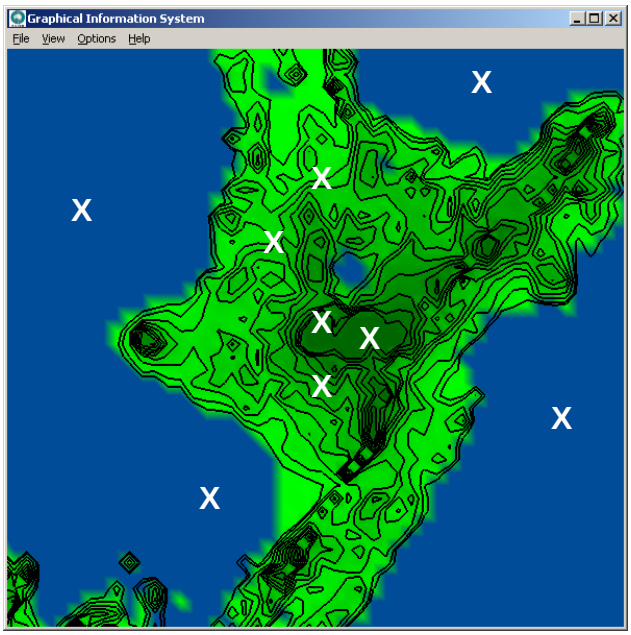

Figure 7. 54
Locations of grid points where data was extracted to analyse the depth of the boundary layer in and near the North Island.

Table 7. 3 shows that the minimum values of the marine boundary layer are equal (25 m) at all locations, including White Island, whereas the minimum depth of the boundary layer over land is lower and vary between 20 and 24 metres. The maximum depths are also higher for the marine boundary layer, varying between 2238 over the Tasman Sea and 6725 in the Cook Strait. The latter value is particularly high and differs also from the other maximum values. The maximum depths of the boundary layer over the North Island (besides Ruapehu) varies from 1522 m in the south to 2518 m at the east of Ruapehu. As can be seen in the line graphs, the maximum values of the marine boundary layer are characterised by few individual peaks, particularly in the Cook Strait and on the eastern side of the North Island. The line graphs for the boundary layer over land show much more variation, indicating more turbulence than over sea. An exception is the graph for the location east of Ruapehu, where one single peak reaches a value of 2518 metres. A possible explanation for this is that the prevailing westerly winds are deflected by the Tongariro massif and consequently, the boundary layer experiences less turbulence east of Ruapehu.

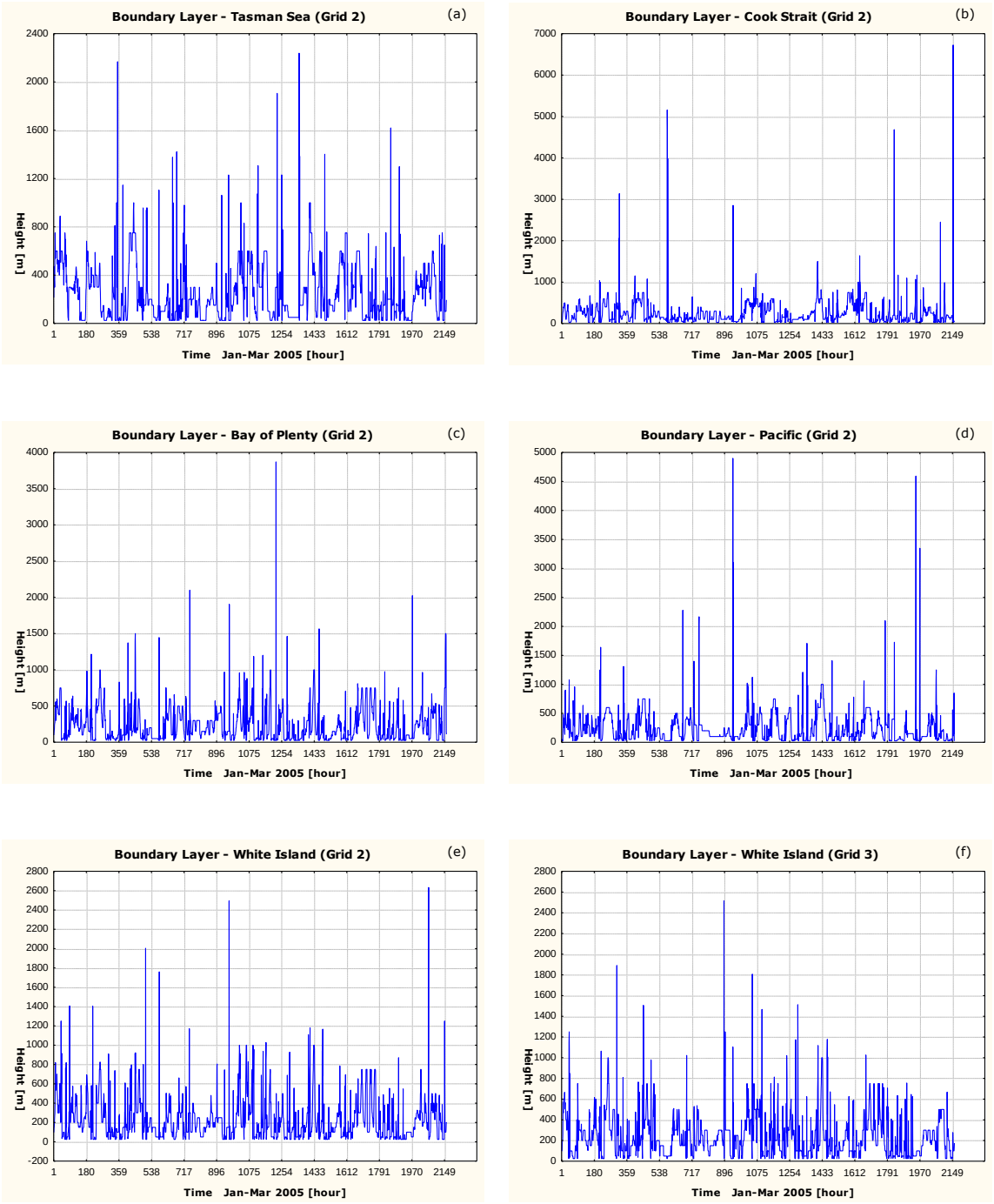

Figure 7. 55 Variation of depth of the boundary layer near the North Island.

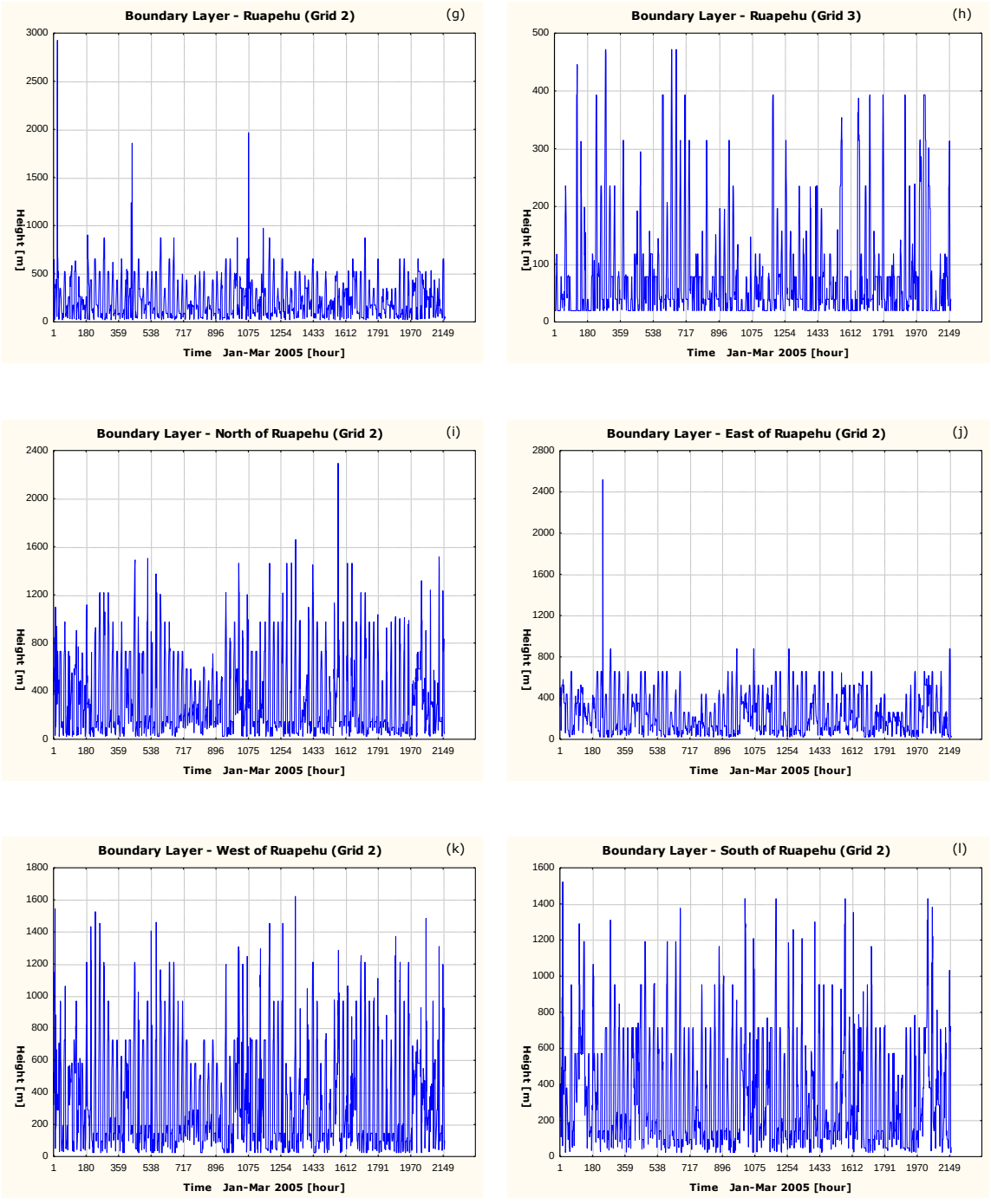

Figure 7. 55 continued.

As expected, the depth of the boundary layer over Ruapehu volcano is much less since the volcanic massif is already at a considerably height, with the vent at nearly 3000 metres. The values modelled for the grid domains 2 and 3 at Ruapehu vary considerably, but as mentioned earlier, the calculations for grid 3 are more accurate due to higher resolution. The boundary layer heights over White Island between grids 2 and 3 are similar, which is probably due to the small size of the volcanic island in comparison to the size of the grid domains. The average values are all higher over land than over sea.

CHAPTER 8: Hazard assessment to population

8. 1. Introduction

As mentioned in chapter 2, the Ministry for the Environment of New Zealand introduced several National Environmental Standards (NES) for protecting air quality for people and environment of New Zealand, in which the threshold values for SO_2 are 350 and 570 μg m^{-3}, respectively. While the first value is allowed to be exceeded for nine hours per year, the second value is not to be exceeded at all.

The results of SO_2 dispersion modelling in chapter 6 showed that the plumes of White Island volcano do not exceed the threshold value of 350 μg m^{-3} at all during quiescent degassing. The plume of Ruapehu volcano, however, exceed both threshold values 350 and 570 μg m^{-3} at ground level but affects mainly sparsely populated or unpopulated areas. Largest plume dispersions and highest SO_2 concentrations reached the plumes in model 4, although the resulted concentration values from White Island are less than from Ruapehu. If populated areas are affected by a plume with concentrations of ≥350 or 570 μg m^{-3}, respectively, then it is from modelling where Ruapehu volcano is the source.

After an introduction about urban areas and population distribution in the North Island, this chapter is focused on detailed SO_2 pollution analysis of several locations in the North Island, including all main urban areas, using the results of plume dispersion of model 4 from White Island and Ruapehu volcanoes. Hazard assessment is performed by comparing the modelled SO_2 dispersion data with issued concentration values of the National Environmental Standard (NES) of New Zealand.

In the NES, the threshold value for PM_{10} is 50 μg m^{-3} in 24-hour mean [Ministry for the Environment of New Zealand 2005], but this concentration is not exceeded during present modelling. Therefore they are not considered for further analysis of hazard assessment.

8. 2. Urban areas and population in the North Island

New Zealand has an area of c. 270,000 km^2, of which the North Island covers 116,000 km^2. The 2006 Census of Population and Dwelling shows the total population in New Zealand is nearly 4.03 Million, which represents a national

average population density of 14.9 people per square kilometre. Although population is increasing, New Zealand is still a sparsely populated country. Statistics New Zealand [2006] defined an urban-rural classification for New Zealand that is based on population size and the diversity of the social and economic characteristics of people living in all areas of the urban-rural spectrum. The geographic location and extension of the urban and rural areas overall the North Island are shown in Figure 8. 1.

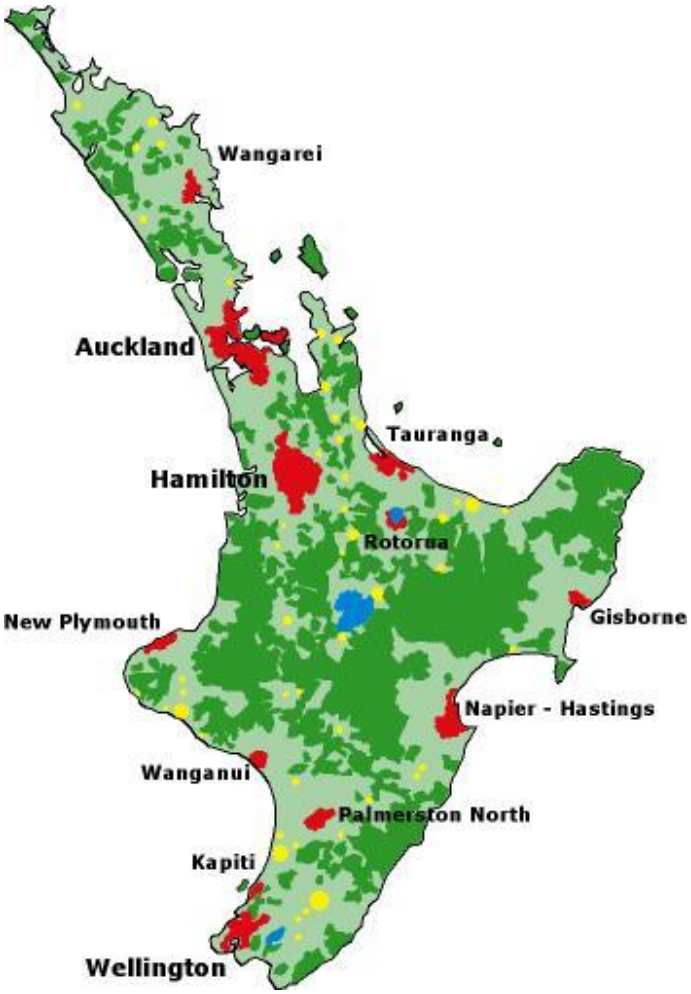

Figure 8. 1 Simplified map showing the distribution of urban and rural areas in the North Island. There are main urban areas including satellite urban communities (red-coloured areas), independent urban communities (yellow-coloured points), rural areas with high, moderate and low urban influence (grey-greenish colour) and highly rural/remote areas (green-coloured areas). Amount, size and distribution of these locations are based on the Census of Population and Dwellings in 2001.

Urban areas in New Zealand are divided into three sub-areas and communities: main urban areas, satellite urban communities and independent urban communities. According to Statistics New Zealand [2006], main urban areas are centred on a city or a main urban centre with a minimum population of 30,000 people.

Main urban areas in New Zealand cover 5078 km^2, which represents about 1.9 percent of country. Based on the Census of Population and Dwellings in 2001, approximately 70 percent of New Zealand's population (2,654,850 people) live in main urban centres. They have also the highest population density with 522.8 people/km^2 in comparison to 14.2 people/km^2 nationally [Statistics New Zealand 2006]. There are 12 main urban centres are located in the North Island, which cover an area of 3945 km^2 and the majority of the population (2,113,662 people) live in these centres (Table 8. 1). For comparison, there are only four main urban areas on the South Island: Nelson, Christchurch, Dunedin and Invercargill, which have a population of 541,188 people [Statistics New Zealand 2006].

Table 8. 1 The main urban areas that are located overall the North Island and their population density [Statistics New Zealand 2006]. These main urban areas but Kapiti and other smaller towns and settlements were chosen to extract the pollution data from the individual modelled SO_2 dispersion scenarios.

Main urban area	Population	Population density [People per km^2]
Whangarei	46,047	347.3
Auckland	1,074,507	989.1
Hamilton	166,128	151.0
Tauranga	95,694	536.9
Rotorua	52,605	593.0
Gisborne	31,719	373.4
Napier-Hastings	113,673	302.8
New Plymouth	47,763	424.9
Wanganui	39,423	375.9
Palmerston North	72,681	407.5
Kapiti	33,669	563.4
Wellington	339,747	765.4

Satellite urban communities include urban areas with strong connections to main urban centres, and where at least 20 percent of the residents are employed in the main urban centres Statistics New Zealand [2006]. They cover 478 km^2 (0.2 percent of New Zealand) and at the time of the 2001 Census of Population and Dwelling, 113,047 people lived in satellite urban communities. This is c. 3 percent of New Zealand's population and increased by 12.1 percent between March 1991 and March 2001. Satellite urban communities in the North Island cover an area of 356 km^2, with 85,122 people Statistics New Zealand [2006].

Statistics New Zealand [2006] defines independent urban communities as towns and settlements that are mainly independent from the main urban centres and have less than 20 percent of the population with workplaces in a main urban area. They are distributed throughout New Zealand and cover an area of 1646 km^2, of which 1013 km^2 is in the North Island. At the time of 2001 Census, almost half a million people lived in independent urban communities that represents almost 12 percent of the whole population in NZ. They have an average population density of 265.9 people/km^2, which is the second highest of any profile area. As in the two previous mentioned urban areas, most of the population living in independent urban communities (269,718 people) have their home in the North Island Statistics New Zealand [2006]. Examples for independent urban communities in the North Island, used for SO_2 dispersion analyses in the present study, are Whakatane and Taupo that were, next to main urban areas, also.

Rural areas in New Zealand are divided into four sub-areas, which is based on the amount of urban influence of the individual rural area. At the time of the 2001 Census, nearly 100,000 people lived in rural areas with high urban influence and the population in rural areas with moderate urban influence was more than 135,000 people. The population density was 12.9 and 6.5 people/km^2, respectively. In rural areas with low urban influence and in highly rural/remote areas lived more than 220,000 and 76,000 people. Population projections assume a further increase in population of main urban areas, satellite urban communities and rural areas with high and moderate urban influence. In contrast, they presume a decrease in population for independent urban communities and highly rural/remote areas Statistics New Zealand [2006]. However, besides of the volcanic centres of White Island and Ruapehu volcanoes any rural areas were not taken into consideration during the present study and for more detailed information the reader is referred to Statistics New Zealand [2006].

DATE	HOUR	TIME	CONC(ppb)	CMAX(ppb)	CLOC(ppb)
20050109	1	193	0	5,084098	0
20050109	2	194	0	0,059723	0
20050109	3	195	0	0,000001	0
20050109	4	196	0	0,001309	0
20050109	5	197	0	4,215639	0
20050109	6	198	0	10,131005	0
20050109	7	199	0	0,017682	0
20050109	8	200	0	0,000001	0
20050109	9	201	0	2,347346	0
20050109	10	202	0	46,3689	0
20050109	11	203	0	94,813202	0
20050109	12	204	0	28,243473	0
20050109	13	205	0	0,025484	0
20050109	14	206	0	8,173588	0
20050109	15	207	0	73,781166	0
20050109	16	208	0	102,277107	0
20050109	17	209	0	89,37545	0
20050109	18	210	0	54,02813	0
20050109	19	211	0	4,779903	0
20050109	20	212	0	0,180598	0
20050109	21	213	0	0,010031	0
20050109	22	214	0	0,006248	0
20050109	23	215	0	0,006586	0
20050109	24	216	0	0,003929	0
20050110	1	217	0	0,00052	0,00031
20050110	2	218	0	0,109324	0,010352
20050110	3	219	0	4,411452	0
20050110	4	220	0	16,557224	0
20050110	5	221	0	39,917595	0,000132
20050110	6	222	0,000238	69,686012	4,006326
20050110	7	223	0,000203	64,874542	7,132929
20050110	8	224	0	48,529991	0,144098
20050110	9	225	0	40,362793	0,001612
20050110	10	226	88,381287	236,285873	236,285873
20050110	11	227	1057,8092	1631,77869	1631,77869
20050110	12	228	599,727661	1073,97583	1073,97583
20050110	13	229	194,590393	372,338867	314,910828
20050110	14	230	67,58931	236,348007	112,591911
20050110	15	231	24,760094	163,620071	56,440899
20050110	16	232	8,841099	489,329193	489,329193
20050110	17	233	2,122203	389,892609	40,092163
20050110	18	234	5,049736	194,868866	5,556928
20050110	19	235	6,721664	106,425171	9,212729
20050110	20	236	6,416059	55,044231	11,086429
20050110	21	237	3,787189	36,646076	6,845273
20050110	22	238	0,942707	19,471519	1,820954
20050110	23	239	0,04055	6,471063	0,079997
20050110	24	240	0,00449	5,168889	0,007065
20050111	1	241	0,000423	3,626173	0,001384
20050111	2	242	0,000022	1,886049	0,003247
20050111	3	243	0,000002	1,072885	0,000006
20050111	4	244	0	0,46533	0,000001
20050111	5	245	0	0,140323	0
20050111	6	246	0	0,035098	0
20050111	7	247	0	0,011844	0
20050111	8	248	0	0,004662	0
20050111	9	249	0	0,004138	0
20050111	10	250	0	0,009208	0
20050111	11	251	0	1,611608	0
20050111	12	252	0	12,106016	0
20050111	13	253	0	44,757462	0
20050111	14	254	0	42,711315	0
20050111	15	255	0	31,024132	0
20050111	16	256	0	23,06283	0,000352
20050111	17	257	0	21,837347	0,000711
20050111	18	258	0	14,19955	0,000196
20050111	19	259	0	9,800135	0,000001
20050111	20	260	0	7,234076	0
20050111	21	261	0	5,184544	0
20050111	22	262	0	7,504987	0,000022
20050111	23	263	0	6,276024	0,000056
20050111	24	264	0	4,986694	0,000006

Figure 8. 2 Part of a list showing the time series of SO_2 concentration at a grid point. The individual columns (left to right) contain information of the date, the hour of the day (e.g. hour 1 is the hourly average from hours 0-1), the model run time (elapsed hour from the start of the model run), the average concentration at the selected grid point (CONC), the maximum concentration on the whole grid field (CMAX) and the local maximum concentration for a 5x5 sub-grid region surrounding the selected grid point (CLOC). The concentration unit is ppbv. Data used for analysis are shown in the box.

8. 3. Results of analysis

For detailed SO_2 pollution analysis of model 4 at the different locations in the North Island, the modelled average concentration data from extracted time series files, described in chapter 6. 3, are used. Depending on the location, the analysis was performed using the grid points of the two innermost grids (Grids 2 and 3) with grid spacings of 10,000 and 3,500 metres. Grid points and corresponding locations in the North Island of the time series files, chosen for detailed analysis of modelled SO_2 pollution data, were already listed in Table 6. 2. A part of such file is shown in Figure 8. 2. Due to the large size of the extracted files, they are only given in the CD-ROM, attached to the thesis.

While the dispersion models and their analyses were performed in quarterly periods, for this analysis the data were summarised to one file. The resulting distributions of the average SO_2 concentration at all chosen locations are presented as line graphs in Figures 8. 3a-n for Ruapehu and Figures 8. 4a-n for White Island volcano. The highest modelled SO_2 concentrations at each analysed location are listed in Table 8. 2.

As described in the previous chapter, TAPM calculated the modelled pollution concentrations of the dispersed plumes from White Island (Figure 6. 17 – 6. 20) are lower than those from Ruapehu volcano (Figure 6. 34 – 6. 37). The highest calculated values (from White Island modelling) are ≥100 µg m^{-3} at all analysed grid points in both grid domains 2 and 3. At grid 3, the main urban area of Wanganui is more affected (526 µg m^{-3}) from the plume than the urban community of Taupo (120 µg m^{-3}). The highest SO_2 ground level concentrations at the different locations in grid 2 were modelled for the urban area of Napier with 578 µg m^{-3}. After follow the cities of Wanganui (547 µg m^{-3}), Palmerston North (397 µg m^{-3}), Gisborne (353 µg m^{-3}), New Plymouth (335 µg m^{-3}), Hamilton (266 µg m^{-3}) and Taupo (233 µg m^{-3}). Lower maximum concentration peaks in grid domain 2 were modelled for the main urban areas of Wellington (181 µg m^{-3}) in the south as well as Whakatane and Tauranga (140 µg m^{-3}) and the remote and rural area of Hicks Bay (120 µg m^{-3}).

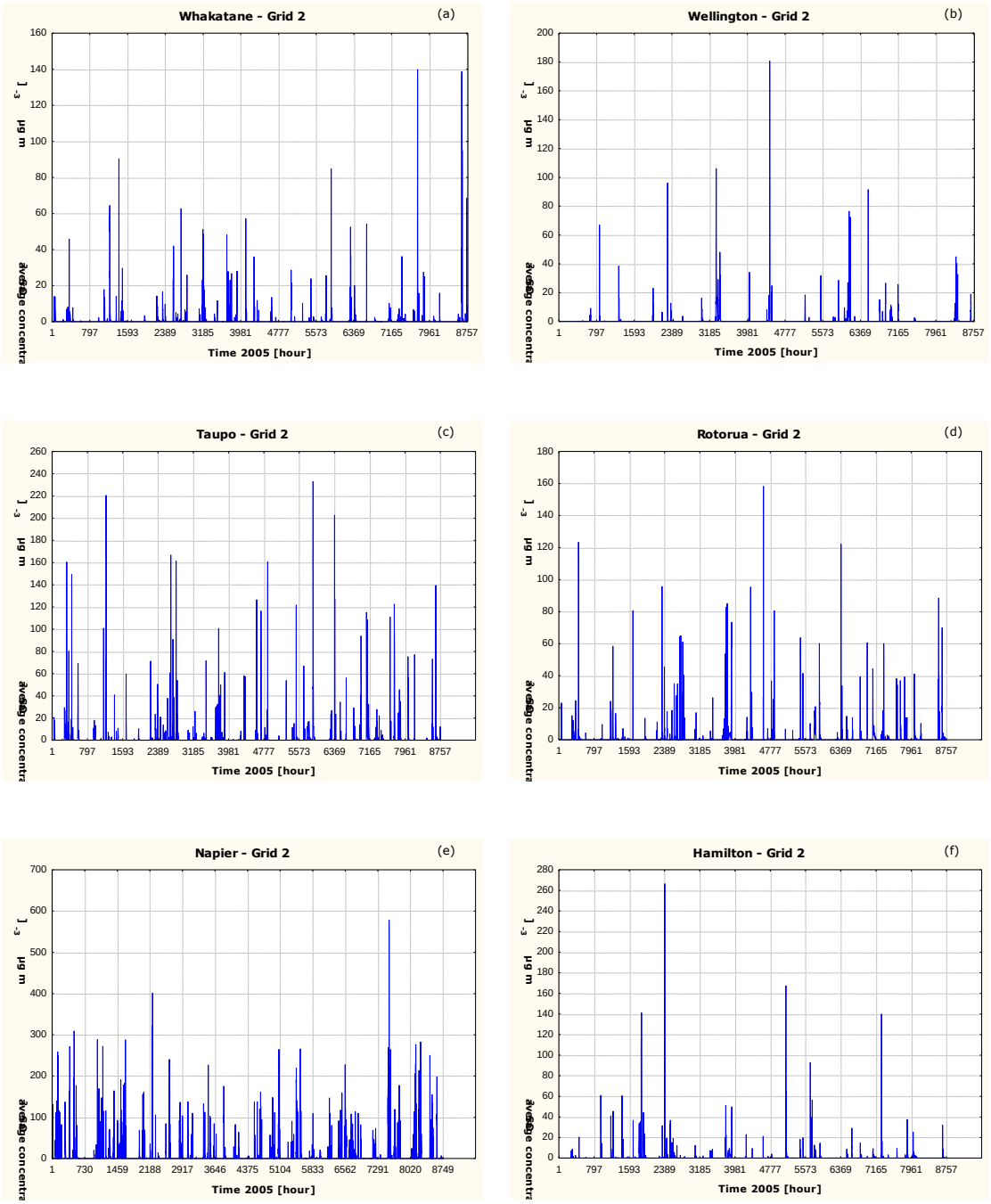

Figure 8. 3 Modelled SO_2 concentration distribution at various locations in the North Island throughout the year 2005 with Ruapehu volcano as point source.

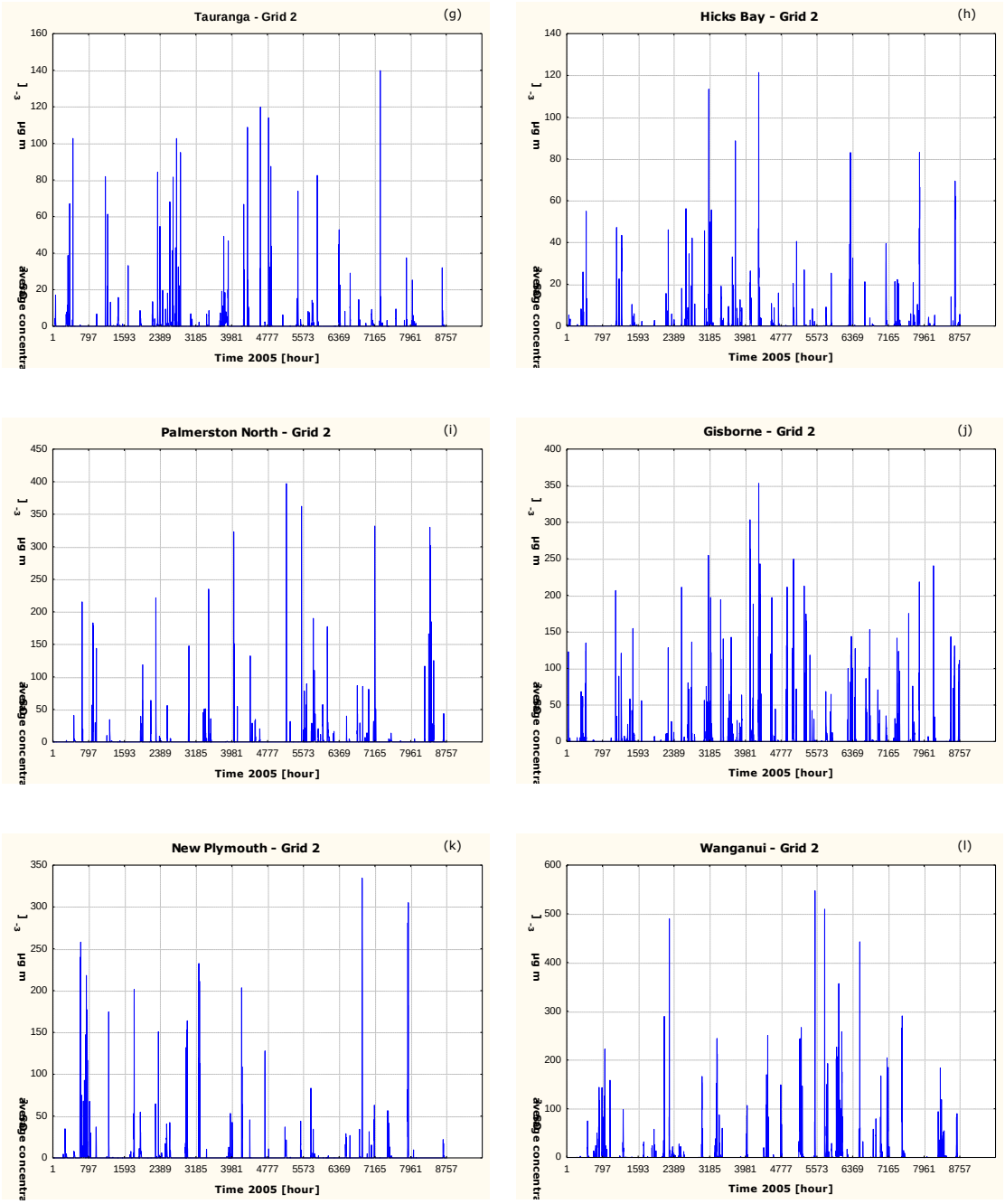

Figure 8. 3 continued.

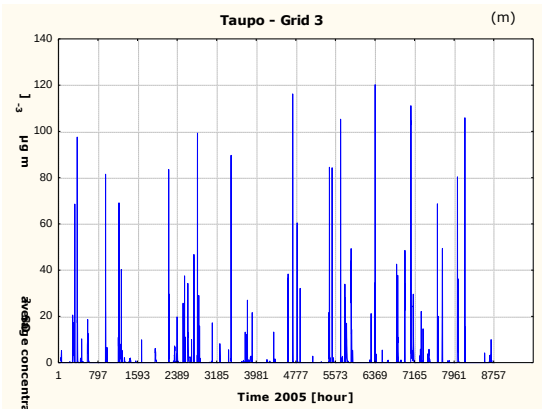

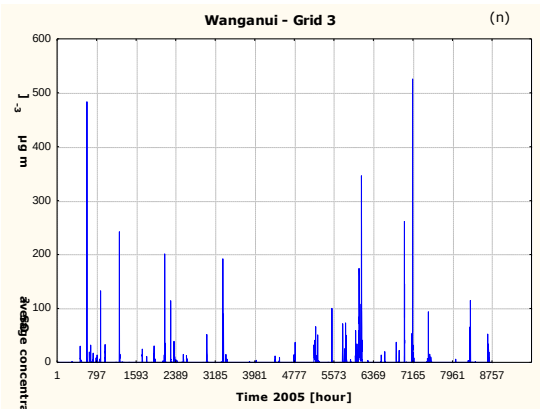

Figure 8. 3 continued.

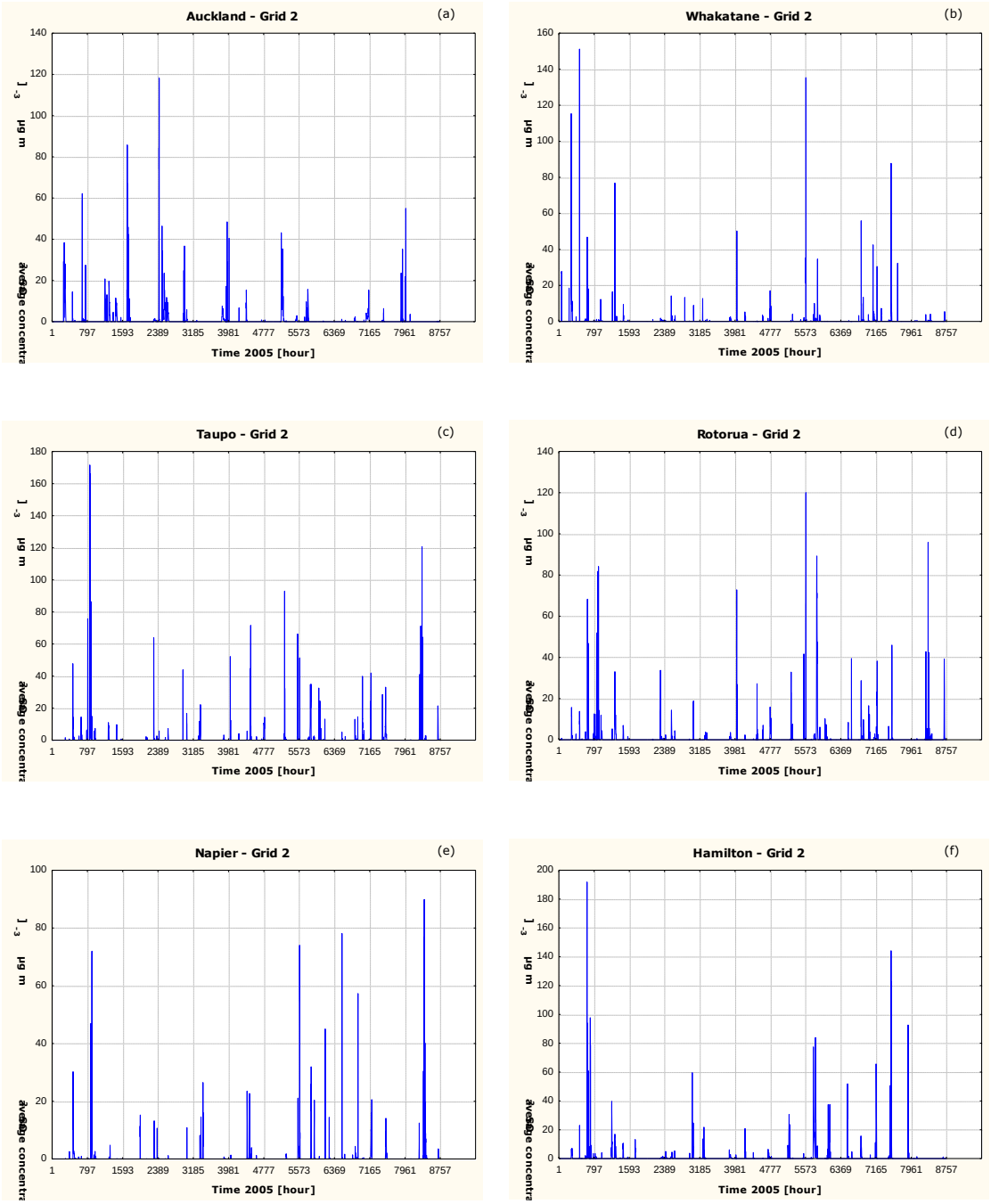

Figure 8. 4 Modelled SO_2 concentration distribution at various locations in the North Island throughout the year 2005 with White Island volcano as point source.

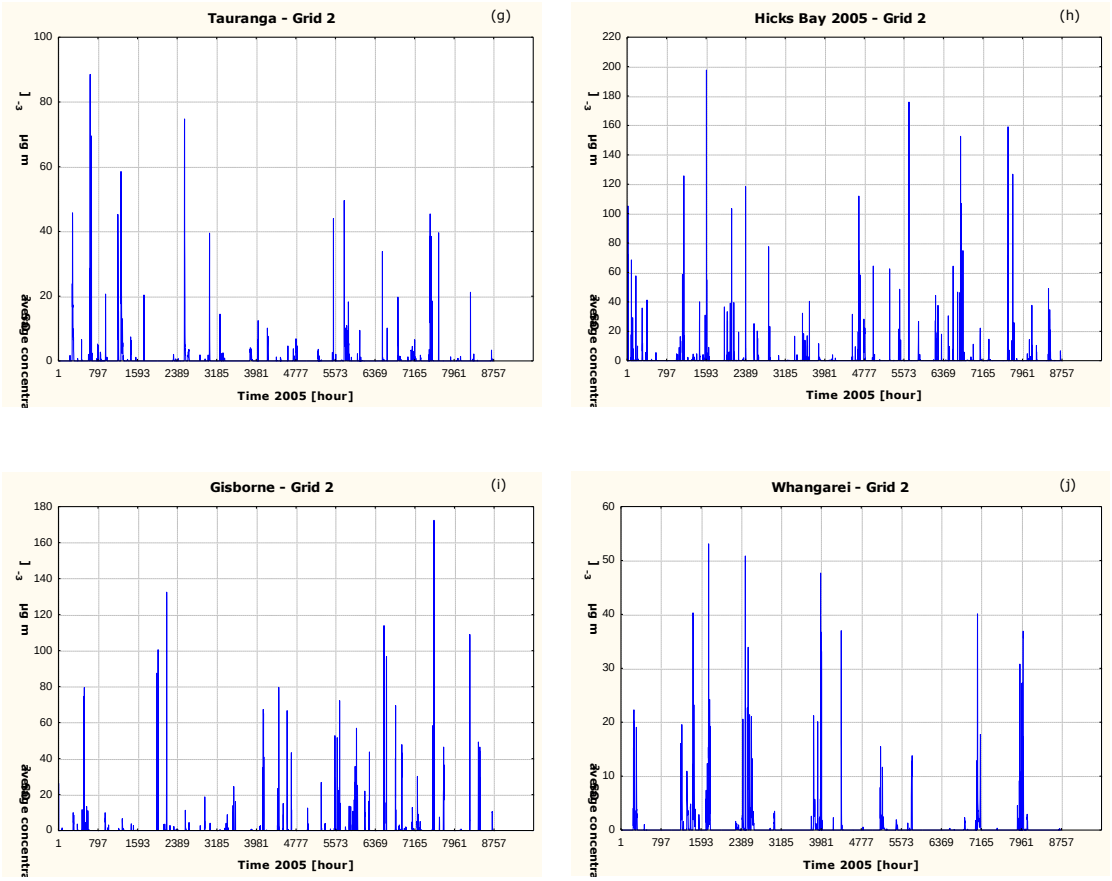

Figure 8. 4 continued.

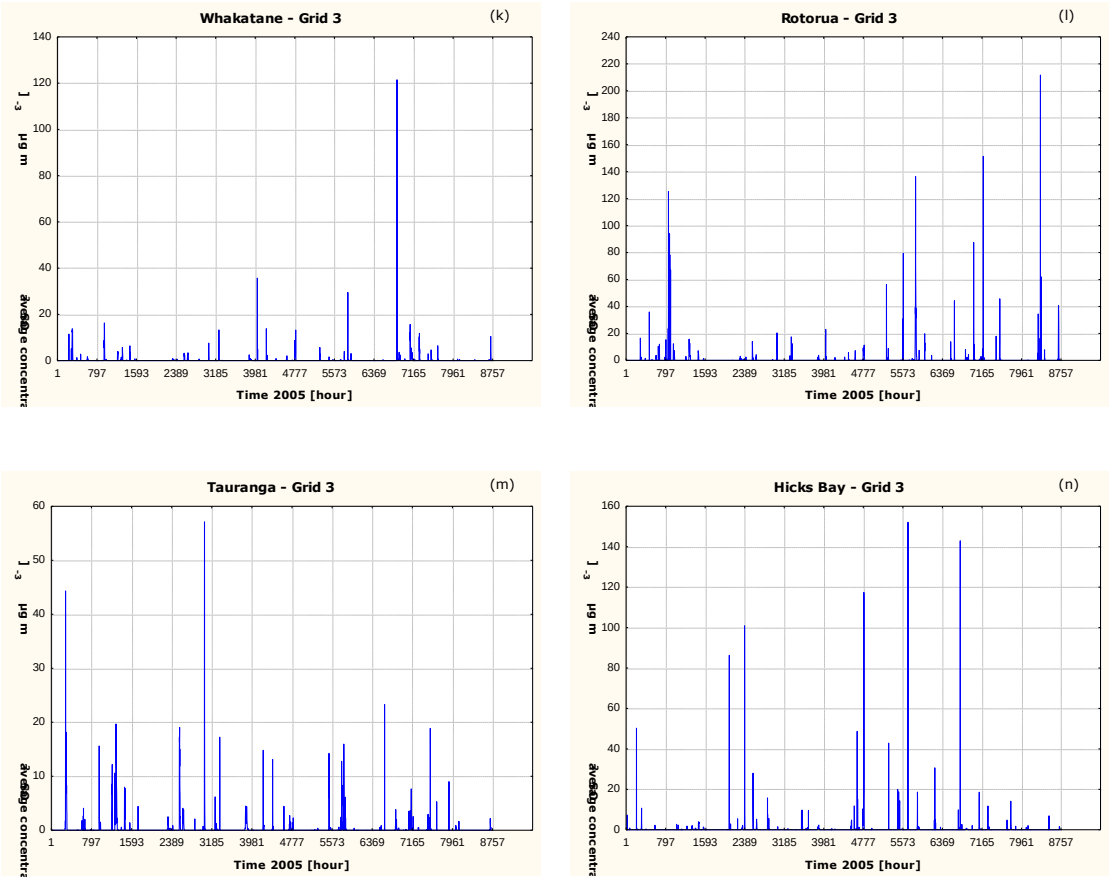

Figure 8. 4 continued.

The few areas covered with plume concentrations of ≥350 µg m^{-3} (from Ruapehu modelling) are near the volcanic vent and in the south-eastern part of the modelled grid domains. The highest value in grid 3 was modelled for Rotorua, reaching a SO_2 concentration of 212 µg m^{-3}, whereas the highest value in grid 2 was calculated for Hicks Bay with 198 µg m^{-3}. However, since wind direction is changing throughout the year, the dispersing plumes also affect other parts of the North Island. Urban areas, which are affected by SO_2 concentrations of ≥100 µg m^{-3} in grid 2, are Hamilton (192 µg m^{-3}), Gisborne and Taupo (172 µg m^{-3}), Whakatane (151 µg m^{-3}), Rotorua (120 µg m^{-3}) and Auckland (118 µg m^{-3}). The cities of Napier, Tauranga and Whangarei experienced SO_2 concentrations of ≤100 µg m^{-3} (Table 8. 2).

Table 8. 2 Highest calculated SO_2 concentrations in model 4 for various locations in the North Island.

Ruapehu volcano		**White Island volcano**	
Location	SO_2 concentration [µg m^{-3}]	Location	SO_2 concentration [µg m^{-3}]
Whakatane	140 (Grid 2)	Whakatane	151 (Grid 2) 121 (Grid 3)
Wellington	181 (Grid 2)	Auckland	118 (Grid 2)
Taupo	233 (Grid 2) 120 (Grid 3)	Taupo	172 (Grid 2)
Rotorua	158 (Grid 2)	Rotorua	120 (Grid 2) 212 (Grid 3)
Napier	578 (Grid 2)	Napier	90 (Grid 2)
Hamilton	266 (Grid 2)	Hamilton	192 (Grid 2)
Tauranga	140 (Grid 2)	Tauranga	89 (Grid 2) 57 (Grid 3)
Hicks Bay	121 (Grid 2)	Hicks Bay	198 (Grid 2) 152 (Grid 3)
Palmerston North	397 (Grid 2)	Whangarei	53 (Grid 2)
Gisborne	353 (Grid 2)	Gisborne	172 (Grid 2)
New Plymouth	335 (Grid 2)		
Wanganui	547 (Grid 2) 526 (Grid 3)		

8. 4. Summary and discussion

Detailed analyses for hazard assessment to population at different locations in the North Island were conducted for model 4, describing the dispersion of volcanic plumes from White Island and Ruapehu with SO_2 emission rates of 15,000 Mg d^{-1} at intervals of five hours.

The present analysis shows that the people in the North Island are more affected by the volcanic plume from Ruapehu volcano than from White Island. While the NES value of 350 µg m^{-3} for SO_2 from the White Island model is not reached by any of the chosen locations in the North Island, there are four urban areas (Napier, Wanganui, Palmerston North and Gisborne) where this threshold value is exceeded from Ruapehu volcano. Additionally, the city of Napier is affected once by the plume, exceeding the higher NES value of 570 µg m^{-3}.

Although the ground level concentrations from the Ruapehu model exceed the threshold value of 570 µg m^{-3} and thus cross the NES value issued by the Ministry for the Environment, it is not necessarily a serious hazard for the people. The same is applied for the NES value of 350 µg m^{-3}, which is exceeded 13 times. Apart from the fact that these crossings of the threshold values are the results from the whole modelled year, these peaks appear sporadically and the population is not exposed permanently to these high concentrations. Most crossings of the 350 µg m^{-3} threshold value in grid 2 were modelled for Wanganui (7), Palmerston North (3), Napier (2) and Gisborne (1). Additionally, in grid 3 this value is exceeded twice at Wanganui.

As explained in chapter 6, the pollution concentration at ground level at Ruapehu is decreasing steadily from the source to the distal parts, whereas the pollutants from White Island often sink to the ground when the plume reaches the coastline. There, the pollutants are influences by the conditions of the continental boundary layer. Due to decreasing temperature of the boundary layer at night, the dispersing gas sinks and is deposited over land. This corresponds to the result that most SO_2 peaks of ≥350 µg m^{-3} at ground level were modelled in the morning hours between 7-12 am (Table 8. 3).

Table 8. 3 The time modelled of SO_2 concentrations ≥350 µg m^{-3} at ground level at urban areas in the North Island.

Urban area	SO_2 concentration [µg m^{-3}]	Time at ground level
Grid 2		
Napier	148	4 April, 5 pm
Napier	578	11 November, 7 am
Napier	547	11 November, 8 am
Wanganui	490	6 April, 7 am
Wanganui	547	19 August, 10 am
Wanganui	471	19 August, 11 am
Wanganui	473	28 August, 10 am
Wanganui	509	28 August, 11 am
Wanganui	356	10 September, 1 pm
Wanganui	443	30 September, 1 am
Palmerston North	397	5 August, 11 am
Palmerston North	372	5 August, 12 am
Palmerston North	362	19 August, 1 pm
Grid 3		
Wanganui	483	26 January, 2 am
Wanganui	526	26 October, 7 am

The present model results show that the dispersing plumes from White Island affect the population in the North Island but the SO_2 concentrations are less than the lower NES value of 350 µg m^{-3} throughout the year, even during very strong gas emissions. Like in the model from Ruapehu volcano, all calculated data with higher concentrations represent single peaks and do not represent permanent pollution values (Figure 8. 3 and 8. 4a-n).

Detailed hazard analysis was not performed for grid points corresponding to the sources of White Island and Ruapehu themselves. According to the different plume dispersions described in chapter 6, the model results from Ruapehu volcano are obvious, covering a large area at and near the volcanic edifice with constant high SO_2 concentrations at ground level even during quiescent degassing.

The results from White Island are less evident, where such high concentrations are not reached or do not cover the whole proximal region. However, the threshold values are still exceeded in model 4 and thus these results should not underestimate the existing hazard for people visiting the volcanic island for scientific or touristy reasons.

However, two important aspects are emphasised. First, as described in chapter 6, the model scenario 4 describes the plume dispersion with puff discharges of 15,000 Mg d^{-1}. Because such high gas discharges are not common for continuous emissions, the model was defined to release SO_2 at intervals of five hours. It is emphasised that, according to the model, no SO_2 is emitted between the 5-hour intervals. This situation is not realistic, since even in the time when no puffs are released, continuous emission keeps ongoing although with lower emission rates, such as defined for models 1-3. Consequently, the resulted SO_2 concentrations in model 4 represent minimum values for that model. Second, the two volcanoes of White Island and Ruapehu are considered to be the only source of pollution in the individual models. Therefore it is emphasised that the modelled concentration data need to add-up to the pollution values from other sources known, such as industrial chimneys and traffic.

Chapter 9: Verification of meteorology and SO_2 dispersion modelling from WIV

9. 1. Introduction

In order to verify the modelled SO_2 dispersion of this study, airborne plume measurements were undertaken using a COSPEC instrument on 22 November 2006 at various distances from the vent of White Island volcano. Modelling was performed for two days, the day before and the day of plume measurement itself: 21-22 November 2006. The first day was modelled as "spin-up day" to initialise the model, but the output data were ignored in further analysis. The distal airborne plume measurements were carried out at an average height of 66 metres.

Verification of the model is performed using the same set of statistical measures that enable the comparison of modelled prediction data by TAPM with recorded observation data, described in chapter 8. For evaluation of the meteorological data the recorded observation data of the weather stations from Whakatane airport and White Island was used. Model evaluations of the meteorology as well as the SO_2 concentration from plume traverses at 3 km distance were also performed using scatter plots. The consequence of data extraction from low-resolution grid domains (all but grid 5) is to have more observed data than model data. Therefore scatter plots are not useful for the plume traverses at 10 and 20 km distances.

9. 2. Summary of TAPM input parameters

All the important input parameters chosen for this modelling scenario of SO_2 plume dispersion on 22 November 2006 are summarised in Table 9. 1. For this period, meteorological modelling was performed with five nested grid domains (each 50 x 50 x 25 grid points) with grid spacings of 20 000, 6000, 2000, 600 and 200 metres. Still centred on the meteorology grid, but to achieve higher resolution of SO_2 dispersion, the grid spacings for pollution modelling were decreased by the factor of '4' to grid widths of 5000, 1500, 500, 150 and 50 metres. Figures 9. 1 shows the different grid domains chosen for SO_2 dispersion modelling. To save

computer run time and storage space, there was chosen a smaller territory for pollution modelling was chosen (Figure 9. 1e).

The continuous emission of SO_2 from White Island volcano originated from all fumaroles on the crater floor, rather than from one single vent. For simplification one single point source of 600 m in diameter was taken, which represents the largest possible value for point sources in TAPM. The input parameters for exit temperature and SO_2 emission rate were chosen according to information supplied by scientists from GNS who reported emission rate of 362±98 Mg d^{-1}. The actual exit temperature at the fumaroles on 22 November 2006 is unknown, but measurements on 31 October 2006, at different fumaroles were between 99.5 and 120.0 °C.

Table 9. 1 Model configuration for meteorological and SO_2 dispersion modelling on 21/22 November 2006.

	Model version	TAPM V3.0.7	
Databases	Terrain data		
	Modelled period	• from 21/11/2006 to 22/11/2006 Note that the first days (21/11/2006) were used as a "spin-up day" to initialise the model. Results from these days were not used for output purposes	
	Grid centre coordinates	• Latitude and Longitude - Lat. 37° 31' S (World Geodetic System 1984) - Long. 177° 10' E (World Geodetic System 1984) Equivalent Easting and Northing - 6400974 mN (NZ Map Grid 1949) - 2878459 mE (NZ Map Grid 1949)	
Meteorological Grid Parameters	Number of grid points	50	50
	Outer grid resolution [m]	20,000	20,000
	Grid 2 resolution [m]	6,000	6,000
	Grid 3 resolution [m]	2,000	2,000
	Grid 4 resolution [m]	600	600
	Grid 5 resolution [m]	200	200
	Number of vertical levels (levels in italics are not included in output files)	25 (10, 25, 50, 75, 100, 150, 200, 250, 300, 400, 500, 600, 750, 1000, 1250, 1500, 1750, 2000, 2500, 3000, 3500, *4000, 5000, 6000, 7000 and 8000*)	

Table 9. 1 continued.

Pollution Grid	Number of grid points	21-22/11/2006	46
	Outer grid resolution [m]	5,000	5,000
	Grid 2 resolution [m]	1,500	1,500
	Grid 3 resolution [m]	500	500
	Grid 4 resolution [m]	150	150
	Grid 5 resolution [m]	50	50
	Pollution Mode	• Chemistry mode with SO_2 • Output 3-d concentration files • Point source • Use of EGM + LPM (Eulerian grid + Lagrangian near-source particle mode	
	Source Characterisations	Number of point sources	1
		Source height	10 m
		Source radius	300 m
		Emission rate_time	Constant
		Exit velocity	1 m s^{-1}
		Exit temperature	373 K
		SO_2 flux 21/22 Nov 2006	4200 gs^{-1}

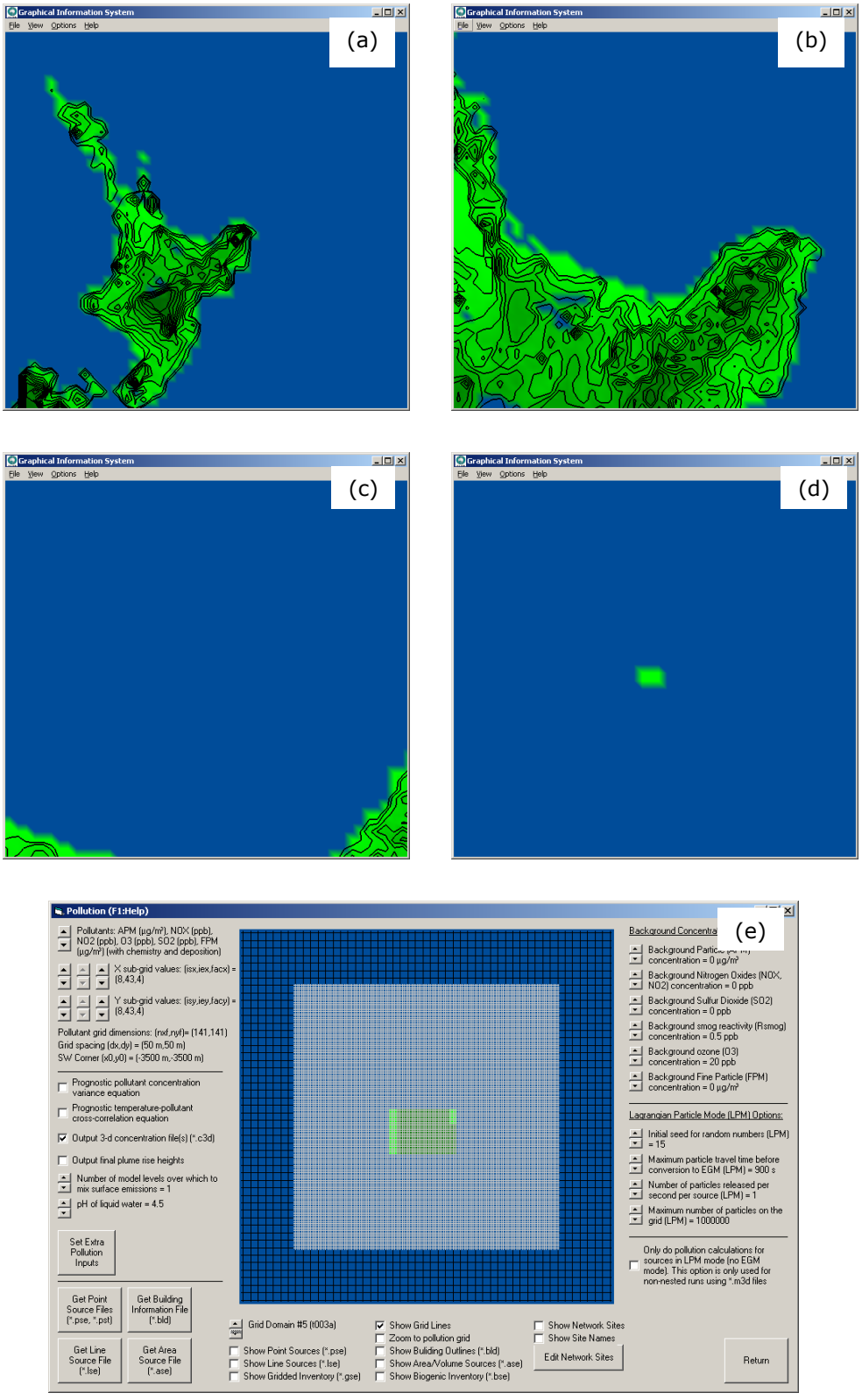

Figure 9. 1 Images of the grid domains for plume dispersion modelling on 21/22 November 2006. Figures a-d are images show a general view of the area modelled. Figure (e) shows the 'Pollution window', which is used to enter optional input for pollution modelling. There is also a set of controls to decrease the pollution grid width. While the outer black grating shows the meteorological grid, the inner white grating represents the pollution grid. For present modelling the pollution grid width was decreased by the factor of '4'.

9. 3. TAPM output data

For evaluation of the meteorological data, the synoptic hourly data of wind speed, wind direction, temperature and relative humidity were extracted at the nearest grid point to each of the monitoring sites. While the weather data from Whakatane was extracted from ground level (≤10 m), the data from White Island was extracted from the vertical level 8 (250-300 m above the ground), because the weather station is located at this height. Additionally, the weather data at White Island was extracted from grid domains 3–5, the same grid domains as SO_2 data was extracted.

Six plume traverses were undertaken on 22 November 2006 at 3 km distance, as well as three plume traverses at 10 and 20 km distances, respectively. Due to the close vicinity of the six plume traverses at 3 km distance, only three of them were analysed. Plume measurements were carried out using a COSPEC instrument, which detects the vertical SO_2 column mass in the atmosphere by differential measurements (Figure 9. 2a, b).

Regarding the geographic location of White Island, there was recognised an error in TAPM. While for modelling was used the geographic coordinates (37° 31’ S, 177° 10’ E), the correct coordinates are (37° 31’ S, 177° 11’ E). This error of one minute in the Easting value makes a difference of c. 68 m in N-S and 1471 m in E-W direction. While this error is irrelevant for large scale modelling in the previous chapter, it had to be involved for data extraction from high resolution modelling in this part of the study to determine the correct distances of locations during COSPEC measurements in the modelled grid and to extract the right grid points.

Since the Easting and Northing coordinates of plume measurements are given in New Zealand Map Grid (NZMG) coordinates based on Geodetic Datum 1949, the geographic coordinates used for TAPM had to be converted (6400974 S, 2878459 E). For conversion of the coordinates were used the online conversion website of Land Information New Zealand (LINZ):
http://www.linz.govt.nz/apps/coordinateconversions/index.html

Using the NZMG coordinates from airborne plume measurements and the Theorem of Pythagoras, all grid points for data extraction could be determined as accurately as possible, depending on grid spacing. As mentioned earlier, each grid domain consists of the same numbers of horizontal and vertical grid points. Depending on the distance of plume traverses from the vent and the area covered of each grid domain, 3-d files containing the time series of the modelled period are extracted (Figure 9. 2c, d).

Figure 9. 2
The correlation spectrometer (COSPEC) is installed in a small aircraft to measure the SO_2 concentration of the volcanic plume. The opening of a tube of the instrument (a) shows into the upper sky while flying underneath the plume (b). During the flight, COSPEC measures permanently the total SO_2 concentration in the column above the point.

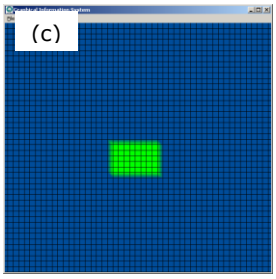

Figure (c) shows the innermost grid domain (Grid 5), from where the modelled data from the proximal plume traverses (3 km) was extracted. While each extracted grid point corresponds to one scan of the COSPEC instrument (d), the number of extracted grid points is decreasing with lower grid resolution or larger grid spacing, respectively. The elevations in Figure (d) are not in scale with the photograph.

The data of airborne plume measurements were provided by scientists from GNS and are given in parts per million by volume per metre [ppmv-m]. The extracted data from TAPM are 3-d files with time series, showing the hourly averaged SO_2 concentration at each vertical grid level or of each grid cube, respectively. A section of such file is shown in Table 9. 2. All files used for analyses are saved on CD-ROM, which is attached to this thesis. Since the output unit is given in parts per billion by volume [ppbv], the modelled output data were further calculated into the same unit [ppmv-m] from plume measurements.

Table 9. 2 Section of a 3-d file of pollution dispersion modelling from White Island volcano on 22 November 2006, showing the SO_2 concentration at different heights. The individual columns (left to right) contain information of: the **Date**, the **Hour** of the day (e.g. hour 12 is the hourly average from hours 11-12), the model run **Time** (elapsed hour from the start of the model run), the average concentration (**CONC**) at the selected grid point (the concentration unit is ppbv) and the corresponding **Height** of SO_2 concentration above sea level.

DATE,	**HOUR,**	**TIME,**	**LEVEL,**	**CONC(ppb) ,**	**HEIGHT(m)**
20061122,	12,	36,	1,	0.000000,	10
20061122,	12,	36,	2,	0.000000,	25
20061122,	12,	36,	3,	0.000000,	50
20061122,	12,	36,	4,	0.000000,	100
20061122,	12,	36,	5,	0.000000,	150
20061122,	12,	36,	6,	0.000000,	200
20061122,	12,	36,	7,	0.000000,	250
20061122,	12,	36,	8,	0.000000,	300
20061122,	12,	36,	9,	0.000000,	400
20061122,	12,	36,	10,	0.000000,	500
20061122,	12,	36,	11,	0.000000,	600
20061122,	12,	36,	12,	0.000000,	750
20061122,	12,	36,	13,	0.000000,	1000
20061122,	12,	36,	14,	24.342932,	1250
20061122,	12,	36,	15,	241.850861,	1500
20061122,	12,	36,	16,	0.075471,	1750
20061122,	12,	36,	17,	0.000000,	2000
20061122,	12,	36,	18,	0.000000,	2500
20061122,	12,	36,	19,	0.000000,	3000
20061122,	12,	36,	20,	0.000000,	3500

9. 4. Results of model evaluation on 22 November 2006

9. 4. 1. Results of model performance statistics for meteorology

Meteorological evaluation for 22 November 2006 was performed with the recorded data from the monitoring sites of White Island and Whakatane airport. Model performance statistics for TAPM meteorology are shown in Table 9. 3. In Figures 9. 3 to 9. 6 are shown scatter plots, where observed and predicted data for wind speed, wind direction, temperature and relative humidity are correlated.

9. 4. 1. 1. White Island

The scatter plots of observed vs. modelled data for wind speed, wind direction, temperature and relative humidity for the three innermost grid domains (Grid 3-5) are presented in Figure 9. 3 to 9. 5a-d. Generally, the data for all weather components between the three grids are almost equal. The only difference was calculated for the relative humidity between data of grid 5 and 4 to the value of grid 3, which is slightly lower. The model data for the ambient temperature are slightly lower than the observation data. TAPM calculated a little stronger value for wind speed, U- and V-components and relative humidity than the observation data suggest. The predicted ambient temperature is slightly underestimated but shows best results regarding the correlation coefficient (≥0.89). The mean observed and predicted west-east components (U) and south-north (V) have the same positive sign, indicating that the wind was correctly modelled coming from the south-west quadrant.

The correlation of the other weather factors shows very good results for wind speed and U-component, in which the two components reached values between 0.80 and 0.77. Not much correlation is found for the relative humidity. The $RMSE_S$ value for the relative humidity is smaller than $RMSE_U$, which is a result as it should be. The unsystematic error for all other weather factors reached lower values than the systematic error. Similar to the correlation coefficient, the indices of agreement (IOA) for wind speed, U-component and temperature reached very good model values in all three grid domains. The IOA for the relative humidity reached just satisfying results with values slightly larger than 0.50, whereas the values for the V-component are little lower than 0.50.

The measures of skill show that the standard deviations for wind speed and the wind components were predicted well, which is indicated by the $SKILL_V$ values. The $SKILL_E$ values for the relative humidity and the $SKILL_R$ values for relative humidity and the V-component are larger than 1.0. All other values are smaller than 1.0, indicating good model results.

9. 4. 1. 2. Whakatane

The scatter plots of observed vs. modelled data for wind speed, wind direction, temperature and relative humidity for the three innermost grid domains (Grid 3-5) are presented in Figure 9. 6a-d. The model calculates for Whakatane stronger mean wind speed (4.5 m s^{-1} vs. 4.1 m s^{-1}) as well as higher values for the U-component (4.3 m s^{-1} vs. 3.5 m s^{-1}) and V-component (1.2 m s^{-1} vs. 0.5 m s^{-1}). The mean observed and predicted wind components U and V have the same positive sign, indicating that the wind was correctly modelled coming from the south-west quadrant.

The correlation coefficient (r) shows satisfying results for the two wind components (U=0.48, V=0.43) but well to very good predicted results for wind speed (0.60), ambient temperature (0.91) and relative humidity (0.83). $RMSE_S$ is smaller than $RMSE_U$ for wind speed, V-component and relative humidity, whereas the values of the U-component and temperature are larger. The index of agreement (IOA) for the V-component (0.47) reached the least good result. All other variables show values are between 0.68 and 0.90, thus indicating good and very good model results. The values of $SKILL_V$ are varying between 0.36 for the V-component and 1.03 for the relative humidity, compared to the ideal value of 1.0. The other two skill variables ($SKILL_E$ and $SKILL_R$) show values less than '1', also indicating good model results.

Table 9. 3 Meteorology (WS = wind speed [m s^{-1}], U = west-east component [m s^{-1}], V = south-north component [m s^{-1}], T = ambient temperature [°C], RH = relative humidity [%]) statistics for TAPM simulation on 22 November 2006. The model data from White Island was extracted from vertical level 8 (300 m), since the weather station is located at this height. The data from Whakatane are near-surface (≤10 m) data.

Site: White Island, Grid 5													
Variable	**N**	**O_{mean}**	**P_{mean}**	**O_{Std}**	**P_{Std}**	**r**	**RMSE**	**$RMSE_S$**	**$RMSE_U$**	**IOA**	**$SKILL_V$**	**$SKILL_E$**	**$SKILL_R$**
WS	24	9.1	9.6	2.2	1.6	0.78	1.42	1.05	0.97	0.85	0.74	0.45	0.66
U	24	8.9	9.1	2.2	1.6	0.80	1.36	0.99	0.93	0.86	0.70	0.42	0.61
V	24	1.1	2.9	1.2	1.0	0.31	2.21	2.00	0.95	0.46	0.84	0.79	1.84
T	24	13.0	12.6	2.6	1.6	0.91	1.38	1.24	0.62	0.88	0.60	0.24	0.53
RH	24	77.4	79.4	4.7	8.2	0.38	7.89	2.51	7.48	0.59	1.75	1.58	1.67

Site: White Island, Grid 4													
Variable	**N**	**O_{mean}**	**P_{mean}**	**O_{Std}**	**P_{Std}**	**r**	**RMSE**	**$RMSE_S$**	**$RMSE_U$**	**IOA**	**$SKILL_V$**	**$SKILL_E$**	**$SKILL_R$**
WS	24	9.1	9.6	2.2	1.6	0.78	1.43	1.06	0.97	0.84	0.73	0.45	0.67
U	24	8.9	9.1	2.2	1.6	0.80	1.36	1.00	0.92	0.86	0.70	0.41	0.60
V	24	1.1	2.9	1.2	1.0	0.34	2.22	2.02	0.94	0.46	0.84	0.77	1.84
T	24	13.0	12.6	2.6	1.6	0.90	1.40	1.24	0.66	0.88	0.60	0.25	0.54
RH	24	77.4	79.1	4.7	8.5	0.30	8.36	2.68	7.92	0.54	1.80	1.68	1.77

Table 9. 3 continued.

Site: White Island, Grid 3													
Variable	**N**	**O_{mean}**	**P_{mean}**	**O_{Std}**	**P_{Std}**	**r**	**RMSE**	**$RMSE_S$**	**$RMSE_U$**	**IOA**	**$SKILL_V$**	**$SKILL_E$**	**$SKILL_R$**
WS	24	9.1	9.6	2.2	1.5	0.77	1.43	1.07	0.95	0.84	0.71	0.44	0.67
U	24	8.9	9.1	2.2	1.5	0.80	1.35	1.01	0.89	0.86	0.68	0.40	0.60
V	24	1.1	2.9	1.2	1.0	0.35	2.23	2.03	0.91	0.46	0.82	0.75	1.84
T	24	13.0	12.6	2.6	1.6	0.89	1.44	1.26	0.70	0.87	0.60	0.27	0.55
RH	24	77.4	78.9	4.7	8.5	0.27	8.48	2.82	8.00	0.52	1.80	1.70	1.80

Site: Whakatane, Grid 3													
Variable	**N**	**O_{mean}**	**P_{mean}**	**O_{Std}**	**P_{Std}**	**r**	**RMSE**	**$RMSE_S$**	**$RMSE_U$**	**IOA**	**$SKILL_V$**	**$SKILL_E$**	**$SKILL_R$**
WS	24	4.1	4.5	2.1	1.7	0.60	1.73	1.13	1.31	0.75	0.80	0.63	0.83
U	24	3.5	4.3	2.3	1.7	0.48	2.21	1.66	1.46	0.68	0.73	0.62	0.94
V	24	0.5	1.2	1.8	0.6	0.43	1.73	1.63	0.57	0.47	0.36	0.32	0.97
T	24	14.7	14.7	5.1	3.1	0.91	2.57	2.24	1.27	0.89	0.60	0.25	0.51
RH	24	71.2	68.4	13.0	13.4	0.83	8.03	3.33	7.31	0.90	1.03	0.56	0.62

KEY: O = observation, P = model prediction, mean = arithmetic mean, Std = standard deviation, r = Pearson correlation coefficient (0 = no correlation, 1 = exact correlation), RMSE = root mean square error, $RMSE_S$ = systematic root mean square error, $RMSE_U$ = unsystematic root mean square error, IOA = index of agreement (0 = no agreement, 1 = perfect agreement), $SKILL_V$ = (P_{Std}/O_{Std}) (near to 1 shows skill), $SKILL_E$ = ($RMSE_U/O_{Std}$) (<1 shows skill), $SKILL_R$ = ($RMSE/O_{Std}$) (<1 shows skill).

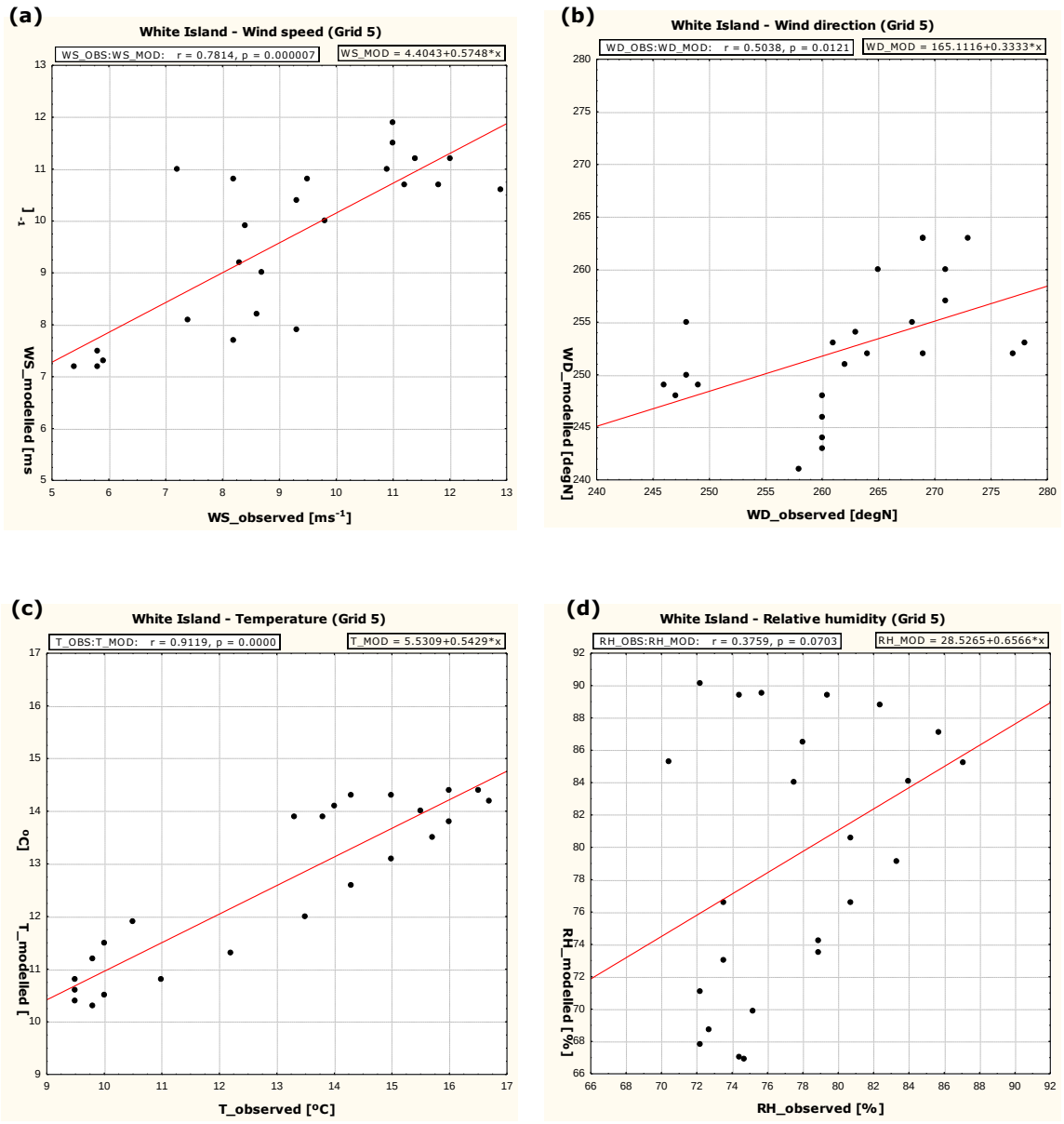

Figure 9. 3 Scatter plots of model predictions vs. observed data for wind speed (a), wind direction (b), temperature (c) and relative humidity (d) for White Island (Grid 5).

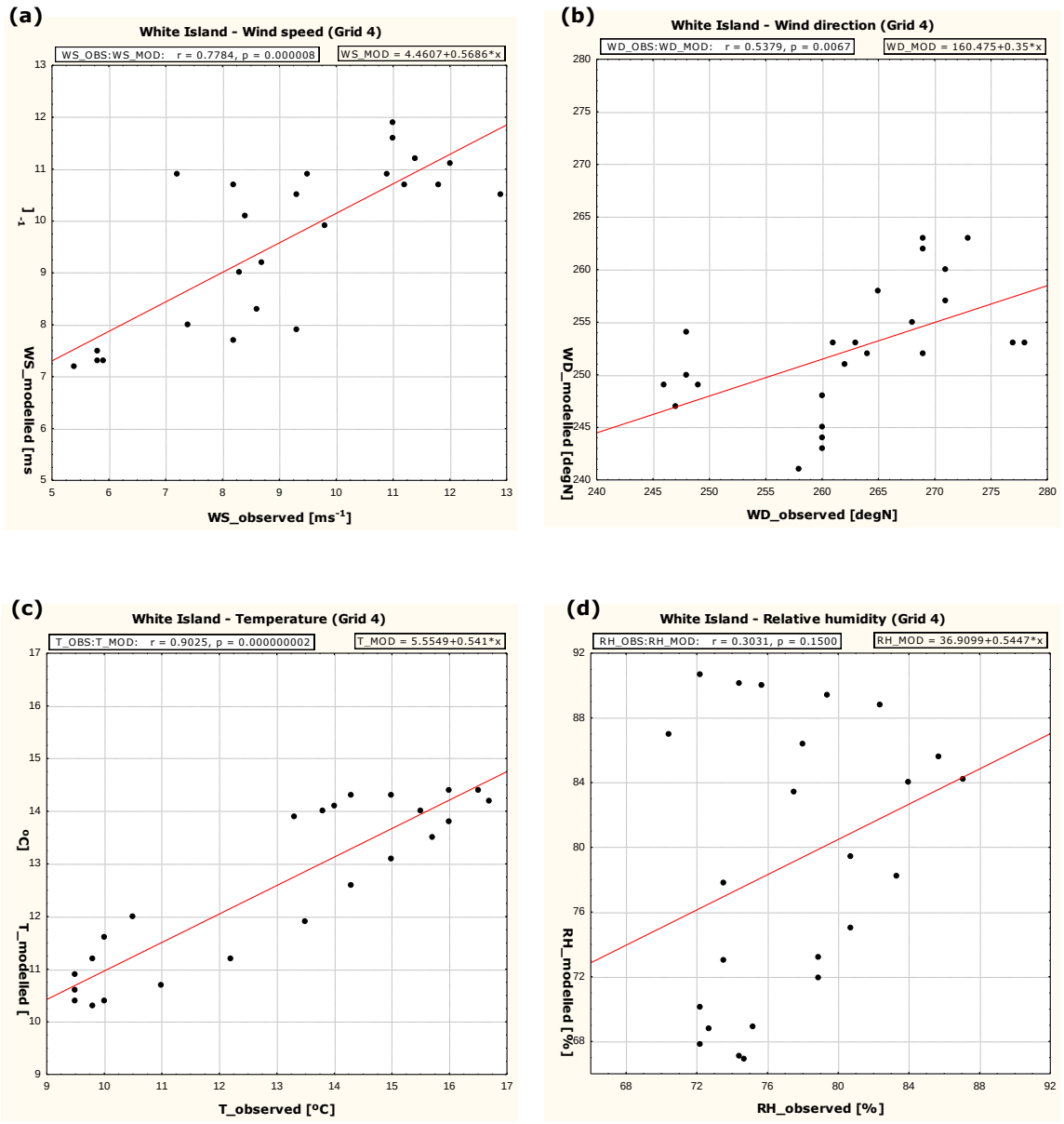

Figure 9. 4 Scatter plots of model predictions vs. observed data for wind speed (a), wind direction (b), temperature (c) and relative humidity (d) for White Island (Grid 4).

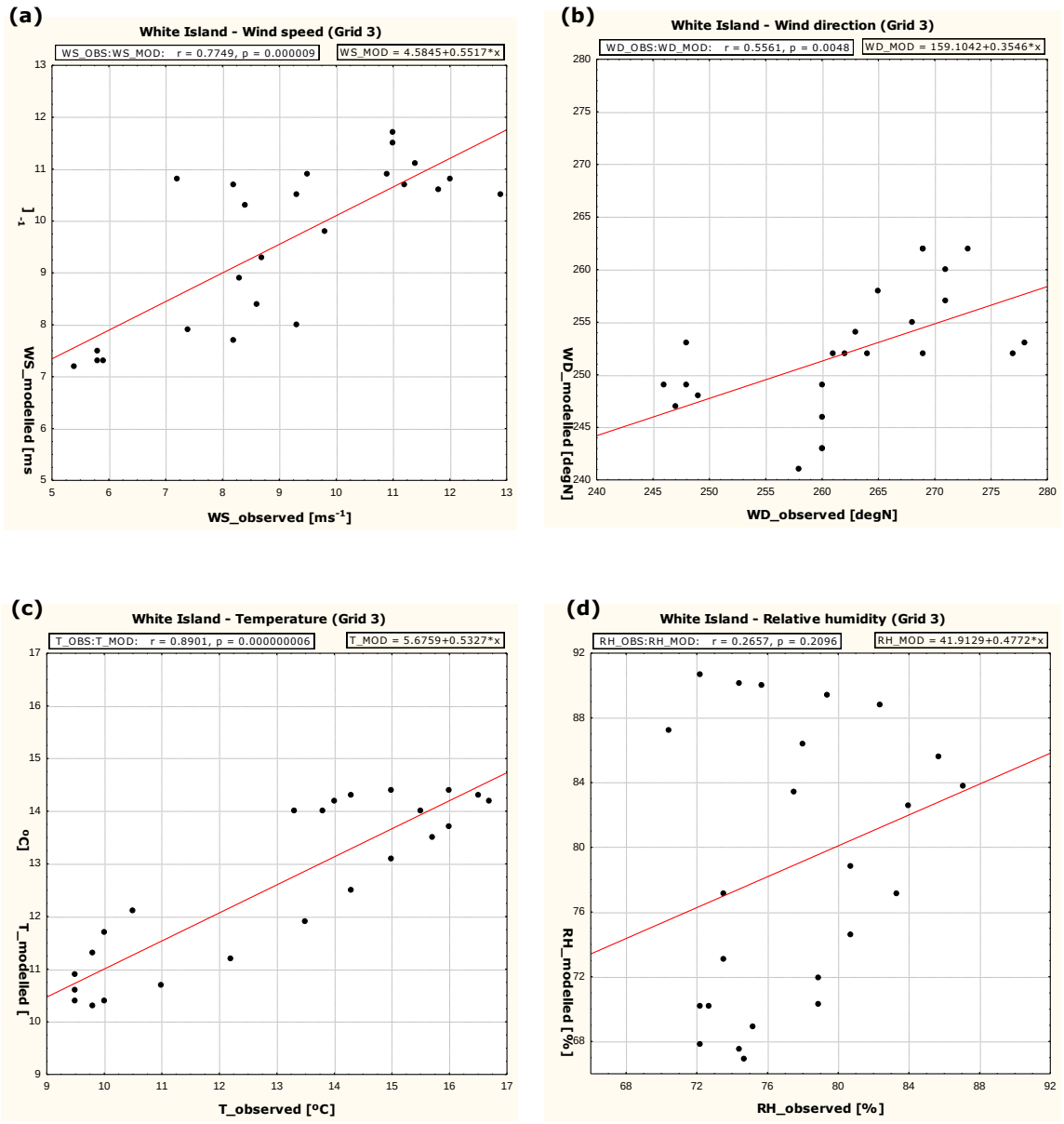

Figure 9. 5 Scatter plots of model predictions vs. observed data for wind speed (a), wind direction (b), temperature (c) and relative humidity (d) for White Island (Grid 3).

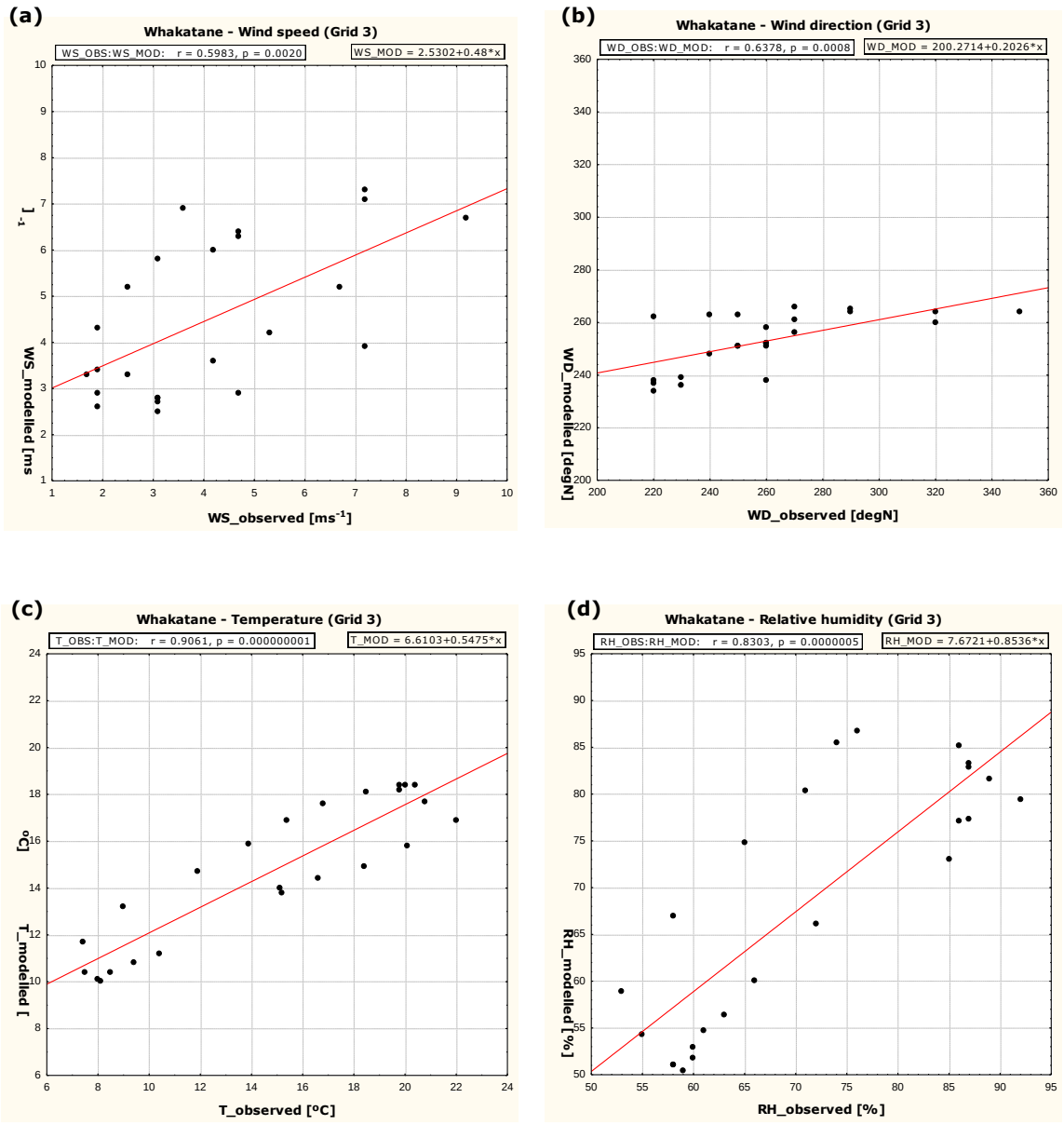

Figure 9. 6 Scatter plots of model predictions vs. observed data for wind speed (a), wind direction (b), temperature (c) and relative humidity (d) for Whakatane (Grid 3).

9. 4. 2. Results of model performance statistics for SO_2 dispersion

The data for evaluation of plume dispersion at a distance of c. 3 km were extracted from grid 5, at a distance of 10 km from grid 4 and at a distance of 20 km from grid 3. The complete lists of all extracted grid points and their corresponding locations of airborne plume measurements are saved on the CD-ROM attached to this thesis. Airborne plume measurements were carried out midday between 11 am and 2 pm. Therefore the statistical measures were calculated for two hours per plume transfer: 11-12 am and 12 am-1 pm (3 km distance) and 12 am-1 pm and 1-2 pm (10 and 20 km distances).

Depending on the distance to the point source, the data of plume concentration were extracted from the three innermost grids with the best possible resolution of grid spacing. For each distance were extracted the grid points of three different airborne plume transfers. The same statistical measures, as used for model evaluation of the meteorological data, are also applied in order to verify the modelled plume dispersion with data from COSPEC measurements. The results of these calculations are shown in Table 9. 4.

9. 4. 2. 1. Plume at 3 km distance

Scatter plots of modelled versus observed concentrations are shown in Figure 9. 8a-f. The straight red-coloured line is the trend line, which shows the linear relationship between the observed and modelled data. The best prediction is found for the plume peaks 1 and 3, which consequently correspond to the highest calculated correlation coefficient values (Figure 9. 7a, b and 9. 7e, f). Here the best correlation is found for the low values, whereas the largest differences are found for the medium values. The two scatter plots of plume peak 2 show no correlation, which is in agreement with the low correlation coefficients (Figure 9. 7c, d).

The model underestimates the average values and standard deviations of SO_2 concentration at all three plume transfers but particularly for the second plume peak. Well-predicted result was reached for plume peak 3 (Table 9. 4). The correlation coefficient (r), which describes the co-linearity between observed and modelled data, shows similar results. While the values for peaks 1 and 3 (0.57–0.69) indicate good modelling results, the coefficients for peak 2 (0.40 and 0.33) are not good.

The systematic error ($RMSE_S$) for the peaks 1 and 2 are larger than the unsystematic error ($RMSE_U$), which do not represent good model results. On the other hand, $RMSE_S$ is less than $RMSE_U$ for plume peak 3 as it should be for an unbiased simulation. The average indices of agreement (IOA) are all larger than 0.5, which indicate good model results. The highest values (0.77 and 0.73) were reached of plume peak 3 again.

The values of $SKILL_V$ of plume peaks 1 and 2 are varying between 0.42–0.49, although they are supposed to be near to '1'. Best calculated values (0.92 and 0.81) of $SKILL_V$ are reached for plume peak 3, which was expected, since the difference between the observed and predicted values for standard deviations are lowest in comparison to the other two peaks. The other two measures of skill show different results. While the values of $SKILL_E$ are all less than '1' and indicate good model results, the values of $SKILL_R$ plume peak 2 are larger than '1'.

Table 9. 4 SO_2 concentration [ppbv] statistics for TAPM simulation for the 22 November 2006.

Site: White Island, Grid 5, Distance to point source: 3 km													
Variable	**N**	**O_{Mean}**	**P_{Mean}**	**O_{Std}**	**P_{Std}**	**r**	**RMSE**	**$RMSE_S$**	**$RMSE_U$**	**IOA**	**$SKILL_V$**	**$SKILL_E$**	**$SKILL_R$**
Peak 1 11-12am	36	57.3	36.3	53.4	26.4	0.63	46.49	41.86	20.21	0.65	0.49	0.38	0.87
Peak 1 12am-1pm	36	57.3	34.3	53.4	22.9	0.69	47.06	43.64	16.42	0.62	0.43	0.32	0.88
Peak 2 11-12am	32	72.2	38.0	53.1	25.5	0.40	59.07	54.41	23.00	0.56	0.48	0.43	1.11
Peak 2 12am-1pm	32	72.2	35.4	53.1	22.2	0.33	61.96	58.17	20.78	0.53	0.42	0.39	1.17
Peak 3 11-12am	35	43.8	36.8	27.6	25.4	0.60	24.38	14.04	19.93	0.77	0.92	0.72	0.88
Peak 3 12am-1pm	35	43.8	34.1	27.6	22.3	0.57	24.78	17.61	17.80	0.73	0.81	0.64	0.90

Site: White Island, Grid 4, Distance to point source: 10 km													
Variable	**N**	**O_{mean}**	**P_{mean}**	**O_{Std}**	**P_{Std}**	**r**	**RMSE**	**$RMSE_S$**	**$RMSE_U$**	**IOA**	**$SKILL_V$**	**$SKILL_E$**	**$SKILL_R$**
Peak 1 12am-1pm	94	18.0	35.7	8.4	33.0	0.65	33.23	21.94	24.96	0.43	3.92	2.96	3.94
Peak 1 1-2pm	94	18.0	36.6	8.4	22.8	0.53	27.00	18.91	19.27	0.43	2.70	2.28	3.20
Peak 2 12am-1pm	68	19.5	44.4	12.3	32.1	-0.17	43.78	30.49	31.41	0.19	2.60	2.55	3.55
Peak 2 1-2pm	68	19.5	41.0	12.3	14.4	-0.19	29.65	26.13	13.97	0.31	1.16	1.13	2.40
Peak 3 12am-1pm	101	15.7	33.4	10.5	34.8	-0.18	41.82	24.22	34.09	0.13	3.32	3.25	3.99
Peak 3 1-2pm	101	15.7	31.4	10.5	22.6	-0.38	32.25	24.63	20.82	0.16	2.16	1.99	3.08

Table 9. 4 continued.

Site: White Island, Grid 3, Distance to point source: 20 km													
Variable	**N**	**O_{mean}**	**P_{mean}**	**O_{Std}**	**P_{Std}**	**r**	**RMSE**	**$RMSE_S$**	**$RMSE_U$**	**IOA**	**$SKILL_V$**	**$SKILL_E$**	**$SKILL_R$**
Peak 1 12am-1pm	163	12.8	20.7	7.7	15.5	0.61	14.63	8.04	12.26	0.59	2.01	1.59	1.90
Peak 1 1-2pm	163	12.8	19.1	7.7	8.2	0.71	8.69	6.52	5.71	0.72	1.06	0.74	1.13
Peak 2 12am-1pm	99	14.3	28.8	6.7	14.5	0.84	17.44	15.53	7.94	0.53	2.18	1.19	2.61
Peak 2 1-2pm	99	14.3	24.4	6.7	6.1	0.76	11.09	10.37	3.95	0.58	0.91	0.59	1.66
Peak 3 12am-1pm	177	8.9	18.6	5.6	15.6	-0.01	19.25	11.33	15.56	0.21	2.77	2.76	3.41
Peak 3 1-2pm	177	8.9	17.3	5.6	9.6	-0.14	14.49	10.96	9.48	0.29	1.70	1.68	2.57

KEY: O = observation, P = model prediction, mean = arithmetic mean, Std = standard deviation, r = Pearson correlation coefficient (0 = no correlation, 1 = exact correlation), RMSE = root mean square error, $RMSE_S$ = systematic root mean square error, $RMSE_U$ = unsystematic root mean square error, IOA = index of agreement (0 = no agreement, 1 = perfect agreement), $SKILL_V$ = (P_{Std}/O_{Std}) (near to 1 shows skill), $SKILL_E$ = ($RMSE_U/O_{Std}$) (<1 shows skill), $SKILL_R$ = ($RMSE/O_{Std}$) (<1 shows skill).

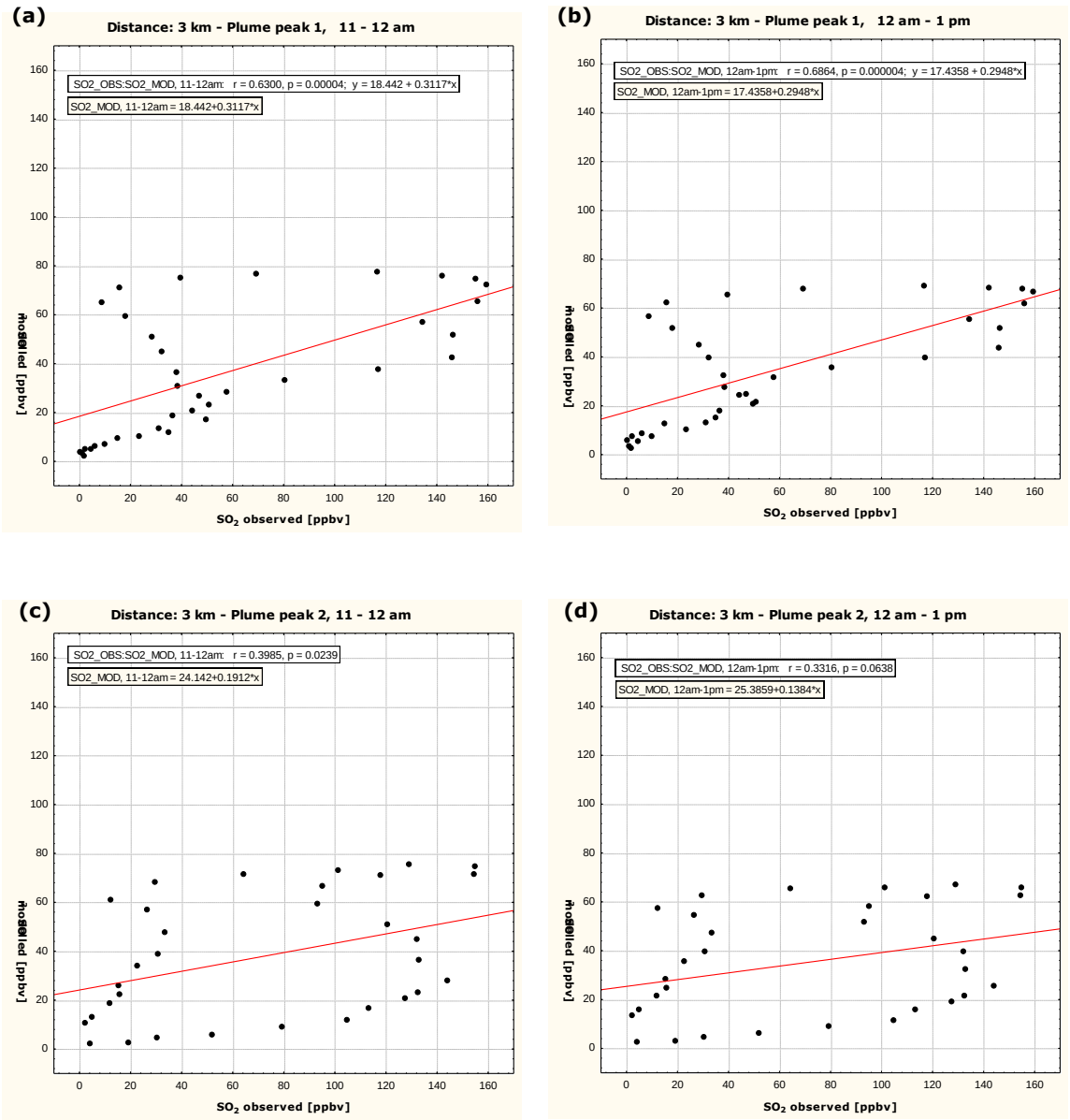

Figure 9. 7 Scatter plots of model predictions vs. observed SO2 concentrations for three plume traverses at a distance of c. 3 km.

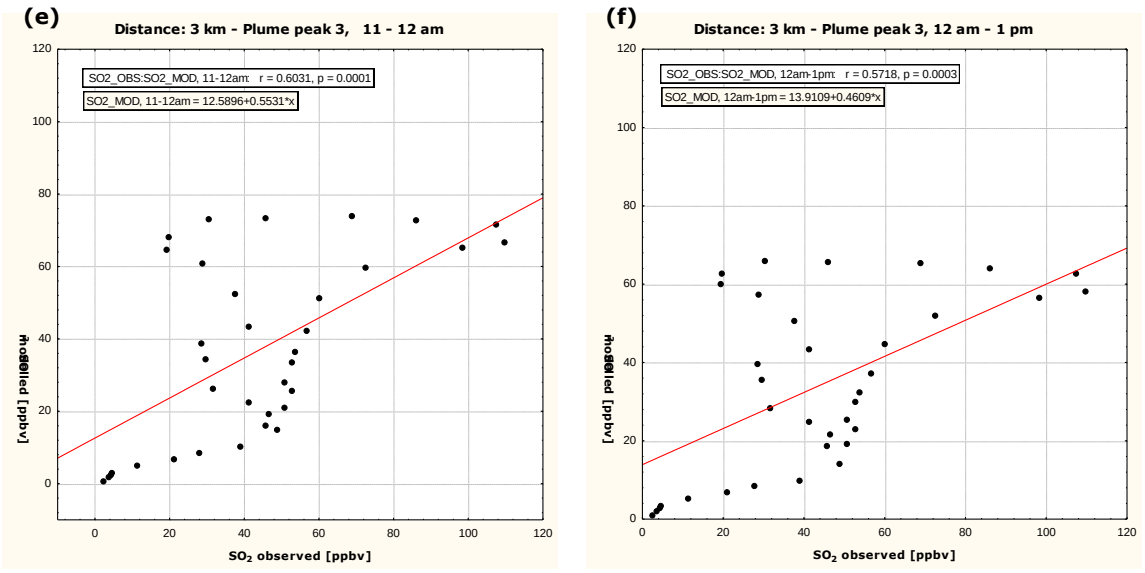

Figure 9. 7 continued.

9. 4. 2. 2. Plume at 10 km distance

TAPM calculated a strong overestimation of the arithmetic means and standard deviations for all three plume transfers at 10 km distance. The highest values for the correlation coefficient (0.65 and 0.53) were reached for plume peak 1. The other plume peaks have a negative sign with the highest of -0.38 for plume peak 3. The systematic error is less than the unsystematic error for all three plume peak but only for the time between 12 am and 1 pm, which is a good characteristic feature for models. For the time between 1-2 pm, $RMSE_S$ is larger than $RMSE_U$. The values of IOA are all less than 0.5, which do not represent good model results. The highest and just satisfying IOA are reached from plume peak 1 with a value of 0.43 for both hours 12 am-1 pm and 1-2 pm. The $SKILL_V$ values for all three plume peaks are larger than '1', in which the best value reached peak 2 with 1.16. The other two measures of skill also indicate not good model results, since their values are larger than '1', although they are supposed to be less than '1'.

9. 4. 2. 3. Plume at 20 km distance

TAPM predicted the average values and standard deviations of SO_2 concentration with an overestimation for all three plume peaks. This overestimation is stronger than the underestimation in model evaluation at 3 km distance. Therefore the correlation coefficients do not reach the good results. The correlation coefficient reached good values (>0.60) for the plume peaks 1 and 2. On the other hand, plume peak 3 shows no correlation, reaching values of –0.01 and –0.14. The systematic error ($RMSE_S$) for the peaks 1 and 3 are less than the unsystematic error ($RMSE_U$), but only for the time of 12 am-1 pm, which represent good model results for an unbiased simulation. On the other hand, $RMSE_S$ is larger than $RMSE_U$ for all other plume peaks. Similar to the correlation coefficient, the indices of agreement (IOA) show good model results for peak 1 and 2, whereas the values for plume peak 3 are smaller than 0.5. According to good results of low differences between predicted and observed standard deviations of plume peaks 1 and 2 for the time between 1-2 pm, they reached very good $SKILL_V$ values (1.06 and 0.91). All other results are larger, in which the highest values (2.77 and 1.70) reached peak 3. Similar are the results of $SKILL_E$ values. While plume peak 1 and 2 (1-2 pm) reached good model results (<1.00), the values for all other plume peaks are larger than '1'. The $SKILL_R$ values of all plume peaks are larger than 1.00, although they are supposed to be less than '1'.

9. 5. Summary

Airborne plume measurements on 22 November 2006 were carried out at approximately 60 m above sea level with three plume traverses at 3, 10 and 20 km distances from the vent of White Island volcano. The recorded SO_2 data were used for comparison with modelled data of the same day. Time series files of individual grid points were extracted from TAPM, which have the approximate same distance from the source as the COSPEC data from airborne measurements. These files contain information about the hourly-averaged vertical SO_2 concentration in the troposphere (≤8000 m) throughout the modelled period. For model evaluation, statistical calculations were performed for both, meteorological and SO_2 data. Additionally, scatter plots show the relationship between model and observation data for meteorology and recorded SO_2 data from plume traverses at 3 km distance.

The indices of agreement (IOA) for SO_2 data vary largely between 0.53-0.77 (3 km), 0.16-0.43 (10 km) and 0.21-0.72 (20 km), in which all values >0.5 represent good model results. Although the scatter plots do not show a strong linear relationship between observed and modelled SO_2 data, the calculated correlation coefficients still indicate good model results for two of the plume traverses at 3 and 20 km and one plume traverse at 10 km distance.

The IOA values from statistical calculation of the meteorological data are mainly >0.5, which represent good or very good results. They vary between 0.75-0.85 (wind speed), 0.68-0.86 (U-component), 0.46-0.47 (V-component), 0.87-0.89 (temperature) and 0.52-0.59 (relative humidity).

Chapter 10: Dimension of the non-eruptive plumes from WIV

10. 1. Introduction

A useful outcome of distal plume measurements was the possibility of studying the dimensions of dispersed plumes from White Island volcano. As mentioned earlier, diffusion of eddies results in lateral spreading of the plume with increasing distance from the vent. McGee [1992] studied the structure and dimensions of the non-eruptive plume from Mount St. Helens volcano and plotted 20 data sets in a diagram that shows the relationship between plume width and distance from the source. According to these data, McGee [1992] derived an empirical relationship (Equation 10. 1) between plume width (W) of Mount St. Helens and distance from the vent (D):

$$W\,[km] = 0.66D\,[km] + 3.09 \qquad (10.\ 1)$$

For example, the plume widths of Mount St. Helens volcano are expected to be c. 10 km and 20 km at distances of 10 km and 25 km, respectively [McGee 1992]. The author also summarised the plume of other volcanoes, which are listed in Table 10. 1. It is emphasised that Equation 10. 1 was intended only to represent the data collected in the Mount St. Helens wind regime in a mathematical way and it was not proposed to explain or predict the plume widths from other volcanic centres [K. McGee 2007, *pers. comm.*]. Therefore the plume dimensions of the other volcanoes are listed for comparison only and do not correspond to the results of the plume from Mount St. Helens. In fact, the calculated plume widths can vary widely (100% or more), depending on the volcanic setting, local wind speed and at what elevation the plume is released into the atmosphere [K. McGee 2007, *pers. comm.*].

The airborne plume measurements during the present study are used to analyse the dimension of the plumes from the quiescent degassing vent from White Island volcano. These results are then compared with the plume dimension data from other volcanoes.

Table 10. 1 Dimensions of quiescent degassing plumes from various volcanoes. List adopted from McGee [1992].

Volcano	Distance from vent [km]	Plume width [km]	Reference
Mt. Baker, U.S.A.	8.0 3.7	7.3 6.0	Radke et al. [1978]
La Soufrière, St. Vincent	4.5	5.0	Hoff & Gallant [1980]
Colima, Mexico	1-20	2-5	Casadevall et al. [1984]
Poás, Costa Rica	1-20	10-17	Casadevall et al. [1984]
Masaya, Nicaragua	14	4-9	Stoiber et al. [1986]

10. 2. Results of airborne plume measurements

Airborne measurements of the quiescent degassing plume of White Island volcano were carried out on 2 December 2004 and 22 November 2006 at several distances from the volcanic vent. As mentioned earlier, the plume widths were measured using a COSPEC instrument. One plume traverse was undertaken at each distance on 2 December 2004, whereas three or more plume traverses were completed on 22 November 2006. The distances of all plume traverses on White Island volcano and their measured plume widths are summarised in Table 10. 2.

Figures 10. 1a, b present the data of the two days of measurements (2 December 2004 and 22 November 2006) individually. The relationship between the plume width and distance from the crater summarised from the two days is shown in Figure 10. 1c. For plotting, the two plume traverses at 3.5 km and the three traverses at 3.7 km from the 22 November 2006 were condensed into one value each.

Table 10. 2 Data of plume width from all plume traverses on White Island volcano based on COSPEC measurements.

Date	Distance [km]	Measured plume width [km]
2 December 04	2.9	1.2
2 December 04	4.7	1.3
2 December 04	6.6	2.4
2 December 04	7.2	1.9
2 December 04	7.6	1.9
2 December 04	8.9	2.9
2 December 04	10.1	3.3
2 December 04	13.4	3.4
2 December 04	14.5	1.6
2 December 04	20.3	2.3
2 December 04	25.8	4.7
22 November 06	3.5	2.0
22 November 06	3.5	2.0
22 November 06	3.6	2.3
22 November 06	3.7	2.2
22 November 06	3.7	2.5
22 November 06	3.7	2.7
22 November 06	9.8	7.2
22 November 06	10.2	8.0
22 November 06	11.3	5.8
22 November 06	20.9	6.0
22 November 06	21.2	10.9
22 November 06	22.2	9.1

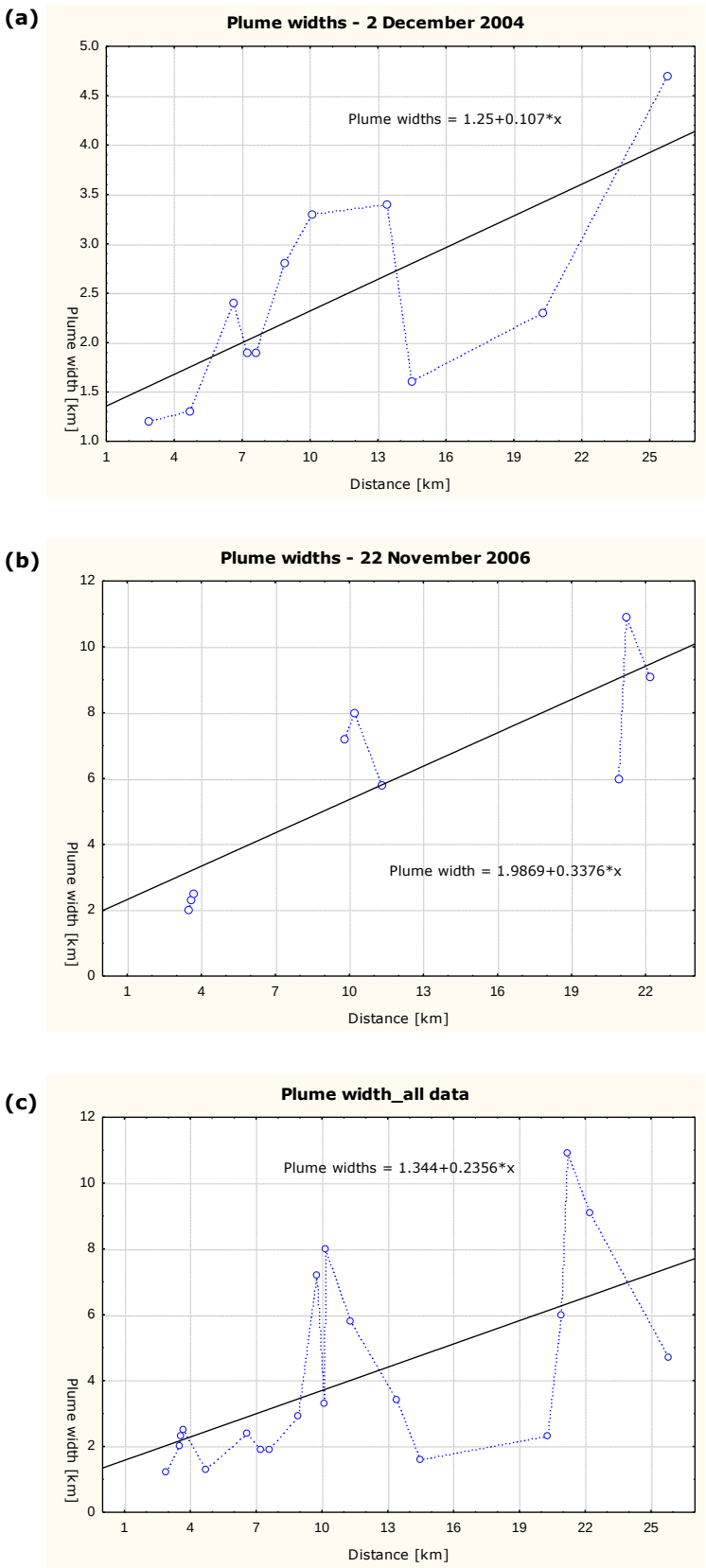

Figure 10. 1 Graphs showing the SO_2 plume widths at various distances from the vent of White Island. Measurements were carried out using COSPEC instrument on 2 December 2004 (a), and on 22 November 2006 (b). The graph in Figure (c) includes the data of both days.

Generally, it can be recognised that the plume width increases progressively (up to 10 km) with little variations. Indeed the values are close to the trend line. Beyond 10 km, however, the plume width begins to vary largely. First there is a short increase of the plume width, followed by a large decrease. This decrease can be seen in the data of both plume-measuring days. While this decline happened at a distance of approximately 13.5 km on 2 December 2004, the shrinking plume width on occurred at a distance of c. 10.5 km on 22 November 2006.

A clear result can be seen at the distal parts (c. 20 km) of plume measurements. While the plume width was quite narrow with 2.3 km on 2 December 2004, it reached a value of 6.0 km on 22 November 2006 (Table 10. 2). This value, although twofold larger, seems to be a minimum value since a few hundred metres further was determined to have a plume width of 10.9 km. This result is maybe the consequence of higher wind speeds. During the flights average wind speeds of 8.8 m s^{-1} on 2 December 2004 and 12.6 m s^{-1} on 22 November 2006 were recorded with standard deviations of 0.3 and 0.4 m s^{-1}, respectively (J. Cole-Baker 2007, *pers. comm.*).

10. 3. Summary and discussion

Based on a publication of McGee [1992] about the dimension of the quiescent degassing plume from Mount St. Helens volcano, the dimension of the quiescent degassing plumes from White Island volcano were studied using the data of several plume traverses at different distances from the vent.

As expected, the linear fit of the data from Mount St. Helens volcano that produces the relationship of Equation 10. 1 does not correspond to the present results of plume measurements from White Island volcano. Based on available data and their results, McGee [1992] generally expects plume widths of 10 and 20 km at distances of 10 and 25 km, respectively. The available data and their results from White Island volcano produce a different relationship between plume width (W) and distance from the vent (D), which is shown in Figures 10. 1a-c. The difference of plume widths in comparison to Mount St. Helens or other volcanoes is probably caused by different existing wind pattern, which in turn are due to different geographic locations of the volcanic edfices as well as different elevations of the degassing vents. Due to the small amount of available data and the resulting large variations, any predictions about the plume widths from White Island volcano are not useful.

CHAPTER 11: Summary and conclusions

11. 1. Objectives recalled

There are two aims of this study. Firstly, the characterisation of particulate matter (PM_{10}) from degassing fumaroles at White Island volcano. Secondly, to perform dispersion modelling of SO_2 and PM_{10} from the presently two most active volcanoes in New Zealand, White Island and Ruapehu.

The following outcomes were successfully achieved by this study:

(1) PM_{10} was sampled from the crater floor of White Island volcano, their concentration and chemical composition determined and the results compared with studies from previous samples as well as other volcanoes.
(2) Annual modelling of SO_2 and PM_{10} plume dispersion was performed from White Island and Ruapehu volcanoes using different input parameter and the model was evaluated the meteorological data are evaluated using statistical measures
(3) The results of all SO_2 and PM_{10} dispersion models are illustrated on DEM images for hazard assessment.
(4) Detailed hazard assessment of modelled SO_2 dispersion was performed for the scenario with the highest ground level concentration (from each source) for various locations in the North Island by comparing the modelled SO_2 dispersion data with issued concentration values of the National Environmental Standard (NES) of New Zealand.
(5) SO_2 dispersion from White Island volcano was modelled for one individual days and the accuracy of the model was verified by comparing the model data with recorded observation data from airborne plume measurements on the same day.
(6) The dimensions of the quiescent degassing plumes from White Island volcano were determined by airborne plume measurements and the results compared with studies from other volcanoes.

This chapter summarises the key findings in relation to the study objectives and outlines a justification for the program 'The Air Pollution Model' concerning future applications in hazard assessments of volcanic degassing.

11. 2. Summary of key findings

11. 2. 1. Aerosol sampling on White Island volcano

Two aerosol-sampling sessions were carried out on the crater floor of White Island volcano, in which two *MiniVol Portable Air Samplers* were used. An impactor with 10-µm cut-off point as particle size pre-separator was used and different filters of various pore sizes were exposed for the collection of particulate matter (PM_{10}) from plumes of the fumaroles. Four analysing methods were applied to analyse the filters for numerous anions and cations.

Several suggestions about the relationship of detected ions have been made, although many of them are uncertain. Best correlations of both sampling days are found for Na^+ and Cl^-, in which they also reached the highest particle mass concentrations (Na^+: 413 µg m^{-3}, Cl^-: 1520 µg m^{-3}) as well as molar concentrations (Na^+: 17.97 µmoles m^{-3}, Cl^-: 42.88 µmoles m^{-3}). Another correlation, from first aerosol sampling, is assumed between the ions of Ca^{2+} and PO_4^{3-} and to a certain extent Mg^{2+}. These relationships are considered to be caused by sampled dust particles, which were eroded from the surrounding pyroclastic deposits.

Another compound collected during the first aerosol-sampling session are NO_3^-, which is possibly due to HNO_3. On three filters from the second sampling NH_4 was detected, which is maybe due to the collection of NH_4Cl particles. A last and very weak correlation is suggested for K^+ and SO_4^{2-}, which would result from the deposition of K_2SO_4 onto two filters.

The results of present aerosol-sampling sessions were used for comparisons with previous studies on White Island by Rose et al. [1986] and samplings from the quiescent degassing plumes of Soufriere Hills volcano (Montserrat) by Allen et al. [2000] and La Fossa (Vulcano, Italy) by Mather et al. [2004b]. The concentration values of the present study are in the range as the sampling results from the other two workers. However, the concentrations from White Island show some variations, particularly chlorine, and some ions are uncertain to be detected. Therefore, an accurate interpretation is not possible and more aerosol-sampling sessions are suggested.

One exposed filter was used for SEM study and the results are comparable with previous work of Rose et al. [1986]. The typical cubic shape of halite particles is recognised. Additional particles are probably silicate particles with their irregular shape and sharp edges. Two less certain particles were found, in which one of

them has a very similar, spherical shape, which Rose et al. [1986] analysed to contain peaks of Ti and S in the EDS spectrum. However, since no EDS study was carried out for the present sample, it could not be proven that this is the same kind of particle.

11. 2. 2. Dispersion modelling by TAPM

11. 2. 2. 1. Annual SO_2 and PM_{10} dispersion modelling

A major part of this study is the presenting of results from pollution dispersion modelling using The Air Pollution Model (TAPM). Various model scenarios were performed for the dispersion of SO_2 (models 1-4) and PM_{10} (model 5 and 6) during quiescent degassing (models 1-3 and 5) as well as the discharge by puffs in intervals of five hours (models 4 and 6). Different input parameters were used, including emission rates, exit temperatures and exit velocities. The models were performed quarterly for the year 2005, in which the output data are gridded summary statistic files, showing the average and the maximum concentrations of all grid points in all defined grid domains.

Since no observation data of SO_2 or PM_{10} are available for the annual model, the accuracy of pollution dispersion could not be verified. Thus, evaluation of annual modelling was performed by comparing the meteorological data (wind speed, wind direction, temperature and relative humidity) from the model with observation data from different monitoring sites in the North Island using statistical calculations and scatter plots. The most important statistical measure is the index of agreement (IOA). The resulting values range between 0 and 1, in which '1' represent perfect agreement and values greater 0.5 symbolise good results [Hurley et al. 2002, Hibberd et al. 2005]. The average values from the present model are 0.75 (wind speed), 0.81 (U-component), 0.83 (V-component), 0.91 (ambient temperature) and 0.76 (relative humidity). The results of the present work were also compared with the results of other TAPM studies, suggesting good model results.

The results of all plume dispersion models are illustrated on DEM images, showing the approximate distribution of the plumes using three different concentrations levels. The first result is that the dispersed plumes from White Island were calculated with lower concentration values than from Ruapehu volcano for both, SO_2 and PM_{10}, and during all model scenarios. Although the SO_2 plumes from White Island are sometimes widespread, they often show very low concentrations. This is particularly valid for the scenarios of quiescent degassing, where the average and maximum concentrations do not exceed the value of 5.0 and 350 µg m^{-3} at all during the modelled periods. The results of model 4 are even more widespread and TAPM calculated higher SO_2 ground level concentrations. The threshold values of 350 µg m^{-3} and/or 570 µg m^{-3}, respectively, are only exceeded at small areas near the vent or remote rural areas and do not affect any urban communities.

The dispersing plumes from Ruapehu volcano are characterised by higher plume concentrations and affect the complete surroundings up to several tens of kilometres away from the source. However, this area has a very low population density and urban areas affected in models 1-2 are only Wanganui in the south and Taupo in the north. More affected are the urban communities in model 3 where the plume with concentrations of ≥350 µg m^{-3} travelled until the city of Napier. Still higher plume concentrations were modelled for scenario 4, where this threshold value is exceeded in several urban areas, including Napier, Gisborne, Wanganui, Palmerston North, New Plymouth and Taupo. The city of Napier even experienced SO_2 concentration of ≥570 µg m^{-3}.

The models also indicate that the volcanic plumes from White Island often reached ground level when they are over land. On the other hand, the ground level concentrations from the plume of Ruapehu volcano are decreasing steadily from the source to the distal parts. This is probably caused by the individual characteristics of the marine boundary layer with less turbulence than the boundary layer over the land [Arya 1999].

For models 4 from the two volcanic centres of White Island and Ruapehu volcanoes, a detailed analysis for hazard assessment to population in the North Island was performed. This analysis is based on NES values for SO_2 of 350 µg m^{-3} and 570 µg m^{-3}, respectively, which was issued by the Ministry for the Environment of New Zealand in 2005. Time series files from different locations in the North Island, including all main urban areas, were used and the extracted data show the distribution of SO_2 concentration at these locations throughout the modelled year.

As mentioned above, the results show that the SO_2 plumes from White Island affect the population in the North Island less than from Ruapehu volcano. While the NES value of 350 µg m^{-3} for SO_2 from the White Island model is not reached by any of the chosen locations in the North Island, there are four urban areas (Napier, Wanganui, Palmerston North and Gisborne) where this threshold value is exceeded. Additionally, the city of Napier is affected once by the plume, exceeding the higher NES value of 570 µg m^{-3}. Although against the regulation, this single peak cannot be considered to be a serious hazard for people in Napier. The same conclusion is applied for the NES value of 350 µg m^{-3}, which is exceeded 13 times in that model. These exceedings are distributed over four cities as well as throughout the modelled year. Most crossings of the 350 µg m^{-3} threshold value in grid 2 were modelled for Wanganui (7), Palmerston North (3), Napier (2) and Gisborne (1). Additionally, in grid 3 this value is exceeded twice at Wanganui. Most SO_2 concentrations were modelled to be at ground level in the morning hours between 7-12 am.

For dispersion modelling of PM_{10}, TAPM calculated extremely low ground level concentrations. Particularly the two model scenarios with White Island as point source indicate very low hazard, where only several smaller areas are affected by ground concentrations of ≥1.0 µg m^{-3}. The highest value was calculated with 4.2 µg m^{-3} near Whakatane.

The dispersed plumes from Ruapehu volcano cover larger areas of the North Island and also reached higher concentrations at ground level than the White Island model. However, the results are still low. Napier and Wanganui are the only urban areas affected by plume concentrations of ≥1.0 µg m^{-3}. Concentration values of ≥5.0 µg m^{-3} were only modelled for rural areas near the edifice of Ruapehu volcano.

11. 2. 2. 2. SO_2 dispersion modelling from WIV on 22 November 2006

Airborne plume measurements using a COSPEC instrument were carried out on 22 November 2006. Measurements were performed by several plume traverses at three distances (3, 10 and 20 km) from the vent of White Island volcano.

In order to verify the calculated pollution dispersion of TAPM, two days (21/22 November 2006) were modelled. The first day was modelled as "spin-up day" to initialise the model, but the output data were ignored from further analysis. The meteorological and SO_2 output data from 22 November were used to compare the model data with observation data. Model evaluation was performed using statistical measures and scatter plots show the relationship between model and observation data.

The indices of agreement (IOA) for SO_2 data vary largely between 0.53-0.77 (3 km), 0.16-0.43 (10 km) and 0.21-0.72 (20 km), in which all values >0.5 represent good to very good model results. Although the scatter plots do not show a strong linear relationship between observed and modelled SO_2 data, the calculated correlation coefficients still indicate good model results for two of the plume traverses at 3 and 20 km and one plume traverse at 10 km distance.

The IOA values from statistical calculation of the meteorological data are mainly >0.5, which represent good or very good results. They vary between 0.75-0.85 (wind speed), 0.68-0.86 (U-component), 0.46-0.47 (V-component), 0.87-0.89 (temperature) and 0.52-0.59 (relative humidity).

11. 2. 3. Dimension of the non-eruptive plume from WIV

Airborne plume measurements were carried out on 2 December 2004 at an average height of 245 m, where the plume peak was highest during the contouring method. These measurements were conducted to see how far the quiescent degassing plume from White Island is travelling or can be detected. Plume measurements of 22 November 2006 were included into this study. The farthest distance of plume traverse was carried out at 25.8 km in December 2004 and 22.2 km in November 2006.

Generally, it can be recognised that the plume width increases progressively (up to 10 km) with little variation. Beyond 10 km, however, the plume width begins to vary largely. First there is a short increase of the plume width, followed by a large decrease. This decrease can be seen in the data from both plume-measuring days. While this decline happened at a distance of approximately 13.5 km on 2 December 2004, the shrinking plume width on occurred at a distance of c. 10.5 km on 22 November 2006. Although minor, different values were also measured at c. 20 km distance, in which the plume width from November 2006 with 6.0 km is twice as much as the plume width in December 2004 with 2.3 km. The variations in plume widths measured may be the consequence of different wind speeds at these days. During the flights average wind speeds of 8.8 m s^{-1} on 2 December 2004 and 12.6 m s^{-1} on 22 November 2006 were recorded with standard deviations of 0.3 and 0.4 m s^{-1}, respectively (J. Cole-Baker 2007, *pers. comm.*). However, it is emphasised that plume measurements at these two days were carried out at different elevations because of different motivation of measurements.

11. 3. Suggestions for future work

11. 3. 1. Aerosol sampling

Two aerosol-sampling sessions were carried out during the present study using *MiniVol Portable Air Sampler*. As mentioned earlier, this instrument is sensitive against acidic air and therefore not useful for further work in a volcanic environment. Consequently, other instruments must be purchased for possible future work. If expensive instruments are not available, the use of filter packs represent a less expensive and common method for sampling of particulate matter.

While during the present study only particles with an aerodynamic diameter of 10 µm (PM_{10}) were examined, future sampling can be performed using an impactor with 2.5 µm cut-off point to collect fine particles ($PM_{2.5}$). On the other hand, the impactor can be avoided to study the total suspending particles (TSP) from volcanic plumes.

Future study of particulate matter can use the present results to examine further the chemical composition as well as the shape of collected particles. Although the results of analyses of the present work are satisfying, they still keep open questions, particularly regarding the relationship between detected ions. To complete more successful analyses, future sampling should be aware to use longer exposure times of the filters, which might be too short during the present study.

Future work could also be undertaken to study the amount of trace metals from White Island volcano or other volcanic environments and to determine the emission rate of particulate matter. This was not performed during the present work, since this would have increased the costs for analyses.

For human health studies White Island is only of interest concerning people who are visiting the volcano. While tourists are only exposed to the plume for a couple of hours, their guides inhale the volcanic gases and particulate matter more often, which can cause health problems for individuals at a later date. Rose et al. [1986] reported the detection of sulphuric acid (H_2SO_4) during their measurements, which represent the most known aerosol in volcanic environments. The detection of H_2SO_4 particles could not be confirmed doubtless during the present study and might be a future outlook too.

11. 3. 2. Dispersion modelling by TAPM

Most previous models using TAPM were performed to study air pollution due to anthropogenic sources, such as industrial chimneys. Additionally, these models analysed the ground level concentration of different pollutants within a small area and compared the results with pollution data from monitoring sites. This study, on the other hand, was performed to study the dispersion of volcanic plumes (SO_2 and PM_{10}) within a large region.

The largest error during present modelling occurred for the height of the SO_2 plume on 22 November 2006 with a difference of c. 1000 metres. On the other hand, the analysis of the meteorological data was performed successfully. The calculated statistical measures indicate good results, which means that TAPM has proven to be a model that is recommended for future studies. Since the statistical analysis of meteorological data includes long-term data of one whole year, the results can also be considered to be significant.

Model evaluations for SO_2 could only be performed for one single day and for PM_{10} not at all. Some correlation coefficients from model evaluations with SO_2 data show values below 0.5 and do not represent good model results. However, most values are >0.5 and thus indicate good agreement with the model. Although this is a good result of TAPM application, the analysis of data from one single day is not very meaningful for model evaluations. Consequently, more long-term pollution data are needed for more significant model verification.

For model evaluations for pollution, data from monitoring sites several kilometres away from the source are required. Since such data is hard to collect from White Island volcano, it is more easily available from the mainland. For example, more detailed modelling can be performed for Ruapehu volcano. Since the population density is very low, monitoring sites that record SO_2 concentrations do not measure the pollution from anthropogenic sources.

On the other hand, the presented results suggested that the modelled plumes from White Island and Ruapehu volcanoes hardly affect the population in the North Island since the two vents are located at remote and less populated areas. Although White Island and Ruapehu volcanoes are the two most active volcanoes in New Zealand in recent time, they are not the only volcanic vents. Thus, future modelling can also be performed for volcanic terrains in higher populated areas, such as Rotorua.

References

Aberkane, T., M. Harvey and M. Webb (2005). Annual ambient air quality monitoring report 2004. Report **No. U05/61**. Environment Canterbury.

Ackerman, S.A. and K.I. Strabala (1994). Satellite remote sensing of H2SO4 aerosol using the 8- to 12-µm window region: Application to Mount Pinatubo. *J. Geophys. Res.* **99 (D9):** 18,639 – 18,649.

Aiuppa, A., P. Bonfanti, L. Brusca, W. D'Alessandro, C. Federico and F. Parello (2001). Evaluation of the environmental impact of volcanic emissions from the chemistry of rainwater: Mount Etna area (Sicily). *Appl. Geochem.* **16:** 985 – 1000.

Amdur, M.O., W.W. Melvin and P. Drinker (1953). Effects of inhalation of sulfur dioxide by man. *Lancet* **2:** 758 – 759.

Albrecht, B.A. (1989). Aerosols, cloud microphysics, and fractional cloudiness. *Science* **245:** 1227 – 1230.

Allen, A.G., P.J. Baxter and C.J. Ottley (2000). Gas and particle emissions from Soufrière Hills volcano, Montserrat, West Indies: characterization and health hazard assessment. *Bull. Volcanol.* **62:** 8 – 19.

Allen, A.G., C. Oppenheimer, M. Ferm, P.J. Baxter, L.A. Horrocks, B. Galle, A.J.S. McGonigle and H.J. Duffell (2002). Primary sulfate aerosol and associated emissions from Masaya volcano, Nicaragua. *J. Geophys. Res.* **107 (D23)**. doi: 10.1029/2002JD002120

Andres, R.J. and A.D. Kasgnoc (1998). A time-averaged inventory of subaerial volcanic sulfur emissions. J. Geophys. Res. **103:** 25,251 – 25,261.

Arya, S.P. (1999). Air Pollution, Meteorology and Dispersion, published by: Oxford University Press, 310 pp.

Barratt, R. (2001). Atmospheric Dispersion Modelling: An introduction to practical applications, published by: Earthscan Publications Limited, 151 pp.

Baxter, P.J., R.E. Stoiber and S.N. Williams (1982). Volcanic gases and health: Masaya volcano, Nicaragua. *Lancet* **2:** 150 – 151.

Bethel, R.A., J. Epstein, D. Sheppard, J.A. Nadel and H.A. Boushey (1983). Sulfur dioxide-induced bronchoconstriction in freely breathing, exercising, asthmatic subjects. *Am. Rev. Respir. Dis.* **129:** 987 – 990.

Bethel, R.A., D. Sheppard, J. Epstein, E. Tam, J.A. Nadel and H.A. Boushey (1984). Interaction of sulfur dioxide and cold dry air in causing bronchoconstriction in asthmatic subjects. *J. Appl. Physiol.* **57:** 419 – 423.

Black, P.M. (1970). Observations on White Island volcano, New Zealand. *Bull. Volcanol.* **34:** 158 – 167.

Bobrowski, N., G. Hönninger, B. Galle and U. Platt (2003). Detection of bromine monoxide in a volcanic plume. *Nature* **423:** 273 – 276.

Boubel, R.W., D.L. Fox, D.B. Turner and A.C. Stern (1994). Fundamentals of Air Pollution, published by: Academic Press, 574 pp.

Brasseur, G.P., P. Artaxo, L.A. Barrie, R.J. Delmas et al. (2003). An integrated view of the causes and impacts of atmospheric changes. In: Brasseur, G.P., R.G. Prinn and A. A.P. Pszenny (eds.) Atmospheric Chemistry in a Changing World - An Integration and Synthesis of a Decade of Tropospheric Chemistry Research – The International Global Atmospheric Chemistry Project of the International Geosphere-Biosphere Programme, published by: Springer, pp. 207 – 230.

Brenstrum, E. (1998). The New Zealand Weather Book, published by: Craig Potton Publishing, 128 pp.

Brimblecombe, P. (1996). Air composition & chemistry, published by: Cambridge University Press, 253 pp.

Bryan, C.J. and S. Sherburn (1999). Seismicity associated with the 1995-1996 eruptions of Ruapehu volcano, New Zealand: narrative and insights into physical processes. *J. Volcanol. Geotherm. Res.* **90:** 1 – 18.

Camuffo, D. and S. Enzi (1995). Impact of clouds of volcanic aerosols in Italy during the last 7 centuries. *Natural Hazards* **11:** 135 – 161.

Casadevall, T.J., W.I. Rose, W.H. Fuller, W.H. Hunt, M.A. Hart, J.L. Moyers, D.C. Woods, R.L. Chuan and J.P. Friend (1984). Sulfur dioxide and particle in quiescent volcanic plumes from Póas, Arenal, and Colima volcanoes, Costa Rica and Mexico. *J. Geophys. Res.* **89 (D6):** 9633 – 9641.

Christenson, B.W. (2000). Geochemistry of fluids associated with the 1995-1996 eruption of Mt. Ruapehu, New Zealand: signatures and processes in the magmatic-hydrothermal system. *J. Volcanol. Geotherm. Res.* **97:** 1 – 30.

Christenson, B.W. and C.P. Wood (1993). Evolution of a vent-hosted hydrothermal system beneath Ruapehu Crater Lake, New Zealand. *Bull. Volcanol.* **55:** 547 – 565.

Christoffel, D.A. (1989). Variations in magnetic field intensity at White Island volcano to the 1976-82 eruption sequence. In: Houghton, B.F. and I.A. Nairn (eds.) The 1976-82 eruption sequence at White Island volcano (Whakaari), Bay of Plenty, New Zealand. *N.Z. Geol. Surv. Bull.* **103:** 109 – 118.

Clark, R.H. (1970). Volcanic activity on White Island, Bay of Plenty 1966-69. Part 1 – Chronology and crater floor level changes. *N.Z. J. Geol. Geophy.* **13:** 565 – 574.

Clark, R.H. (1973). Surveillance of White Island volcano 1968-72. Part 1 – Volcanic events and deformation of the crater floor. *N.Z. J. Geol. Geophy.* **25:** 317 – 324.

Clark, R.H. and J.W. Cole (1989). Volcanic monitoring and surveillance at White Island before the 1976-82 eruption sequence. In: Houghton, B.F. and I.A. Nairn (eds.) The 1976-82 eruption sequence at White Island volcano (Whakaari), Bay of Plenty, New Zealand. *N.Z. Geol. Surv.* **103:** 9 – 11.

Clark, R.H. and P.M. Otway (1989). Deformation monitoring associated with the 1976-82 White Island eruption sequence. In: Houghton, B.F. and I.A. Nairn (eds.) The 1976-82 eruption sequence at White Island volcano (Whakaari), Bay of Plenty, New Zealand. *N.Z. Geol. Surv.* **103:** 69 – 84.

Clarke, A.G. (1992). The atmosphere. In: Harrison, R.M. (ed.) *Understanding Our Environment: An introduction to Environmental Chemistry and Pollution*, published by: Royal Society of Chemistry, pp. 5 – 52.

Clarkson, B.D. (1990). A review of vegetation development following recent (<450 years) volcanic disturbance in North Island, New Zealand. *N.Z. J. Ecol.* **14:** 59 – 71.

Clarkson, B.D. and B.R. Clarkson (1994). Vegetation decline following recent eruptions on White Island (Whakaari), Bay of Plenty, *New Zealand. N.Z. J. Botany* **32:** 21 – 36.

Cole, J.W. (1986). Monitoring White Island volcano. In: International Volcanological Congress New Zealand, 1986 - Volcanic Hazards Assessment in New Zealand, published by: New Zealand Geological Survey.

Cole, J.W., T. Thordarson and R.M. Burt (2000). Magma origin and evolution of White Island (Whakaari) volcano, Bay of Plenty, New Zealand. *J. Petrol.* **41:** 867 – 895.

Cronin, S.J., V.E. Neall, J.A. Lecointre, M.J. Hedley and P. Loganathan (2003). Environmental hazards of fluoride in volcanic ash: a case study from Ruapehu volcano, New Zealand. *J. Volcanol. Geotherm. Res.* **121:** 271 – 291.

De Lisle, J.F. and I.S. Kerr (1963). The climate and weather of the Bay of Plenty region. *N.Z. Meteor. Serv. Misc. publ.* **115 (1):** 1st. Edition, 12 pp.

Delmelle, P. and J. Stix (2000). Volcanic Gases. In: Sigurdsson, H. et al. (eds.) Encyclopedia of Volcanoes, published by: Academic Press, pp. 803 – 815.

Delmelle, P., J. Stix, C.P.-A. Bourque, P.J. Baxter, J. Garcia-Alvarez and J. Barquero (2001). Dry deposition and heavy acid loading in the vicinity of Masaya volcano, a major sulfur and chlorine in Nicaragua. *Environ. Sci. Techn.* **35 (7):** 1289 – 1293.

Delmelle, P., J. Stix, P. Baxter, J. Garcia-Alvarez and J. Barquero (2002). Atmospheric dispersion, environmental effects and potential health hazard associated with the low-altitude gas plume of masaya volcano, Nicaragua. *Bull. Volcanol.* **64:** 423 – 434.

Delmelle, P. (2003). Environmental impacts of tropospheric volcanic plumes. In: Oppenheimer, C., D.M. Pyle and J. Barclay (eds.) Volcanic Degassing, published by: *Geological Society, London, Spec. Publ.* **213:** 381 – 399.

Donoghue, S.L., V.E. Neall, A.S. Palmer and R.B. Stewart (1997). The volcanic history of Ruapehu during the past 2 millennia based on the record of Tufa Trig tephras. *Bull. Volcanol.* **59:** 136 – 146.

Drost, F., J. Renwick, B. Bhaskaran, H. Oliver and J. McGregor (2007). Simulation of New Zealand's climate using a high-resolution nested regional climate model. *Int. J. Climatol.* **27:** 1153 – 1169.

Duncan, A.R. (1970). The petrology and petrochemistry of andesite and dacite volcanoes in eastern Bay of Plenty, New Zealand. Ph.D. thesis, Victoria University, Wellington, New Zealand (unpubl.).

Edmonds, M., D. Pyle and C. Oppenheimer (2001). A model for degassing at the Soufrière Hills volcano, Montserrat, West Indies, based on geochemical data. *Earth Planet. Sci. Lett.* **186:** 159 – 173.

Fiacco, R.J. Jr., Th. Thordarson, M.S. Germani, S. Self, J.M. Palais, S. Withlow and P.M. Grootes (1994). Atmospheric aerosol loading and transport interpreted from ash particles and acidity due to the 1783-1784 Laki eruption in the GISP2 ice core. *Quaternary Res.* **42:** 231 – 240.

Folinsbee, L.J. (1993). Human health effects of air pollution. *Environ. Health Perspect.* **100:** 45- 56.

Frank, N.R., M.O. Amdur, J. Worcester and J.L. Whittenburger (1962). Effects of acute controlled exposure to SO_2 on respiratory mechanics in healthy adult males. *J. Appl. Physiol.* **17:** 252 – 258.

Gallaher, M. and B. Depro (2005). Economic impact analysis (EIA) for the proposed stationary combustion turbines NSPS: Final report. **EPA-452/R-05-001**, 103 pp.

Gamble, J.A., I.C. Wright and J.A. Baker (1993). Seafloor geology and petrology in the oceanic to continental transition zone of the Kermadec-Havre-Taupo Volcanic Zone Arc System, New Zealand. *N.Z. J. Geol. Geophys.* **36:** 417 – 435.

Gamble, J.A., C.P. Wood, J.G. Price, I.E.M. Smith, R.B. Stewart and T. Waight (1999). A fifty year perspective of magmatic evolution on Ruapehu volcano, New Zealand: verification of open-system behaviour in an arc volcano. *Earth Planet. Sci. Lett.* **170:** 301 – 314.

Garland, J.A., W.S. Clough and D. Fowler (1973). Deposition of sulfur dioxide on grass. *Nature* **242:** 256 – 257.

Gauthier, P.-J. and M.-F. Le Cloarec (1998). Variability of alkali and heavy metal fluxes released by Mt. Etna volcano, Sicily, between 1991 and 1995. *J. Volcanol. Geotherm. Res.* **81:** 311 – 326.

Giggenbach, W.F. (1982). The chemical and isotopic composition of gas discharges from New Zealand andesitic volcanoes. *Bull. Volcanol.* **45:** 253 – 255.

Giggenbach, W.F. (1983). Chemical surveillance of active volcanoes in New Zealand. In: Tazieff, H. & J.C. Sabroux (eds.) Forecasting Volcanic Events, published by: Elsevier, pp. 312 – 322.

Giggenbach, W.F. (1987). Redox processes governing the chemistry of fumarolic discharges from White Island, New Zealand. *Appl. Geochem.* **2:** 143 – 161.

Giggenbach, W. and D.S. Sheppard (1989). Variations in temperature and chemistry of White Island fumarole discharges, 1972-85. In: Houghton, B.F. and I.A. Nairn (eds.) The 1976-82 Eruption Sequence at White Island Volcano (Whakaari), Bay of Plenty, New Zealand. *N.Z. Geol. Surv. Bull.* **103:** 119 – 126.

Giggenbach, W.F. and R.L. Goguel (1989). Collection and analysis of geothermal and volcanic water and gas discharges. *DSIR Chem. Div. Report* **CD2401**, pp. 1 – 81.

Gimson, N.R. (2005). Modelling the air quality of Auckland – A comparison between CALGRID and TAPM simulations based on observed and modelled meteorology. *Clean Air and Environmental Quality* **39 (2):** 38 – 46.

Goodin, W.R., G.J. McRae and J.H. Seinfeld (1980). An objective analysis technique for constructing three-dimensional urban-scale wind fields. *J. Appl. Meteorol.* **19:** 98 – 108.

Gordon, N.D. (1986). The Southern Oscillation and New Zealand Weather. *Monthly Weather Review* **114:** 371 – 387.

Graedel, T.E. and P.J. Crutzen (1993). Atmospheric Change – An Earth System Perspective, published by: W.H. Freeman and Company, 446 pp.

Graf, H.-F., J. Feichter and B. Langmann (1997). Volcanic sulfur emissions: estimates of source strength and its contribution to the global sulfate distribution. J. Geophys. Res. **102:** 10,727 – 10,738.

Grattan, J., M. Durand and S. Taylor (2003). Illness and elevated human mortality in Europe coincident with the Laki Fissure eruption. In: Oppenheimer, C., D.M. Pyle and J. Barclay (eds.) Volcanic Degassing, published by: *Geol. Soc. Lond. Spec. Pub.* **213:** 401 - 414.

Grattan, J.P. and F.B. Pyatt (1994). Acid damage in Europe caused by the Laki fissure eruption – an historical review. *Sci. Total. Environ.* **151:** 241 – 247.

Graziani, G., A. Martilli, M.T. Pareschi and M. Valenza (1997). Atmospheric dispersion of natural gases at Vulcano island. *J. Volcanol. Geotherm. Res.* **75:** 283 – 308.

Hackett, W.R. and B.F. Houghton (1989). A facies model for a Quaternary andesite composite volcano: Ruapehu, New Zealand. *Bull. Volcanol.* **51:** 51 – 68.

Halmer, M.M., H.-U. Schmincke and H.-F. Graf (2002). The annual volcanic gas input into the atmosphere, in particular into the stratosphere: a global data set for the past 100 years. *J. Volcanol. Geotherm. Res.* **115:** 511 – 528.

Hansell, A. and C. Oppenheimer (2004). Health hazards from volcanic gases: a systematic literature review. *Archives of Environ. Health* **59:** 628 – 639.

Harding, D. and J.M. Miller (1982). The influence on rain chemistry of the Hawaiian volcano Kilauea. *J. Geophys. Res.* **87:** 1225 – 1230.

Havas, M. (1986). Effects of acidic deposition on aquatic ecosystems. In: Stern, A. (ed.) *Air Pollution*, Vol. IV, published by: Academic Press, pp. 351 – 389.

Hibberd, M., I. Galbally, P. Hurley, A. Luhar, M. Edwards, S. Bentley and S. Lee (2005). Final Report – Meteorological and Dispersion Modelling using TAPM for Wagerup, Phase 3B: HRA (Health Risk Assessment) Concentration Modelling – Expanded Refinery Scenario, 133 pp.

Hill, A.C. (1971). Vegetation: a sink for atmospheric pollutants. *J. Air Pollut. Control Assoc.* **21:** 341 – 346.

Hill, J. and P.J. Hurley (2005). Fluoride dispersion in a coastal environment. In: Towards a new agenda: 17th International Clean Air & Environment Conference proceedings, Hobart. Clean Air Society of Australia and New Zealand. 7 pp.

Hobbs, P.V., J.P. Tuell, D.A. Hegg, L.F. Radke and M.K. Eltgroth (1982). Particles and gases in the emissions from the 1980-1981 volcanic eruptions of Mt. St. Helens. *J. Geophys. Res.* **87:** 11,062 – 11,086.

Hoff, R.M. and A.J. Gallant (1980). Sulfur dioxide emissions from La Soufrière volcano, St. Vincent, West Indies. *Science* **209:** 923 – 924.

Horrocks, L.A., C. Oppenheimer, M.R. Burton and H.J. Duffell (2003). Compositional variation in tropospheric volcanic gas plumes: evidence from ground-based remote sensing. In: Oppenheimer, C., D.M. Pyle and J. Barclay (eds.) *Volcanic Degassing*, published by: Geological Society, London. *Geol. Soc. Spec. Pub. No.* **213:** 349 – 369.

Hosking, G. (1993). *Nothofagus* decline in New Zealand: Separating causes from symptoms. In: Huettl, R.F. & D. Mueller-Dombois (eds.) Forest decline in the Atlantic and Pacific region, published by: Springer, Berlin.

Houghton, B.F. and I.A. Nairn (1989). A model for the 1976-1982 phreatomagmatic and strombolian eruption sequence at White Island volcano, New Zealand. In: Houghton, B.F. and I.A. Nairn (eds.) The 1976-82 eruption sequence at White Island volcano (Whakaari), Bay of Plenty, New Zealand. *N.Z. Geol. Surv.* **103:** 127 – 136.

Houghton, B.F., C.J.N. Wilson, M.O. Lanphere, S.D. Weaver, R.M. Briggs and M.S. Pringle (1995). Chronology and dynamics of a large silicic magmatic system: central Taupo Volcanic Zone, New Zealand. *Geology* **23:** 13 – 16.

Hurley, P. (2000). Verification of TAPM meteorological predictions in the Melbourne region for a winter and summer month. *Austral. Meteorol. Mag.* **49:** 97 – 107.

Hurley, P.J. (2005a). The Air Pollution Model (TAPM) Version 3. Part 1: Technical Description. *CSIRO Atmospheric Research Technical Paper* No. 71, 54 pp.

Hurley, P.J. (2005b). The Air Pollution Model (TAPM) Version 3. User Manual. *CSIRO Atmospheric Research Internal Paper* No. 31, 37 pp.

Hurley, P.J. and A.K. Luhar (2005). An evaluation and inter-comparison of AUSPLUME, CALPUFF and TAPM – Part 1: The Kincaid and Indianapolis field datasets. *Clean Air and Environmental Quality* **39 (1):** 39 – 45.

Hurley, P.J., J. Hill and A. Blockley (2005). An evaluation and inter-comparison of AUSPLUME, CALPUFF and TAPM – Part 2: Anglesea and Kwinana annual datasets. *Clean Air and Environmental Quality* **39 (1):** 46 – 51.

Hurley, P.J., A. Blockey and K. Rayner (2001). Verification of a prognostic meteorological and air pollution model for year-long predictions in the Kwinana industrial region of Western Australia. *Atmos. Environ.* **35:** 1871 – 1880.

Hurley, P.J., W.L. Physick and A.K. Luhar (2002). The Air Pollution Model (TAPM) Version 2. Part 2: Summary of some verification studies. *CSIRO Atmospheric Research Technical Paper* **No. 57**, 46 pp.

Hurley, P., P. Manins, S. Lee, R. Boyle, Y. Leung Ng and P. Dewundege (2003). Year-long, high-resolution, urban airshed modelling: verification of TAPM predictions of smog and particles in Melbourne, Australia. *Atmos. Environ.* **37:** 1899 – 1910.

Hurley, P.J. (2006). An evaluation and inter-comparison of AUSPLUME, AERMOD and TAPM for seven field datasets of point source dispersion. *Clean Air and Environmental Quality* **40 (1):** 45 – 50.

Hurst, A.W. (1980). Temperature observations of Crater Lake, Mt. Ruapehu, New Zealand, using temperature telemetry buoys. *Bull. Volcanol.* **43:** 121 – 129.

Hurst, A.W. and D.A. Christoffel (1973). Surveillance of White Island volcano, 1968-1972: part 3 thermo-magnetic effects due to volcanic activity. *N.Z. J. Geol. Geophys.* **16:** 965 – 972.

Hurst, A.W., H.M. Bibby, B. Scott and M.J. McGuinness (1991). The heat source of Ruapehu Crater Lake: deductions from the energy and mass balances. *J. Volcanol. Geotherm. Res.* **46:** 1 – 20.

Hurst, A.W. and J. Vandemeulebrouck (1996). Acoustic noise and temperature monitoring of the crater lake of Mount Ruapehu volcano. *J. Volcanol. Geotherm. Res.* **71:** 45 – 51.

Hurst, A.W., P.C. Rickerby, B.J. Scott and T. Hashimoto (2004). Magnetic field changes on White Island, New Zealand, and the value of magnetic changes for eruption forecasting. *J. Volcanol. Geotherm. Res.* **136:** 53 – 70.

Hutchinson, T.C. and M. Havas (1994). Ecological impact of acid deposition on natural ecosystems. In: Calvert, J.G. (ed.) *The Chemistry of the Atmosphere: Its Impact on Global Change*, published by: Blackwell Scientific, London, pp. 297 – 315.

Jane, G.T. and T.G.A. Green (1983). Episodic forest mortality in the Kaimai Ranges, North Island, New Zealand. *NZ J. Botany* **21:** 21 – 31.

Johnson, N. and R.A. Parnell (1986). Composition distribution and neutralization of 'acid rain' derived from Masaya volcano, Nicaragua. *Tellus* **38B:** 106 – 117.

Kaufman, Y.D., D. Tanra and O. Boucher (2002). A satellite view of aerosols in the climate system. *Nature* **419 (6903):** 215 – 223.

Kellogg, W.W., R.D. Cadel and E.R. Allen (1972). The sulfur cycle: Man's contributions are compared to natural sources of sulfur compounds in the atmosphere and oceans. *Science* **175:** 587 – 596.

Kinoshita, K. (1996). Observation of flow and dispersion of volcanic clouds from Mt. Sakurajima. *Atmos. Environ.* **30:** 2831 – 2837.

Kreisman, H., C.A. Mitchell, H.R. Hosein and A. Bouhuy (1976). Effects of low concentrations of sulfur dioxide on respiratory function in man. *Lung* **154:** 25 – 34.

Latter, J.H. (1986). Volcanic risk and surveillance in New Zealand. *N.Z. Geol. Surv. Rec.* **10:** 5 – 22.

Leet, R.C. (1988). Saturated and subcooled hydrothermal boiling in groundwater flow channels as a source of harmonic tremor. *J. Geophys. Res.* **93:** 4835 – 4849.

Linacre, E. and B. Geerts (1997). Climates and Weather Explained, published by: Routledge, 432 pp.

Luhar, A.K. and K.S. Rao (1994). Lagrangian stochastic dispersion model simulations of tracer data in nocturnal flows over complex terrain. *Atmos. Environ.* **28:** 3417 – 3431.

Luhar, A.K. and P.J. Hurley (2003). Evaluation of TAPM, a prognostic meteorological and air pollution model, using urban and rural point-source data. *Atmos. Environ.* **37:** 2795 – 2810.

Luhar, A.K., I. Galbally and P. Hurley (2004). Meteorological and dispersion modelling using TAPM for Wagerup; Phase 1: Meteorology. Report **C/0986**, 103 pp.

Lutgens, F.K. and E.J. Tarbuck (1979). The Atmosphere – An Introduction to Meteorology, published by: Prentice-Hall, 413 pp.

Mannino, D.M., S. Ruben, F.C. Holschuh, M.D. Wilson and T. Holschuh (1996). Emergency department visits and hospitalisations for respiratory disease on the island of Hawaii, 1981 to 1991. *Hawaii Med. J.* **55:** 48 – 53.

Marty, B. and W.F. Giggenbach (1990). Major and rare gases at White Island volcano, New Zealand: origin and flux of volatiles. *Geophys. Res. Lett.* **17:** 247 – 250.

Mather, T.A., A.G. Allen, C. Oppenheimer, D.M. Pyle and A.J.S. McGonigle (2003a). Size-resolved characterisation of soluble ions in the particles in the tropospheric plume of Masaya volcano, Nicaragua: Origins and plume processing. *J. Atmos. Chem.* **46:** 207 – 237.

Mather, T.A., D.M. Pyle and C. Oppenheimer (2003b). Tropospheric volcanic aerosol. In: Robock, A. & C. Oppenheimer (eds.) Volcanism and the Earth's Atmosphere. *Geophysical Monograph* **139:** 189 – 212.

Mather, T.A. and D.M. Pyle (2004). Volcanic emissions of mercury to the atmosphere: global and regional inventories: comment. *Sci. Total Environ.* **327:** 323 – 329.

Mather, T.A., A.G. Allen, B.M. Davison, D.M. Pyle, C. Oppenheimer and A.J.S. McGonigle (2004a). Nitric acids from volcanoes. *Earth Planet. Sci. Lett.* **218:** 17 – 30.

Mather, T.A., C. Oppenheimer, A.G. Allen and A.J.S. McGonigle (2004b). Aerosol chemistry of emissions from three contrasting volcanoes in Italy. Atmos. Environ. **38:** 5637 – 5649.

Mather, T.A., V.I. Tsanev, D.M. Pyle, A.J.S. McGonigle, C. Oppenheimer and A.G. Allen (2004c). Characterisation and evolution of tropospheric plumes from Lascar and Villarrica volcanoes, Chile. J. Geophys. Res. **109. (D21304).** doi: 10.1029/2004JD004934.

McGee, K. (1992). The structure, dynamics and chemical composition of non-eruptive plumes from Mount St. Helens. *J. Volcanol. Geotherm. Res.* **51:** 269 – 282.

McGonigle, A.J.S., C. Oppenheimer, B. Galle, T.A. Mather and D.M. Pyle (2002). Walking traverse and scanning DOAS measurements of volcanic gas emission rates. Geophys. Res. Lett. **29 (20)**. doi:10.1029/2002GL015827.

McGonigle, A.J.S., C. Oppenheimer, A.R. Hayes, B. Galle, M. Edmonds, T. Caltabiano, G. Salerno, M. Burton and T.A. Mather (2003). Sulphur dioxide fluxes from Mount Etna, Vulcano, and Stromboli measured with an automated scanning ultraviolet spectrometer. *J. Geophys. Res.* **108 (B9).** doi:10.1029/2002JB002261.

Miller, A. and R.A. Anthes (1980). Meteorology, published by: Charles E. Merrill Publishing Company, 170 pp.

Mills, M.J. (2000). Volcanic aerosol and global atmospheric effects. In: Sigurdsson, H. et al. (eds.) Encyclopedia of Volcanoes, published by: Academic Press, pp. 931 – 943.

Ministry for the Environment, New Zealand (1995). Environmental performance indicators. NIWA: National ambient air quality monitoring network for New Zealand, prepared by Fisher, G.W., B.W. Graham and M.J. Bell. *Technical Report* **No. 2**, Air, 151 pp.

Ministry for the Environment, New Zealand (1998). The Effects of Air Pollution on New Zealand Ecosystems – Review of National and International Research. *Air Quality Technical Report* **No. 1**, 77 pp.

Ministry for the Environment, New Zealand (2000a). Good-practice guide for air quality monitoring and data management, 111 pp.

Ministry for the Environment, New Zealand (2000b). Proposals for revised and new ambient air quality guidelines – Discussion document, 79 pp.

Ministry for the Environment, New Zealand (2002). Ambient Air Quality Guidelines – update. *Air Quality Report* No. 32, 66 pp.

Ministry for the Environment, New Zealand (2003a). Monitoring of CO, NO2, SO_2, ozone, benzene and benzo(a)pyrene in New Zealand. *Air Quality Technical Report* **No. 42**, October 2003, 87 pp.

Ministry for the Environment, New Zealand (2003b). Health effects of CO, NO_2, SO_2, ozone, benzene and benzo(a)pyrene in New Zealand. *Air Quality Technical Report* **No. 43**, November 2003, 28 pp.

Ministry for the Environment, New Zealand (2003c). Emission inventories for CO, NOx, SO_2, ozone, benzene and benzo(a)pyrene in New Zealand. *Air Quality Technical Report* **No. 44**, November 2003, 48 pp.

Ministry for the Environment (2005). Updated users guide to resource management (National Environmental Standards relating to certain air pollutants, dioxins and other toxics), Regulations 2004 (including amendments 2005), 79 pp.

Ministry for the Environment, New Zealand (2006). New Zealand's Fourth National Communication under the United Nations Framework Convention on Climate Change, Including the Report on the Global Climate Observing System and the report on Demonstrable Progress under the Kyoto Protocol. 232 pp.

Ministry of Health, United Kingdom (1954). Report on Public Health and Medical Subjects, No 95, HMSO, London.

Nadel, J.A., H. Salem, B. Tamplin and Y. Tokiwa (1965). Mechanism of bronchoconstriction during inhalation of sulfur dioxide. *J. Appl. Physiol.* **20:** 164 – 167.

Nakagawa, M., K. Wada, T. Thordarson, C.P. Wood and J.A. Gamble (1999). Petrologic investigations of the 1995 and 1996 eruptions of Ruapehu volcano, New Zealand: formation of discrete and small magma pockets and their intermittent discharge. *Bull. Volcanol.* **61:** 15 – 31.

Nakagawa, M., K. Wada and C.P. Wood (2002). Mixed magmas, much chambers, and eruption triggers: evidence from zoned clinopyroxene phenocrysts in andesite scoria from the 1995 eruptions of Ruapehu volcano, New Zealand. *J. Petrol.* **43:** 2279 – 2303.

Neiburger, M., J.G. Edinger and W.D. Bonner (1973). Understanding our atmospheric environment, published by: W.H. Freeman and Company, 293pp.

Neubert, D. (2001). Gutachten: Feinstaub-Exposition (Außenluft) und Morbidität (Mortalität) – Zusammenstellung von Daten zur biologischen Wirkung von Sulfat-Aerosolen und Versuch einer medizinischen Risikoabschätzung, 59 pp.

Niinimaa, V., P. Cole, S. Mintz and R. Shephard (1980). The switching point from nasal to oronasal breathing. *Respir. Physiol.* **42:** 61 – 67.

Nishi, Y., S. Sherburn, B.J. Scott and M. Sugihara (1996). High-frequency earthquakes at White Island volcano, New Zealand: insights into the shallow structure of a volcano-hydrothermal system. *J. Volcanol. Geotherm. Res.* **72:** 183 – 197.

Obenholzner, J.H., H. Schroettner, P. Golob and H. Delgado (2003). Particles from Popocatepetl volcano, Mexico. In: Oppenheimer, C., D.M. Pyle and J. Barclay (eds.) Volcanic Degassing. *Geol. Soc. London Spec. Pub.* **213:** 123–148.

Oden, S. (1967). *Dagens Nyheter*, Stockholm.

Ogden, J., C.H. Lusk and M.G. Steel (1993). Episodic mortality, forest decline and diversity in a dynamic landscape: Tongariro National Park, New Zealand. In: Huettl, R.F. & D. Mueller-Dombois (eds.). Forest decline in the Atlantic and Pacific region, published by: Springer, Berlin.

Oke, T.R. (1987). Boundary layer climates, published by: Methuen London and New York, 435 pp.

Oliver, W.R.B. (1915). The vegetation on White Island, New Zealand. *J. Linnaean Soc. London, botany* **43:** 41 – 47.

Operator Manual – White Island Met Station (2004).

Oppenheimer, C., P. Francis and J. Stix (1998). Depletion rates of sulfur dioxide in tropospheric volcanic plumes. *Geophys. Res. Lett.* **25:** 2671 – 2674.

Oppenheimer, C. (2003). Volcanic degassing. In: Rudnick, R.L. (ed.) Treatise on Geochemistry, Vol. 3: The Crust, published by: Elsevier, pp. 123 – 166.

Otway, P.M. (1986). Volcanic deformation surveys in the Tongariro Volcanic Centre. In: Gregory, J.G. & W.A. Watters (eds.) Volcanic Hazards assessment in New Zealand. *NZ Geol. Surv. Rec.* **10:** 35 – 40.

Pareschi, M. T., M. Ranci, M. Valenca and G. Graziani (1999). The assessment of volcanic gas hazard by means of numerical models: an example from Vulcano Island (Sicily). *Geophys. Res. Lett.* **26:** 1405 – 1408.

Phlean, J.M., D.L. Finnegan, D.S. Ballantine, W.H. Zoller, M.A. Hart and J.L. Moyers (1982). Airborne aerosol measurements in the quiescent plume of Mount St. Helens: September 1980. *Geophys. Res. Lett.* **9:** 1093 – 1095.

Physick, W.L., P.J. Hurley, A. Blockley, K.N. Rayner and P. Mountford (2002). Verification of the air quality models TAPM and DISPMOD in coastal regions. In: Brebbia, C.A. (ed.) Coastal environment: environmental problems in coastal regions IV, Rhodes, Greece, published by: WIT Press, pp. 425-434.

Physick, W.L. and M. Edwards (2005a). Worsley Alumina Pty 4.4 Mtpa efficiency and growth expansion air pollution modeling – Part I: TAPM verification against monitoring data. Final Report C/1036, 32 pp.

Physick, W.L. and M. Edwards (2005b). Worsley Alumina Pty 4.4 Mtpa efficiency and growth expansion air pollution modeling – Part II: Effect of expansion on sulfur dioxide, nitrogen dioxide and ozone concentrations. Final Report C/1036, 25 pp.

Pielke, R.A. (2002). Mesoscale Meteorological Modelling, published by: Academic Press, 676 pp.

Piironen, A. K. (1994). Analysis of Volume Imaging Lidar Signals. Ph.D. Thesis, University of Joensuu, Department of Physics, Vaisala Laboratory, Finland.

Quayle, A.M. (1984). The climate and weather of the Bay of Plenty region. *N.Z. Meteor. Serv. Misc. publ.* **115 (1)** 2nd. Edition, 56 pp.

Rampino, M.R. and S. Self (1982). Historic eruptions of Tambora (1815), Krakatau (1883), and Agung (1963), their stratospheric aerosols, and climatic impact. *Quaternary Res.* **18 (2):** 127 – 143.

Ratto, C.F., R. Festa, C. Romeo, O.A. Frumento and M. Galluzzi (1994). Mass-consistent models for wind fields over complex terrain. *Environ. Software* **9:** 247 – 268.

Reid, S.J. (1981). New Zealand winds and wind power. *N.Z. Met. S. Misc. Pub.* **172:** 14 pp.

Robock, A. (2000). Volcanic eruptions and climate. *Rev. Geophys.* **38:** 191 – 219.

Roedel, W. (2000). Physik unserer Umwelt – Die Atmosphäre, published by: Springer, pp. 498.

Roger, L.J., H.R. Kehrl, M.J. Hazucha and D.H. Horstman (1985). Bronchoconstriction in asthmatics exposed to sulfur dioxide during repeated exercise. *J. Appl. Physiol.* **59:** 784 – 791.

Rose, W.I., R.L. Chuan, W.F. Giggenbach, P.R. Kyle and R.B. Symonds (1986). Rates of sulfur dioxide and particle emissions from White Island volcano, New Zealand, and an estimation of the total flux of major gaseous species. *Bull. Volcanol.* **48:** 181 – 188.

Salinger, M.J. (1979). New Zealand climate: The temperature record, historical data and some agriculture implications. *Climatic Change* **2:** 109 – 126.

Scott, A.J. (2005). Source apportionment and chemical characterisation of airborne fine particulate matter in Christchurch, New Zealand. *Ph.D. thesis* (unpubl.) University of Canterbury, 255 pp.

Scott, B.J. (1991). A simple method for continuously recording the temperature of Crater lake, Mt. Ruapehu, New Zealand. *NZ DSIR Geol. Geophys. Geol. Rec.* **43:** 51 – 55.

Seinfeld, J.H. (1986). Atmospheric Chemistry and Physics of Air Pollution, published by: John Wiley, pp.

Seinfeld, J.H. and S.N. Pandis (1998). Atmospheric Chemistry and Physics: From Air Pollution to Climate Change, published by: John Wiley & Sons, 1326 pp.

Sheppard, D., W.L. Eschenbacher, H.A. Boushey and R.A. Bethel (1984). Magnitude of the interaction between the bronchomotor effects of sulfur dioxide and those of dry (cold) air. *Am. Rev. Respir. Dis.* **130:** 52 – 55.

Sherburn, S., C.J. Bryan, A.W. Hurst, J.H. Latter and B.J. Scott (1999). Seismicity of Ruapehu volcano, New Zealand, 1971-1996: a review. *J. Volcanol. Geotherm. Res.* **88:** 255 – 278.

Siebke, K., F.W. Badeck, G.H. Kohlmaier et al. (1990). Modelling pollutant exchange between plant and environmental uptake and metabolism of sulfur dioxide by different leaf cell compartments. In: *Developments in environmental modelling* **16:** Modelling in Ecotoxicology, published by: Elsevier Science Publishing Co., Inc.

Simpson, P. (1993). The cabbage trees (Cordyline australis) are dying: Investigations of sudden decline in New Zealand. In: Huettl, R.F. & D. Mueller-Dombois (eds.). Forest decline in the Atlantic and Pacific region, published by: Springer, Berlin.

Smith, S. (1992). Ecological and health effects of chemical pollution. In: Harrison, R.M. (ed.) *Understanding Our Environment: An introduction to Environmental Chemistry and Pollution*, published by: Royal Society of Chemistry, pp. 245 – 296.

Smith, W.H. (1990). Air Pollution and Forests: Interaction Between Air Contaminants and Forest Ecosystems, published by: Springer, 618 pp.

Sparks, R.S.J., M.I. Bursik, S.N. Carey, J.S. Gilbert, L.S. Glaze, H. Sigurdsson and A.W. Woods (1997). Atmospheric effects. In: *Volcanic Plumes*, published by: John Wiley & Sons, pp. 493 – 525.

Speizer, F.E. and N.R. Frank (1966). A comparison of changes in pulmonary flow resistance in healthy volunteers acutely exposed to SO_2 by mouth and by nose. Br. J. Ind. Med. 23: 75 – 79.

Spinks, K.D., V. Acocella, J.W. Cole and K.N. Bassett (2005). Structural control of volcanism and caldera development in the transtensional Taupo Volcanic Zone, New Zealand. *J. Volcanol. Geotherm. Res.* **144:** 7 – 22.

Statistics New Zealand (2006). Defining Urban and Rural New Zealand, http://www.stats.govt.nz/urban-rural-profiles/defining-urban-rural-nz/default.htm and related pages.

Steiner, J.T. (1980). The climate and weather of the South-West Pacific Region. *N.Z. Meteor. Serv. Misc. publ.* **166**, 35 pp.

Stevenson, D.S., C.E. Johnson, W.J. Collins and R.G. Derwent (2003). The tropospheric sulphur cycle and the role of volcanic SO_2. In: Oppenheimer, C., D.M. Pyle and J. Barclay (eds.) Volcanic Degassing. *Geol. Soc. London Spec. Pub.* **213:** 295 – 305.

Stern, A.C., R.W. Boubel, D.B. Turner and D.L. Fox (1984). Fundamentals of Air Pollution, published by: Academic Press, 530 pp.

Stull, R.B. (1989). An introduction to Boundary Layer Meteorology, published by: Kluwer Academic Press, 670 pp.

Stull, R.B. (1995). Meteorology Today for Scientists and Engineers – A Technical Companion Book, published by: West Publishing Company, 385 pp.

Sturman, A.P. and N.J. Tapper (1996). The Weather and Climate of Australia and New Zealand, published by: Oxford University Press.

Sutton, A.J. and T. Elias (1993). Volcanic gases create air pollution in the island of Hawai'i. *Earthquakes and Volcanoes* **24:** 178 – 196.

Symonds, R.B., W.I. Rose, G.J. Bluth and T.M. Gerlach (1994). Volcanic –gas studies: methods, results and applications. In: Carroll, M.R. & J.R. Holloway (eds.) Volatiles in Magmas. *Reviews in Mineralogy* **30:** 1 – 66. Mineralogical Society of America, Washington D.C.

Tam, E.K., J. Liu, B.G. Bigby and H.A. Boushey (1988). Sulfur dioxide does not acutely increase nasal symptoms or nasal resistance in subjects with rhinitis or in subjects with bronchial responsiveness to sulfur dioxide. *Am. Rev. Respir. Dis.* **138:** 1559 – 1564.

Tedesco, D. and J.-P. Toutain (1991). Chemistry and emission rate of volatiles from White Island volcano (New Zealand). *Geophys. Res. Lett.* **18:** 113 – 116.

Tomari, T., T. Yanagihashi, T. Ando et al. (1990). Comparison study on pulmonary function in school children: effect of volcanic activity from Mt. Sakurajima and athletic capability on the health of schoolchildren. Bu*ll. Phys. Fitness Res. Inst.* **75:** 74 – 85.

Torgersen, T., J.E. Lupon, D.S. Sheppard and W.F. Giggenbach (1982). Helium isotope variations in the thermal areas of New Zealand. *J. Volcanol. Geotherm. Res.* **12:** 283 – 295.

Turco, R. (2005). Earth Under Seige, published by:

Uda, T., S. Akiba, H. Hatano et al. (1999). Asthma-like disease in the children living in the neighborhood of Mt. Sakurajima. *J. Epidemiol.* **9 (1):** 27 – 31.

US Department of Health and Human Services (1998). Toxicological profile for sulfur dioxide. US Department of Health and Human Services, Public Health Service, Agency for Toxic Substances and Disease Registry 223 pp.

van Breemen, N., C.T. Driscoll and J. Mulder (1984). Acidic deposition and internal proton sources in acidification of soils and waters. *Nature* **307:** 599 – 604.

Vié Le Sage, R. (1983). Chemistry of the volatile aerosol. In Tazieff, H. & J.-C. Sabroux (eds.) *Forecasting Volcanic Events*, published by: Elsevier, Amsterdam, pp. 445 – 474.

Wakisaka, I., T. Yanagihashi, T. Tomari et al. (1988). Effects of volcanic activity on mortality figures for respiratory diseases. *Jpn. J. Hyg.* **42 (6):** 1101 – 1110.

Walker, G.T. (1924). Correlation of seasonal variations of weather, IX. *Mem. India Meteor. Dept.* **24:** 275 – 332.

Wardell, L.J., P.R. Kyle, N. Dunbar and B. Christenson (2001). White Island volcano, New Zealand: carbon and sulfur dioxide emission rates and melt inclusion studies. *Chem. Geol.* **177:** 187 – 200.

Wardle, J.A. and B.B. Allen (1983). Dieback in New Zealand *Nothofagus* forests. Pac. Sci. **37:** 397 – 404.

Warneck, P. (2000). Chemistry of the Natural Atmosphere, published by: Academic Press, 927 pp.

Werner, C., B.W. Christenson, M. Hagerty and K. Britten (2006). Variability of volcanic gas emissions during a crater lake heating cycle at Ruapehu volcano, New Zealand. *J. Volcanol. Geotherm. Res.* **154:** 291 – 302.

White Island Met Station – Operator Manual (2004).

Whiteman, C.D. (1990). Observations of thermally developed wind systems in mountainous terrain. In: Atmospheric Processes over Complex Terrain, published by: American Meteorological Society, pp. 5 – 42.

Willmott, C.J. (1981). On the validation of models. *Phys. Geography* **2:** 184 – 194.

Wilson, C.J.N., B.F. Houghton, M.O. McWilliams, M.A. Lanphere, S.D. Weaver and R.M. Briggs (1995). Volcanic and structural evolution of Taupo Volcanic Zone, New Zealand: a review. *J. Volcanol. Geotherm. Res.* **68:** 1 – 28.

Wilson, J.G. and P. Zawar-Reza (2006). Intraurban-scale dispersion modelling of particulate matter concentrations: Applications for exposure estimates in cohort studies. *Atmos. Environ.* **40:** 1053 – 1063.

Zawar-Reza, P., S. Kingham and J. Pearce (2005). Evaluation of a year-long dispersion modeling of PM_{10} using the mesoscale model TAPM for Christchurch, New Zealand. *Science Total Environ.* **349:** 249 – 259.

Zielinski, G.A., P.A. Mayewski, L.D. Meeker, S. Whitlow and M.S. Twickler (1996). A 110,000-yr record of explosive volcanism from GISP2 (Greenland) ice core. *Quaternary Res.* **45:** 109 – 118.

Zreda-Gostynska, G., P.R. Kyle, D. Finnegan and K. Meeker Prestbo (1997). Volcanic gas emissions from Mount Erebus and their impact on the Antarctic environment. *J. Geophys. Res.* **102:** 15,039 – 15,055.